Microencapsulation of omega-3 fatty acid rich oil via complex coacervation

A Thesis Submitted to the
College of Graduate and Postdoctoral Studies
in Partial Fulfillment of the Requirements
for the Degree of Doctor of Philosophy
in the Department of Food and Bioproduct Sciences
University of Saskatchewan
Saskatoon, Saskatchewan, Canada

By
Yingxin Wang
2022

PERMISSION TO USE

In presenting this thesis in partial fulfillment of the requirements for a Postgraduate degree from the University of Saskatchewan, I agree that the Libraries of this University may make it freely available for inspection. I further agree that permission for copying of this thesis in any manner, in whole or in part, for scholarly purposes may be granted by the professor or professors who supervised my thesis work or, in their absence, by the Head of the Department or the Dean of the College in which my thesis work was done. It is understood that any copying or publication or use of this thesis or parts thereof for financial gain shall not be allowed without my written permission. It is also understood that due recognition shall be given to me and to the University of Saskatchewan in any scholarly use which may be made of any material in my thesis.

Requests for permission to copy or to make other uses of materials in this thesis in whole or part should be addressed to:

Head of the Department of Food and Bioproduct Sciences
Room 3E08, Agriculture Building, 51 Campus Drive
University of Saskatchewan
Saskatoon, Saskatchewan, S7N 5A8, Canada

OR

Dean
College of Graduate and Postdoctoral Studies
University of Saskatchewan
116 Thorvaldson Building, 110 Science Place
Saskatoon, Saskatchewan S7N 5C9 Canada

ABSTRACT

The overall goal of this thesis was to use plant-based materials to encapsulate omega-3 oils to produce microencapsulated powders with improved stability against oxidative stresses. This research includes four studies (Chapter 3, 4, 5 & 6). Chapter 3 examined the complexation behaviour of lentil protein isolate (LPI) and carboxymethyl cellulose (CMC) with different degree of substitution (DS; 0.7, 0.9, and 1.2) and molar mass (MM; 90 and 250 kDa), and their thermodynamic properties. For complexation behaviour, max optical density was conducted at 4:1 LPI: CMC mixing ratio. MM and DS had no significant effect on critical pH values but impacted the size and number of complexes formed. The complexation reactions of all LPI-CMC mixtures at pH 3 was energetically favorable. Chapter 4 and 5 compared the complexation behaviour of LPI with various polysaccharides, including CMC, gum Arabic (GA), alginate (AL), ι-carrageenan (ι-C), and κ-carrageenan (κ-C), and the resulting emulsifying properties. For chapter 4, at 4:1 LPI-polysaccharide mixing ratio, LPI-GA and LPI-CMC mixtures formed coacervate-type of complexes, while precipitate-type of complexes were formed with LPI-AL and LPI-ι-C systems. Their resulting complexes at pH_{opt} were used to make emulsions. LPI-ι-C emulsion displayed the highest emulsion stability (ES) due to its high emulsion viscosity, lower mean droplet sizes, and highly negative-charged droplets. For chapter 5, incorporating ι-C and κ-C into the LPI solution led to suppression of complexes formed. Emulsions prepared with the resulting soluble complexes at pH 6 showed significantly higher stability than those made with insoluble complexes at pH 3.5 for each sample. The greatest ES was attributed to 4:1 LPI-κ-C and LPI-ι-C emulsions at pH 6. Chapter 6 developed the LPI-polysaccharide based microcapsules to encapsulate flaxseed oil. LPI-κ-C and LPI-ι-C emulsions with maltodextrin at pH 6 were prepared, followed by spray-drying or freeze-drying to yield the dried capsules. Spray-dried capsules showed higher oil encapsulation efficiency, but the encapsulated oil was oxidized significantly due to heat effect during drying and lower water activity of the capsules. Flaxseed oil was stable in all freeze-dried capsules during 8 weeks of storage. For *in vitro* oil release profile, more oil was released from LPI-κ-C powders under simulated gastric fluid, but more oil was released from LPI-ι-C powders under subsequent simulated gastric fluid and simulated intestinal fluid regardless of drying method and oil content.

This research suggested that there is great potential to use the resulting emulsions to make plant-based microcapsules to deliver omega-3 oils.

ACKNOWLEDGEMENTS

I would like to express my sincere thanks and gratitude to my supervisor, Dr. Michael Nickerson, for his continuous support, valuable guidance, encouragement, patience, and tremendous contribution. All made it possible for me to complete my research project and made my four-year research a rewarding and enjoyable journey. I would also like to thank to my advisory committee, Drs. Phyllis Shand, Supratim Ghosh, Yongfeng Ai, Filiz Koksel, and Rex Newkirk for taking time out of their busy schedules and giving a lot of valuable advice and insightful comments, which inspires and widens my research. Special thanks to my external examiner, Dr. Jiajia Rao from North Dakota State University for her time and her thoughtful comments.

Special thanks to Yuriy Kryachko and Maria Romero from the Department of Food and Bioproduct Sciences for the training on confocal laser scanning microscopy, Daniel Wiens and Jianheng Shen from the Department of Plant Sciences for their assistance and training on spray dryer and freeze dryer, and Guosheng Liu from the Department of Biology for his help on scanning electron microscopy for my research.

Many thanks go to my lab mates Pillai Prasanth, Burcu Guldiken, Andrea Stone, Dellaney Konieczny, Erin Hopkins for all the training, assistance, and support for my research and also providing a friendly working environment. I would also like to say thank you to Yuanlong Cao, YanRan Tang, Chi Doan, Pravin Gadkari, Kunal Kadiya, Athira Mohanan for all the help on my research. Also, I am grateful to the staff in the Department of Food and Bioproduct Sciences, especially Ann Harley and Donna Selby, for their administrative support.

Finally, I would like to express my warmest thanks to my parents and my boyfriend Siyang Shen, for their precious support, consistent encouragement, and love through my research and all the achievements in Canada.

I greatly appreciate for the financial support from the Natural Sciences and Engineering Research Council of Canada (NSERC) Discovery Program (RGPIN-2014-05661) and the NSERC-CREATE Program (Canadian Agri-food Protein Training, Utilization and Research Enhancement).

TABLE OF CONTENTS

LIST OF TABLES

LIST OF FIGURES

LIST OF SIMBOLS AND ABBREVIATION

O_2	Oxygen
U_E	Electrophoretic mobility
V_{stokes}	Velocity of a droplet
η_C	Continuous phase viscosity
η_D	Disperse phase viscosity
ρ_c	Continuous phase
ρ_d	Dispersed phase
$\Delta G_{formation}$	Free energy of emulsion formation
ΔS_{config}	Change of configurational entropy of droplets in system
ΔA	Change in oil-water interfacial area
ΔG	Total Gibbs free energy
ΔH	Enthalpy
ΔS	Entropy
°C	Degree Celsius
µL	Microliter
µm	Micrometer
a	Redness
AL	Alginate
ANOVA	Analysis of variance
a_w	Water activity
b	Yellowness
BHT	Butylated hydroxytoluene
Ca^{2+}	Calcium ion
CLSM	Confocal laser scanning microscopy
cm	Centimeter
CMC	Carboxymethyl cellulose
CPI	Canola protein isolate
d.b.	Dry basis
$d_{3,2}$ / $D_{3,2}$	Surface-average diameter

$d_{4,3}$ / $D_{4,3}$	Volume-average diameter
DE	Dextrose equivalent
DMSO	Dimethyl sulfoxide
DS	Degree of substitution
EE	Encapsulation efficiency
EEP	Electric equivalence point
Eq	Equation
ES	Emulsion stability
$f(\kappa\alpha)$	Smoluchowski approximation
g	Gram
GA	Gum Arabic
GDL	Glucono-δ-lactone
GMO	Genetically modified organism
h	Hour
HCl	Hydrochloric acid
ITC	Isothermal titration calorimetry
K	Binding constant/ affinity constant
K^+	Potassium ion
kDa	Kilodalton
kg	Kilogram
KI	Potassium iodide
L	Liter
L	Length
L	Lightness
LPI	Lentil protein isolate
m	Consistency coefficient
M	Morality
m^3/h	Cubic meter per hour
MD	Maltodextrin
MDA	Malondialdehyde
meq	Milliequivalents

Mg^{2+}	Magnesium ion
Min	Minute
mL	Milliliter
MM	Molar mass
mM	Micromolar
mN/m	Millinewton per meter
mPa s	Millipascal per second
mPa	Millipascal
mV	Millivolt
n	Flow behavior index
N	Normality
Na^{+}	Sodium ion
$Na_2S_2O_3$	Sodium thiosulfate
N_i	Number of droplets
nm	Nanometer
O/W	Oil in water
O/W/O	Oil in water in oil
OD	Optical density
OD_{Max}	Maximun optical density
$pH_{\phi 1}$	Insoluble complex
$pH_{\phi 2}$	Complete dissolution
pH_c	Soluble complexes
pH_{opt}	Maximum coacervation
pI	Isoelectric point
PV	Peroxide value
q	Binding stoichiometry
rpm	Revolutions per minute
S	Second
S	Svedberg unit
SDS	Sodium dodecyl sulfate
SEM	Scanning electron microscope

SGF	Simulated gastric fluid
SIF	Simulated intestinal fluid
SO	Surface oil
T	Absolute temperature
TBA	2-Thiobarbituric acid
TBARS	2-Thiobarbituric acid reactive substances
v/v	Volume by volume
V_A	Volume of the aqueous phase after drainage
V_B	Volume of the aqueous phase before emulsification
W/O	Water in oil
w/w	Weight by weight
α	Particle radius
ζ	Zeta potential
ι-	Iota
ι-C	ι-Carrageenan
κ	Debye length
κ	Kappa
κ-C	κ-Carrageenan
λ	Lambda
d	Diameter of the droplet
$f(\kappa\alpha)$	A function related to the ratio of particle radius (α)
g	Gravitational acceleration
γ	Interfacial tension
ε	Permittivity
η	Viscosity
θ	Contact angle

1. INTRODUCTION

1.1. **Overview**

The interactions between proteins and polysaccharides play an important role in controlling food structure and functionality (Schmitt et al., 1998; Ye, 2008). Mixed systems involving animal proteins (e.g., casein, whey gelatin) and food polysaccharides (e.g., carboxymethyl cellulose, pectin, carrageenan, alginate, and gum Arabic) have been extensively investigated (Engbal et al., 2016; Weinbreck et al., 2003; Devi & Maji, 2011); however, those involving plant proteins are more limiting, where the main difference observed is associated with a greater role of protein aggregation during biopolymer interactions for plant proteins (Liu et al., 2009; Klemmer et al., 2012). The use of plant protein ingredients within the food industry is increasing rapidly due to their lower cost, greater environmental sustainability, perceived safety concerns related to consuming animal products, and consumer dietary preferences based on ethical, religious and moral views.

Complex coacervation (also known as associative phase separation) involves attractive interactions (via electrostatics) at solution pH values where biopolymer mixtures (e.g., proteins and polysaccharides) have opposing net charges. The result is that phase separation occurs into a biopolymer (protein + polysaccharide)-rich and solvent-rich phase (Bungenberg et al., 1929; deKruif et al., 2004; Ye, 2008). Solvent conditions (e.g., pH, salt concentration), biopolymer characteristics, and mixing ratio and concentration can affect the structure and functions of the coacervates formed. Electrostatically complexed protein-polysaccharides can be widely used for the development of controlled release materials for use for food, nutraceutical, or drug delivery (Schmitt et al., 1998; Ye, 2008), and biodegradable edible films.

Encapsulation technology has been widely studied and applied in the pharmaceutical, cosmetic, chemical, printing, and food industries (Madene et al., 2006; Heinzen, 2002). Encapsulation can provide better production to the core material against environmental changes, regulates the nutritional loss, and controls the release (Narsaiah et al., 2014). Microencapsulation

using the complex coacervation method is one of the most widely encapsulation techniques for entrapping a lipid core due to the simple, solvent-free, non-thermal, and low-cost process with great controlled release properties, heat resistance, and stability (Bakry et al., 2016; Wang et al., 2014). A stabilized emulsion is first prepared during the production, followed by drying to yield dried powders (Koupantsis et al., 2014). Protein-polysaccharide stabilized emulsions can form either a bilayer or mixed layer at the interface to stabilize the emulsion, and the biopolymer, solvent, and shearing conditions would greatly affect the stability of the emulsion.

Within this research, interactions between lentil proteins and carboxymethyl cellulose (CMC) will be examined as a function of CMC molar mass and degree of substitution. Lentil has received great interest due to its high nutritional value (high in protein, fibre and low in fat) and high digestibility (Campos-Vega et al. 2010; Jarpa-Parra, 2018). In addition, lentils provide a series of health benefits, such as lowering the incidence of colon cancer and type-2 diabetes, and reducing the cholesterol and lipid levels in human bodies (Roy et al., 2010; Jarpa-Parra, 2018). Lentil protein also provides desired functional properties such as emulsifying, water binding, fat binding, foaming, and gelling properties and can be made into many value-added products (Boye et al., 2010; Aydemir & Yemenicioglu, 2013). CMC is a polysaccharide with a wide range of application in foods (Biswal & Singh, 2004). CMC can be modified with different substitution degrees of their carboxy methyl group and to have different molecular mass. Further, complexation involving LPI will also be examined with other anionic polysaccharides for comparative purposes, including alginate, gum Arabic and iota-carrageenan. All biopolymers selected for this study represent industrially important food biopolymers. Gum Arabic is a branched carboxylated polysaccharide with highly heterogeneous structure. Alginate is also a carboxylated polysaccharide with considerably high linear charge density, while κ-carrageenan and ι-carrageenan are sulfated polysaccharides. The emulsifying properties of all formed complexes will be examined. Stable emulsions prepared under the use of complex coacervates were reported in a whey protein-gum Arabic system (Weinbreck et al., 2004), pea protein isolate-gum Arabic (Liu et al., 2010), canola protein isolate-carrageenan (Stone et al., 2013), chitosan-alginate (Li & McClements, 2011), β-lactoglobulin-CMC (Chuah et al., 2014), and milk protein-CMC (Koupantsis et al., 2014). The most stable emulsion stabilized by one of the LPI-polysaccharide complex combinations will then be selected for further implement to increase the stability of the emulsion, and the microencapsulation process will be applied for further study.

The first goal of this thesis is to examine the complexation behaviour of lentil protein isolate and CMC with different degrees of substitution and molecular mass, as a function of pH and biopolymer mixing ratio. Then, to compare the complexation behaviour of LPI with a range of polysaccharide and the resulting emulsifying properties. And finally, to integrate knowledge gained relating to conditions where the most stable emulsion will form for development of lentil protein-polysaccharide based microcapsules.

1.2. **Objectives**

Specific objectives include:

- To examine the effect of degrees of substitution and molecular mass of CMC on the complexation behaviour with lentil protein isolate, as a function of pH and biopolymer ratio.
- To examine the effect of degrees of substitution and molecular mass of CMC on the thermodynamic properties during complexation with LPI by isothermal calorimetry.
- To examine the effect of pH on the complexation behavior of LPI with other anionic polysaccharides, including alginate, gum Arabic and iota-carrageenan.
- To examine the emulsifying properties of formed LPI-polysaccharide complexes.
- To examine the effect of biopolymer, solvent, and shearing conditions on the interfacial and emulsifying properties for LPI-polysaccharide complexes (i.e. LPI-ι-C complexes)
- To obtain microcapsules using the LPI, ι-C, and maltodextrin as the wall materials and the canola oil or flaxseed oil as the core material, followed by spray drying.

1.3. **Hypotheses**

The following hypotheses will be tested as part of this research:

- Different degrees of substitution and molecular mass of CMC will have different complexation behaviours with LPI as a function of pH and biopolymer ratio. More coacervates will be achieved between lentil protein isolate and CMC with a higher degree of substitution or high molecular mass.
- Complexation between a higher charge density of CMC and LPI will lead to a larger enthalpy and binding stoichiometry.

- LPI-CMC and LPI-GA systems will form soluble coacervate structures, while insoluble precipitate-type structures will be formed in LPI-AL and LPI-ι-C.
- Increased emulsion stability will be observed under LPI-polysaccharide complex stabilized emulsions because a stronger viscoelastic film formation can be formed under complexation of LPI and polysaccharides.
- More stable emulsions will be obtained as the mixing ratio of lentil protein isolate and ι-carrageenan increases. Also, emulsions prepared at pH 6 might be more stable than those prepared at pH 3.
- Microcapsules with higher stability against oxidative stress can be achieved compared to the unencapsulated oil.

2. LITERATURE REVIEW

2.1 Phase separation in biopolymer mixtures

Protein-polysaccharide interactions play an important role in controlling food structure, as well as in the development of controlled release materials (e.g., films and microcapsules) for use for nutraceutical or drug delivery (Schmitt et al., 1998; Ye, 2008). Phase separation behaviour of biopolymer mixtures have primarily been examined involving food based polysaccharides (e.g., pectin, carrageenan, alginate and gum Arabic) with animal-derived proteins such as from milk (e.g., casein, whey, beta-lactoglobulin and alpha-lactalbumin) (Engbal et al., 2016; Weinbreck et al., 2003; Weinbreck et al., 2004; Girard et al., 2004), gelatin (Devi & Maji, 2011) and egg (e.g., Ovalbumin) (Souza & Garcia-Rojas, 2015); or with plant-derived proteins such as from pulses (Liu et al., 2009; Klemmer et al., 2012), soy (Conto et al., 2013; Hsiao et al., 2017) or oilseeds (Klassen et al., 2011; Stone et al., 2014). Unlike the much smaller animal-derived proteins, interactions involving polysaccharides and the larger plant proteins tend to have greater impact on protein aggregation (Liu et al., 2009; Klemmer et al., 2012). Mechanisms describing coacervation formation and growth have been previously reviewed based primarily on mixtures with animal derived proteins (Weinbreck et al., 2003; Weinbreck et al., 2004; Devi & Maji, 2011); however, further understanding of systems involving plant proteins is needed.

In brief, depending on the biopolymer concentration and electrostatic charge within the system, various phase separating behaviour may ensue. In very dilute solutions, biopolymers are co-soluble, with both remaining in solution and non-interacting due to the large entropic effect (Figure 2.1) (Ye, 2008; Tolstoguzov, 1991). As the biopolymer concentration increases, either segregative or associative (also known as complex coacervation) phase separation occurs depending on the functional groups and charges present (Schmitt et al., 1998). In segregative phase separation, proteins and polysaccharides are incompatible as they carry similar net charges resulting in electrostatic repulsion and the separation into a protein-rich and polysaccharide-rich phase (Figure 2.1) (Liu et al., 2010; Klassen et al., 2011; Klemmer et al., 2012; Stone et al., 2014).

In this case, solvent-biopolymer interactions are more favored than biopolymer-biopolymer interactions (Ye, 2008). In the case of associated phase separation, proteins and polysaccharides carry opposing net charges and experience electrostatic attraction between biopolymers and phase separation into a biopolymer (protein + polysaccharide)-rich and solvent-rich phase (Figure 2.1) (Bungenberg et al., 1929; de Kruif et al., 2004; Ye, 2008). Depending on the charge density and the functional group, associative phase separation may lead to the formation of either a soluble coacervate or an insoluble precipitate-type structure (Figure 2.1) (Schmitt et al., 1998; de Kruif et al., 2004; Kayitmazer, 2017; Singh et al., 2007; Klemmer et al., 2012). Coacervate structures tend to entrap water inside, remain suspended in solution and retain a high level of chain mobility within it (Ye, 2008). The coacervate structure also tends to be reversible upon changes in pH, and typically involves polysaccharides that are more weakly charged (i.e., lower linear charge density), such as gum Arabic (Stone et al., 2014). Precipitate structures entrap little water, have significantly less chain mobility inside, and tend to sediment to the bottom of the solution rather quickly (Ye, 2008). The structures are more strongly interacting leading to a less reversible structure. Precipitate formation tends to involve protein mixtures with highly charged polysaccharides (i.e., high linear charge density) such as carrageenan and alginate (Klemmer et al., 2012).

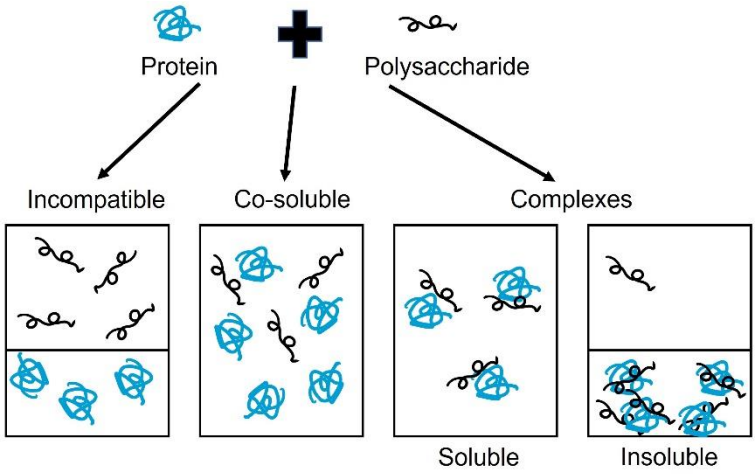

Figure 2.1 Depicts the phase separation behaviour between proteins and polysaccharides (reproduced based on Ye, 2008).

Although the main driving force behind complex coacervation is electrostatic attractive forces, non-Coulombic interactions such as hydrophobic interactions, hydrogen bonding, and

covalent linkages also play a role in the formation and stability of coacervate structures (Schmitt et al., 1998; deKruif et al., 2004; Ye, 2008; Klemmer et al., 2012). From a thermodynamics perspective, the formation of protein-polysaccharide complexes becomes possible and occurs spontaneously when the change of total Gibbs free energy within the system is negative (i.e., $\Delta G = \Delta H - T\Delta S < 0$) (Schmitt et al., 1998; Turgeon & Laneuville, 2009). The value of ΔG is determined by the balance between the favourable entropy (- $T\Delta S$) and the unfavourable enthalpy (ΔH). It is generally agreed that coacervation is mainly driven by entropy gained through the release of condensed counter ions (deKruif et al., 2004; Tyrgeon & Laneuville, 2009; Sulatha & Natarajan, 2015; Kayitmazer, 2017). The entropically driven process has been confirmed and by isothermal titration calorimetry (de Kruif et al., 2004; Sulatha & Natarajan, 2015).

2.2 Factors affecting complex coacervation

2.2.1 Solvent factors

Since complex coacervation is dominated by electrostatic forces, both solvent pH and the presence of salts have the greatest impact on biopolymer interactions. Depending on the pH, reactive sites on both biopolymers may be protonated or deprotonated. Typically, complex formation occurs between negatively charged polysaccharides and positively charged proteins (at pH < isoelectric point of the protein) (Ye, 2008); however, in the case of highly charged polysaccharides interactions can occur at pH values above the pI due to the presence of positively charged patches on the protein's surface (Tolstoguzov, 1997; Ye, 2008; Turgeon & Laneuville 2009). The interactions between positively charged patches on the protein's surface at pH above pI and negative charged polysaccharides have been reported in a LPI-gum Arabic (GA) system (Aryee & Nickerson, 2021), a whey protein-gum Arabic mixture (Weinbreck et al., 2003b), and a bovine serum albumin-heparin mixture (Seyrekan et al., 2003).

The formation of coacervate or precipitate structures follows a number of pH-induced structure forming events identified using a turbidity curve during an acid titration (Kizilay et al., 2011). Typically, initial biopolymer interactions occur at or near the pI of the protein, where it starts to assume a positive charge to allow it to electrostatically attract to the anionic polysaccharide and form a soluble complex (denoted as pH_c) (Schmitt et al., 1998; Turgeon & Laneuville, 2009; Stone et al., 2014). At this pH, a slight reflection in the turbidity vs. pH curve can be observed (Tolstoguzov, 1997; Ye, 2008; Turgeon & Laneuville, 2009). As pH is lowered

further, protein-polysaccharide interactions become greater leading to the formation of a greater number of larger complexes via nucleation and growth kinetics (Stone et al., 2014). Once it reaches a critical pH (denoted as $pH_{\phi 1}$), associated with the formation of insoluble complexes, a large rise in turbidity within the curve is evident (Schmitt et al., 1998; Turgeon & Laneuville, 2009; Stone et al., 2014). It is noteworthy to mention that the terms 'soluble' and 'insoluble' complexes refer to terminology used in the coacervation literature, rather than having to do with a functional property of solubility. Turbidity reaches a maximum absorbance at a pH denoted as pH_{opt} (Li et al., 1994). At pH_{opt}, the protein and polysaccharide mixtures reach an electrical equivalence point (EEP), where two biopolymers have exactly opposite charges with a zeta potential of zero; and typically corresponds to maximum coacervate yield (Li et al., 1994; Schmitt et al., 1998; Stone et al., 2014; Kayitmazer, 2017). As pH is further lowered, coacervates start to break up as the reactive side chains on the anionic polysaccharides start to become protonated as evident by a reduction in turbidity (Stone et al., 2014). This continues until reaching a pH corresponding to near the pK_a of the polysaccharide (denoted as $pH_{\phi 2}$), where complete disassociation of the biopolymers is observed and they become co-soluble again (Klemmer et al., 2012; Stone et al., 2014).

The presence of counter ions in solution can act to screen charges on both the protein and the polysaccharides to reduce their Debye length or thickness of their electrical double layer (EDL) (Kayitmazer, 2017). This process, depending on the types of ions present and the ionic strength, will act to reduce the electrostatic attraction forces between opposite charged groups (Ye, 2008). Since coacervation is an entropically driven process, it depends on the release of counter ions. Under high salt levels, the release of counter ions condensed on the biopolymer's surface is more difficult and the entropic driving force is suppressed (Schmit et al., 1998; Perry et al., 2014). Further, protein-protein aggregation due to hydrophobic interactions between the proteins would be favoured over protein-polysaccharide interactions if there were little attractive forces. Perry et al. (2014), Burgess (1990), and Weinbreck et al. (2003) reported the presence of small amounts of salt could improve the coacervation process by softening the strength of the electrostatic attractive forces to allow for increased conformational entropy of the biopolymers and exposure of additional reactive sites.

Solution temperatures can impact the stability of the formed complexed structures by altering the protein conformation and non-Coulombic interactions. Globular proteins tend to denature at higher temperatures allowing for more sites that are reactive (e.g., hydrophobic groups)

to become exposed. This conformational change might result in a process mainly driven by hydrophobic interactions instead of electrostatic effects, where the protein-protein aggregation would become more significant (Tsianou et al., 1999; Borrega et al., 1999). At low temperature, hydrogen bonding is preferred (Schmitt et al., 1998; Turgeon & Laneuville, 2009). With stronger hydrogen bonding occurring, less electrostatic interactions are required to form coacervate structures. This effect was reported by Weinbreck et al. (2004) for a whey protein-carrageenan system, and by Antonov et al. (2006) involving fava bean legumin-type proteins with carboxymethyl cellulose.

2.2.2 Biopolymer characteristics

Depending on the type of biopolymer (protein or polysaccharide) present, the coacervation process could differ based on their molecular mass, conformation and flexibility, and the type and density of reactive sites present. Typically, proteins are mixed with sulphated polysaccharides ($-OSO_3^-$ groups; and include κ- or ι-type carrageenan) or carboxylated polysaccharides ($-COO^-$ groups; and include alginate, pectin, gellan gum, gum Arabic and carboxymethyl cellulose) (Ye, 2008). The former type tends to form stronger interactions with the proteins. In the case of carboxylated polysaccharides, the linear charge density becomes important. For instance, pea protein isolate has been shown to form precipitate-type structures in the presence of alginate (Klemmer et al., 2012), whereas a coacervate-type structure was formed in the presence of gum Arabic (Liu et al., 2010). Linear proteins such as gelatin and caseins are more flexible, and they can interact with polysaccharides more strongly than globular proteins such as beta-lactoglobulin (Grindrod and Nickerson, 1968). Proteins with more flexibility could lead to increasing contacts with oppositely charged polysaccharides (Ye, 2008). Also, Schmitt et al. (1998) noted that increasing the molecular weight of biopolymers should affect the coacervation since a higher molecular weight could lower the entropy of mixing which reduces the biopolymer compatibility in the solution, and there might be less coacervates formed and a tendency of phase separation.

The number of reactive sidechains /groups carried by proteins or polysaccharides per unit of length is defined as the linear charge density (Schmitt et al., 1998). In the case of proteins, charge density is largely dependent on pH. Normally, a protein would only interact with an anionic polysaccharide when the pH is below its isoelectric point (pI) (i.e., when a protein carries positive charges); however, as mentioned earlier (see section 2.2.1) they can associate at pH values above

the pI. Turgeon and Laneuville (2009) noted that coacervation between highly charged biopolymers is mostly driven by entropy (ΔS) due to release of counter ions and opposed by a positive enthalpy change (ΔH); in contrast, with weakly charged biopolymers, complex formation is driven by a negative enthalpy with less entropic effect (Turgeon & Laneuville, 2009).

2.2.3 Mixing ratio and concentration

The biopolymer-mixing ratio plays a role in the coacervation process by influencing the overall charge balance of the protein and polysaccharide, which eventually impacts the degree of the coacervation. Typically, at a given solution condition (i.e., pH and ionic strength), the maximum yield of the coacervate is reached at a specific mixing ratio for different biopolymer combinations (Schmitt et al., 1998; Ye, 2008). At this mixing ratio, the overall charge of the complex is neutral. For instance, canola protein isolate (CPI) -gum Arabic (GA) complexes achieved maximum yield at ratio 2:1 at pH 4.20 (Stone et al., 2014). If one of the biopolymers is in excess, there will be excess positive or negative charges present in the system, and soluble complexes would form because of these unbalanced charges (Girard et al., 2004, Espinosa-Andrews et al., 2007; Perry et al., 2014). In whey protein-gum Arabic systems (with minimal protein-protein aggregation), critical pH values (i.e., pH_c, $pH_{\phi 1}$, pH_{opt} and $pH_{\phi 2}$) were found to be independent of biopolymer mixing ratio (Weinbreck et al., 2003). However, in the case of plant proteins, they tend to be mixing ratio dependent because polysaccharide chains are interacting with protein aggregates of varying sizes rather than individual macromolecules. Stone et al. (2014) reported that critical pH values increased with increasing mixing ratios within a canola protein isolate (CPI) -gum Arabic (GA) system until a ratio of 4:1 before reaching a plateau at higher ratios. The authors explained ratio dependence of the critical pH values was the result of interactions between a GA molecule and CPI-CPI aggregates rather than single proteins. Furthermore, Weinbreck et al. (2003) reported that coacervation occured up to a maximum total biopolymer concentration (dependent on the system), after which attractive interactions are suppressed by the increased release of counter ions which in turn would then screen charges between the proteins and polysaccharides.

2.3 Emulsion formation

Emulsions are dispersions of two or more immiscible liquids where one phase is dispersed as small droplets in the other. Food emulsions normally contain droplets with sizes ranging from 0.1 to 100 μm and can be classified as oil in water (O/W) emulsions such as milk, salad dressings, and mayonnaise, or water in oil (W/O) emulsions including butter and margarine (Dickinson, 1992; Friberg & Larsson, 1997; Lam & Nickerson, 2013). Emulsions are stabilized through the use of emulsifiers, which are surface active components that can absorbed into the oil – water interface due to their amphiphilic nature (McClements, 2005). Emulsifiers include small surfactants, for example, lecithin, fatty acid salts, Tweens, and Spans, and biopolymers such as proteins, gum Arabic, modified starches, modified cellulose, and protein-polysaccharide complexes (McClements, 2005).

Emulsions stabilized by protein-polysaccharide complexes have been drawing more attention by industry. Proteins, either animal or plant-based, stabilized emulsions have been studied extensively due to the excellent emulsifying properties (Agyare et al., 2009; Can Karaca et al., 2011; Djordjevic et al., 2004; Popineau et al., 2002), however their stability can be affected under environment stresses such as pH, ionic strength and temperature (Yin et al., 2012). Incorporating the anionic polysaccharides alongside the proteins could result in more stable emulsions, if conditions are right (McClements, 2005; Yin et al., 2012). Protein-polysaccharide stabilized emulsions can form either a bilayer or mixed layer at the interface to stabilize the emulsion. The former is prepared through a multi-step procedure, where a primary protein stabilized emulsion is formed, followed by the addition of polysaccharides to adsorb on the protein layer (Figure 2.2a) (Guzey & McClements, 2006; Evans et al., 2013; Lam & Nickerson, 2013). The latter is prepared involving a premixed coacervate solution, in which the pre-formed protein-polysaccharide complexes align at the interface to develop a viscoelastic film (Evans et al., 2013). A simple preparation route of coacervate emulsions is showed in Figure 2.2b. During the emulsification process, the formed surface-active protein-polysaccharide complexes migrate, adsorb and become integrated at the oil-water interface to reduce the interfacial tension, which is a force to minimize the contact area between the oil and water phase (Uruakpa & Arntfield, 2005; Walstra & van Vliet, 2008). At the interface, the formed complexes re-align to position the hydrophobic amino acids towards the oil phase and hydrophilic moieties towards the aqueous phase, leading to the formation of viscoelastic films that can resist mechanical stresses, and to

provide steric stabilization and electrostatic repulsion depending on the conditions of complexes (i.e. charge and sizes) (Lam & Nickerson, 2013). Stable emulsions prepared under the use of complex coacervates were reported in a whey protein-gum Arabic system (Weinbreck et al., 2004), pea protein isolate-gum Arabic (Liu et al., 2010), canola protein isolate-carrageenan (Stone et al., 2013), chitosan-alginate (Li & McClements, 2011), β-lactoglobulin-CMC (Chuah et al., 2014), and milk protein-CMC (Koupantsis et al., 2014).

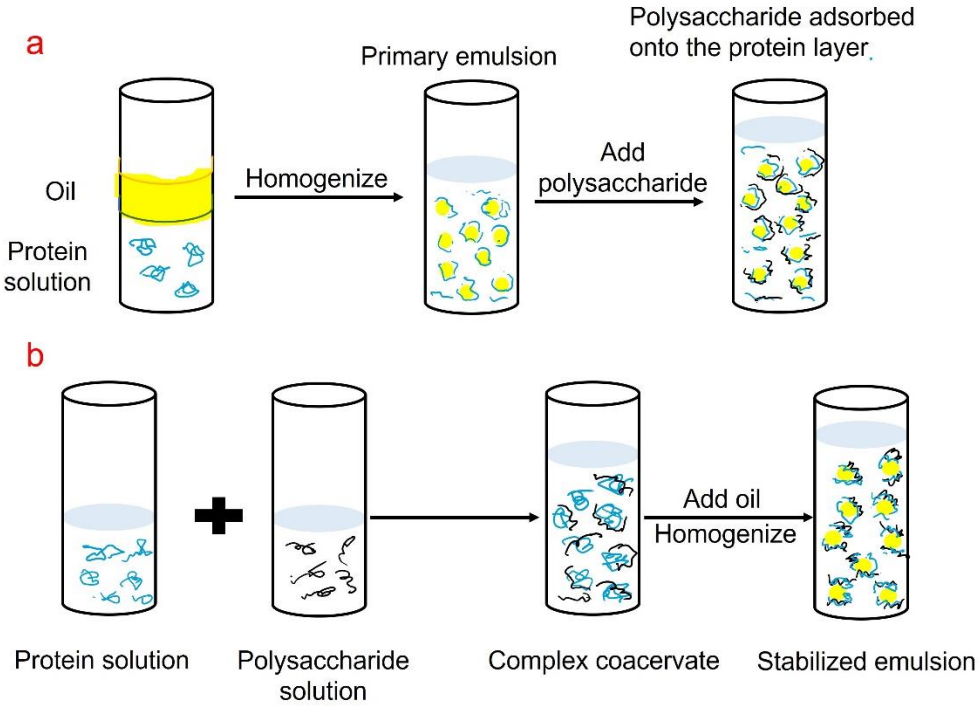

Figure 2.2 Schematic of preparation of bilayer emulsion (a) and coacervate emulsion (b), reproduced based on Evans et al. (2013).

Emulsions can be prepared through varies mechanical devices, such as rotor-stator homogenizers, high-pressure homogenizers, microfluidizers, and ultrasonic homogenizers (McClements & Rao, 2011; Liu et al., 2013a). These devices can generate intensively disruptive forces to break down the oil and water phases into very small droplets, which are widely used to manufacture food emulsions (McClements & Rao, 2011; Liu et al., 2013a). Rotor-stator homogenizers consist of a rotor that could rotate rapidly to generate extreme turbulence, cavitation, and mechanical shearing within the gap between the rotor and the stator (Figure 2.3a-b). The droplets reduce in size as they pass through the gap, and smaller droplets are achieved as the rotor

stator speed increases (Liu et al., 2013a). Small droplet size at around 1 μm can be produced using rotor-stator homogenizer. Monomodal or bimodal droplet size distribution could be resulted depending on the rotor speed. High-pressure homogenizers can produce more uniform droplets with smaller sizes (i.e. less than 1 μm) since it can generate stronger disruptive forces (Maindarkar et al., 2015; Lee et al., 2009). However, rather than preparing emulsion from two phases, high-pressure homogenizers are more efficient in preparing fine emulsions from existing coarse emulsions due to the unique design, where a high shear mixer or a rotor-stator homogenizer is usually used to prepare a coarse emulsion (McClements & Rao, 2011). As shown in Figure 2.3c, the coarse emulsion is pulled in the chamber and passes through the narrow valve, where intensively disruptive forces are created to lead to droplet disruption. The droplet size usually decreases as the number of cycles to pass the homogenizer, or the pressure increases. A third way is to use a microfluidizer for emulsion preparation. Similar to high-pressure homogenizer, the microfluidizer also uses high pressure to facilitate droplet disruption. A coarse emulsion flows into a channel and splits it into two streams, and these two fast-moving streams will then run into each other to generate intense disruptive forces to break down the large droplets into smaller one (Figure 2.3d). Droplet size decreases as homogenization pressure and number of passing cycles increase. Ultrasonic homogenization involves the use of highly intensive ultrasonic waves to create disruptive forces for emulsion preparation from the oil and water phases (Lin & Chen, 2008; McClements & Rao, 2011). The sonicator probe is placed at the oil-water interface during emulsification, and energy is released from the probe due to an alternating electrical voltage to generate intensive vibration leading to droplet disruption (Figure 2.3e). Mixed surfactants-based β-carotene nanoemulsions (Mehmood et al, 2018), olive oil-based O/W nanoemulsions (Mehmood et al, 2017), and the W/O as well as O/W/O emulsions (Lin & Chen, 2008) were successfully prepared using ultrasonic homogenizers.

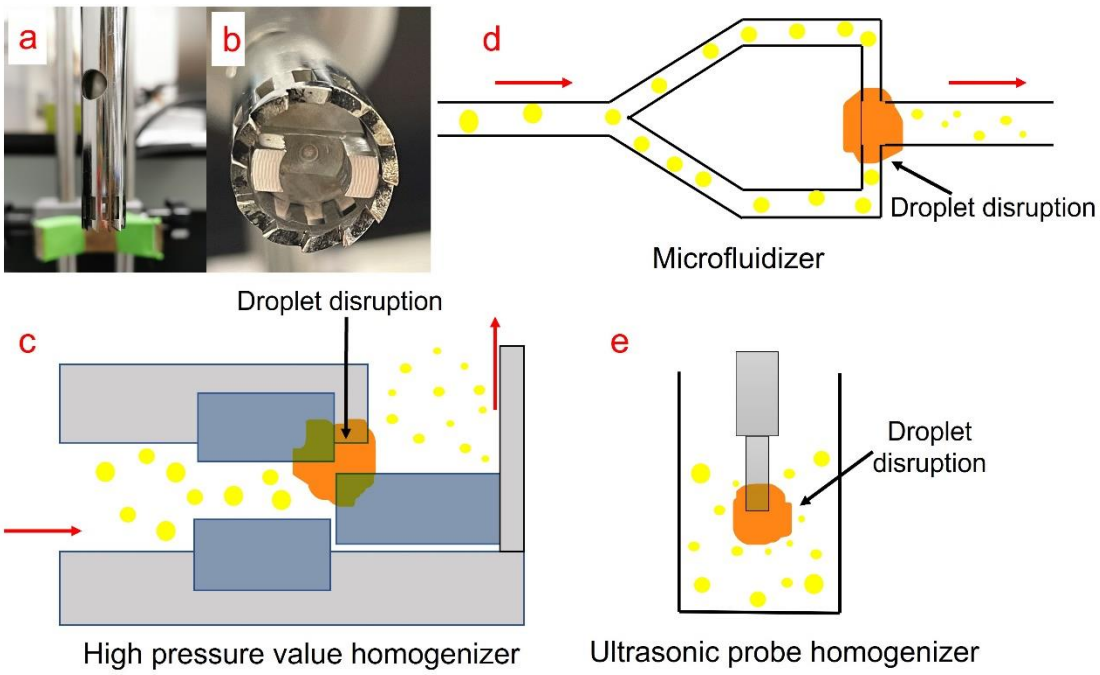

Figure 2.3 Different devices used to prepare a coacervate emulsion: a-b) rotor-stator homogenizer; c) high pressure homogenizer; d) microfluidizer; and e) ultrasonic homogenizer (reproduced based on McClements & Rao, 2011; Liu et al., 2013a).

2.4 Emulsion stability

Emulsion stability is defined as the ability of an emulsion to resist changes over time-period (McClements, 2005). From a thermodynamic aspect, the free energy change in a food emulsion system can be expressed as:

$$\Delta G_{formation} = \gamma \Delta A - T \Delta S_{config} \quad (2.1)$$

where, $\Delta G_{formation}$ is free energy of emulsion formation, γ is interfacial tension, ΔA is change in oil-water interfacial area, T is the absolute temperature, and ΔS_{config} is the change of configurational entropy of droplets in system (Note: this can be ignored in most food emulsions). If an oil droplet is created, ΔA increases, and more $\Delta G_{formation}$ is required. Therefore, a food emulsion is always thermodynamically unstable, and the oil and water phases are trying to separate to minimize free energy of emulsion formation (McClements, 2005).

Destabilization of a food emulsion might occur due to physical and chemical processes. Physical in-stabilization results from gravitational separation, droplet aggregation including flocculation and coagulation, droplet coalescence, Ostwald ripening, partial coalescence, and emulsion inversion, while chemical instability normally refers to hydrolysis and oxidation processes (Lam & Nickerson, 2013; McClements, 2005). The emulsion destabilization mechanisms due to physical instability have been well studied (McClements, 2012; Ercelebi & Ibanoglu, 2007; Capek, 2004; Shi, 2002). The rate at which an emulsion breaks down and the corresponding mechanisms depend on the composition of the emulsion, the microstructure of the surface-active compounds, and its environmental conditions. Ostwald ripening happens when mass transfer of dispersed phase (e.g. flavor oil) occurs from small droplets to large droplets through continuous phase. Partial coalescence normally is involved in a cold process such as ice cream and whipped toppings manufacturing, while phase inversion happens during butter production (McClements, 2005). In a coacervate emulsion, destabilization is mainly driven by gravitational separation, droplet aggregation, and coalescence.

Gravitational separation occurs due to the density difference of the dispersed and continuous phases, in which the lower density phase rises, and the other phase with higher density will settle down under the gravitational force resulting in either creaming (O/W emulsions) or sedimentation (W/O emulsions). This process can influence the texture, mouthfeel, and taste of the emulsion, as well as enhances droplet flocculation and coalescence (McClements, 2005). The rate of creaming or sedimentation can be determined by Stokes' law:

$$V_{stokes} = \frac{g(\rho_d - \rho_c)d^2}{18\eta} \tag{2.2}$$

Where, V_{stokes} is velocity of a droplet, g is gravitational acceleration, ρ_d is the dispersed phase, ρ_c is the continuous phase, d is the diameter of the droplet, and η is the continuous phase's viscosity. Based on the Stokes' law, it will be efficient to slow down the gravitational separation by decreasing the density difference between dispersed and continuous phases (Piorkowski & McClements 2014), reducing the droplet sizes, and increasing the continuous viscosity by adding thickening agents. Gravitational separation can be measured through visual observation (Stone et al., 2013), turbidity measurement (McClements, 2005), backscattered light measurement (McClements, 2005), and accelerated gravitational separation (Primozic et al., 2018).

As the droplets in the emulsions are always moving, collision occurs, and droplets might become aggregated. Droplet aggregation can be reversible (weak interaction) or irreversible (strong interaction). Flocculation is a reversible form of aggregation, where two or more droplets aggregate without losing their individual characteristics and can become separated easily, while coagulation is irreversibly aggregated due to significant interaction between droplets (McClements, 2005). Coalescence occurs when two or more droplets aggregate significantly and eventually merge into a large droplet. Droplet aggregation involves a few physiochemical processes including droplets encounter, film thinning, thin film formation, and thin film rupture. Droplets might come into each other due to Brownian motion, gravity, or applied shear, and a thin film of continuous phase may form between the droplets. This film may continuously become thinning until a crtical point is reached, and then the droplets might move apart, remain in flocculation or coagulation, or move closer to coalesce depending on the colloidal and hydrodynamic interactions of the droplets (Dukhin et al., 2001, 2003; McClements, 2005; Mishchuk, 2005). Figure 2.4 shows the total interaction energy between two droplets. No aggregation (droplets move apart) occurs when there are a small secondary minimum and a high energy barrier. Flocculation takes place under a deep secondary minimum and a high energy barrier. However, if the secondary minimum and energy barrier are both small but with a short-range repulsion, the droplets will move to the primary minimum and become coagulated with the presence of a thin film of continuous phase between the droplets. Film rupture happens when there is no strong short-range repulsion between the droplets, and droplets coalesce into a large droplet.

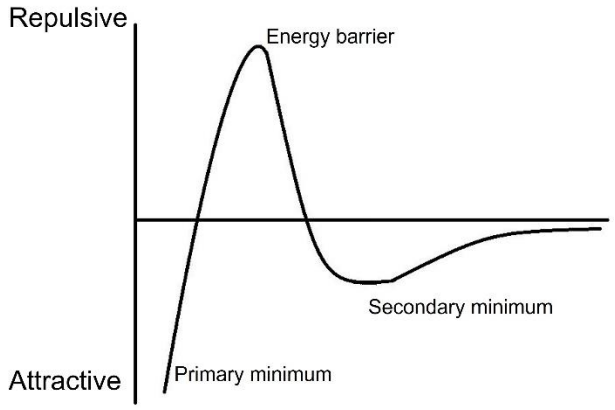

Figure 2.4 The total interaction energy between two droplets in emulsions: a secondary minimum, an energy barrier, a primary minimum, and a strong short-range repulsion (reproduced based on McClements, 2005).

Flocculation can be advantageous especially in an emulsion gel system; however, it is normally undesirable because it accelerates the gravitational separation rate in dilute systems leading to the changes of texture, appearance, and shorter shelf-life of food products. Flocculation can be prevented through controlling the frequency and the efficiency of the collision of the droplets (McClements, 2005). As the droplets move depending mainly on Brownian motion and gravity, collision rates increase as the droplet size decreases or droplet concentration increases. Therefore, it is important to increase the continuous phase viscosity to slow down the droplet movement. Increased emulsion stability with increasing continuous phase viscosity was observed in a hydroxypropylmethyl cellulose-sodium dodecylsulfate stabilized O/W emulsion (Sovilj & Petrovic, 2006). On the other hand, collision efficiency can be controlled by manipulating the colloidal interactions including electrostatic, steric, hydrophobic, and van der Waals interactions (Lam & Nickerson, 2013; McClements, 2005). It is efficient to stabilize emulsions through electrostatic repulsion by using charged surface-active compounds such as proteins and protein-polysaccharide complexes. For example, emulsion stabilized by 2.0% (w/w) pea protein isolate were unstable at pH 5, where the surface charge of pea protein isolate was closed to zero, but emulsion stability remained at 85% after 24 h at pH 3, where the protein's surface charge was at + 32.5 mV (Chang et al., 2015). Steric repulsion could be another efficient way to prevent droplet

flocculation, and protein-polysaccharide complexes would be the great emulsifier due to the relatively large size than small surfactants.

Coalescence is also undesirable since it accelerates creaming or sedimentation in emulsions. Generally, coalescence can be reduced through increasing the viscoelasticity of the interfacial layer or the interfacial layer thickness (Dickinson, 1992). A thicker interfacial layer surrounding the droplet could provide greater stability by preventing the rupture of the film more efficiently (McClements, 2005); thus, coacervate complex due to the relatively large size is a great option to be the emulsifier. Protein-polysaccharide complexes also provide stronger viscoelasticity at the interfacial layer to against mechanical shear. Stronger viscoelastic films were formed at the oil-water interface with the incorporation of the carrageenan (including kappa-, iota-, or lambda- type) in the whey protein isolate compared to using whey protein isolate alone (Lam & Nickerson, 2014). It has also been observed that applying heat treatment could result in stronger protein-polysaccharide interactions, achieving the stronger oil-water interfacial films formation, for example, in a soy protein-soy polysaccharide emulsion system (Yin et al., 2012) and in a beta-lactoglubulin-carboxymethyl cellulose stabilized emulsion system (Chuah et al., 2014).

2.5 Encapsulation by complex coacervation

Encapsulation technology has been widely studied in the literature and used in the pharmaceutical, cosmetic, chemical, printing, and food products (Madene et al., 2006; Heinzen, 2002; Eghbal & Ghoudhary, 2018; Gharsallaoui et al., 2007). Encapsulation is defined as a process, where bioactive particles are entrapped in coating materials, with the particle sizes ranging from less than 1 μm to more than 1000 μm. The wall materials ensure the functionality of the active compounds and can provide their controlled delivery (Aloys et al., 2016; Chang et al., 2016; Gharsallaoui et al., 2007; Eghbal & Ghoudhary, 2018; Madene et al., 2006). Generally, encapsulation can offer many advantages in food industry, such as: a) protection to the core materials against adversely environmental factors including pH, temperature, oxygen, light, and moisture; b) regulating the loss due to evaporation or transfer of the core materials; c) controlling the release (time and environment) of the core materials; d) masking the undesirable smells and tastes of the core active compounds; e) convenient transportation due to the solid-formed particles; and f) dilution to the core compounds when it is needed (Bakry et al., 2016; Narsaiah et al., 2014).

The entrapped compounds are known as the active or core materials, and the coating material is called shell, carrier, or wall material (Tyagi et al., 2011; Madene et al., 2006). For core materials, food compounds such as omega fatty acid oils, volatile essential oils, flavor compounds, enzymes, vitamins, and polyphenols can be encapsulated (Koupantsis et al., 2014; Liu et al., 2013b). Wall materials act to protect the core and should consist of materials that will not react with the core. Ideal wall materials should also have good emulsifying properties to stabilize the microparticles prior to drying, high solubility, desirable controlled release properties, and proper rheological properties (i.e. low viscosity) for drying (Chang et al., 2016; Gharsallaoui et al., 2007). Common wall materials used in food products for encapsulation are carbohydrates such as gum Arabic, maltodextrin and sucrose, and biopolymers such as proteins, polysaccharides, and coacervates complexes (Bakry et al., 2016; Gharsallaoui et al., 2007).

Microencapsulation using the complex coacervation method is one of the most widely used encapsulation techniques for entrapping a lipid core (Bakry et al., 2016). Generally, coacervation encapsulation is a simple, solvent-free, non-thermal, and low-cost process, which is good for the industrial scale (Xiao et al., 2014). More importantly, high encapsulation efficiency (up to 99%) can be achieved (Gouin, 2004; Eghbal & Ghoudhary, 2018). It also provides excellent controlled release properties, heat resistance and stability (Wang et al., 2014; Xiao et al., 2011). Successful microencapsulation made from coacervate complexes were prepared in a milk proteins-carboxymethyl cellulose system (Koupantsis et al., 2014); a sodium alginate-guar gum system (Narsaiah et al., 2012); a soybean protein isolate-gum Arabic system (Xiao et al., 2011); a kappa-carrageenan-chitosan system (Devi & Maji, 2009); and a gelatin-sodium carboxymethyl cellulose system (Devi & Maji, 2011). In terms of production, a coacervate-based emulsion containing the core materials is first prepared, followed by drying, typically spray drying and freeze dry, to yield dried powders (Koupantsis et al., 2014; Chang et al., 2016).

2.5.1 Spray drying

Spray drying is a common drying method widely used in food industry with the lowest cost compared to other drying techniques and easy handled (Gharsallaoui et al., 2007). It involves the atomization of the emulsion into dry powders at elevated temperature. According to Figure 2.5, the emulsion is pumped into the spray dryer and sprayed out from the spraying nozzle from the top. A hot air stream is then blown through the chamber to evaporate the water, leading to the

formation of microcapsules as they fall (Bakry et al., 2016). Usually, spherical shaped microcapsules with embedded oil are obtained. The emulsion should have low viscosity to prevent the formation of large or elongated droplets and air inclusion in the droplets (Drusch, 2006). Feed temperatures (including air-inlet and air-outlet temperatures) should be optimized during the drying process since it influences the drying rate and the final moisture content of the capsules, and the inlet temperature should not be too high to damage the products (Gharsallaoui et al., 2007; Liu et al., 2004). However, spray drying requires wall materials with good solubility only and leads to a lot of energy waste due to heat loss in the drying chamber and final products with lower oxidative stability (Bakry et al., 2016; Gharsallaoui et al., 2007). Palm oil encapsulated microcapsules were prepared by chitosan-xanthan coacervates with spray drying for making yogurt and bread (Rutz et al., 2017).

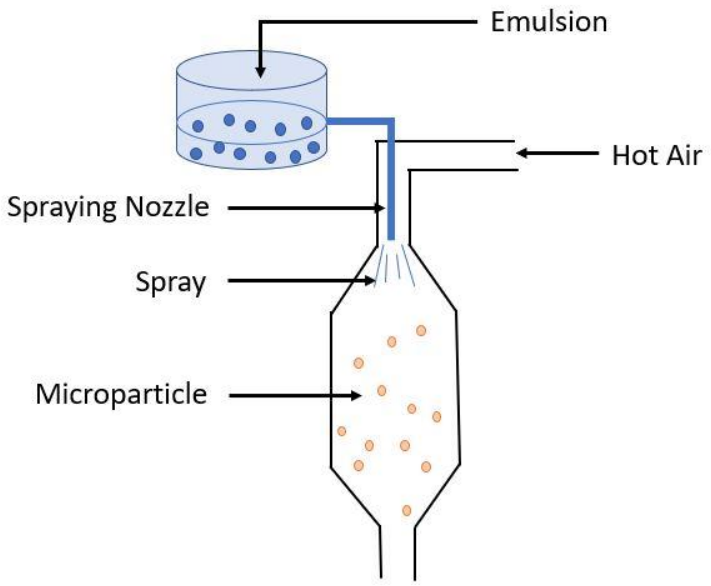

Figure 2.5 Schematic representation of the microencapsulation process by spray-drying.

2.5.2 Freeze drying

Freeze drying is an attractive drying method due to simple process and easy handling. Freeze drying is normally applied for heat sensitive products, and generally longer retention time of the volatile compounds is achieved compared to other methods (Heinzelmann et al., 2000; Heinzelmann et al., 2000; Krokida & Philippopoulos, 2006). During the process, the emulsion sample is frozen between -90 °C to – 40 °C, and the pressure is also reduced by the vacuum pump,

which leads to the sublimation of the frozen water from its solid state to the gas phase (Bakry et al., 2016). Nevertheless, freeze drying requires long processing time, higher cost, and high energy consumption. Beta-pinene containing microcapsules were prepared by complex coacervation of milk proteins and carboxymethylcellulose (CMC), followed by freeze dry (Koupantsis et al., 2014). Beta-carotene containing microcapsules were prepared by chitosan-sodium tripolyphosphate coacervates or chitosan-carboxymethyl cellulose coacervates with freeze drying (Rutz et al., 2016).

Different types of microcapsules can be obtained depending on the core materials, the composition of the wall, or the encapsulation process. As shown in Figure 2.6, there are three main kinds of microcapsules: a mononuclear capsule that contains a core coated with a layer of wall; a polynuclear capsule consisting of continuous wall materials where multiple cores that are dispersed, and a matrix design, where the core is distributed in the wall materials homogeneously (Tyagi et al., 2011). The size and morphology of coacervate capsules are significantly affected by the processing conditions (Lemetter et al., 2009). It was reported that low homogenization rate produced mononuclear microcapsules while high homogenization rate created multinuclear microcapsules (Dong et al., 2011).

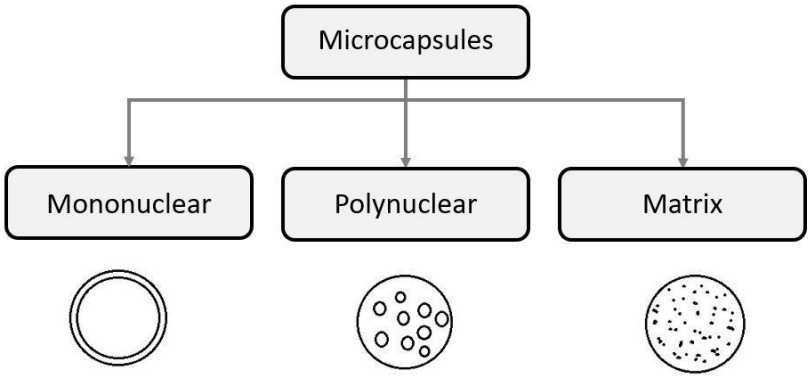

Figure 2.6 Types of microcapsules.

2.6 Microcapsule characterization

The wall materials and processing parameters affect the characteristics of the microcapsules, which are critical to different applications. These microcapsules can be characterized with physical, oxidative stability, and physicochemical properties (Kaushik et al., 2015). Physical properties of the microcapsules include moisture content, water activity, particle

size, wettability, surface oil, encapsulation efficiency, and payload (Kaushik et al., 2015; Koc et al., 2015).

2.6.1 Physical properties

Moisture content and water activity are critical to the shelf-life of the microcapsule. A high moisture content might lead to caking of the capsules during storage, and a high-water activity value might also lead to microbial spoilage in food (Madene et al., 2006). In flavor microencapsulation, off-flavor process is accelerated with high moisture. It was reported that a dry surface of the capsule with water activity lower than 0.90 could act as a semipermeable membrane to retain flavor compounds but permit small water molecules (Reineccius, 2004). A smaller particle size of the microcapsules can provide a smoother mouth feel to the food products. It is generally agreed that microcapsules should be less than 100 μm to avoid the impacts on mouth feel (Kaushik et al., 2015). Smaller particles can be achieved through optimizing emulsion preparation conditions (e.g. pH, wall materials, homogenization device) and drying conditions (i.e. temperature and air flow rate) (Madene et al., 2006). Producing smaller capsules can also increase the encapsulation efficiency and stability since more droplets are created; however, it might result a lower oxidative stability due to the increase of the surface area to the air (Kaushik et al., 2015). Wettability of microcapsules gives information of the ability for microcapsules to dissolve into water. Particle size and wall material composition have strong impact on the wettability. Research showed that the addition of sodium alginate to the lentil protein isolate-maltodextrin system decreased the microcapsules' wettability (Chang et al., 2016).

Encapsulation efficiency (EE) is defined as the percentage of the encapsulated core material to the percentage of core material used in the process, whereas surface oil is the non-encapsulated oil on the surface of the capsules (Kaushik et al., 2015). It is important to ensure a high encapsulation efficiency, in other words, the lower surface oil on the microcapsules, for the surface oil can oxidize rapidly leading to free radical formation and off flavor. Improving encapsulation efficiency can be achieved through the formation of the stronger interfacial film. For example, encapsulation efficiency increased from 75% in a lentil protein isolate-maltodextrin (LPI-MD) based system to 88% in a lentil protein isolate-maltodextrin-sodium alginate (LPI-MD-AL) system (Chang et al., 2016). However, EE value decreased to 42% with the addition of lecithin due to the increased viscosity of the system used for spray drying. It is ideal for surface oil lower

than 2% (w/w) in food industry applications. Payload refers to the percentage of the oil or active compounds per gram of the capsules, and a higher payload should be obtained from an economic scale (Kaushik et al., 2015).

2.6.2 Oxidative stability

Oxidative rancidity of lipids is a primary cause of deterioration of the food products such as colour change and loss of flavour and odour. To protect the omega fatty acids-rich oils against oxidation is the primary purpose of encapsulation; therefore, wall materials should act as an oxygen barrier to prevent the transfer of oxygen. Oxidative rancidity involves three important steps: initiation, propagation, and termination. In initiation, two free radicals are produced due to the breakdown the peroxide resulting from the reaction between singlet state oxygen (i.e. at excited state) and unsaturated site in a lipid molecule. The free radicals then undergo several types of reactions during propagation, such as abstraction, addition to a site of unsaturation, or decomposition. Aldehydes and ketones that are volatile might form during the process leading to off flavours and aromas. Also, rearrangement of the site of unsaturation might result from the addition of free radicals, which causes the formation of conjugated double bonds or trans fat formation. Termination can occur when two free radicals react with one another, or when a free radical react with an antioxidant to from a stable radical compound. Oxidative stability of oil in microcapsules is determined through measuring the oxidative products formed (e.g. conjugated dienes, aldehydes, trans fats, and peroxides) under a set of temperature and relative humidity (Kaushik et al., 2015). Different composition of wall materials can provide different protective effects to the core materials. According to Chang and co-workers, (2016), the oxidative stability of the canola oil increased significantly in lentil protein isolate-maltodextrin-sodium alginate (LPI-MD-AL) capsules compared to the lentil protein isolate-maltodextrin (LPI-MD) capsules.

2.6.3 Oil release properties

The main purpose for encapsulation in foods includes improving the effective use of the active compounds such as omega fatty acid oils and to reduce the required dose (Gouin, 2004). Controlled release refers to a process where one or more active agents or ingredients are available at a desired site and time and at a specific rate (Pothakamury & Barbosa-Canovas, 1995). Developing an effective controlled release system has become one of the main challenges in food

products to achieve a high bioavailability during consumption (Eghbal & Ghoudhary, 2018). The release characteristics of the core materials can be affected by the wall materials (e.g. compositions, viscosity, and solubility), the physical properties (e.g. particle size and wettability), types and morphology of the capsules (da Silva et al., 2014). For instance, the bioavailability of a core material should be higher in a protein-based capsule than a cellulose-based capsule since proteins have a higher digestibility than cellulose (Kaushik et al., 2015). Core materials will be released easily from mononuclear capsules than polynuclear capsules, and the more complex of the wall structure might lead to a slower release. Release might occur under changes of environmental conditions such as heating, pH, or shearing (Nesterenko et al., 2013). Studies have been conducted on the release properties of coacervate microcapsules, for example, chitosan-xanthan coacervate microcapsules were used to encapsulate palm oil for yogurt and bread (Rutz et al., 2017).

2.7 Choice of materials

2.7.1 Wall materials

Lentil proteins, like other pulse proteins are gaining tremendous interests by the food industry since they are non-soy, gluten-free and non-animal based. Pulse proteins tend to have excellent functional attributes, which include water/fat binding, emulsification, foaming, solubility, and gelation depending on how they are prepared (Nunes et al., 2006; Boye et al., 2010; Liang & Tang, 2014; Graca et al., 2016). Lentils are an economically important crop to Saskatchewan and Canada, and they are rich in protein (28-31%, dry basis, d.b.), carbohydrates (56-63%, d.b.), crude fibre (5-7%), along with many vitamins and minerals (Bhatty, 1988; EL-Adawt et al., 2003). They are also low in fat (about 1%, d.b.) (Bhatty, 1988; EL-Adawt et al., 2003). Protein isolates can be prepared from lentils through alkaline extraction followed by isoelectric precipitation or ultrafiltration, followed by drying (Can Karaca et al., 2011; Aryee & Nickerson, 2012). Isolates tend to be >85% (d.b.) in protein content (Can Karaca et al., 2011). Lentil proteins are dominated by globulin-type [salt soluble; 50-65% of the total protein] and albumin-type [water soluble; 10-25% of the total proteins] proteins (Gueguen & Barbot, 1988; Boye et al., 2010; Jarpa-Parra, 2018) with small amounts of prolamins and glutelins (Stone et al., 2015). Globulin can be fractionated into two major proteins, a 11S (S is a Svedberg unit) legumin [hexameric protein; molecular mass of 350-400 kDa; each subunit (60 kDa) is comprised of a α-chain (40 kDa) and β-chain (20 kDa) linked by a disulfide bond] and a 7S vicilin [trimeric protein; molecular mass of 150 kDa, with

each subunit (50 kDa) being held together by non-covalent forces] (Chakraborty et al., 1979; Liu et al., 2009; Boye et al., 2010; Stone et al., 2015; Graca et al., 2016). A third minor globulin protein is the 7S convicilin protein which has a molecular mass of ~290 kDa) (Croy, 1980). Albumin proteins are comprised of enzymatic proteins, protease inhibitors, amylase inhibitors, and lectins with molecular weight ranging from 6-100 kDa (Park et al., 2010; Boye et al., 2010; Dziuba et al., 2014).

Carboxymethyl cellulose (CMC) is a polysaccharide with a wide range of industrial application in foods (e.g. ice creams, puddings, pie fillings), drugs, paper, and detergents etc. that is derived from cellulose (Biswal & Singh, 2004). Cellulose is the major structural component of the protective cell wall of the higher plants (O'Sullivan, 1997). Cellulose, as a homopolysaccharide, is made up of linear chains of $(1 \rightarrow 4)$ - β –D-glucopyranosel units (Janjarasskul & Krochta, 2010). CMC (as shown in Figure 2.7) is obtained by the reaction between alkali cellulose and sodium monochloroacetate (Ducel et al., 2004; Biswal & Singh, 2004). The molecular weight of the CMC, substitution degree (e.g. the number of hydroxyl groups substituted on per anhydroglucose unit (Ducel et al., 2004)), and the distribution of the substituents greatly influence the properties of the CMC such as solubility and permeability (Kamide et al., 1985; Biswal & Singh, 2004; Janjarasskul & Krochta, 2010). Theoretically, the maximum substitution degree is three, and degree of substitute affects the solubility significantly (Hader et al., 1952). Normally, cellulose is insoluble in aqueous solution due to the highly crystalline structure with the tightly packed polymer chains under the align of hydroxyl groups (Janjarasskul & Krochta, 2010). The water solubility can be improved through the etherification process to produce cellulosic derivatives. Under the processing, the bulkier carboxymethyl groups are substituted on the hydroxyl groups on the glycosyl units, and because of this substitution process intramolecular hydrogen bonds are disrupted, which increases the separation of the polymer chains in crystalline structure resulting in improved water solubility (Janjarasskul & Krochta, 2010). Generally, CMC is soluble in both hot and cold water. Also, the substitution degree has an impact on thickening property, emulsion stability, suspending, acid resistance as well as salt tolerance (Hader et al., 1952). CMC forms a shear-thinning dispersion, and the viscosity of the solution increases along with the chain length and the substitution degree (Ducel et al., 2004). Furthermore, CMC has desirable film-forming properties (Janjarasskul & Krochta, 2010) and forms good complex coacervates with proteins (e.g. gelatin-sodium carboxymethyl cellulose coacervate (Devi & Maji,

2011; Duhoranimana et al., 2018), whey-CMC complex (Girard et al., 2002), and potato protein-CMC complex (Vikelouda & Kiosseoglou, 2004).

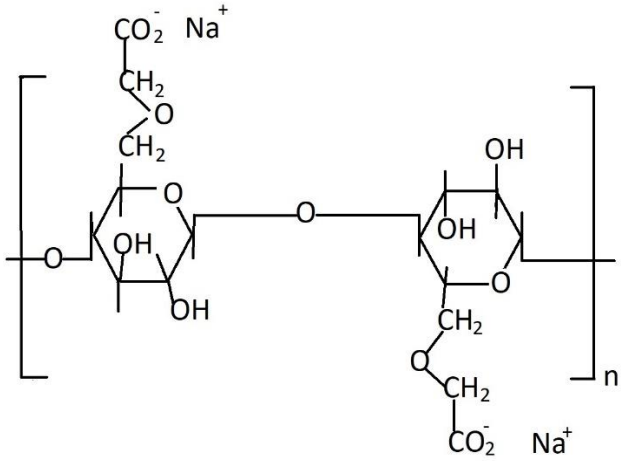

Figure 2.7 Shows structure of carboxymethyl cellulose (CMC) with substitution degree of 1 (modified based on Biswal & Singh, 2004).

Gum Arabic (GA) is an edible, dried, gummy exudate from the stems and branches of *Acacia sene* and *A. seyal* (Ali et al., 2009). GA is widely applied in food applications (e.g. soft drinks, marshmallows, and gummy candies), cosmetics, and pharmaceutical industries (Verbeken et al., 2003; Ali et al., 2009). Gum Arabic (GA) is highly water-soluble, and it is an excellent emulsifying agent. In contrast to CMC, GA is a branched carboxylated anionic arabinogalactan polysaccharide; it has a highly heterogeneous structure with three main fractions. About 89% of the GA is made up of a highly branched acidic polysaccharide (i.e. β-(1-3) galactopyranose (galactan) polysaccharide backbone highly branched with β-(1-6) galactopyranose residues terminating in arabinose and glucuronic acid and/or 4-O-methyl glucuronic acid units). About 10% of the gum is comprised of an arabinogalactan–protein complex, in which a polypeptide backbone and arabinogalactan chains are linked covalently (Aryee & Nickerson, 2012; Dror et al., 2006; Liu et al., 2009). And a third fraction (about 1%) is a low molecular weight glycoprotein. According to Idris and co-workers (1998), GA consists of galatose (39-42%), arabinose (24-27%), rhamnose (12-16%), glucuronic acid (15-16%), protein (1.5-2.6%), and moisture. Nevertheless, the chemical composition of GA varies from the sources, age of the trees, and environmental conditions (Verbeken et al., 2003). GA is primarily non-digestible to humans or animals; however, it can be

fermented in the large intestine by microorganisms to short-chain fatty acids, particularly propionic acid (Kishimoto et al., 2006).

Alginate (AL) comes from the intracellular matrix of marine algae (brown seaweeds) and is non-toxic, biodegradable and biocompatible (Mi, Sung, & Shyu, 2002). Alginate is a linear polysaccharide that is composed of segments of β-(1-4)-linked D-mannuronic acid (M block) and α-(1-4)-linked L-guluronic acid (G block) with M/G ratio varying from 0.5 to 2.0 (Figure 2.8) (Harnsilawat et al., 2006; Klassenet al., 2011; Yang et al., 2011). Free hydroxyl and carboxyl groups are distributed along the polymer chain backbone leading to its' anionic nature. Alginate can form gel in the presence of divalent cations (e.g. Ca^{2+}), in which two polysaccharide chains are linked together though the cations with the carboxyl groups (i.e. $-COO^{-}-Ca^{2+}-COO^{-}$) in an 'egg-box' liked junction zone. AL can also form gel at pH below the pKa of the uronic acid residues, and this acidic gel is stabilized by intermolecular hydrogen bonds (Bu et al., 2004).

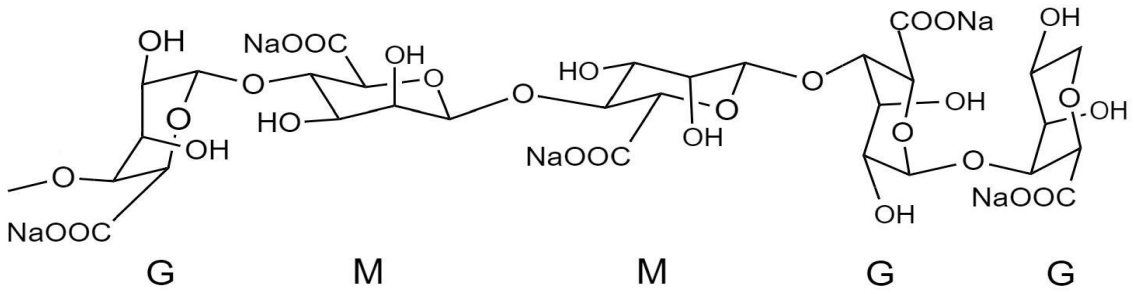

Figure 2.8 Structure of alginate with M block and G block (modified based on Yang et al., 2011).

Carrageenan is also extracted from marine algae (red seaweeds) from the class *Rhodophyceae* (Necas & Bartosikova, 2013). Carrageenan is commonly used in food products due to their excellent gelling, thickening, texture improving, and emulsifying properties and is also applied to the control-released system due to the high encapsulation efficiency (Li et al., 2014; Van de Velde et al. 2002). Carrageenan is a sulfated polygalactan containing 15 to 40% of ester-sulfate with an average molecular mass above 100 kDa. Carrageenan can be classified into three types based on the number of sulphate groups per disaccharide unit which are kappa-1 (κ-), iota-2 (ι-), and lambda-3 (λ-) (Necas & Bartosikova, 2013). Lower solubility temperature and weaker gel strength are observed as the content of ester sulfate increases from kappa, iota to lambda type, respectively (Barbeyron et al. 2000). ι-Carrageenan (ι-C) contains a disaccharide repeating unit of

(1-3)-β-D-galactopyranose-4-sulphate-(1-4)-3,6-anhydro-α-D-galactose-2-sulphate (de Jong & de Velde, 2007; Lam & Nickerson, 2014). Similar to alginate, carrageenan is linear polysaccharides and can form gel in the present of cations.

Maltodextrin (MD) is an ingredient obtained from the enzymatic (e.g. α-amylase) or acid hydrolysis of starch, followed by drying (Rezende, 2018). Maltodextrin is the most common starch hydrolysate used in the food applications such as soups, sauces, baby food, and fat replacer due to the low costs, low bulk density, mild flavor, and excellent mouthfeel (Rezende, 2018; Suryabhan et al., 2019; Carneiro et al., 2013). Maltodextrin is also a common secondary wall material for microencapsulation due to the excellent functional properties such as high solubility, low viscosity at higher concentration, and low affinity to hydrophobic compounds (Suryabhan et al., 2019; Carneiro et al., 2013; Kyriakoudi & Tsimidou, 2018). Stable microcapsules coated with lentil protein isolate or lentil protein isolate-alginate (primary wall materials) with maltodextrin (secondary wall material) were successfully prepared by Chang and co-workers (2016). Maltodextrin has dextrose equivalent (DE) value less than 20, and a larger DE value means a higher degree of hydrolysis of starch (Qi & Tester, 2018). Generally, Maltodextrins with larger DE value are more susceptible to browning reaction and provide more sweetness, but they can form microcapsules with lower oxygen permeability (Wang et al., 2015). The DE value of maltodextrin could influence the surface oil content during encapsulation. Can Karaca and co-authors (2013) found that microcapsules prepared with MD with a smaller DE value (e.g. DE of 9) had lower surface oil content compared with those prepared with MD of DE 18, which could be attributed to a more hydrophilic microcapsule surface due to the orientation of higher molecular weight MD towards the entrapped oil (i.e. lower DE value) resulting in lower encapsulation efficiency.

2.7.2 Core materials

Canola oil is one of the most important edible oils and occupies the third largest production for vegetable oil in the world, with Canada as the largest producer (Lin et al., 2013). The canola plant was originally selected from rapeseed cultivars (high-erucic acid crops) through traditional plant breeding to achieve low levels of erucic acid (<2%) and glucosinolates (<30 umol/g) for safety consumption (Velasco et al., 2008). Canola oil can provide health benefits against cardiovascular disease, type 2 diabetes, and osteoporosis risk through regulating plasma lipids and

low-density lipoprotein, which can be attributed to the high content of monounsaturated fatty acids and polyunsaturated fatty acids, including 61% oleic acid, 21% linoleic acid, and 11% α-linolenic acid (Johnson et al., 2007; Rajaram, 2014). Only about 7% of saturated fatty acids is found in canola oil; therefore, canola oil is susceptible to oil rancidity due to oxidation, and microencapsulation technology can provide proper protection.

Flaxseed (*Linum usitatissimum* L.) is a commercial oilseed that contains a rich source of α-linolenic acid (ALA; ~50%), oleic acid (~20%), linoleic acid (~15%), vitamin E, and vitamin A (Mohanan et al., 2018; Rubilar et al., 2012; Shim et al., 2015). As an essential fatty acid in human, ALA provides health benefits such as developing the brain and nervous system in infants, preventing cardiovascular diseases and immune response disorders, reduction of cholesterol levels; also, ALA acts as the precursor of the for eicosapentaenoic acid (EPA) and docosahexaenoic acid (DHA) (Menin et al., 2018). However, polyunsaturated fatty acids are highly susceptible to oxidation in the presence of light, heat, or reactive oxygen species leading to oil rancidity, loss of nutritional value and flavor, as well as texture and color changes (Mohanan et al., 2018). Microencapsulation would be an effective method to enhance the oxidative stability of flaxseed oil; studies of encapsulation using protein-based materials has been conducted on Avramenko et al. (2016), Can Karaca et al. (2013), and Carneiro et al. (2013).

3. EFFECT OF MOLECULAR MASS AND DEGREE OF SUBSTITUTION OF CARBOXYMETHYL CELLULOSE ON THE FORMATION ELECTROSTATIC COMPLEXES WITH LENTIL PROTEIN ISOLATE[1]

3.1 Abstract

The electrostatic interaction between lentil protein isolate (LPI) and carboxymethyl cellulose (CMC) of different molar mass (MM; 90 and 250 kDa) and degree of substitution (DS; 0.7, 0.9 and 1.2) was examined during a turbidimetric pH acid-titration over a pH (8.0-1.5) and mixing ratio (LPI: CMC; 1:1-10:1) rang. For LPI-CMC (0.7 DS, 250 kDa) at a 1:1 ratio, critical structure forming events associated with the formation of soluble (pH_c) and insoluble complexes ($pH_{\phi 1}$), maximum coacervation (pH_{opt}) and the dissolution of complexes ($pH_{\phi 2}$) occurred at pH values of 6.8, 2.6, 2.1 and 1.7, respectively. As the mixing ratio increased, pH_c and $pH_{\phi 2}$ remained unchanged; however, $pH_{\phi 1}$ and pH_{opt} shifted to higher pH values until plateauing at a 4:1 mixing ratio. MM and DS had no significant effect on critical pH values but did have an impact on the size and number of complexes formed. The maximum optical density at pH_{opt} was found to decrease from 0.495 to 0.406 as the DS increased from 0.7 to 1.2 on the CMC (constant at 250 kDa), suggesting that complexes were likely smaller as they scattered less light. As the MM of CMC decreased from 250 to 90 kDa (at 0.7 DS), maximum optical density increased from 0.495 to 0.527, respectively. Confocal laser scanning microscopy preformed at pH_{opt} showed an

[1] Wang, Y., Pillai, P. K., & Nickerson, M. T. (2019). Effect of molecular mass and degree of substitution of carboxymethyl cellulose on the formation electrostatic complexes with lentil protein isolate. *Food Research International*, *126*, 108652. doi: 10.1016/j.foodres.2019.108652 (*Reproduced with permission*). Y. Wang contributed to the experimental design, data collection and analysis, and drafting of the manuscript. P. Pillai aided in the isothermal titration calorimetry experiments, whereas M. Nickerson was the primary supervisor, contributed to the experimental design and was corresponding author for the manuscript.

increasing number of aggregates as the DS or MM of CMC decreased. From isothermal titration calorimetry (ITC), larger enthalpy values in LPI-CMC with increased DS and MM were observed.

3.2 Introduction

Applications involving protein-polysaccharide interactions are becoming more of interest for protein purification processes, in the design of controlled delivery systems, and in the development of edible films (Schmitt et al., 1998; Ye, 2008). Complex coacervation (also known as associative phase separation) occurs between proteins and polysaccharides of opposing net charge, where the electrostatic attraction between biopolymers induces phase separation into a biopolymer (protein + polysaccharide)- and solvent-rich phase (de Kruif et al., 2004; Ye, 2008). During an acid pH titration, the first detectable change in turbidity within the biopolymer mixture due to protein-polysaccharide interactions results in the formation of a soluble complex (denoted as pH_c) (Schmitt et al., 1998; Tolstoguzov, 1997; Turgeon & Laneuville, 2009; Ye, 2008). Protein-polysaccharide interactions become greater with further acidification leading to the formation of insoluble complexes via nucleation and growth kinetics at $pH_{\phi 1}$ (Schmitt et al., 1998; Stone et al., 2014; Turgeon & Laneuville, 2009). Maximum turbidity is reached at a pH denoted by pH_{opt}, where an electrical neutrality point is reached (Kayitmazer, 2017; Li et al., 1994; Schmitt et al., 1998; Stone et al., 2014). Further protonation results in the complete dissolution of coacervates at a pH corresponding to near the pK_a of reactive sites on the polysaccharide (denoted as $pH_{\phi 2}$) (Klemmer et al., 2012; Stone et al., 2014). Depending on the charge density and the functional groups, a soluble coacervate or an insoluble precipitate-type structure may form (de Kruif et al., 2004; Kayitmazer, 2017; Schmitt et al., 1998; Singh et al., 2007).

Apart from the electrostatic attractive forces, non-Coulombic interactions (hydrophobic interactions, hydrogen bonding, and steric interactions) also play a role in the formation and stability of complex structures (de Kruif et al., 2004; Klemmer et al., 2012; Schmitt et al., 1998; Ye, 2008). From a thermodynamics perspective, the formation of protein-polysaccharide complexes becomes possible and occurs spontaneously when the change in total Gibbs free energy within the system is negative (i.e., $\Delta G = \Delta H - T\Delta S < 0$) (Schmitt et al., 1998; Turgeon & Laneuville, 2009). Studies conducted on systems of ovalbumin-CMC (Xiong et al., 2017), sodium caseinate-low methoxyl pectin (Wang et al., 2019), β-lactoglobulin-κ-carrageenan (Hosseini et al., 2013) and β-lactoglobulin-pectin (Girard et al., 2003; Xu, Melton et al., 2015) suggest that

enthalpy played an important role in complex formation especially with biopolymers of different charge density or molar mass.

Selection of the protein and polysaccharide within the mixture is critical as coacervation is greatly influence by the characteristics of biopolymers itself, such as charge density, size and conformation. Lentil protein for instance is an attractive protein alternative to those from animal sources due to their lower cost, abundance and nutritional value (high in protein, fibre and low in fat) (Campos-Vega et al., 2010; Jarpa-Parra, 2018). Lentil proteins also display excellent functionality such as emulsifying, water binding, fat binding, foamin, and gelling (Aydemir & Yemenicioglu, 2013; Boye et al., 2010). Lentil proteins are dominated by globulin-type [salt soluble; 50-65% of the total protein] and albumin-type [water soluble; 10-25% of the total proteins] proteins (Boye et al., 2010; Gueguen & Barbot, 1988; Jarpa-Parra, 2018) with small amounts of prolamins and glutelins (Stone et al., 2015a). Globulin can be fractionated into two major proteins, a 11S (S is a Svedberg unit) legumin [hexameric protein; molecular mass of 350-400 kDa; each subunit (60 kDa) is comprised of a α-chain (40 kDa) and β-chain (20 kDa) linked by a disulfide bond] and a 7S vicilin [trimeric protein; molecular mass of 150 kDa, with each subunit (50 kDa) being held together by non-covalent forces] (Boye et al., 2010; Chakraborty et al., 1979; Graça et al., 2016; Liu et al., 2009; Stone et al., 2015a; Stone et al., 2015b). A third minor globulin protein is the 7S convicilin protein which has a molecular mass of ~290 kDa) (Croy et al., 1980). Albumin proteins are comprised of enzymatic proteins, protease inhibitors, amylase inhibitors, and lectins with molecular weight ranging from 6-100 kDa (Boye et al., 2010; Dziuba et al., 2014; Park et al., 2010).

Carboxymethyl cellulose (CMC) is a polysaccharide with a wide range of applications in foods (e.g. ice creams, puddings, pie fillings), drugs, paper and detergents (Biswal & Singh, 2004). Cellulose is the major structural component of the cell wall of the higher plants (O'Sullivan, 1997), and is as a homo-polysaccharide made up of linear chains of $(1 \rightarrow 4)$- β –D-glucopyranosyl units (Janjarasskul & Krochta, 2010). CMC is obtained by the reaction between alkali cellulose and sodium monochloroacetate (Biswal & Singh, 2004; Ducel et al., 2004). The molecular mass of the CMC, substitution degree (e.g. the number of hydroxyl groups substituted on per anhydroglucose unit, Ducel et al., 2004), and the distribution of the substituents greatly influence the properties of the CMC, such as solubility and permeability (Biswal & Singh, 2004; Janjarasskul & Krochta, 2010; Kamide et al., 1985).

This study aims to investigate the complexation behaviour of LPI and CMC with different degrees of substitution and molecular mass as a function of pH and biopolymer mixing ratio through turbidimetric and ITC measurements. The different thermodynamic parameters [binding stoichiometry (q), affinity constant (K), enthalpy (ΔH), entropy (ΔS) contributions and Gibbs free energy change (ΔG)] of the LPI-CMC complexation were investigated with respect to the DS and MM of CMC. Obtaining a greater understanding of LPI-CMC interaction behaviours might provide more information on the development of new functional blended ingredients for the food industry.

3.3 MATERIALS AND METHODS

3.3.1 Materials

Lentil protein isolate was given to the project by KeyLeaf Corp. (Saskatoon, SK). CMC of differing levels of substitution (0.7, 0.9 and 1.2) at a constant molecular mass (250 kDa), and CMC of differing molecular mass (90 and 250 kDa) with a constant degree of substitution (0.7) were purchased from Sigma-Aldrich Co (Oakville, ON, Canada). All other chemicals were purchased through Sigma-Aldrich Co.

3.3.2 Proximate analysis

Moisture, ash, fat, and protein (%N×6.25) were measured according to the Association of Official Analytical Chemists (AOAC) methods 925.10, 923.03, 920.85 and 984.13A, respectively (AOAC, 2003) (reported on a dry weight basis). Carbohydrate content was determined based on percent differential from 100%. Measurements were made in triplicate and reported as the mean ± one standard deviation (n=3). Mineral measurements were conducted by KeyLeaf Corp. (Saskatoon, SK).

3.3.3 Turbidimetric measurements

Critical pH values (pHc, pHϕ1, pHopt and pHϕ2) within LPI-CMC mixtures were examined using a turbidimetric pH acid titration over a pH (8.0–1.5) and mixing ratio (1:1, 2:1, 4:1, 6:1, 8:1 and 10:1 of LPI: CMC on a LPI weight by weight basis) range, at a constant biopolymer concentration of 0.05% (w/w). Biopolymer solutions were prepared by dissolving each powder in water under constant mechanical stirring (500 rpm) for 2 h at room temperature (21–

23 °C) and then overnight at 4 °C to help facilitate protein solubility. The pH of the solutions was 6.5. The LPI and CMC solutions were then mixed and allowed to stir for 30 min, and the pH was corrected to pH 9.0 prior to measurements.

Turbidimetric acid pH titrations of biopolymer mixtures were carried out according to Liu et al. (2009) to determine the pH values associated with structure forming events (pH_c, $pH_{\phi 1}$, pH_{opt} and $pH_{\phi 2}$) at 600nm using an ultraviolet-visible spectrophotometer (Genesys 10 UV/Vis, Thermo Scientific, Waltham, MA, USA). Measurements were made using triplicate stock solutions. The critical pH values were reported as the mean ± one standard deviation (n = 3). Controls were run using 0.05% (w/w) LPI and CMC solutions.

3.3.4 Surface charge (zeta potential)

The zeta potential (ζ) for homogenous and mixed LPI and CMC solutions was determined using a Zetasizer Nano-ZS90 (Malvern Instruments, Westborough, MA) according to Liu et al. (2009). In brief, homogenous and mixed samples were prepared at total biopolymer concentration of 0.05%. Solutions were pH adjusted using 0.25M HCl every 0.5 units between the pH range of 8.0 and 1.5. Electrophoretic mobility (velocity of a particle within an electric field) is related to the zeta potential (ζ), which gives the information of surface charge density, using the Henry equation (Eq. 3.1).

$$U_E = \frac{2\varepsilon \times \xi \times f(\kappa\alpha)}{3\eta} \tag{3.1}$$

where, η donates the dispersion viscosity, ε is the permittivity, $f(\kappa\alpha)$ is a function related to the ratio of particle radius (α) and κ is the Debye length (Liu et al., 2009). Using the Smoluchowski approximation, $f(\kappa\alpha)$ is equal to 1.5. All measurements were made at room temperature (21–23 °C) in triplicate.

3.3.5 Confocal laser scanning microscopy

Confocal laser scanning microscopy (CLSM) was used to image mixtures of 4:1 LPI-CMC solutions at pH_{opt} as a function of the degrees of substitution and molecular mass of the CMC polysaccharides according to Liu et al. (2010) at room temperature. Solutions were prepared in a similar manner as the turbidimetric analysis, with the addition of rhodamine B (0.01%, w/w), which has a maximum excitation and emission wavelength of 543 and 567 nm, respectively. The

solution was placed on a cover slide and imaged using a Nikon Eclipse LV100 CLSM microscope (Nikon, Tokyo, Japan). All mixtures were prepared in triplicate and 4 images were taken per slide. A representative image from each slide was shown.

3.3.6 Isothermal titration calorimetry

Isothermal titration calorimetry was conducted for LPI and CMC as a function of the degrees of substitution and molecular mass of the CMC polysaccharides at pH 3 using ITC model CSC 4200 (Calorimetry Science Corportation, Lindon, UT, USA) at room temperature (25℃). LPI (5%, w/w) and 0.1% (w/w) CMC solutions were prepared in a similar manner as previous (2 h at room temperature and then overnight at 4 °C) except dissolving powders in 5 mM citric buffer (pH 3). Solutions were then warmed at room temperature and stirred for 30 min, and the LPI solution was centrifuged at 4,032 x g for 2 min. The supernatant was collected, and solubility measured (53.9 ± 0.7%) to determine its concentration. Then, 250 µL of the soluble LPI (0.1055 mM) and 1420 µL CMC (0.004 mM) solution were placed in syringe and reaction cell, respectively. The titration was performed with 25 successive 10 µL injection of LPI solution, with an equilibration time of 200 s between the injections and at 300 rpm stirring speed. The dilution heat of LPI solution was measured by their titration with citric buffer at pH 3 and subtracted from the raw data. Measurements were carried out in duplicates. Thermodynamic parameters such as binding stoichiometry (q), binding constant (K) and enthalpy (H) were calculated by curve fitting of the binding isotherms with Bind Work software using the independent binding model. The entropy and Gibbs free energy was calculated using the Eq. (3.2) and (3.3), respectively.

$$\Delta G = -RT \ln K \tag{3.2}$$

$$\Delta G = \Delta H - T\Delta S \tag{3.3}$$

A SDS-page gel and densometry was performed on the LPI to show approximately 50% of the proteins were legumin (MM 60 kDa x 6 subunits = 360 kDa) and 50% were vicilin (MM 50 kDa x 3 subunits = 150 kDa) (data not shown); therefore, an average MM of 255 kDa was assumed and used in ITC calculations of protein molar concentration.

3.3.7 Statistics

A one-way analysis of variance with a Scheffe post-hoc test was preformed to access differences for each critical pH as a function of mixing ratio, degree of substitution, and molar mass. All statistics were preformed using SPSS software (IBM, Armonk, NY, USA).

3.4 RESULTS AND DISCUSSION

3.4.1 Composition

Proximate composition of the LPI material was found to be comprised of 80.6% (dry weight basis, d.b.) protein, 0.8% (d.b.) lipid, 13.0% (d.b.) carbohydrate, and 5.6% (d.b.) ash. In contrast, all CMC polymers had carbohydrate and ash contents ranging between 80.4-81.4% (d.b.) and 18.6-19.6% (d.b.), respectively except for CMC polymers with a MM of 250 kDa and DS of 1.2% which has a carbohydrate and ash content of 75.0% (d.b.) and 25% (d.b.), respectively. Protein and lipid contents were considered as negligible in all CMC polysaccharides. In terms of major minerals, the LPI contained 1.80% Na^+ and 0.67% K^+ with minor amounts of Ca^{2+} and Mg^{2+}, whereas all CMC polymers were high in Na^+ (8.10-10.00%). Further proximate data can be found in the Appendix, Table A1.

3.4.2 Formation of electrostatic complexes as a function of LPI: CMC mixing ratio

Changes to the optical density (OD) of the solution during an acid pH titration for LPI alone, and for LPI-CMC blends involving only the CMC with 0.7 DS and a MM of 250 kDa, at differing mixing ratios is given in Figure 3.1A. The optical density of CMC biopolymers was not plotted as they were negligible. For LPI alone, a bell-shaped OD curve as a function of pH was observed, ranging between pH 6.9 and 2.4, with a maximum OD of 0.476 occurring at pH 4.4 near the protein's isoelectric point (pH 4.6; Figure 3.2) where it carries no net charge (zeta potential = 0 mV). However, OD remained relatively flat at the maximum over the pH range of 3.6-4.8 due to reduced solubility caused by the increased protein-protein interactions. In general, as the amount of CMC increases within the mixing ratio, the scattering curves shifted to lower pH values, and the bell-shaped curve changed to have a longer rise in OD as pH decreased prior to the maximum, a narrower peak region and, a lower maximum OD (Figure 3.1A). In Figure 3.1A, it was observed that some LPI-CMC systems (at 4:1, 8:1, 10:1 ratios) had larger OD values than homo LPI system at pH 5.5-7.5. At this pH range, low OD values should have been observed since the systems were

at thermodynamically incompatible states due to intermolecular electrostatic repulsions between net negatively charged proteins and CMCs. However, it is hypothesized that a stronger electrostatic repulsion could occur between the highly negative charged CMC polysaccharides, and that led to a depletion effect in which an effective attraction between the protein molecules occurred (Liu et al., 2013) causing increasing LPI-LPI aggregations. Therefore, an increase in OD was observed, and this increase became more intensive overall as LPI:CMC ratio increased.

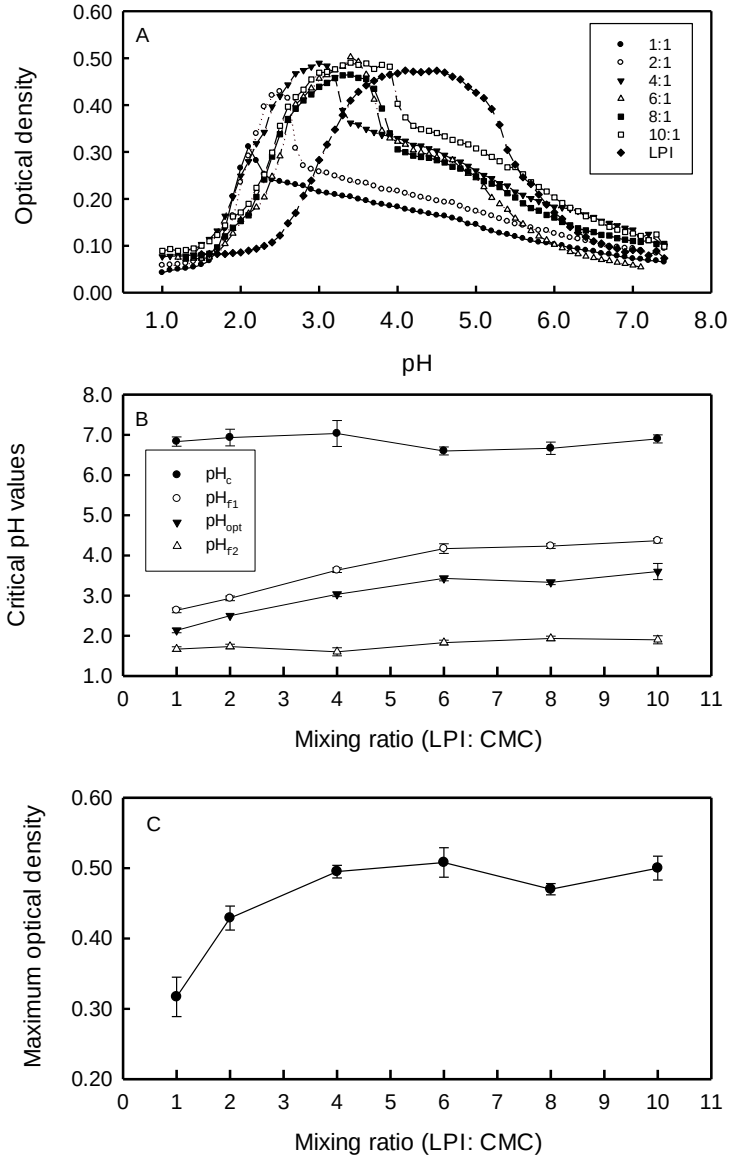

Figure 3.1 Complex coacervation behavior within mixtures of lentil protein isolate (LPI) and carboxymethyl cellulose (CMC, 0.7 DS; molecular mass of 250 kDa) at different mixing ratios, as outlined in: (a) A turbidimetric pH-titration during coacervation; (b) critical pH values associated with complex formation and breakdown [pH_c – soluble complexes, $pH_{\phi 1}$ – insoluble complexes, pH_{opt} – optimal complexation and $pH_{\phi 2}$ – dissolution of complexes]; and (c) maximum optical density (OD) occurring at pH_{opt}. Data in (a) represents the mean data points from triplicate curves; whereas data in (b, c) represent the mean ± one standard deviation (n = 3).

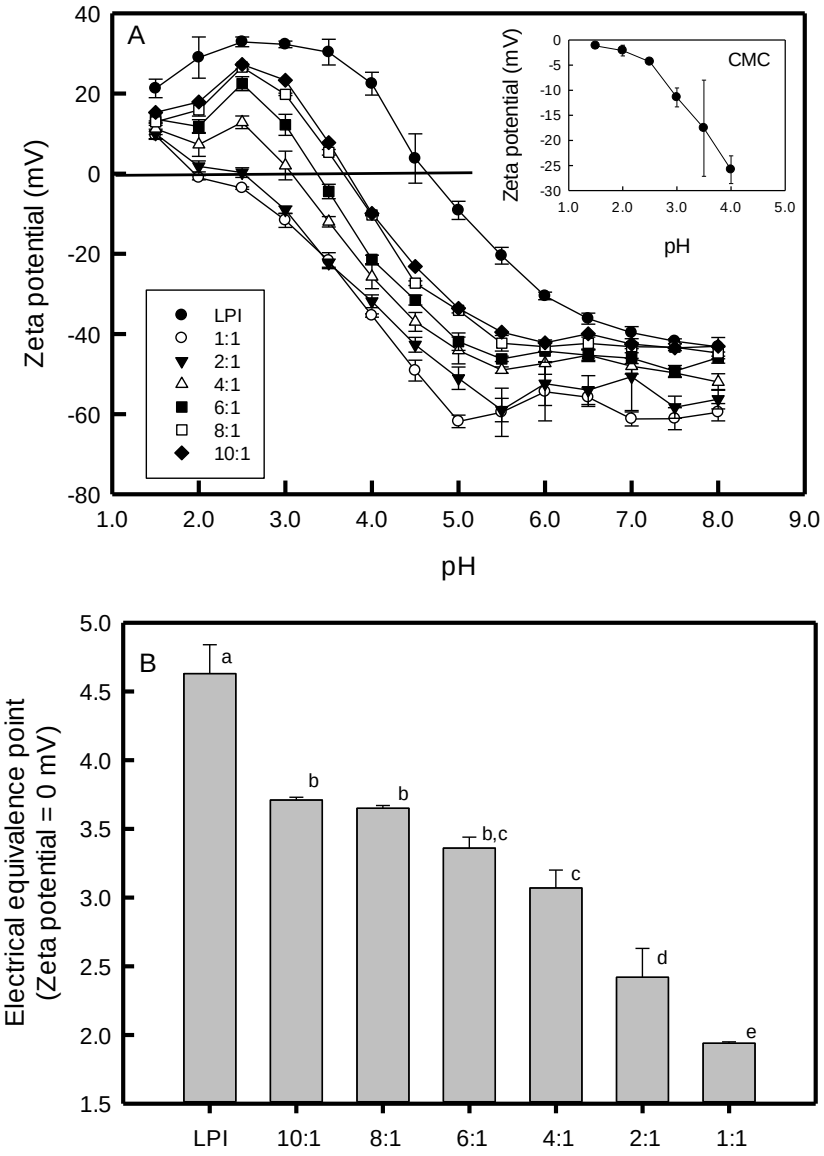

Figure 3.2 (A) The surface charge (zeta potential) as a function of pH for mixtures of lentil protein isolate (LPI) and carboxymethyl cellulose (CMC, 0.7 DS; molecular mass of 250 kDa) at different mixing ratios, and for homogenous solutions of LPI and CMC (see insert). (B) Electrical equivalence point (zeta potential = 0 mV) determined for the same systems (except for the CMC control which remained negatively charged at all pH's examined. Data represent the mean ± one standard deviation (n = 3).

Phase diagrams showing changes to the critical pH values associated with the formation and dissolution of electrostatic complexes as a function of mixing ratio is given in Figure 3.1B. For all mixtures, the formation of soluble complexes was found to occur at ~pH 7.0 regardless of the mixing ratio ($p>0.05$). At this pH, both biopolymers carry a net negative charge. It is presumed that interactions take place between CMC and positive patches on the protein(s) surface, as was noted by Seyrekan and co-authors (2003) for bovine serum albumin-heparin mixture, Weinbreckand et al. (2003a) for whey proteins-exocellular polysaccharide mixtures, Weinbreck and co-authors (2003b) for whey protein-gum Arabic mixtures, and Aryee and Nickerson (2012) for LPI-gum Arabic (GA) mixtures. Independence of pH_c to biopolymer mixing ratio has been reported in aggregate-free (removed by filtration) whey protein-exocellular polysaccharide (Weinbreck et al., 2003a), whey protein-carrageenan (Weinbreck et al., 2004), and β-lactoglobulin-pectin (Girard et al., 2004) mixtures where it was presumed that soluble complexes formed between individual proteins and polysaccharides. Since the initial rise in OD in the presence study of LPI (control) also occurred at pH 7.0, it is presumed that the initial interactions with CMC occurred with individual LPI proteins or very small LPI-LPI aggregates. In contrast, mixing ratio dependence of pH_c has been previously reported within mixtures where protein aggregation was more prevalent prior to initial complexation, including gelatin (Type-A and Type-B)-agar (Singh et al., 2007), pea protein isolate-GA (Liu et al., 2009), canola protein isolate-alginate/ι-carrageenan (Klassen et al., 2011), and LPI-GA (Aryee & Nickerson, 2012).

With further acidification, insoluble complexes were formed at $pH_{\phi 1}$ indicating macroscopic structure formation. Of note, the terms ‘soluble’ and ‘insoluble’ are terms used in the coacervation literature and no refer to solubility in a protein functionality sense. As shown in Figure 3.1B, $pH_{\phi 1}$ increased as the mixing ratios increase ($p<0.05$), where $pH_{\phi 1}$ occurred at pH 2.6 at 1:1 and at pH 4.2 at 6:1, then becoming more stable ($p>0.05$). It was hypothesized that this trend was the result of an increase in number and size of LPI-LPI aggregates due to the weaker electrostatic repulsive forces generated by the smaller amount of CMC polysaccharides as mixing ratios increased. Also, as the LPI concentration increased, there would be more protein molecules available for CMC chain for binding with increasing biopolymer mixing ratio (Aryee & Nickerson, 2014; Liu et al. 2009). As the pH decreased further, OD reached a maximum at pH_{opt} indicating pH conditions that yielded the greatest number of complexes. Similar to $pH_{\phi 1}$, pH_{opt} increased along with mixing ratios from pH 2.1 at the 1:1 ratio to pH 3.0 at the 4:1 ratio ($p<0.05$) and became

more stable at 6:1, 8:1 and 10:1 at pH ranging from 3.3-3.6 (Figure 3.1B). At pH_{opt}, the LPI and CMC mixtures reach an electrical equivalence point, where two biopolymers reached an overall neutral charge (Kayitmazer, 2017; Li et al., 1994; Schmitt et al., 1998; Stone et al., 2014). The maximum OD as a function of LPI-CMC mixing ratio is shown in Figure 3.1C, where it was found to increase quickly from a 1:1 mixing ratio to 2:1 ($p<0.05$) and then more gradually to 4:1, afterwards reaching a steady state. OD_{Max} at 4:1 LPI-CMC ratio was 0.495, which was greater than that of the control (LPI alone; OD_{Max} = 0.476). Further acidification showed a decline in OD as the dissolution of complexes began as the carboxyl sites along the CMC became protonated. This reduction continued until reaching $pH_{\phi 2}$ (at pH 1.6-1.9). Only small fluctuation was found for $pH_{\phi 2}$ with mixing ratios in this study (Figure 3.1B).

Figure 3.2 shows the surface charge of LPI-CMC blends as a function of mixing ratios and homogeneous biopolymers (LPI and CMC) over the range from pH 8.0 to 1.5. Net neutrality (pI) for LPI alone occurred at pH 4.6 (Figure 3.2), which corresponded to OD_{max} from Figure 3.1. The LPI carried a net negative charge above pH 4.6 and positive charges below this pH. Surface charges of the homogeneous CMC solution remained below zero during the entire titration but increased to close to zero at pH 1.5; results were reported from pH 4.0 because the values fluctuated largely between pH 4.5 to 8.0. The variability in the CMC data also was thought to impact readings of the blends between pH values 5-8 where ZP was relatively constant. Net neutrality for all mixing ratios was determined at pH values < pI of LPI alone, and was found to increase from pH 1.9 at the 1:1 ratio to pH 3.7 at the 10:1 ratio (Figure 3.2B) with increment more steeply from 1:1 to 4:1 ($p<0.05$) then more gradually from 4:1 to 10:1. Net neutrality shifted closer to the pI of LPI with higher mixing ratios indicating more contribution of LPI aggregates in the complexation processes.

3.4.3 Effect of degree of substitution of CMC on the formation of electrostatic complexes with LPI

The effects of degree of substitution (DS 0.7, 0.9, 1.2) of CMC (molecular mass of 250 kDa) on the formation of complexes at LPI: CMC at 4:1 mixing ratio was determined through a turbidimetric pH-titration (Figure 3.3A). The mixture of LPI-CMC (DS 0.7) displayed the greatest OD_{Max} (0.495), followed by CMC with degrees of substitution of 0.9 (0.471) and 1.2 (0.406) (Table 3.1). It was originally hypothesized that a higher charge density (higher DS) would have more reactive sites to bind with LPI to give greater complexation. However, this inhibition has been

reported in use of some highly charged polysaccharide involving complex such as pea protein isolate-alginate (Klemmer et al., 2012), LPI- κ-carrageenan and LPI-gellan gum (Aryee & Nickerson, 2014), and pea protein isolate-high methoxy citrus pectin (Warnakulasuriya et al., 2018). Thus, is presumed that the higher charge density of CMC (DS 1.2) would generate more electrostatic repulsive forces between CMC chains to suppress the formation of LPI-LPI aggregates and slowed down the rate of forming LPI-CMC (Warnakulasuriya et al., 2018). The structural differences in these CMCs might be another factor affecting complexation behavior. In addition to substituting more $-COO^-$ groups, increased DS also means generating bigger constituent groups ($-CH_2OH \rightarrow -CH_2OCH_2COOH$), which would induce steric effect and negatively influences the complexation between LPI and CMC (Zhivkov, 2013) resulting lower maximum OD values.

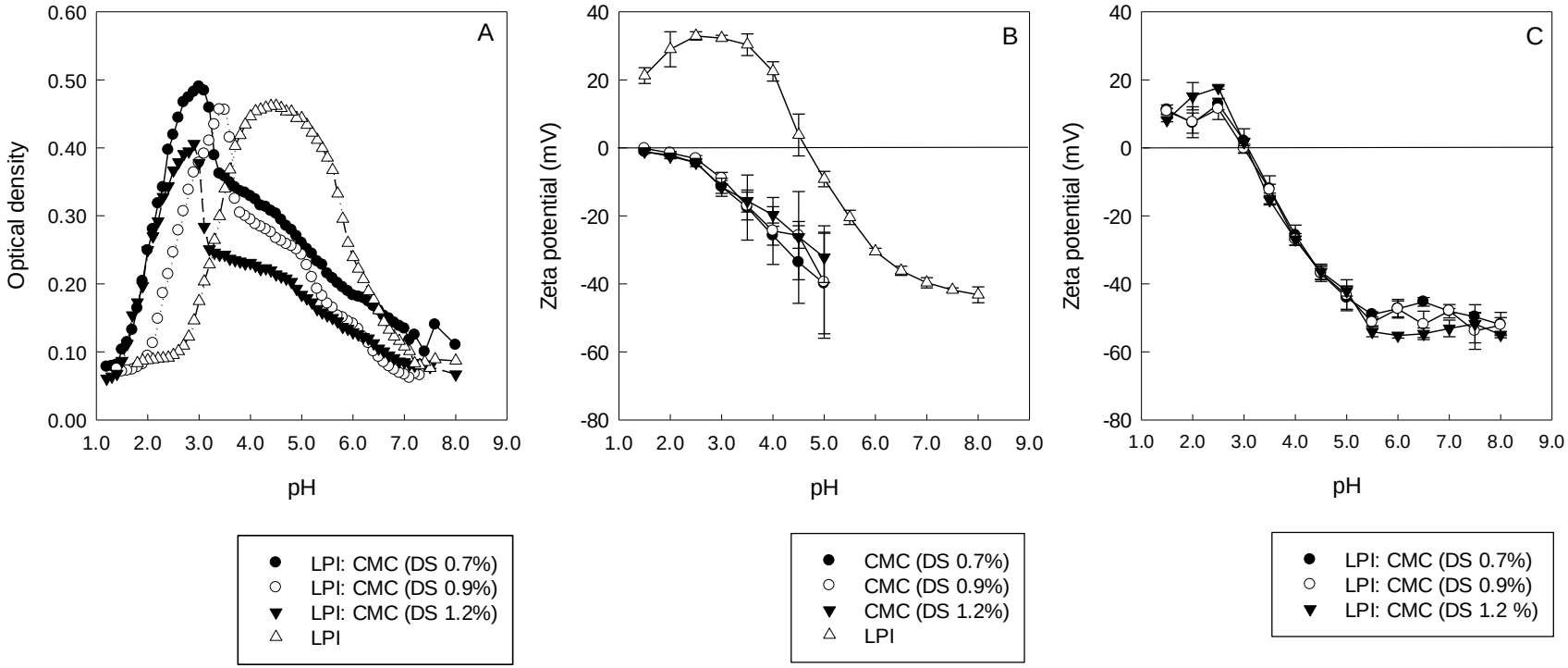

Figure 3.3 Effect of DS of carboxymethyl cellulose (CMC, molecular mass of 250 kDa) on its coacervation behavior in mixtures with lentil protein isolate (LPI), as described by (A) a turbidimetric pH-titration and surface charge. (B) homogenous polymer solutions and (C) mixed polymer solutions, so as a function of pH. Data in (A) represents the mean data points from triplicate curves; whereas data in (B, C) represent the mean ± one standard deviation (n = 3).

Table 3.1 Effect of DS and molecular mass on critical parameters associated with the complex coacervation of lentil protein isolate – carboxymethyl cellulose mixtures (4:1 blending ratio) relative to lentil protein isolate alone. Data represents the mean ± one standard deviation (n = 3).

Materials	**pH_c**	**$pH_{\phi 1}$**	**pH_{opt}**	**$pH_{\phi 2}$**	**Max. OD**	**EEP**
a) LPI (control)	6.93 ± 0.12^{aA}	5.93 ± 0.12^{aA}	4.37 ± 0.15^{aA}	2.40 ± 0.10^{aA}	0.476 ± 0.017^{aB}	4.63 ± 0.17^{aA}
b) Effect of degree of substitution[1]						
LPI: CMC (0.7)	7.03 ± 0.32^{a}	3.63 ± 0.06^{c}	3.03 ± 0.06^{b}	1.60 ± 0.10^{b}	0.495 ± 0.009^{a}	3.07 ± 0.13^{b}
LPI: CMC (0.9)	6.57 ± 0.21^{a}	3.90 ± 0.00^{b}	3.10 ± 0.10^{b}	1.70 ± 0.10^{b}	0.471 ± 0.008^{a}	2.99 ± 0.06^{b}
LPI: CMC (1.2)	6.93 ± 0.06^{a}	3.37 ± 0.06^{d}	2.90 ± 0.00^{b}	1.50 ± 0.00^{b}	0.406 ± 0.009^{b}	3.05 ± 0.02^{b}
c) Effect of molecular mass of CMC[2]						
LPI: CMC (90 kDa)	6.93 ± 0.12^{A}	3.83 ± 0.15^{B}	3.00 ± 0.10^{B}	1.77 ± 0.12^{B}	0.527 ± 0.013^{A}	3.11 ± 0.05^{B}
LPI: CMC (250 kDa)	7.03 ± 0.32^{A}	3.63 ± 0.06^{B}	3.03 ± 0.06^{B}	1.60 ± 0.10^{B}	0.495 ± 0.009^{AB}	3.07 ± 0.13^{B}

Abbreviations:

- Lentil protein isolate (LPI) and carboxymethyl cellulose (CMC)
- Critical pH values corresponding to the formation of soluble complexes (pH_c), insoluble complexes ($pH_{\phi 1}$), optimal complexation (pH_{opt}) and the dissolution of complexes ($pH_{\phi 2}$).
- Optical density (OD)
- EEP: electric equivalence point

Representative confocal scanning microscopy images of LPI and LPI-CMC solutions at corresponding pH_{opt} values as a function of DS at the 4:1 mixing ratio are given in Figure 3.4. In Figure 3.4A, some small-sized and a few medium-sized of aggregates were observed for the LPI control. With the addition of CMC (DS 0.7, 250 kDa), the number of aggregates increased compared to the LPI control, as more medium-sized aggregates and a few larger aggregates were present (Figure 3.4C), which would cause the higher OD seen in Figure 3.1. In general, as the degree of substitution of CMC chains increased, fewer aggregates were observed (Figure 3.4C-E). More medium but fewer large aggregates were observed in system LPI-CMC with 0.9 DS relative to the 0.7 DS, leading to a smaller OD value. And in the case of CMC 1.2 DS, a few large aggregates were observed resulting in the least scattered light (OD reduced) (Figure 3.4E).

No obvious difference ($p>0.05$) in critical pH values (pH_c, pH_{opt} and $pH_{\phi 2}$) were observed as a function of degrees of substitution (Table 3.1). For $pH_{\phi 1}$, values differed most likely due to the change in the turbidity curves where the CMC (DS 0.7) saw gradual increase in OD between pH_c and $pH_{\phi 1}$, whereas the curves of LPI-CMC (DS 0.9, 1.2) changed with multiple inflection points over the same pH range indicating that structure formation was somewhat variable (Table 3.1, Figure 3.3A). Surface charge as a function of pH is given for homogenous systems of LPI and CMC (Figure 3.3B) and for the mixed LPI-CMC systems (Figure 3.3C). All homogenous CMC solutions were negatively charged at pH 5.0, and progressively increased to close to zero at pH 1.5 (Figure 3.3B). Net neutrality for LPI-CMC (DS 0.7, 0.9, 1.2) systems were found near pH 3.0 respectively ($p>0.05$), which corresponding pH_{opt} values (Table 3.1).

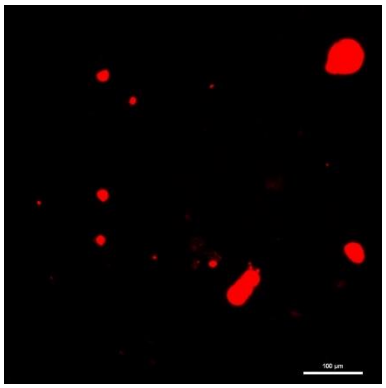

A) LPI alone

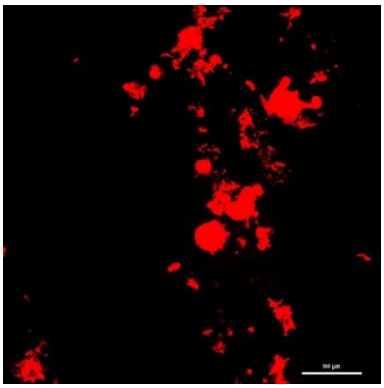

(B) LPI-CMC (0.7 DS, 90 kDa)

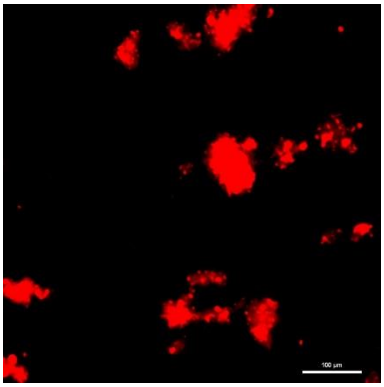

C) LPI-CMC (0.7 DS, 250 kDa)

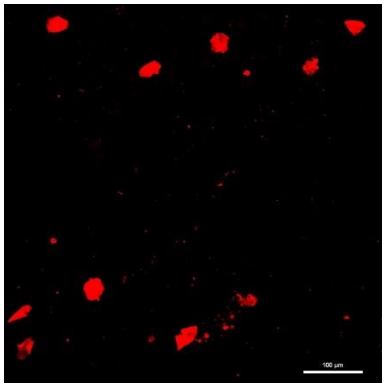

D) LPI-CMC (0.9 DS, 250 kDa)

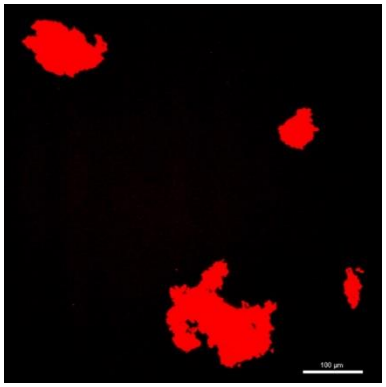

E) LPI-CMC (1.2 DS, 250 kDa)

Figure 3.4 Confocal laser scanning microscopy images of LPI alone and mixtures at the 4:1 LPI: CMC (at difference DS and molecular mass) mixing ratio taken at pH_{opt}. The scale bar represents 100 µm.

3.4.4 Effect of molecular mass of CMC on the formation of electrostatic complexes with LPI

The effects of CMC molecular mass (90 and 250 kDa) on the formation of complexes with LPI were investigated at a 4:1 mixing ratio and a constant CMC DS of 0.7 through a turbidimetric acid titration (Figure 3.5A). It was hypothesized that by increasing the molecular mass of CMC, the amount of complexation would decrease since the lower entropy of mixing would result in reduced biopolymer compatibility in solution (Schmitt et al., 1998). Increased maximum OD value with smaller molecular mass was also observed in a pea protein isolate-alkaline de-esterified pectin system (Pillai et al., 2019). In the present study, OD_{Max} decreased from 0.527 to 0.495 as molecular mass of CMC increased from 90 to 250 kDa (Table 3.1). It was also presumed that CMC (90 kDa) with smaller sizes could approach LPI easier compared to CMC (250 kDa) due to less steric effects resulting more LPI-CMC interaction. CSLM images showed a greater number of larger aggregates were present with 90 kDa CMC (Figure 3.4B) relative to that with 250 kDa CMC (Figure 3.4C) allowing it to scatter more light. No difference ($p>0.05$) was observed with all the critical pH values between the two systems, with neutrality occurring near pH 3 ($p>0.05$) (Table 3.1). Complementary surface charge measurements were given in Figure 3.4B and 3.4C. Greater turbidity was reported for a hyaluronic acid (HA)-chitosan system during an acid titration with decreasing HA molecular weight (Kayitmazer et al., 2015) and a pea protein isolate-alkaline de-esterified pectin system with decreased pectin molecular weight (Pillai et al., 2019). In contrast, Shieh and Glatz (1994) found little effect of molecular weight on a lysozyme-polyacrylic complexation.

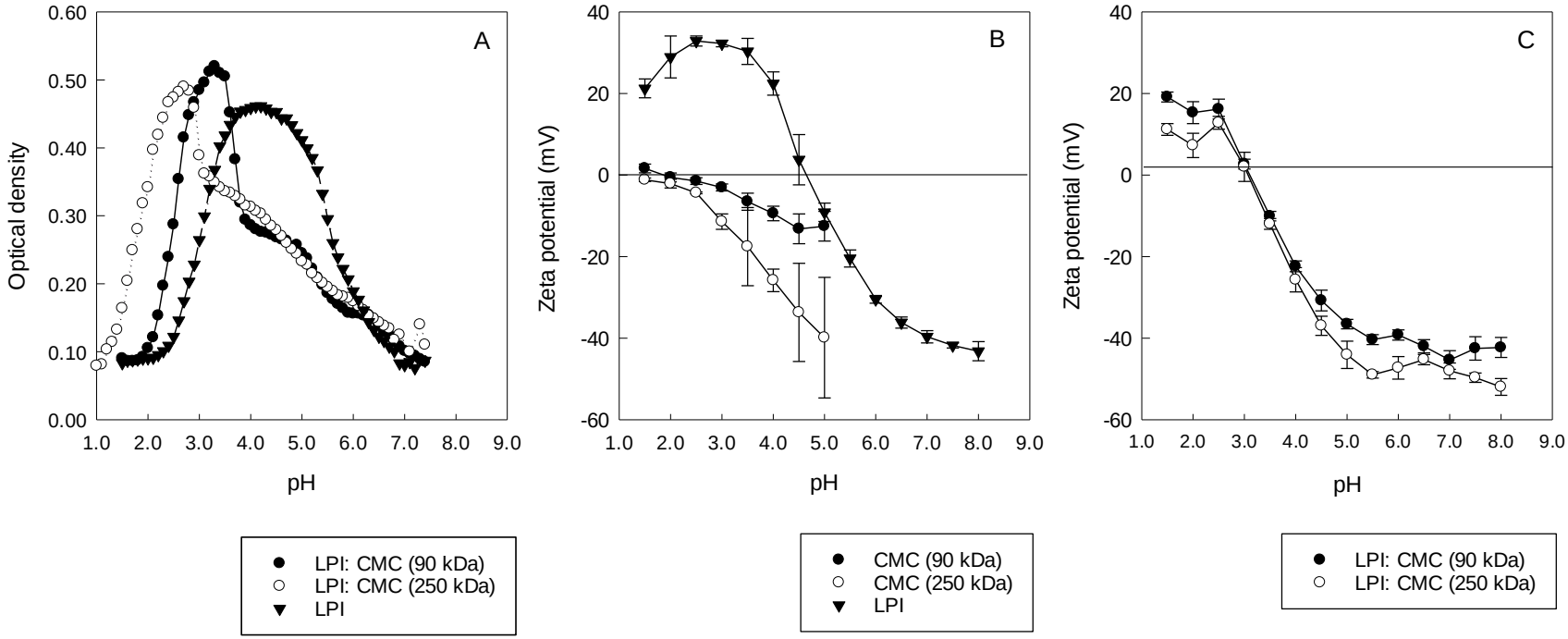

Figure 3.5 Effect of molecular mass of carboxymethyl cellulose (CMC, DS 0.7) on its coacervation behavior in mixtures with lentil protein isolate (LPI), as described by (A) a turbidimetric pH-titration and surface charge (B) homogenous polymer solutions and (C) mixed polymer solutions, so as a function of pH. Data in (A) represents the mean data points from triplicate curves; whereas data in (B, C) represent the mean ± one standard deviation (n = 3).

3.4.5 Isothermal titration calorimetry

Isothermal titration calorimetry (ITC) was performed to understand the thermodynamic parameters [binding stoichiometry (q), affinity constant (K), enthalpy (ΔH), entropy (ΔS) contributions and Gibbs free energy change (ΔG)] of LPI-CMC complexation. It directly measures the energetics through heat changes associated with the complexation reaction of LPI and CMC at a constant temperature (Freire et al., 1990; Jelesarov & Bosshard, 1999; Kayitmazer, 2017; Xiong et al., 2017). The thermodynamics properties of LPI-CMC coacervates as a function of CMC substitution degree and molecular mass were determined at pH 3 for all LPI-CMC systems based on the optimal coacervation pH determined and 25℃. The interaction of LPI and CMC (0.7, 250 kDa) was taken as an example to show a typical heat flow curve and binding isotherm (Figure 3.6A, B). The thermodynamic parameters determined for all four systems are given in Table 3.2.

As seen in Fig 3.6A, after each injection of LPI solution (0.1055 mM) into the reaction cell containing CMC solution (0.004 mM), the amount heat released as a result of complexation was monitored and showed as the area of the peaks in the heat flow curve. The thermograms obtained for all systems were exothermic, which indicated that the complexation reaction was energetically favorable. The area of peaks reduced gradually due to the reduction of free CMC chains available for complexation in the cell and until reaching a steady equilibrium state, which indicates the saturation point of the LPI-CMC interaction. Note that the saturation points for the LPI-CMC (0.7, 250 kDa) interaction was reached after 18 injections (Figure 3.6A). For the rest of the LPI-CMC systems, the saturation point occurred at 19, 9, and 11 injections for LPI-CMC (0.9, 250 kDa), LPI-CMC (1.2, 250 kDa), and LPI-CMC (0.7, 90 kDa), respectively (data not shown). The heat flow curves were then fitted into binding isotherms using an “independent binding site” model based on the assumption that each LPI molecule contained only one independent binding site and the carboxylate group on CMC was the only binding group to LPI since the interaction of LPI and CMC was mainly driven by positively charged proteins and negatively charged carboxylate groups on CMC chains through electrostatic attraction.

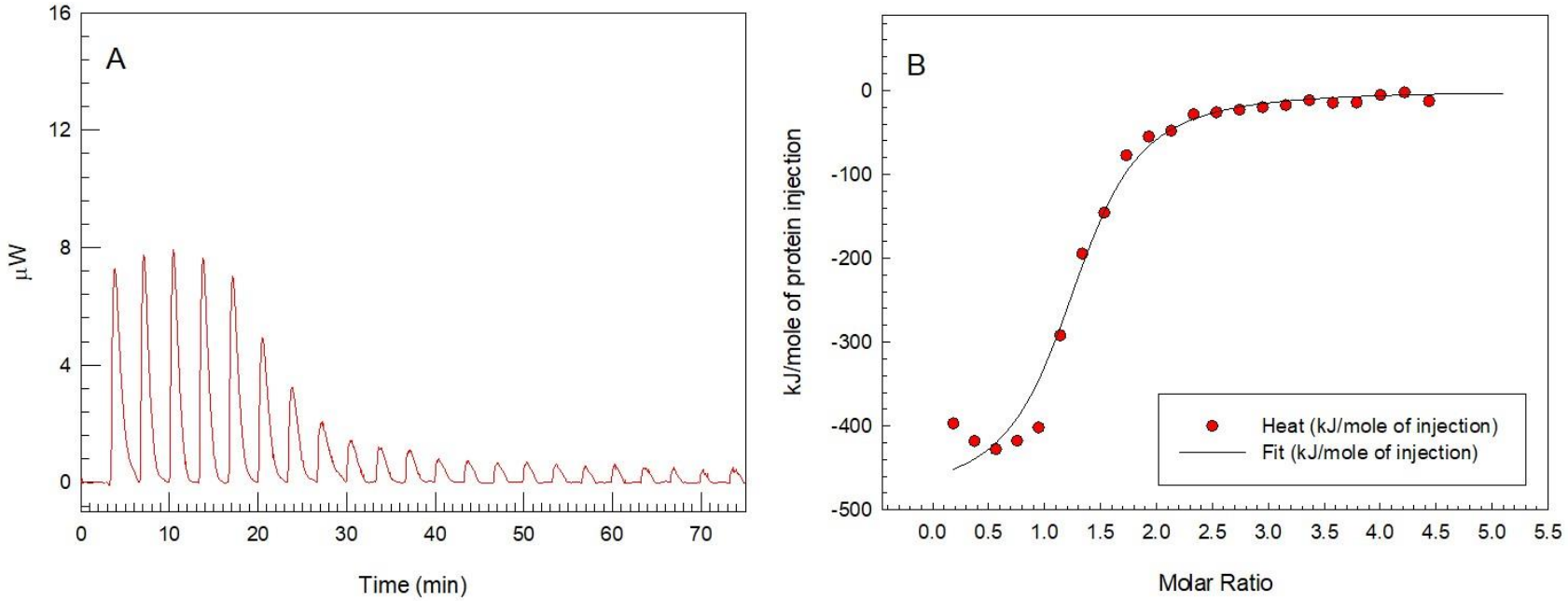

Figure 3.6 Heat flow curve (A) and binding isotherm (B) of titration of LPI into CMC (DS 0.7, 250kDa) in pH 3 citric buffer.

Table 3.2 Thermodynamic parameters for LPI-CMC samples. Data represents the mean ± one standard deviation (n = 2).

Samples	**q**	**K** ($\times 10^6$)	**ΔH [KJ/mol]**	**TΔS [KJ/mol]**	**ΔG [KJ/mol]**
LPI-CMC (0.7, 250kDa)	1.25 ± 0.01	2.78 ± 0.51	-466.28 ± 22.79	-429.52 ± 22.33	-36.76 ± 0.46
LPI-CMC (0.9, 250kDa)	1.49 ± 0.43	6.82 ± 1.91	-468.01 ± 16.44	-429.05 ± 15.74	-38.96 ± 0.70
LPI-CMC (1.2, 250kDa)	1.19 ± 0.04	21.2 ± 12.1	-759.30 ± 1.70	-717.71 ± 3.21	-41.59 ± 1.50
LPI-CMC (0.7, 90kDa)	0.73 ± 0.05	3.84 ± 1.76	-540.06 ± 14.00	-502.62 ± 12.82	-37.44 ± 1.18

Abbreviations:

- q: binding stoichiometry
- K: association constant
- ΔH: enthalpy
- T: the temperature on the Kelvin scale
- ΔS: entropy
- ΔG: Gibbs free energy

A binding isotherm of LPI-CMC (0.7, 250kDa) fitted from a heat flow curve (Figure 3.6A) was shown in Figure 3.6B with a stable enthalpy determined at LPI-CMC molar ratio of 3.6 corresponding to optimal LPI-CMC coacervation mixing ratio of 4. The stable enthalpy was observed at molar ratio of 3.7, 1.7, and 2 for LPI-CMC (0.9, 250 kDa), LPI-CMC (1.2, 250 kDa), and LPI-CMC (0.7, 90 kDa), respectively (data not shown). ΔH, q and K were derived from the binding isotherm, where ΔH is the amount of heat released per mole of LPI injection; q represents the number of identical and independent binding site for LPI on CMC, and K indicates the strength of association. Entropy and Gibbs free energy were calculated from Eq 3.2 and Eq 3.3; all the critical parameters were shown in Table 3.2. Enthalpy, entropy, and Gibbs free energy from four LPI-CMC systems were all negative suggesting the exothermic complex coacervation processes of LPI and all CMC polysaccharides were dominated by enthalpy change (Table 3.2). Girard et al. (2003), Hosseini et al. (2013), and Xiong et al. (2017) also reported a spontaneous exothermic enthalpy driven process in a β-lactoglobulin-low methoxyl pectin, a β-lactoglobulin-κ-carrageenan system, and an ovalbumin-CMC, respectively, while an exothermic-endothermic sequenced process driven by enthalpic and entropic contribution for a sodium caseinate-low methoxyl pectin system at pH 3 was observed by Wang et al (2019c). A negative entropy indicated that the effects of release of counter ions in the present study were unfavourable. The similar values of ΔH and TΔS suggested that the binding between LPI and CMC and the release of the counter ions from the biopolymer chains are compensation (Ou & Muthukumar, 2006). For LPI and CMC as a function of CMC degree of substitution, the enthalpy obtained for LPI-CMC (0.7) and LPI-CMC (0.9) were similar corresponding to the similar maximum OD obtained from turbidity (Figure 3.3A). The higher exothermic values (i.e. more negative ΔH) for LPI-CMC (1.2) complexation suggested that the interaction was more intense which could be attributed to the higher charge density of CMC (1.2), and that might be the reason for the larger complexes' formation observed in Figure 3.4E. Increased association constant was also observed as CMC charge density increased in LPI-CMC (1.2) indicating its high affinity for the complexation reaction compared to the rest. Increased enthalpy and association constant values with higher biopolymer charge density were also observed in an ovalbumin-CMC system (Xiong et al. 2017) and in a β-lactoglobulin-low methoxyl pectin system compared with high-methoxyl pectin (Girard et al. 2003). The effect of CMC degree of substitution was minor on binding stoichiometry, where approximately one protein was interacting with one CMC chain. However, binding stoichiometry was greatly affected by the

molecular weight of CMC; results showed about one protein was interacting with two CMC (90kDa) polysaccharides chains instead. It was reported that the smaller biopolymer molecular size reflected by lower molecular mass could accelerate the biopolymer-biopolymer interaction (Doublier et al., 2000; Pillai et al., 2019). In this study, CMC (90kDa) chains could move more quickly compared to CMC (250kDa) to bind with LPI molecules leading to a larger enthalpy value, which corresponded to the higher maximum OD value (Figure 3.5A).

3.5 Conclusions

The complexation behavior of LPI and CMC with different degrees of substitution (0.7. 0.9, and 1.2) and different molecular mass (90 and 250 kDa) was investigated through a turbidimetric pH acid-titration and ITC. For LPI-CMC (0.7, 250 kDa), the level of complex formation was found to increase from an OD_{max} of 0.317 at the 1:1 LPI: CMC mixing ratio to an OD_{max} of 0.495 at the 4:1 ratio, followed by a plateau region. Critical pH values ($pH_{\phi 1}$ and pH_{opt}) were also found to increase as the mixing ratio increased indicating more LPI-LPI aggregates were interacting with CMC. This corresponded to a shift to higher pH values within increasing mixing ratio where the electrical equivalence points were reached; all of which was below the isoelectric point of LPI. The effects of substitution degree (DS) and molecular mass of CMC on the critical pH values were minor. Higher DS of CMC seemed to suppress of formation of LPI-LPI aggregates resulting in less complexes being formed (lower OD_{max} readings) due to the higher charge density on the CMC chains which generated more electrostatic repulsion within neighboring chains in solution. Increased OD_{max} readings was also observed at a lower molecular mass of CMC with LPI. Larger enthalpy values were found in LPI-CMC as CMC degree substitution increased or CMC molecular mass decreased. Binding stoichiometry was greatly influence by CMC molecular mass as one protein was interacting with two CMC (90 kDa) chains but only one CMC (250 kDa) chain.

3.6 Linkage to the next study

Based on the findings from chapter 3, among 1:1 to 10:1 LPI-CMC mixing ratios, 4:1 mixing ratio was found to have the greatest electrostatic interactions between LPI and CMC (0.7 DS, 250 kDa). Therefore, 4:1 mixing ratio was selected for the following experiments. At 4:1 LPI-CMC mixing ratio, the effect of molecular mass and substitution degree of CMC only had minor

effects on the electrostatic interaction between LPI and CMC polysaccharides. As there were no big differences in the complexation behavior among the LPI and various CMC mixtures, stronger interacting polysaccharides were introduced into the next study (i.e. Chapter 4). The polysaccharides with different charge density and functional groups such as gum Arabic, alginate, and iota-carrageenan were selected to contrast with the CMC. In the next study, the complexation behavior between LPI and various polysaccharides were examined. Additionally, the emulsifying properties of the forming LPI-polysaccharide complexes were also investigated because a stable emulsion must form prior to the drying process to result in dried microcapsules.

4. EFFECT OF PH ON THE FORMATION OF ELECTROSTATIC COMPLEXES BETWEEN LENTIL PROTEIN ISOLATE AND A RANGE OF ANIONIC POLYSACCHARIDES, AND THEIR RESULTING EMULSIFYING PROPERTIES[2]

4.1 Abstract

This research investigated the effect of pH on forming electrostatic complexes between lentil protein isolate (LPI) and a range of anionic polysaccharides [carboxymethyl cellulose **(**CMC), gum Arabic (GA), alginate (AL), and ι-carrageenan (ι-C)] at 4:1 LPI-polysaccharide mixing ratio, and their resulting emulsifying abilities. Maximum optical densities were found to be 0.486, 0.716, 0.310, and 0.190 for LPI-CMC, LPI-GA, LPI-AL, and LPI-ι-C, respectively indicating the level of aggregate size and growth. LPI-ι-C emulsion displayed the highest emulsion stability (ES) because of its higher continuous phase and emulsion viscosities, lower mean droplet sizes, and negatively charged droplets. They also formed much smaller complexes within solution due to their high negative charge. All other LPI-polysaccharide systems formed less stable emulsions than LPI alone due to the larger sizes of both complexes and oil droplets.

4.2 Introduction

Complex coacervation involves the electrostatic attractive interactions of biopolymer mixtures (e.g., proteins and polysaccharides) with opposing net charges over a narrow pH range

[2] Wang, Y., Ghosh, S., & Nickerson, M. T. (2019). Effect of pH on the formation of electrostatic complexes between lentil protein isolate and a range of anionic polysaccharides, and their resulting emulsifying properties. *Food Chemistry*, *298*, 125023. doi: 10.1016/j.foodchem.2019.125023 (*Reproduced with permission*). Y. Wang contributed to the experimental design, data collection and analysis and drafting of the manuscript; S. Ghosh was second reader on the manuscript; whereas M. Nickerson was the primary supervisor, contributed to the experimental design and acted as corresponding author for the manuscript.

resulting in phase separation into a biopolymer (protein + polysaccharide)- and solvent-rich phase (de Kruif et al., 2004; Ye, 2008). Through an acid titration, critical pH values associated with coacervate or precipitate structure forming events can be identified (Kizilay et al., 2011). For instance, during a turbidimetric pH acid titration, the first indication of structure development is denoted at pH_c associated with the formation of soluble complexes. As the titration continues, macroscopic changes in turbidity starts at $pH_{\phi 1}$ and the formation of insoluble complexes. Turbidity reaches a peak at pH_{opt}, and then eventually dissociates (at $pH_{\phi 2}$) pH as charges on the polysaccharides become protonated. Structure and functions of the resulting mixtures can be greatly affected by biopolymer characteristics (e.g. charge density and the functional groups) leading to the formation of a soluble coacervate or an insoluble precipitate-type structure (de Kruif et al., 2004; Kayitmazer, 2017; Singh et al., 2007). Coacervate structures tend to entrap water inside, remain suspended in solution and retain a high level of chain mobility within it (Ye, 2008), whereas precipitate structures entrap little water, have significantly less chain mobility inside, and tend to sediment to the bottom of the solution rather quickly (Ye, 2008). The coacervate structure also tends to be reversible upon changes in pH, and the precipitate structures are more strongly interacting leading to a less reversible structure (Klemmer et al., 2012; Stone et al., 2014). Manipulating the food structure and the functionality can be achieved through complex coacervation leading to a wide series of applications, such as the development of controlled release materials, encapsulation, biodegradable edible films, and food colloidal systems (Ye, 2008).

Incorporating the anionic polysaccharides alongside the proteins results in either positive or negative effects on emulsion stability depending on the protein-polysaccharide interactions. If a viscoelastic mixed or bilayer protein-polysaccharide film is formed at the oil-water interface, a stable emulsion is formed. Especially if conditions are such that bridging flocculation does not occur. Enhanced emulsion stability has been reported using complex coacervates such as whey protein-gum Arabic (Weinbreck et al., 2004), pea protein isolate-gum Arabic (Liu et al., 2010), canola protein isolate-carrageenan (Stone et al., 2013), chitosan-alginate (Li & McClements, 2011), and milk protein-CMC (Koupantsis et al., 2014). As an example, Stone and co-authors (2015) reported ES increased from 88.7% to 93.3% when canola protein was complexed with low methoxy pectin, whereas when combined with gum Arabic, no differences in ES was observed Stone et al. (2014). Liu et al. (2010) reported ES was improved with pea protein isolate and gum

Arabic relative to pea protein alone using both one-step (mixed layer) and two-step (bilayer) procedure.

Lentil proteins are gaining tremendous interest by the food industry like other pulse proteins because they are non-soy, gluten-free, and non-animal based. Pulse proteins tend to have excellent functional attributes including water/fat binding, emulsification, foaming, solubility and gelation depending on preparation processes (Boye et al., 2010; Liang & Tang, 2014). Lentil proteins are dominated by globulin and albumin representing 50-65% and 10-25% of the total protein, respectively (Boye et al., 2010; Jarpa-Parra, 2018). Small amount (~10% and 3.5%, respectively) of prolamins and glutelins also present (Aryee & Nickerson, 2012). Globulin is comprised of two major proteins: a 11S (S is a Svedberg unit) legumin (molecular mass of 350-400 kDa) and 7S vicilin (molecular mass of 150 kDa) (Boye et al., 2010; Liu et al., 2009). Albumin proteins consists of enzymatic proteins, protease inhibitors, amylase inhibitors, and lectins (molecular weight ranging from 6-100 kDa) (Boye et al., 2010).

Carboxymethyl cellulose (CMC) is a functional ingredient with a wide range of applications in the food industry (e.g. ice creams, puddings, pie fillings) for bulking agent, moisture retention, prevention of syneresis, and sugar crystallization (Biswal & Singh, 2004; Koupantsis et al., 2014). CMC is a linear anionic polysaccharide obtained by the reaction between alkali cellulose and sodium monochloroacetate (Biswal & Singh, 2004; Ducel et al., 2004). The substitution degree of CMC is the average number of carboxymethyl groups substituted on per glucose unit ranging from 0.7-1.2 for commercial grade (Ducel et al., 2004; Janjarasskul & Krochta, 2010). In contrast to CMC, gum Arabic (GA) is a branched carboxylated anionic arabinogalactan polysaccharide; it has a highly heterogeneous structure with three main fractions. About 89% of the GA is made up of a highly branched acidic polysaccharide (i.e. β-(1-3) galactopyranose (galactan) polysaccharide backbone highly branched with β-(1-6) galactopyranose residues terminating in arabinose and glucuronic acid and/or 4-O-methyl glucuronic acid units, and about 10% of the gum is comprised of an arabinogalactan–protein complex, in which a polypeptide backbone and arabinogalactan chains are linked covalently (Aryee & Nickerson, 2012; Dror et al., 2006; Liu et al., 2009). GA is highly water-soluble and is excellent emulsifying agent. Alginate (AL) is extracted from marine algae (brown seaweeds) and is composed of segments of β-(1-4)-linked D-mannuronic acid (M block) and segments of α-(1-4)-linked L-guluronic acid (G block) with M/G ratio varying from 0.5 to 2.0 (Harnsilawat et al.,

2006; Klassen et al., 2011). ι-Carrageenan (ι-C) is also extracted from marine algae (Rhodophyceae family) and contains a disaccharide repeating unit of (1-3)-β-D-galactopyranose-4-sulphate-(1-4)-3,6-anhydro-α-D-galactose-2-sulphate (de Jong & van de Velde, 2007; Lam & Nickerson, 2014). Alginate and ι-carrageenan are linear polysaccharides and can form gel in the present of cations.

The overall goal of this research is to compare the complexation behavior lentil protein isolate with the addition of four different polysaccharides (i.e. CMC, GA, AL, ι-C) as a function of pH, and to explore their potential for stabilizing oil-in-water emulsions. It is hypothesized that smaller LPI-polysaccharide complexes will act as better emulsifiers due to their greater ability to migrate and orient at the oil-water interface.

4.3 Materials and methods

4.3.1 Materials

Lentil protein isolate (LPI) used in this study was generously donated by KeyLeaf Corp. (Saskatoon, SK), and was produced by alkaline extraction (pH 9.5) followed by isoelectric precipitation (pH 4.5), followed by neutralization and spray drying. Anionic polysaccharides included: carboxymethyl cellulose (CMC; molar mass 250 kDa, degree of substitution of 0.7, 400-800 mPa s in 2% solution), gum Arabic (GA; ~250 kDa, branched), alginate (AL; Batch #: 108K1228, medium viscosity), and ι-carrageenan (ι-C; Batch #: 075K1808) were purchased from Sigma-Aldrich Co (Oakville, ON, Canada). Canola oil was purchased from a local supermarket. All other chemicals used in this study were of reagent grade and purchased through Sigma-Aldrich Co (Oakville, ON, Canada). Water was filtered through a Milli-Q purification system (Millipore Corporation, MA, USA).

4.3.2 Proximate analysis

Proximate analysis of all materials was determined according to the Association of Official Analytical Chemists (AOAC) methods 925.10 (moisture), 923.03 (ash), 920.85 (lipid) and 920.87 (crude protein, %N x 6.25), respectively (AOAC, 2003). A percent dry weight basis (d.b.) of ash, fat, and protein levels was reported. Carbohydrate content was calculated based on percent differential from 100%. Measurements were performed in triplicate and reported as the mean ±

one standard deviation (n = 3) for all analyses. Mineral contents were measured by KeyLeaf Corp. (Saskatoon, SK) using atomic absorption spectroscopy.

4.3.3 Turbidimetric measurements

The turbidimetric pH titration was carried out to investigate the critical pH values ($pH_{c,}$ $pH_{\phi1}$, pH_{opt} and $pH_{\phi2}$) associated with phase changes within LPI-polysaccharide mixtures as a function of pH (8.0–1.5) at a 4:1 biopolymer mixing ratio at a constant biopolymer concentration of 0.05% (w/w). The mixing ratio was selected based on preliminary work with LPI-CMC (not shown), with other polysaccharides being combined with LPI at the same ratio for comparative purposes. Biopolymer solutions were prepared by dissolving each powder in Milli-Q water at the 4:1 LPI-polysaccharide mixing ratio under constant mechanical stirring (500 rpm) for 2 h at room temperature (21-23 °C) and then overnight at 4 °C to help facilitate protein solubility. The solutions were mixed and stirred for 30 min at room temperature, and the pH was corrected to pH 9.0 prior to measurements. Critical pH values associated with structure forming events ($pH_{c,}$ $pH_{\phi1}$, pH_{opt} and $pH_{\phi2}$) were determined by turbidimetric acid pH titrations of biopolymer mixtures according to Liu et al. (2009) and Aryee and Nickerson (2012). Biopolymer mixtures were acidified by adding 0.05% (w/w) glucono-δ-lactone (GDL), which slowly lowered the pH from 8.0 to ~4.3. Afterwards, the dropwise addition of HCl was then added to minimize the dilution effects with a gradient of HCl concentrations based on pH (i.e., 0.05 M > pH 3.3; 0.5 M > pH 2.7; 1 M > pH 2.2; 2 M > pH 1.5). The changes in the optical density (O.D.) of the solutions were monitored using an ultraviolet-visible spectrophotometer (Genesys 10, Thermo Scientific, Fair Lawn, NJ, USA) at 600 nm and plastic cuvettes (1 cm path length). Critical pH values (i.e., pH_c, $pH_{\phi1}$, and $pH_{\phi2}$) were determined graphically as the intersection point of two curve tangents (Aryee & Nickerson, 2012; Liu et al., 2009), whereas pH_{opt} was denoted at the pH where maximum optical density occurred. Measurements were performed in triplicate with fresh solutions. The critical pH values were reported as the mean ± one standard deviation (n = 3). Homogenous LPI and polysaccharide solutions under the same solvent conditions at a total biopolymer concentration of 0.05% (w/w) were used as controls.

4.3.4 Surface charge (zeta potential)

Surface charge of mixed and homogeneous solutions was determined over a pH range of

8.0–1.5 with the use of a Zetasizer Nano-ZS90 (Malvern Instruments, Westborough, MA). Solutions were prepared as previously described in turbidimetric measurements. Solutions were titrated with the dropwise addition of titrant HCl (0.1 M > pH 5.0; 0.5 M > pH 3.5; 1.0 M > pH 2.5; 2.0 M > pH 1.5), and surface charge was measured in every 0.5 pH increment. Using the Henry equation, the electrophoretic mobility (i.e., velocity of a particle within an electric field) was used to give an estimate of the zeta potential (ς).

$$U_E = \frac{2\varepsilon \times \xi \times f(\kappa\alpha)}{3\eta} \quad (4.1)$$

where, ε is the permittivity, η is the dispersion viscosity, and $f(\kappa\alpha)$ is a function related to the ratio of particle radius (α) and the Debye length (κ) (Liu et al., 2009; Aryee & Nickerson, 2012). The Smoluchowski approximation *f*(κα) equaled 1.5 was used. All measurements were conducted at room temperature (21–23 °C) in triplicate. The electric equivalence point (EEP) was estimated from where the line from the plot of zeta potential vs pH passes through zero.

For droplet charge, 1.0% (w/w) of LPI control and LPI-polysaccharide emulsions were prepared at their corresponding optimal pH values as previously described. One drop of each of the fresh emulsion was dispersed into 100 mL double distilled water at the corresponding optimal pH values. The dispersions were used to measured droplet charge. Droplet charge of the emulsions was determined from a Zetasizer Nano-ZS90 (Malvern Instruments, Westborough, MA) as described previously.

4.3.5 Emulsion stability (ES)

ES was determined according to Liu et al. (2010) and Stone et al. (2013) based on creaming experiments overtime. Homogenous and mixed (at 4:1 ratio) LPI and polysaccharide solutions were prepared in a similar manner as the turbidimetric analysis except at a total biopolymer concentration of 1.0% (w/w). ES was tested for a 50/50 oil-in-water emulsion (6 g oil/ 6 g aqueous solution) using canola oil. Mixed aqueous solutions were stirred at 500 rpm for 30 min at room temperature, and then adjusted to the pH corresponding to their pH_{opt} values [pH at 4.2 for LPI; 3.0 for LPI-CMC; 4.0 for LPI-GA; 2.6 for LPI-AL; and 4.0 for LPI-ι-C] using 2 N and 0.2 N HCl. Emulsions were then homogenized (Omni International, Inc., Marietta, GA, USA) for 5 min at speed 4 (~7200 rpm) with a saw tooth generating probe (20 mm) with the position at the oil-water

interface in 50 mL screw capped plastic centrifuge tubes. Then, 8 mL of the emulsion was transferred to a 10 mL graduated cylinder (inner diameter = 10.80 mm; height = 100.24 mm; as measured by a digital caliper) and allowed to separate for 0.5, 24, 48, and 72 h. The percentage ES was determined using Eq. (4.2), where V_B and V_A are the volume of the aqueous (or serum layer) before emulsification (4.0 mL) and after drainage at each time point, respectively.

$$\%ES = \frac{V_B - V_A}{V_B} \times 100\% \quad (4.2).$$

All measurements were performed in triplicate.

4.3.6 Droplet size and distribution

Emulsions were prepared as previously described. After homogenization, 4 mL of the emulsion was immediately placed in a Mastersizer 2000 laser light scattering instrument (Malvern Instruments Ltd., Worcestershire, UK) with a Hydro 2000S sample handling unit as described by Can Karaca et al. (2011) for determination of average droplet size and distribution. Milli-Q water was used as the dispersant in the sample handling unit, and the obscuration was brought up to ~14% with the addition of the sample. The relative refractive index of emulsion, which is the ratio of the refractive index of canola oil (1.47) to the refractive index of the dispersant (1.33) was 1.105. The droplet size was reported as surface-average diameter ($d_{3,2}$) that is expressed using Eq. (4.3).

$$d_{3,2} = \frac{\sum_{i=1} N_i d_i^3}{\sum_{i=1} N_i d_i^2} \quad (4.3)$$

where N_i is the number of droplets of diameter (*di*) (McClements, 2005). All measurements were performed in triplicate.

4.3.7 Interfacial tension

Interfacial tension of canola oil and 1.0% (w/w) homogeneous LPI solution and LPI-polysaccharide solutions at their corresponding pH values was measured with the use of a Force Tensiometer-K20 (Kruss, Germany) and a Wilhelmy plate. In brief, 23 mL of solution was added into the glass cup, and the plate was lowered slowly to the air-solution surface. Then, 46 mL of oil

was added carefully on the top. The device measures the force on the plate due to wetting. Each measurement is taken every 3-min, and the results were collected when the standard deviation lower than 0.10 mN/m. Interfacial tension is calculated using the Wilhelmy equation:

$$\gamma = \frac{F}{L\cos(\theta)} \quad (4.4)$$

Where L is the length of the plate perimeter, and θ is the contact angle (normally complete wetting (θ = 0) is assumed. All measurements were performed in triplicate.

4.3.8 Continuous phase and emulsion viscosity

Continuous phase and emulsion viscosity were determined according to Hopkins et al., (2015) for 1.0% (w/w) LPI and LPI-polysaccharide solutions as well as emulsions, prepared as previously described. Each solution or emulsion (~0.6 mL) was placed onto a AR-G2 Rheometer (TA Instruments, New Castle, DE) equipped with a 40 mm diameter 2° acrylic cone. Apparent viscosity was measured as a function of shear rate (2 to 200 s^{-1}) and 10 data points were collected per logarithmic decade. Data was then fitted using the power-law model:

$$\log \text{viscosity} = (n-1) \log \text{shear rate} + \log m \quad (4.5)$$

where 'n' is the flow behavior index and 'm' is the consistency coefficient (which is equivalent to the apparent viscosity at 1 s^{-1}). All measurements were performed in triplicate.

4.3.9 Confocal laser scanning microscopy

Confocal laser scanning microscopy (CLSM) was carried out to image mixtures of 4:1 LPI-polysaccharide solutions at corresponding pH_{opt} at room temperature (Liu et al., 2010). Solutions were prepared in a similar manner as previous measurements. 0.01% (w/w) Rhodamine B (excitation by 543 nm and emission collected at 567 nm) was added into the solutions to bind with proteins. A Nikon Eclipse LV100 CLSM microscope (Nikon, Tokyo, Japan) was used to image the solutions. All mixtures were made in triplicate and 4 images were taken per slide with the use of 20x objectives lens.

LPI and LPI-polysaccharide stabilized emulsions prepared as previously described were also imaged through CLSM using 543 and 633nm lasers (Primozic, Duchek, Nickerson, & Ghosh, 2018). 0.01% (w/w) Nile red with a maximum excitation and emission wavelength of 543 nm and

573-613 nm, respectively was added into the canola oil to dissolve completely under stirring prior to homogenization. Fast green (0.1% w/w in water) with the excitation and emission at 633 and 650 nm, respectively was added after emulsions were made to bind with protein in the continuous phase such that the final concentration of fast green in the emulsion was 0.015% w/w. Similarly, emulsions were made in triplicate, and 4 images were taken per slide with the use of a 20x and a 40x objectives lens.

4.3.10 Statistics

A one-way analysis of variance with a Tukey HSD test was preformed to access differences for each critical pH for the various LPI mixtures, emulsion stability, emulsion initial droplet size, droplet charge, interfacial tension, consistency coefficient, and flow behavior index. All statistics were preformed using SPSS software.

4.4 Results and discussion

4.4.1 Composition

Chemical analysis found LPI to be comprised of 80.6% (d.b., dry weight basis) protein (N×6.25), 0.8% (d.b.) lipid, 13.0% (d.b.) carbohydrate, and 5.6% (d.b.) ash. CMC (0.7, 250 kDa) was comprised of 81.3% (d.b.) carbohydrate and 18.7% (d.b.) ash. GA was found to be comprised of 1.8% (d.b.) protein, 94.8% (d.b.) carbohydrate, 3.4% (d.b.) ash and negligible amounts of lipid. In contrast, AL and ι-C were found to have carbohydrate and ash levels of 73.9% (d.b.) and 26.1% (d.b.), and 71.2% (d.b.) and 28.8% (d.b.), respectively, with both lipid and protein levels considered to be negligible. Major mineral components included Na^+ (1.80%) and K^+ (0.67%) for LPI; Na^+ (8.20%) for CMC; K^+ (0.90%) and Ca^{2+} (0.70%) for GA; Na^+ (10.3%) for AL; and Na^+ (1.4%), K^+ (5.50%) and Ca^{2+} (4.00%) for ι-C. Further compositional data can be found in the Appendix (Table A1).

4.4.2 Effect of pH on the formation of electrostatic complexes between LPI and various anionic polysaccharides

The formation of electrostatic complexes between LPI and various anionic polysaccharides (i.e., CMC, GA, AL, and ι-C) during a turbidimetric pH titration is given in Figure 4.1, along with the homogenous LPI solution. Homogenous polysaccharide solutions were not shown in Figure

4.1 since the optical density (OD) readings were negligible. LPI control showed a bell-shaped OD profile between pH 6.8 and 2.0, with max OD reading of 0.465 occurring at pH 4.3. Overall, the addition of anionic polysaccharides caused a change from a bell-shaped curve to one highly skewed towards more acidic pH values due to the presence of high electrostatic repulsion between neighboring polysaccharide molecules. Only LPI-CMC and LPI-GA mixtures resulted in complexes with greater OD than the LPI control (Figure 4.1). It is believed that these mixtures formed more coacervate-type structures which gave aggregates containing more entrapped water than LPI alone (Stone et al., 2013).

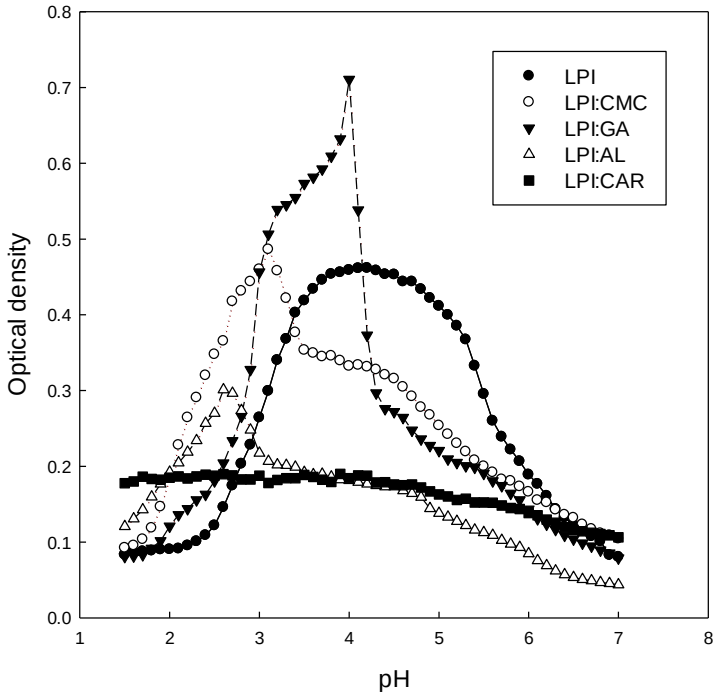

Figure 4.1 Complex coacervation behavior within mixtures of LPI and carboxymethyl cellulose (CMC), gum Arabic, alginate, and ι-carrageenan. Data represents the mean data points from triplicate curves (n = 3).

The critical pH values associated with the structure forming events for each mixture are given in Table 4.1. In the case of the LPI-CMC mixture, the formation of soluble complexes (denoted as pH_c) occurred at pH 6.8, well above the isoelectric point of LPI (pH 4.7, Figure 4.2A) where both biopolymers carried negative net charges (Table 4.1). Findings suggest that initial

interactions are of CMC with the positively charged patches on the protein's surface of LPI-LPI aggregates (Ye, 2008). The OD increased gradually till the pH reached $pH_{\phi 1}$ at 3.8, after which a significant rise in OD occurred indicating the formation of insoluble complexes. The slow rise between pH_c and $pH_{\phi 1}$ is thought to be associated with the formation of LPI-LPI aggregates via hydrophobic interactions which delayed some interactions with CMC chains (Stone et al., 2014). Maximum OD was reached at 0.486 at a pH corresponding to pH_{opt} (pH 3.1), where the LPI and CMC mixtures reached an electrical equivalence point (Kayitmazer, 2017; Stone et al., 2014) (Table 4.1). When the solution was further acidified, a rapid reduction in OD was observed suggesting the LPI-CMC complexes were disassociating as the carboxymethyl groups on the CMC chains were becoming protonated. Complete dissolution of LPI-CMC complexes occurred at $pH_{\phi 2}$ (pH 1.6). Similar to LPI-CMC system, LPI also interacts with gum Arabic through positively charged patches on the protein and negatively charged carboxylate groups. The LPI-GA mixture also was believed to form a coacervate resulting in a greater structure being formed than LPI alone. Associated critical pH values for pH_c, $pH_{\phi 1}$, pH_{opt}, $pH_{\phi 2}$ were at 6.8, 4.5, 4.0 and 1.9, respectively with max OD reaching 0.716 (Table 4.1). LPI-GA provided the greatest maximum OD among all the mixed systems. It might be due to the highly branched structure of the polysaccharide, which allowed intensive LPI-GA interactions through electrostatic attractions but also entrapped a greater amount of water within the structure by hydrogen bonding. de Kruif et al. (2004), Kayitmazer (2017), Singh et al. (2007) all indicated good coacervate formation when complexation is occurred with a protein and weakly charged (i.e., those with a low linear charge density). Figure 4.2A shows both CMC and GA are weakly charged relative to the other polysaccharides tested (< 40 mV). Electrostatic equilibrium point (EEP) was reached for both the LPI-CMC and LPI-GA mixtures at pH 3.1 and 3.7 (Figure 4.2B), respectively, which was very close to their pH_{opt} values (pH 3.0 and 4.0, respectively) (Table 4.1).

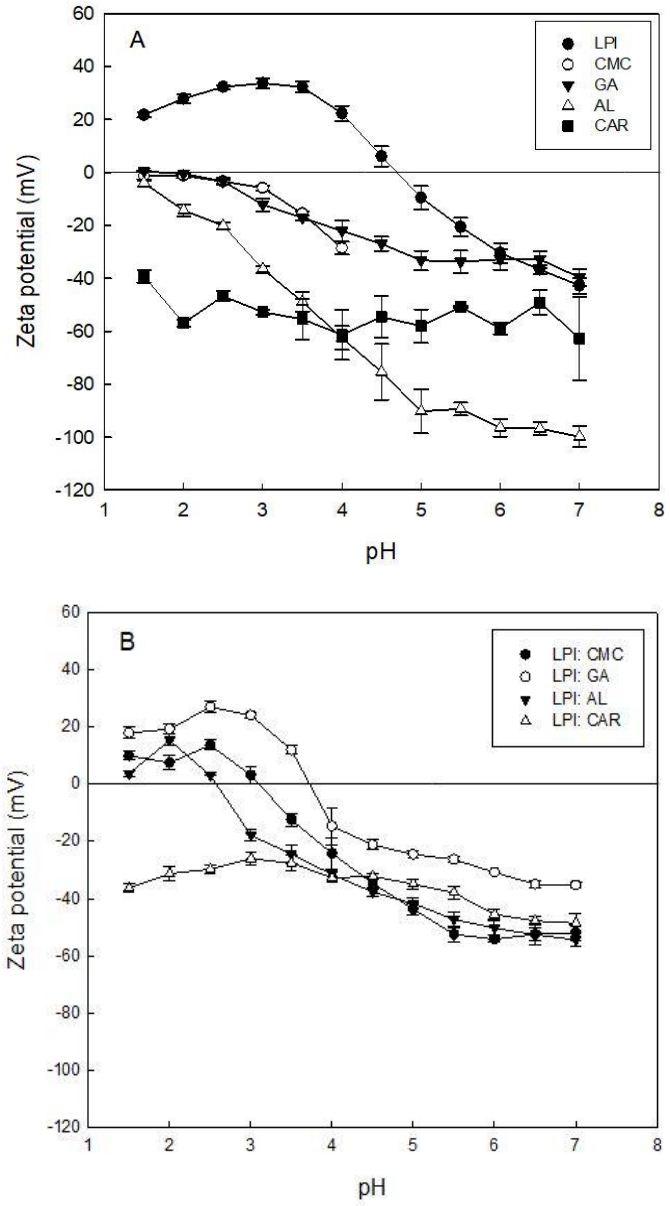

Figure 4.2 Zeta potential (mV) for homogenous (a) and mixed solutions (b) of lentil protein isolate (LPI) and carboxymethyl cellulose (CMC), gum Arabic (GA), alginate (AL) and ι-carrageenan ι-C). Data represents the mean ± one standard deviation (n = 3).

Table 4.1 Critical parameters associated with the complex coacervation for mixtures of lentil protein isolate with various anionic polysaccharides (4:1 blending ratio) relative to lentil protein isolate alone. Data represents the mean ± one standard deviation (n = 3).

Materials	**pH_c**	**$pH_{\phi 1}$**	**pH_{opt}**	**$pH_{\phi 2}$**	**Max. OD**	**EEP**
LPI (control)	6.93 ± 0.21^{a}	6.07 ± 0.06^{a}	4.25 ± 0.23^{a}	2.43 ± 0.12^{a}	0.465 ± 0.021^{b}	4.69 ± 0.12^{a}
LPI: CMC (DS 0.7, 250 kDa)	6.83 ± 0.15^{a}	3.83 ± 0.25^{c}	3.10 ± 0.00^{b}	1.63 ± 0.12^{bc}	0.486 ± 0.010^{b}	3.09 ± 0.09^{c}
LPI: Gum Arabic	6.83 ± 0.12^{a}	4.47 ± 0.06^{b}	4.03 ± 0.06^{a}	1.90 ± 0.10^{b}	0.716 ± 0.011^{a}	3.73 ± 0.07^{b}
LPI: Alginate	6.57 ± 0.15^{a}	3.57 ± 0.12^{c}	2.63 ± 0.06^{c}	1.43 ± 0.12^{c}	0.310 ± 0.010^{c}	2.58 ± 0.02^{d}
LPI: ι-Carrageenan	6.73 ± 0.06^{a}	Nil	4.00 ± 0.17^{a}	Nil	0.190 ± 0.010^{d}	Nil

Abbreviations:

- Lentil protein isolate (LPI) and carboxymethyl cellulose (CMC)
- Critical pH values corresponding to the formation of soluble complexes (pH_c), insoluble complexes ($pH_{\phi 1}$), optimal complexation (pH_{opt}) and the dissolution of complexes ($pH_{\phi 2}$).
- Optical density (OD)
- Electrical equivalence point (EEP)

In contrast, for both LPI-AL and LPI-ι-C mixtures significant chain repulsion of the polysaccharides was thought to occur due to their higher linear charge density resulting in suppression of LPI-LPI aggregation. It is presumed that precipitate structures were formed that trapped less water due to their stronger electrostatic interactions. Formed complexes tend to be smaller and fewer in number. In the case of LPI-AL, associated critical pH values for pH_c, $pH_{\phi 1}$, pH_{opt}, and $pH_{\phi 2}$ were at 6.6, 3.6, 2.6 and 1.4, respectively, with max OD reaching 0.310 which was lower than LPI alone (Figure 4.1, Table 4.1). Due to the pH sensitivity of alginates, charged carboxylate groups ($-COO^-$) along the AL backbone started to become protonated (-COOH) at pH 2.6; therefore, there would be less attraction to form LPI-AL complexes resulting a small maximum OD value of 0.310. The OD curve was also skewed significantly towards lower pH values, and that might be because of the stronger Coulombic forces between positively charged LPI and more negatively charged AL (Stone et al., 2014). In contrast, LPI- ι-C mixtures resulted in even greater precipitation where initial interactions occurred at pH 6.7, and then gradually increased to a max OD at pH 4 without ever going through a transition between pH_c and $pH_{\phi 1}$, nor a dissolution of complexes at $pH_{\phi 2}$ (Figure 4.1, Table 4.1). It was suggested that the strong suppression of LPI-LPI aggregates was caused by the strong electrostatic repulsion between carrageenan polysaccharides associated with the negative charge of sulfate group (Stone et al., 2013). The sulfate group has a pK_a of -10, no protonation could occur during the entire acidic titration; therefore, the OD of the solution was stable at around 0.19 from pH 4.0 to 1.5. It also indicated that at 4:1 ratio ι-carrageenan was saturated, and there should be free sulfate group on ι-carrageenan in the solution. Surface charge as a function of pH for both AL and ι-C given in Figure 4.2A, showing AL to have much greater charge at pH >4, then less charge than ι-C at pH <4. This corresponds to lower OD readings in the turbidity plot for AL than ι-C at pH >4, and more LPI-AL interactions at pH <4 than LPI-ι-C. Surface charge on both AL and ι-C was much greater than CMC and GA (Figure 4.2A) to cause the differences in types of complexes formed (i.e., coacervate vs. precipitate). EEP for the LPI-AL mixture was found to occur at pH 2.6 (Figure 4.2B, Table 4.1), which corresponded to pH_{opt} (pH 2.6) from Figure 4.1. EEP was not obtained in the case of the LPI-ι-C mixture.

Confocal laser scanning microscopy (CLSM) images of LPI and LPI-polysaccharide mixtures taken at their respective pH_{opt} are shown in Figure 4.3. LPI alone showed a few medium sized aggregates (Figure 4.3A). The addition of LPI-CMC resulted in a few large aggregates

(Figure 4.3B), whereas the addition of GA resulting in the formation of many media to large sized aggregates in solution (Figure 4.3C), which was most likely the cause of the highest OD readings from Figure 4.3. In contrast, LPI interactions with more highly charged polysaccharides showed the formation of a few, very small aggregates in the case of LPI-ι-C (Figure 4.3D) relative to LPI alone, which is reflective by the lowest OD reading, and the formation of a few large aggregates in the case of LPI-AL (Figure 4.3E). The fewer structures would allow more light to pass than the LPI-CMC mixture which also had large aggregates but greater in number (Figure 4.3B, E).

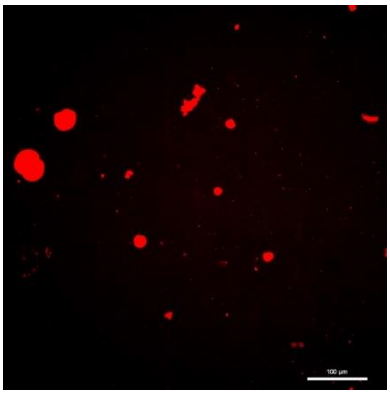

A) LPI alone

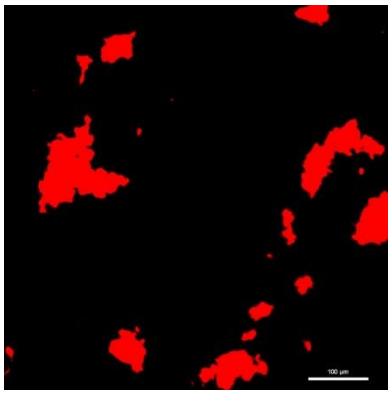

B) LPI-CMC

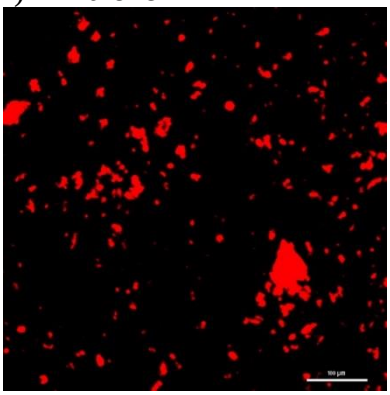

C) LPI-GA

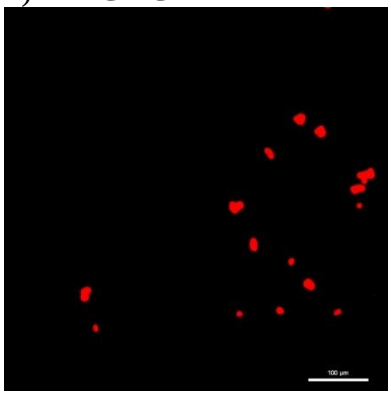

D) LPI-CAR

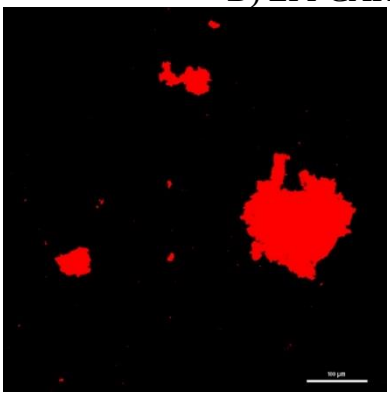

E) LPI-AL

Figure 4.3 Confocal laser scanning microscopy images of LPI alone and mixtures LPI with carboxymethyl cellulose (CMC) (B), gum Arabic (GA) (C), ι-carrageenan (ι-C) (D) and alginate (AL) (E) taken at pH_{opt}. The scale bar represents 100 μm.

4.4.3 Emulsifying properties of formed LPI-polysaccharide complexes

The emulsion stability (via creaming) of LPI and LPI-polysaccharide complexes (at pH_{opt}) stabilized oil-in-water emulsions over time was examined and presented in Table 4.2. Unlike the turbidity studies, total biopolymer concentration was increased to 1.0% (w/w) in the aqueous phase of the emulsion. For LPI-stabilized emulsions, ES was found to be 94% after 30 min but then dropped to ~75% after 24 h, where it remained constant for the 3-d trial ($p>0.05$) (Table 4.2). It is hypothesized that a steady state for ES data was not reached until after 24 h since: a) the integration of LPI into the interface had not reached an equilibrium state; and b) insoluble LPI-LPI aggregates where gradually precipitating over that period leading to disruption of formed oil droplets. In the case of the latter, after 24 h only soluble LPI-LPI aggregates were thought to be present leading to more stable ES values. At this point, the interface is thought to be stabilized by both electrostatic and steric forces. ι-C was the only system to lead to an increase in ES relative to LPI alone, where ES was found to be 100% after 30 min, and then gradually declined to 81% after 3-d (Table 4.2). In contrast, the addition of CMC, GA and AL all led to a decrease in ES relative to LPI alone in decreasing order, where ES was found to be 78%, 81% and 63%, respectively after 30 min. Like LPI alone, ES of LPI-GA dropped after 24 h to become 65% ($p<0.05$) then becoming stable ($p>0.05$), but the decline of ES of LPI-CMC and LPI-AL were minor ($p>0.05$) after 30min (Table 4.2).

The stability of the emulsion can be impacted by coverage of the viscoelastic film, charge on the film, size/conformation of the biopolymers/aggregates, and the continuous phase viscosity, all of which acts to inhibit coalescence which leads to gravitational separation (McClements, 2007; Stone et al., 2013; Walstra & van Vliet, 2008). In order to produce a stable emulsion, surface active biopolymers must migrate, adsorb and become integrated into the oil-water interface to reduce the interfacial tension (Uruakpa & Arntfield, 2005; Walstra & van Vliet, 2008). At the interface, biopolymers re-align to position hydrophobic amino acids towards the oil phase and hydrophilic moieties towards the aqueous phase. The speed of the biopolymers to migrate and the ability of the biopolymers to re-align at the interface would greatly influence the formation of emulsion, droplet size and distribution, as well as emulsion stability.

Table 4.2 Critical parameters of for emulsions stabilized by homogeneous lentil protein isolate (LPI) solutions and mixtures of LPI with various anionic polysaccharides at 4:1 blending ratio. n = 3).

Properties	**LPI**	**LPI-CMC**	**LPI-GA**	**LPI-AL**	**LPI-ι-C**
Emulsion stability (%)					
0.5 h	94.2 ± 1.4^{A}	77.7 ± 4.0^{A}	80.8 ± 2.9^{A}	62.5 ± 2.5^{A}	100.0 ± 0.0^{A}
24 h	75.8 ± 1.4^{B}	71.7 ± 4.4^{A}	65.0 ± 0.0^{B}	57.5 ± 4.3^{A}	92.5 ± 4.3^{AB}
48 h	75.4 ± 0.7^{B}	70.0 ± 5.0^{A}	65.0 ± 0.0^{B}	56.7 ± 5.8^{A}	87.5 ± 2.5^{BC}
72 h	74.2 ± 0.7^{B}	68.3 ± 2.9^{A}	64.2 ± 1.4^{B}	55.8 ± 5.2^{A}	80.8 ± 3.8^{C}
Droplet size D[3.2] (μm)	39.4 ± 0.8^{c}	88.8 ± 4.2^{a}	70.0 ± 1.2^{b}	336.6 ± 49.4*	15.7 ± 1.5^{d}
Droplet charge (mV)	-2.5 ± 1.5*	N/A	N/A	N/A	-49.1 ± 0.7*
Interfacial tension (mN/m)	10.3 ± 0.2^{c}	12.8 ± 0.1^{a}	11.7 ± 0.3^{b}	13.5 ± 0.1^{a}	13.4 ± 0.5^{a}
Continuous phase viscosity					
a) Consistency coefficient (mPa s)	0.02 ± 0.00^{c}	0.02 ± 0.00^{c}	0.01 ± 0.02^{c}	0.040 ± 0.01^{b}	0.07 ± 0.00^{a}
b) Flow behavior index	0.58 ± 0.02^{b}	0.56 ± 0.03^{a}	0.71 ± 0.05^{bc}	0.45 ± 0.07^{c}	0.59 ± 0.00^{ab}
Emulsion viscosity					
a) Consistency coefficient (mPa s)	0.51 ± 0.05^{c}	2.51 ± 0.03^{b}	0.97 ± 0.10^{c}	1.92 ± 0.32^{b}	3.38 ± 0.44^{a}
b) Flow behavior index	0.61 ± 0.02^{a}	0.33 ± 0.00^{b}	0.39 ± 0.03^{b}	0.23 ± 0.04^{c}	0.40 ± 0.02^{b}

- Data represents the mean ± one standard deviation
- Abbreviations: (LPI) lentil protein isolate, (CMC) carboxymethyl cellulose, (GA) gum Arabic, (AL) Alginate and (ι-C) ι-carrageenan.
- *Denotes samples that were not included in the statistical analysis
- Upper letters indicate comparison within samples over time for emulsion stability
- Lower letters indicate comparison between samples for other properties

Droplet size distributions measured immediately after homogenization showed a mono-distributed curve skewed slightly towards small mean droplet sizes for all systems except LPI-ι-C stabilized emulsion (Figure A4.1, Appendix). LPI-ι-C emulsion showed two peaks with one peak at about 5 µm and the other peak at 40 µm, which was confirmed in confocal image (Figure 4.4E). Mean particle diameter (D [3,2]) in each emulsion is given in Table 4.2. The LPI-stabilized emulsion (control) was found to have average droplets of 39 µm, whereas only the LPI-ι-C mixture produced smaller droplet sizes of 16 µm which contributed to the more stable emulsions (Table 4.2). In contrast, droplet size increased to 70 µm, 89 µm and 337 µm in systems stabilized by LPI-GA, LPI-CMC and LPI-AL, respectively (Table 4.2).

Interfacial tension (IT) for all five systems was measured at their corresponding optimal pH values (pH_{op}) (Table 4.2). The interfacial tension was lowered from 21.9 mN/m (control, oil/water) to 10.3, 11.7, 12.8, 13.5 and 13.4 mN/m for LPI alone, LPI-GA, LPI-CMC, LPI-AL, and LPI-ι-C, respectively suggesting that all systems were surface active. During the measurements, settling of the insoluble complexes was observed for all systems indicating the interfacial tension was most likely lowered by soluble complexes. It is worth nothing that interfacial tension increased for all LPI-polysaccharide systems compared to LPI alone, which suggests that the interactions between LPI and polysaccharides under complexation could limit the re-alignment of proteins to position properly on the interface leading to lower emulsion stability and larger droplet formation for LPI-CMC, LPI-GA, and LPI-AL systems. However, LPI-ι-C system displays the highest interfacial tension but provides the highest emulsion stability and the smallest droplet size indicating other factors might be playing important roles.

The number and size of structures will impact the resulting droplet sizes. In terms of biopolymer conformation, formed complexes were quite small and numerous in the case of the LPI-ι-C system (lowest OD in Figure 4.1) allowing it to migrate to the interface faster versus the other mixtures and LPI alone, which led to the smallest mean droplet-size formation (Figure 4.3D). The larger droplet sizes, particularly with LPI-AL relative to LPI alone most likely reflects the size/conformation of complexes formed (Figure 4.3E) and their reduced ability to migrate and align at the oil-water interface. The slower the diffusion to the interface, and the less integration to cover the interface will lead to larger droplet sizes and reduced emulsion stability. Furthermore, both the LPI-CMC and LPI-GA complexes were larger than the LPI-LPI aggregates ($p<0.05$) leading to their reduced ability to migrate as well (Figure 4.3A-C).

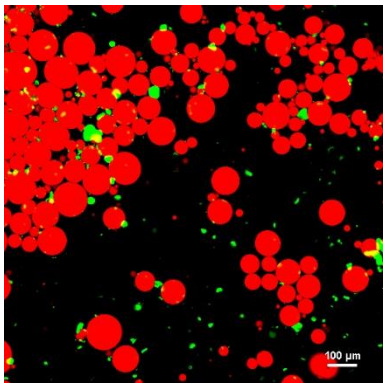

A) LPI

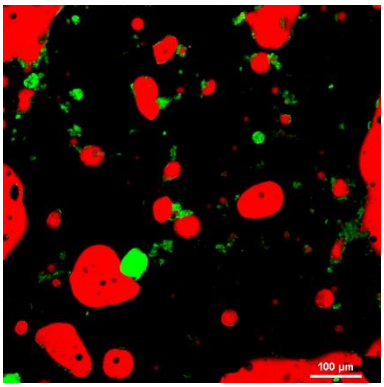

B) LPI-Carboxymethyl cellulose

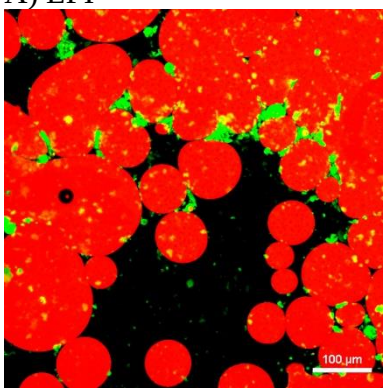

C) LPI-Gum Arabic

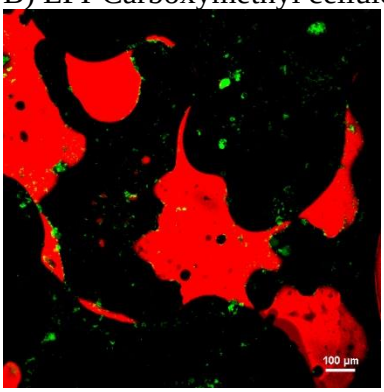

D) LPI-Alginate

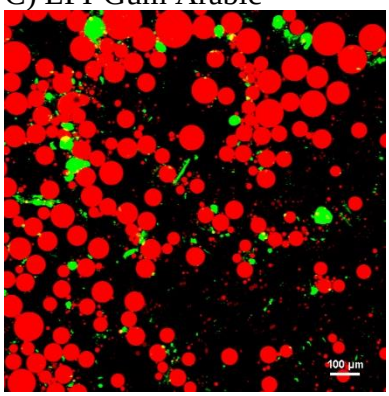

E) LPI-ι-Carrageenan

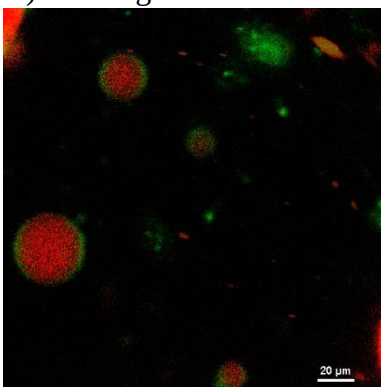

F) LPI-ι-Carrageenan (40x objective)

Figure 4.4 Confocal scanning laser microscopy images oil-in-water emulsions stabilized by lentil protein isolate (LPI) (A), and mixtures of LPI and carboxymethyl cellulose (B), gum Arabic (C), alginate (D) and ι-Carrageenan (E, F).

The charge on the droplets could provide electrostatic repulsion effects to enhance emulsion stability, as shown in Table 4.2. Due to the large droplet formation of LPI-GA, LPI-CMC, and LPI-AL stabilized emulsions, measurement of the droplet charge for these emulsions could not be made since the droplets were easily disrupted during the dispersion process. Droplet

charge of LPI-ι-C emulsion was found at -49.1 mV suggesting sufficient electrostatic repulsive forces were generated to against droplet aggregation. During emulsification, the protein from the LPI-ι-C complexes would unfold to expose the hydrophobic moieties to align inward to the oil phase and leaving the carrageenan outward to the aqueous phase leading to the increase of the charges compared to LPI-ι-C solution of -33 mV (Figure 4.2B). Electrostatic repulsion was thought to be minimal since all other systems were prepared at corresponding pH_{opt} where the net surface charge of the biopolymer mixture was zero. For example, droplet charge of LPI emulsion was -2.5 mV (Table 4.2).

Emulsion rheology could affect emulsion stability as well. Flow curves of continuous phase and emulsion viscosities for each system, given in Figure A4.2 (Appendix), were subsequently fitted using the Power-law model to determine the consistency coefficient (m, equivalent to the apparent viscosity at 1 s^{-1}) and the flow behavior index (n, describing the level of pseudoplastic behavior of the material) (Table 4.2). Emulsion viscosity (as described by the consistency coefficient, Table 4.2) was substantially greater for the LPI-ι-C mixture than the other systems ($p<0.05$), followed by LPI-CMC and LPI-AL ($p>0.05$), and then LPI-GA and LPI ($p>0.05$). The highest viscosity of LPI-ι-C emulsion can be attributed to the largest continuous phase viscosities (Table 4.2). LPI-ι-C solution displayed the largest continuous phase viscosity ($p<0.05$), followed by LPI-AL, LPI-CMC, LPI, and then LPI-GA systems. It is hypothesized that because of the higher electrostatic repulsion in the LPI-ι-C system, a greater amount of unbound ι-C chains will be present contributing to contribute to the higher continuous phase viscosity resulting higher emulsion viscosity. ι-Carrageenan is also more well known for its thickening and gelling abilities (depending on the salts present in solution) than the other polymers, in part because of its larger hydrodynamic volume (Doublier et al., 2017). The continuous phase viscosities could also be attributed to the number and sizes of insoluble complexes formed. LPI-AL solution formed the largest complexes and displayed a higher viscosity, while LPI and LPI-GA formed smaller complexes and thus displayed lower viscosities. The high continuous phase viscosity might also lead to small droplets formation. In order to produce small droplets, an optimum range of disperse-to-continuous phase viscosity ratios ($\frac{\eta_D}{\eta_C}$) needs to be achieved (Qian & McClements, 2011; Wooster et al., 2008). In this study, LPI-ι-C emulsion might display the proper $\frac{\eta_D}{\eta_C}$ resulting small droplets formation. It was found that the mean droplet diameter decreased with increasing

continuous phase viscosity in a β-lactoglobulin emulsion system (Qian & McClements, 2011). It was thought to due to the higher emulsion viscosity of LPI-ι-C, LPI-CMC and LPI-AL, the decreased of ES from 30 min to 24 h of these systems ($p>0.05$) were smaller than less viscous LPI-GA and LPI ($p<0.05$). The addition of polysaccharides also resulted in increased pseudoplastic behavior for emulsions relative to LPI alone, where 'n' decreased from 0.61 for LPI ($p<0.05$), to 0.33, 0.39, 0.40 for LPI-CMC, LPI-GA and LPI-ι-C which were similar ($p>0.05$), and then decreased to 0.23 for LPI-AL ($p<0.05$) (Table 4.2). For continuous phase solutions, LPI, LPI-CMC, and LPI-ι-C preformed similar pseudoplastic behavior ($p>0.05$), and LPI-AL displayed increased pseudoplastic behavior than LPI control ($p<0.05$), while LPI-GA displayed lower pseudoplastic behavior ($p<0.05$). During shearing, viscosity is reduced as oil droplets become elongated and break apart, complexes disassociate, and biopolymers become streamlined within the shear field. Because of this, changes to emulsion viscosity are presumed to be irreversible.

All five emulsions were imaged using confocal microscopy (Figure 4.4). Due to the large droplet formation, droplets of LPI-CMC, LPI-GA, and LPI-AL stabilized emulsions disrupted during preparation of slides (Figure 4.4B-D). LPI-ι-C emulsion image showed two groups of different-sized droplets with one at 2 µm and the other around 40 µm agreed with the two peaks present in droplet size distribution curve (Figure A4.1, Appendix). Image of LPI emulsion showed most droplets were 30-50 µm with a few larger at around 100 µm corresponding to the droplet size distribution (Figure 4.4a, Figure A4.1, Appendix). Confocal images confirmed that oil droplets were covered by LPI/LPI-polysaccharide viscoelastic film; an example was taken from LPI-ι-C (Figure 4.4F), and more LPI/LPI-polysaccharide complexes were observed in the continuous phase (Figure 4.4A-D). That confirms the hypotheses of soluble complexes aligning on the interface to lower the interfacial tension and insoluble complexes contributing to the continuous phase viscosities.

4.5 Conclusions

Complexation behaviour between LPI and four anionic polysaccharides (CMC, GA, AL, and ι-C) at 4:1 LPI-polysaccharide mixing ratio was evaluated, as well as their resulting emulsifying properties. LPI-CMC and LPI-GA mixtures formed coacervate-type structures with OD_{max} occurring at 0.486 and 0.716, respectively, whereas LPI-AL and LPI-ι-C formed precipitate-type of structures with lower OD_{max} values occurring at 0.310 and 0.190, respectively.

Critical pH values (pH_c, $pH_{\phi 1}$, pH_{opt}, $pH_{\phi 2}$) of four mixtures varied significantly. LPI-ι-C stabilized emulsion showed the greatest stability due to the small droplet sizes and higher continuous phase and emulsion viscosity as well as negatively charged droplets formation than the LPI and other LPI-polysaccharide mixtures. They also formed much smaller complexes in solution due to the large electrostatic repulsive forces exerted between ι-C chains in solution. All emulsions stabilized by the other LPI-polysaccharide mixtures showed lower stability than LPI (only) stabilized emulsions mainly due to the larger complex's sizes and droplet size as well as higher interfacial tension, all of which were hypothesized to inhibit their ability to migrate and align at the oil-water interface to form a stable viscoelastic film that prevented coalescence and oil droplet growth.

4.6 Linkage to the next study

Coacervate-type structures were formed within LPI-GA and LPI-CMC systems, and their resulting complexes showed greater OD than the LPI control. In contrast, LPI-AL and LPI-ι-C mixtures resulted precipitate-type structure with lower OD values. The structural differences of the complexes led to different functional properties. In this chapter, emulsifying properties of the resulting insoluble complexes at their corresponding pH_{opt} were examined. The findings suggested that only LPI-ι-C stabilized emulsion showed greater emulsion stability compared to the control LPI emulsion. Therefore, the emulsifying property of LPI-carrageenan complexes were continuously investigated in the next study, and kappa-carrageenan was also introduced to compare with iota-carrageenan as the number of sulfate groups differed. Since this study only examined the emulsifying properties of the insoluble complexes, the resulting soluble complexes were also under consideration for the next study. In Chapter 5, the complexation behavior of LPI-kappa-carrageenan and -iota-carrageenan were investigated, and the emulsifying properties of their resulting soluble and insoluble complexes were also examined.

5. EFFECT OF BIOPOLYMER MIXING RATIOS AND AQUEOUS PHASE CONDITIONS ON THE INTERFACIAL AND EMULSIFYING PROPERTIES FOR LENTIL PROTEIN ISOLATES- κ-CARRAGEENAN AND -ι-CARRAGEENAN COMPLEXES[3]

5.1 Abstract

The use of plant protein ingredients within the food industry is increasing rapidly due to their lower cost, greater environmental sustainability, perceived safety concerns related to consuming animal products, and consumer dietary preferences. Lentil protein, as an emerging non-soy, gluten-free, plant-based protein could play more important role in food processing. However, plant proteins generally contribute lower solubility than animal proteins; incorporation of polysaccharides such as carrageenan could tailor the functionality of lentil protein. This work aimed to investigate the complexation behavior between lentil protein isolate (LPI) and carrageenan (κ-carrageenan: κ-C and ι-carrageenan: ι-C) as a function of pH and biopolymer mixing ratio, and the emulsifying properties of their resulting soluble and insoluble complexes. Incorporation of both κ-C and ι-C into the LPI solution led to the suppression of large protein aggregates being formed during a turbidimetric pH acid-titration. As LPI-carrageenan mixing ratio decreased, maximum optical density (max OD) values for both LPI-κ-C and LPI-ι-C systems decreased. Emulsions made at pH 6 showed higher emulsion stability than those made at pH 3.5

[3] Wang, Y., Ghosh, S., & Nickerson, M. T. (2021). Effect of biopolymer mixing ratios and aqueous phase conditions on the interfacial and emulsifying properties of lentil protein isolate–κ-carrageenan and lentil protein isolate–ι-carrageenan complexes. Cereal Chemistry. https://doi.org/10.1002/cche.10465 (*Reproduced with permission*). Y. Wang contributed to the experimental design, data collection and analysis and drafting of the manuscript; S. Ghosh was second reader on the manuscript; whereas M. Nickerson was the primary supervisor, contributed to the experimental design and acted as corresponding author for the manuscript.

for each sample. Emulsions at pH 6 also formed smaller, more uniform, and higher charged droplets, and showed lower interfacial tension. 4:1 LPI-κ-C and 4:1 LPI-ι-C emulsions at pH 6 showed higher emulsion viscosity and higher corresponding continuous phase viscosity. Soluble and insoluble complexes were formed between LPI and both carrageenan polysaccharides through electrostatic interactions at pH 6 and pH 3.5, respectively. Emulsions prepared at pH 6 showed higher stability than emulsions at pH 3.5, where the highest emulsion stability was contributed to 4:1 LPI-κ-C and 4:1 LPI-ι-C emulsions. Lentil protein interacted with carrageenan through electrostatic attraction, where soluble complexes were formed between the positive patches on LPI and negatively charged carrageenan, and insoluble complexes were formed between positively charged LPI and negatively charged carrageenan. Both types of electrostatic complexes were used to prepare emulsions, and soluble complexes were shown to contribute better emulsion stability than insoluble complexes. Preparation of the stable LPI-carrageenan based emulsion is a low-cost, non-solvent, and relatively easy process, which shows potential for further food applications.

5.2 Introduction

Emulsions are dispersions of two or more immiscible liquids where one phase is dispersed as small droplets in the other. They are stabilized using emulsifiers, which are surface active components that can be absorbed onto the oil-water interface due to their amphiphilic nature (McClements, 2015). Protein stabilized emulsions have been studied extensively (Djordjevic et al., 2004); however, their stability can be affected by environment stresses such as pH, ionic strength, and temperature (Yin et al., 2012). Incorporating polysaccharides to proteins under proper conditions could achieve a more stable emulsion by changing the charge of the system, increasing the thickness of the interfacial layer to provide steric repulsion, and modifying emulsion rheology (McClements, 2015; Yin et al., 2012). Emulsions can be prepared using the premixed protein-polysaccharide complexes stabilized through electrostatic attraction, where a mixed layer is aligned at the interface to stabilize emulsion (Evans et al., 2013). Preparing protein-polysaccharide based emulsion is a simple, solvent-free, non-thermal, and low-cost process, and the emulsion can be applied in a series of food products, such as microencapsulation and emulsion-based edible films (Schmitt et al., 1998). Studies have been conducted on emulsions prepared using protein-polysaccharide electrostatic complexes such as β-lactoglobulin-carboxymethyl cellulose (Chuah et al., 2014), soy protein-soy polysaccharide (Yin et al., 2012), milk protein-carboxymethyl

cellulose (Koupantsis et al., 2014), and ovalbumin- carboxymethyl cellulose (Xiong et al., 2020). Chuah and co-authors (2014) found that the incorporation of carboxymethyl cellulose into β-lactoglobulin was able to improve emulsion stability compared to β-lactoglobulin stabilized emulsion; however, the mixed layer emulsion was also affected by biopolymer concentration ratios and pH. Similar findings were also observed by Xiong and co-authors (2020). They found that the content of ovalbumin-carboxymethyl cellulose complex increased as pH decreased, and a higher emulsion stability was conducted when the system pH increased.

The complexation event between proteins and polysaccharides can be identified during an acid titration (Ye, 2008). The initial point of protein-polysaccharide interaction can first be detected at a slight reflection in optical density (OD) at pH_c, also indicating the formation of soluble complexes. As pH is lowered, more soluble complexes will form until the system reaches a critical pH called $pH_{\phi 1}$, which is the formation of insoluble complexes due to significantly greater and stronger protein-polysaccharide interactions. A large rise is observed in turbidity after $pH_{\phi 1}$, and a maximum turbidity (max OD) will reach at pH_{opt}, where the protein-polysaccharide mixtures reach an electrical equivalence point (EEP). Protein-polysaccharide complexes will start to break up as pH is further lowered, due to the protonation of the reactive side chains on the anionic polysaccharides. The disassociation of the electrostatic complexes will complete at $pH_{\phi 2}$. (Schmitt et al., 1998; Turgeon & Gauthier, 2004; Ye, 2008). In addition to pH, the resulting electrostatic complexes also varies differently based on the biopolymers used (i.e. type and density of the functional groups), and the biopolymer mixing ratio (Schmitt et al., 1998). For instance, suppression of the formation of large protein-protein aggregates can occur in the mixed systems involving highly charged polysaccharides. Formation of smaller complexes was observed in the system of lentil protein-carboxymethyl cellulose of higher charge density (Wang et al., 2019a). Influence of biopolymers with different charge densities on the size and number of complexes formed was also observed in pea protein – pectin systems, where a high methoxy pectin (i.e. less carboxyl group) flavoured the interaction with pea protein, leading to the formation of a larger number and size of complexes (Warnakulasuriya et al., 2018). The biopolymer-mixing ratio affects the overall charge balance of the protein and polysaccharide, impacting the degree of the interaction. At a specific mixing ratio, soluble complexes will be achieved when excess positive or negative charges present in the system due to the excess of one of the biopolymers, while the maximum yield of the complexes is reached when the overall charge of the complexes is neutral

(Girard et al., 2004; Schmitt et al., 1998; Ye, 2008). The differences in size and structure of soluble and insoluble complexes in a pea protein isolate-gum Arabic system was investigated by Liu and co-authors (2010), and they found that irregularly shaped complexes were formed during the titration and soluble complexes were smaller in size compared to insoluble complexes. The difference in charge, size, and extent of interaction between soluble and insoluble complexes suggested that they might contributed different emulsifying properties to affect the stability of their resulting emulsions.

As biopolymers significantly affect complex interactions and the resulting emulsion's stability, selection of the biopolymer is critical. More attentions have been drawn to lentil proteins due to their abundance, low cost, low allergenicity, and good functional properties such as high solubility among plant proteins and good emulsifying properties (Graca et al., 2016; Liang & Tang, 2014). A popular way to prepare lentil protein isolates (LPI) from lentils is through alkaline extraction followed by isoelectric precipitation or ultrafiltration, then drying (Can Karaca et al., 2011). The dominant proteins in lentil proteins are globulin-type and albumin-type with 50-65% and 10-25% of the total proteins, respectively (Gueguen & Barbot, 1988; Jarpa-Parra, 2018). Carrageenan is extracted from marine algae (red seaweeds) from the class *Rhodophyceae* (Necas & Bartosikova, 2013). Carrageenan is commonly used in food products due to their excellent gelling, thickening, and texture improving properties and is also applied to the control-released system due to the high encapsulation efficiency (Li et al., 2014; Van de Velde et al., 2002). Carrageenan is a linear sulfated polygalactan containing 15 to 40% of ester-sulfate with molecular mass above 100,000 and generally forms gel in the present of cations. Carrageenan can be classified into three types based on the number of sulphate groups per disaccharide unit which are kappa-1 (κ-), iota-2 (ι-), and lambda-3 (λ-) (Necas & Bartosikova, 2013). κ-Carrageenan and ι-carrageenan are gelling polysaccharides whereas λ-carrageenan is more contributed to thickening (Li et al., 2014). As κ- and ι-types are more closely related in terms of their functional attributes and developing a weak gel network could possibly help to improve emulsion stability, this study focused on κ- and ι-carrageenan only.

Our previous work (Wang et al., 2019b) worked on the complexation behavior between LPI and different polysaccharides (e.g. gum Arabic, carboxymethyl cellulose, alginate, and iota-carrageenan), and their emulsifying properties of the resulting insoluble complexes were examined. The most stable emulsion was attributed to LPI-ι-C insoluble complexes stabilized emulsions.

Therefore, this study continues to explore the complexation behavior and emulsifying behavior between LPI and carrageenan polysaccharides. The overall goals of this study are to investigate the complexation behavior of LPI-κ-C and LPI-ι-C as a function of biopolymer mixing ratio and pH, and to achieve the most stable emulsion by selecting the resulting mixtures with different structures and functions (i.e. soluble complexes vs insoluble complexes).

5.3 Materials and methods

5.3.1 Materials

Lentil protein isolate (LPI) used in this project was kindly donated by KeyLeaf Corp. (Saskatoon, SK) prepared using an alkaline extraction process (pH 9.5) followed by isoelectric precipitation (pH 4.5). κ-Carrageenan (κ-C; Lot#: 0001432063) and ι-carrageenan (ι-C; Batch #: 075K1808) were purchased from Sigma-Aldrich Co (Oakville, ON, Canada). Canola oil was purchased from a local supermarket. All other reagent-graded chemicals used in this study were also purchased through Sigma-Aldrich Co (Oakville, ON, Canada).

5.3.2 Proximate analysis

Proximate analysis of all materials including moisture, ash, lipid and crude protein (reported on a dry weight basis (d.b.)) was determined according to the Association of Official Analytical Chemists (AOAC) methods 925.10, 923.03, 920.85, and 920.87, respectively (AOAC, 2003). Carbohydrate content was calculated based on percent differential from 100%. Lentil protein isolate (LPI) was found to contain 80.6% (d.b.) protein, whereas κ- (κ-C) and ι- (ι-C) carrageenan had 77.6% (d.b.) and 71.2% (d.b.) carbohydrate, respectively. Complete proximate composition results are given in Table A1 (Appendix).

5.3.3 Turbidimetric measurements

Turbidimetric measurements of biopolymer solutions with a total biopolymer concentration of 0.05% were determined though a turbidimetric pH titration according to Wang et al. (2019b) at 4:1, 8:1, and 12:1 protein to polysaccharide mixing ratios. The critical pH values (pH_c, $pH_{\phi 1}$, pH_{opt} and $pH_{\phi 2}$) associated with phase changes within LPI-carrageenan mixtures as a function of pH (7.0-1.0) were also investigated. Biopolymer solutions were prepared by dissolving each powder in Milli-Q water at 500 rpm for 2 h at room temperature (21-23 °C) and then overnight

at 4 °C. The solutions were then stirred for 30 min at room temperature and mixed to different mixing ratios prior to measurements. Solutions were acidified under mechanical stirring of 750 rpm with the addition of 0.05% (w/w) glucono-δ-lactone (GDL) (pH from 8.0 to ~4.3) and 0.1, 0.5 and 2 N HCl (pH from 4.3 to 1.0, as the decrease of pH due to GDL became minor). The changes in the optical density (O.D.) of the solutions were measured using an ultraviolet-visible spectrophotometer (Genesys 10, Thermo Scientific, Fair Lawn, NJ, USA) at 600 nm. The critical pH values of pH_c, $pH_{\phi 1}$, and $pH_{\phi 2}$ were the intersection points of two curved tangents, determined graphically. Measurements were performed in triplicated fresh solutions. All the critical values were reported as the mean ± one standard deviation (n = 3). The homogenous LPI and both carrageenan solutions were used as controls.

5.3.4 Emulsion preparation

Twenty milli-liters of 20/80 (w/w) oil-in-water coacervate-type emulsions were prepared using homogeneous LPI or LPI-carrageenan solutions at 4:1, 8:1, and 12:1 protein to polysaccharide mixing ratios as a function of pH (3.5 & 6.0) at room temperature (21-23 °C). Biopolymer solutions were prepared similarly as in turbidimetric measurements with the total biopolymer concentration increased to 1.0% (w/w). The pH of solutions was adjusted to pH 3.5 or 6 (selected based on turbidimetric results) using 2 N and 0.2 N HCl, followed by 1 h of stirring (750 rpm). Emulsions were homogenized using a rotor stator system (Polytron PT2100 homogenizer) (Kinematica AG, Lucerne, Switzerland) equipped with a 12 mm PT-DA 2112/2EC generating probe for 5 min at 15,000 rpm. All emulsions were prepared in triplicate.

5.3.5 Zeta potential

The surface charge of mixed and homogeneous biopolymer solutions, prepared similarly in the turbidimetric measurements, was determined over a pH range of 8.0–1.5 with every 0.5 pH increment at 22.5 °C using a Zetasizer Nano-ZS90 (Malvern Instruments, Westborough, MA) (Wang et al., 2019b). For the emulsions' droplet charge, ten drops of each of the fresh emulsion were dispersed into 100 mL Milli-Q water at the corresponding pH values, and the dispersions were shaken gently to become homogeneous and used for measurement.

The electrophoretic mobility (i.e., velocity of a particle within an electric field, U_E) was used to calculate the zeta potential (ς) by using the Henry equation.

$$U_E = \frac{2\varepsilon \times \xi \times f(\kappa\alpha)}{3\eta} \quad (5.1)$$

where η is the dispersion viscosity (water in this study), ε is the permittivity. $f(\kappa\alpha)$ equals to 1.5 according to the Smoluchowski approximation and is a function related to the Debye length (κ) and the ratio of particle radius (α). Measurements were performed in triplicate, and results were reported as the mean ± one standard deviation (n = 3).

5.3.6 Emulsion stability (ES)

Emulsion stability was determined according to Stone et al. (2013) based on creaming for 0.5, 24, and 48 h at room temperature (21-23 °C). For comparison purpose, emulsions of homogeneous κ-C and ι-C at 1% (w/w) and concentrations equivalent to the carrageenan amount (w/w) at their corresponding emulsions at 4:1, 8:1, 4:1 mixing ratios at pH 6 and 3.5 were also prepared similarly to determine ES. Ten milli-liters of each fresh emulsion was transferred to a 10 mL graduated cylinder (inner diameter = 9.60 mm; height = 114.96 mm) and allowed for separation. The percentage of ES was determined using Eq. (5.2), where V_B and V_A are the volume of the aqueous phase before emulsification and after drainage at each time point, respectively.

$$\%ES = \frac{V_B - V_A}{V_B} \times 100\% \quad (5.2)$$

Measurements were performed in triplicate, and results were reported as the mean ± one standard deviation (n = 3).

5.3.7 Droplet size and distribution

The average droplet size and distribution of each freshly prepared emulsion (~1.5 mL) was measured in a Mastersizer 2000 laser light scattering instrument (Malvern Instruments Ltd., UK) equipped with a Hydro 2000S sample handling unit as described by Can Karaca et al. (2011). The relative refractive index of emulsion was 1.105, which was calculated as the ratio of the refractive index of canola oil (1.47) to the refractive index of water (1.33). The particle size was reported as surface-average diameter ($D_{3,2}$) and volume-average diameter ($D_{4,3}$) calculated using Eq. (5.3) and (5.4), respectively.

$$D_{3,2} = \frac{\sum_{i=1} N_i d_i^3}{\sum_{i=1} N_i d_i^2} \quad (5.3)$$

$$D_{4,3} = \frac{\sum_{i=1} N_i d_i^4}{\sum_{i=1} N_i d_i^3} \quad (5.4)$$

where N_i is the total number of particles of diameter (*di*) (McClements, 2005). All measurements were performed in triplicate. $D_{3,2}$ and $D_{4,3}$ values were reported as the mean ± one standard deviation (n = 3).

5.3.8 Interfacial tension

Interfacial tension between canola oil and 1% (w/w) homogeneous LPI solutions and LPI-carrageenan solutions at pH 3.5 and 6.0 were measured at room temperature (21-23 °C) by a Force Tensiometer-K20 (Kruss, Germany) and a Wilhelmy plate according to Wang et al. (2019b). Solutions were prepared as same as previous described. About 25 mL of solution was added into the glass cup, followed by slowly lowering the plate on the air-solution surface. 46 mL of oil was then added carefully on the top to avoid breaking the interface. The force on the plate due to wetting was measured, and each measurement was taken every 3-min till the standard deviation lower than 0.10 mN/m to collect the final result. Interfacial tension was calculated using the Wilhelmy equation:

$$\gamma = \frac{F}{L\cos(\theta)} \quad (5.5)$$

where L is the length of the plate perimeter (40.200 mm), and θ is the contact angle (normally complete wetting (θ = 0) is assumed). Measurements were performed in triplicate, and results were reported as the mean ± one standard deviation (n = 3).

5.3.9 Continuous phase and emulsion viscosity

Continuous phase viscosity and emulsion viscosity were measured for homogeneous LPI solutions, LPI-carrageenan solutions at 1% (w/w) as well as the coacervate emulsions at pH 3.5 & 6.0 using the AR-G2 Rheometer (TA Instruments, New Castle, DE) equipped with a 40 mm diameter 2° acrylic cone at 22 °C (Hopkins et al., 2015). Solutions and emulsions were prepared as previously described. Apparent viscosity was measured as a function of shear rate (2 to 200 s^{-1}), and 10 data points were collected per logarithmic decade. Data were then fitted with the power-law model:

$$\log \text{viscosity} = (n-1) \log \text{shear rate} + \log m \quad (5.6)$$

where m is the consistency coefficient (equivalent to the apparent viscosity at 1 s^{-1}) and n is the flow behavior index, describing the level of pseudoplastic behavior of the material. Measurements were performed in triplicate, and m, n values were reported as the mean ± one standard deviation (n = 3).

5.3.10 Confocal Laser Scanning Microscopy (CLSM)

Lentil protein isolate- and LPI-carrageenan stabilized emulsions prepared as previously described were imaged through a Nikon Eclipse LV100 CLSM (Nikon, Tokyo, Japan) using 543 and 633 nm lasers. Nile red and fast green were added into the oil phase and water phase respectively as described by Wang et al. (2019b). 0.01% (w/w) Nile red with a maximum excitation and emission wavelength of 543 nm and 573-613 nm, respectively were added into the canola oil prior to homogenization process. 0.1% (w/w) of Fast green in water with the excitation and emission at 633 and 650 nm, respectively were added after emulsions were made to bind with protein in the continuous phase with the final fast green concentration of 0.012% (w/w). Emulsions were prepared in triplicate, and 4 images were taken per slide using a 40x objective lens.

5.3.11 Statistics

A one-way analysis of variance with a Tukey HSD test were performed to determine differences for each critical pH values in turbidimetric measurements, and for samples prepared at the same pH in emulsion stability, droplet size ($D_{3,2}$, $D_{4,3}$), droplet charge, interfacial tension, consistency coefficient and flow behavior index of continuous phase and emulsion viscosity. An independent T-test was performed to access the differences for each sample prepared at pH 6 and 3.5 in emulsion stability, droplet size ($D_{3,2}$, $D_{4,3}$), droplet charge, interfacial tension, consistency coefficient, and flow behavior index. The independent t-test was also performed to access the differences between the consistency coefficient of continuous phase and emulsion with each sample. All measurements were done in triplicate, unless otherwise stated. All statistics were performed using SPSS software.

5.4 Results and discussion

5.4.1 Effects of pH and biopolymer mixing ratio on forming LPI-κ-C and LPI-ι-C electrostatic complexes

The formation of electrostatic complexes between LPI and two types of carrageenan through the acidic titration was shown in Figure 5.1. A bell-shaped OD curve was evident in homogeneous LPI with the formation of soluble (pH_c) and insoluble complexes ($pH_{\phi 1}$), maximum complexation range (pH_{opt}) and the dissolution of complexes ($pH_{\phi 2}$), and max OD reading occurring at pH 6.7, 5.7, 3.5-4.5 (with the greatest OD found at pH 4.3), 2.3, and 0.446, respectively (Table 5.1, Figure 5.1). Electrical equivalence point (EEP), which indicates zero net surface charge, was found at pH 4.5 corresponding with maximum complexation (Table 5.1, Figure 5.2A). The overall charge of LPI was negative before EEP and became positive below EEP; however, the OD values between pH 4.5 and 3.5 remained similar suggesting significant protein-protein interactions through not only electrostatic but also hydrophobic interactions within protein aggregates, leading to a delayed decrease of OD values after the maximum point. OD remained flat was also observed in the pea protein system (Klemmer et al., 2012). The changes of optical density (OD) were not provided for homogeneous κ-C and ι-C solutions since the changes were negligible.

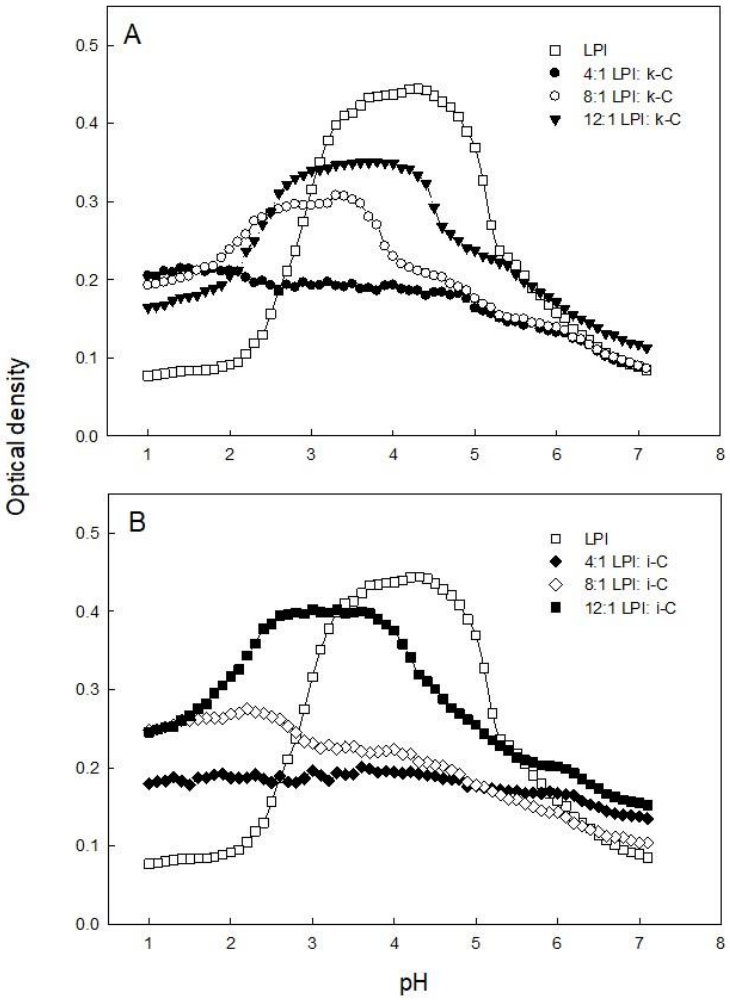

Figure 5.1 Electrostatic complexes within mixtures of LPI and κ-carrageenan (A), and LPI and ι-carrageenan (B) at 4:1, 6:1, 12:1 mixing ratios as a function of pH. Data represent the mean.

Table 5.1 Critical parameters associated with the complex coacervation for mixtures of lentil protein isolate with κ-Carrageenan and ι-Carrageenan at 4:1, 8:1, and 12:1 mixing ratios as well as lentil protein isolate alone. Data represents the mean ± one standard deviation (n = 3).

Materials	**pH_c**	**$pH_{\phi 1}$**	**pH_{opt}**	**$pH_{\phi 2}$**	**Max. OD**	**EEP**
LPI (control)	6.73 ± 0.06^{bc}	5.73 ± 0.06^{a}	4.30 ± 0.10^{a}	2.27 ± 0.06^{a}	0.446 ± 0.013^{a}	4.52 ± 0.05^{a}
LPI: κ-Carrageenan						
4:1	6.97 ± 0.06^{ab}	n.d.	n.d	n.d.	0.210 ± 0.007^{e}	Nil
8:1	7.00 ± 0.17^{a}	4.80 ± 0.10^{c}	3.33 ± 0.06^{c}	1.57 ± 0.12^{c}	0.309 ± 0.004^{d}	3.47 ± 0.03^{d}
12:1	6.83 ± 0.06^{abc}	5.33 ± 0.12^{b}	3.80 ± 0.10^{b}	1.83 ± 0.06^{b}	0.355 ± 0.012^{c}	3.95 ± 0.08^{b}
LPI: ι-Carrageenan						
4:1	6.67 ± 0.06^{c}	n.d.	n.d	n.d.	0.202 ± 0.008^{e}	Nil
8:1	6.83 ± 0.06^{abc}	n.d.	n.d	n.d.	0.279 ± 0.020^{d}	2.23 ± 0.05^{e}
12:1	6.77 ± 0.06^{abc}	5.30 ± 0.20^{b}	3.63 ± 0.06^{b}	1.43 ± 0.06^{c}	0.400 ± 0.007^{b}	3.70 ± 0.09^{c}

Abbreviations:

- LPI: Lentil protein isolate
- Critical pH values corresponding to the formation of soluble complexes (pH_c), insoluble complexes ($pH_{\phi 1}$), optimal complexation (pH_{opt}) and the dissolution of complexes ($pH_{\phi 2}$).
- Optical density (OD)
- Electrical equivalence point (EEP)

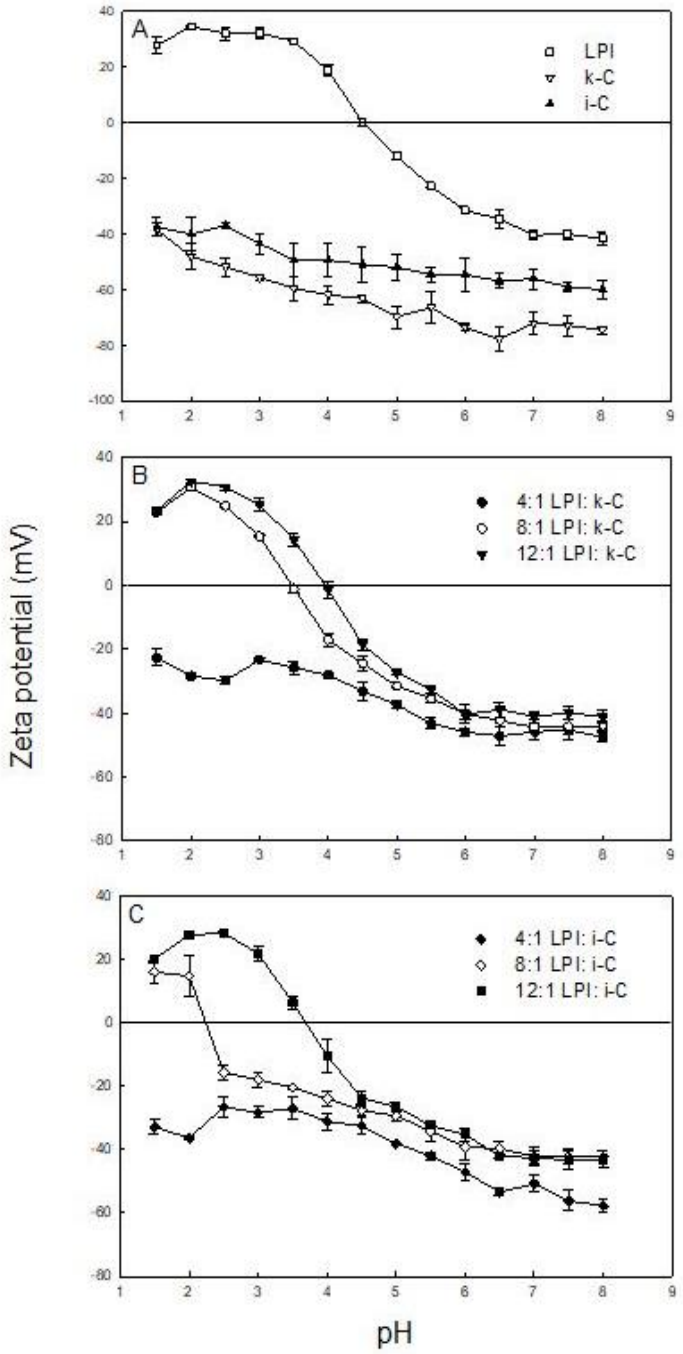

Figure 5.2 The surface charge of homogeneous Lentil protein isolate (LPI), κ-Carrageenan (κ-C), and ι-Carrageenan (ι-C) (A), and mixtures of LPI with κ-C (B) and ι-C (C) at 4:1, 6:1, 12:1 mixing ratios as a function of pH. Data represent the mean ± one standard deviation (n = 3).

The addition of both carrageenan polysaccharides to LPI solution resulted in OD curves more skewed towards acidic pH values and lower maximum OD values. Turbidity curves of LPI-κ-C at 4:1, 8:1, 12:1 mixing ratios as a function of pH was shown in Figure 5.1A. The formation of soluble complexes (pH_c) for all mixing ratios was similar ranging between pH 6.7 to 7.0. It was hypothesized that κ-C was interacting with the positive patches on LPI at pH_c, which was also observed in the LPI-carboxymethyl cellulose system (Wang et al., 2019a) and whey protein-gum Arabic system (Weinbreck et al., 2003). That the pH_c values remained unchanged suggested that the initial interaction occurred between κ-C and very small LPI-LPI aggregates or individual LPI. This has also been reported in LPI-carboxymethyl cellulose (Wang et al., 2019a) and β-lactoglobulin-pectin (Girard et al., 2004) systems. For 12:1 LPI-κ-C system, a bell-shaped curve was also observed. The formation of insoluble complexes, maximum complexation, and complete dissolution were found at pH 5.3, 3.8, 1.8, respectively, with max OD value of 0.355 (Table 5.1). The decrease of $pH_{\phi1}$, pH_{opt}, $pH_{\phi2}$, and max OD value ($p<0.05$) compared to homogeneous LPI solution was due to the presences of κ-C polysaccharides that generated significantly electrostatic repulsion, leading to suppression of larger LPI-LPI aggregates formation, which was also observed in a canola protein isolate-gum Arabic system (Stone et al., 2014) and a pea protein isolate-commercial pectic system (Warnakulasuriya et al., 2018). Titration curve of 8:1 LPI-κ-C also gave a bell-shape, and the decrease for $pH_{\phi1}$, pH_{opt}, $pH_{\phi2}$, and max OD became more significantly to pH 4.8, 3.3, 1.6, and 0.309, respectively ($p<0.05$), due to more κ-C polysaccharides involved in the solution to provide stronger electrostatic repulsion (Table 5.1). For 4:1 LPI-κ-C, electrostatic repulsion was even stronger, and $pH_{\phi1}$, pH_{opt}, $pH_{\phi2}$ was not identified. The OD values increased gradually without going through a transition state of forming insoluble complexes, but the formed complexes started to precipitate out at pH 4.8 with OD values being stable between 0.190 and 0.210 till pH 1.0, suggesting the saturation of κ-C at 4:1 mixing ratio (Figure 5.1).

Formation events of electrostatic complexes between LPI and ι-C at 4:1, 8:1, 12:1 mixing ratios during the acidic titration processes from pH 7.0 to 1.0 was shown in Figure 5.1B. OD curve of 12:1 LPI-ι-C also provided a bell-shape, and the pH_c, $pH_{\phi1}$, pH_{opt} were found at pH 6.8, 5.3, 3.6, respectively, which were also similar ($p>0.05$) to the corresponding critical pH values of 12:1 LPI-κ-C (Table 5.1). However, the complete dissolution ($pH_{\phi2}$) of 12:1 LPI-ι-C was conducted at pH 1.4 that was significantly lower ($p<0.05$). The lower $pH_{\phi2}$ can be attributed to the structural differences between ι-C and κ-C, where ι-C contains two sulphate groups per disaccharide unit

while κ-C only contains one sulphate group per disaccharide unit (Necas & Bartosikova, 2013), and such that stronger electrostatic attraction within each LPI-ι-C complex was formed, resulting in delay of the dissolution point. As greater electrostatic attraction of LPI-ι-C complexes was generated, a significantly higher max OD value of 0.400 was observed ($p<0.05$) (Table 5.1). That might be due to the formation of some ι-C double helices under the presence of residual minerals (Table A1, Appendix), which could also be evident in the less negative surface charge of ι-C compared to κ-C (Figure 5.2A). There would thus be less available sulfate groups in ι-C remained for complexation, leading to formation of larger LPI-LPI aggregates and a greater max OD value. For 8:1 LPI-ι-C, soluble complexes were formed at pH 6.8, similar to 12:1 LPI-ι-C ($p>0.05$) (Table 5.1). The OD values increased gradually from pH 7.0 and reached a small peak at pH 2.3 with OD value of 0.279 without ever going through a transition state of forming insoluble complexes, and then decreased slightly to 0.250 till pH 1.0 with no further dissolution (Figure 5.1B). In this case, since there was lack of obviously prominent part observed in the whole curve, the small peak found at pH 2.3 was not reported as maximum complexation point (Table 5.1). However, the small peak point was corresponding the EEP at pH 2.2 identified in Figure 5.2C, suggesting the neutral-surface charge was achieved at the small peak point. That no obvious dissolution was observed from pH 2.3 to pH 1.0 could be attributed to the strong electrostatic attraction within the formed LPI-ι-C complexes. Formation of soluble complexes for 4:1 LPI-ι-C was found at pH 6.7, similar to other mixing ratios ($p>0.05$). The $pH_{\phi 1}$, pH_{opt}, $pH_{\phi 2}$ points were also not identified. The OD values increased slowly and became stable at around 0.20 from pH 4.0 to 1.0, where precipitated type of structure was formed (Figure 5.1B).

Surface charge of homogeneous LPI, κ-C, and ι-C solutions (Figure 5.2A), and the mixtures of LPI-κ-C (Figure 5.2B) and LPI-ι-C (Figure 5.2C) at 4:1, 6:1, 12:1 mixing ratios as a function of pH was shown. The isoelectric point (pI) of LPI was found at pH 4.5, corresponding to the pH_{opt} of LPI (Figure 5.2A). Surface charge of κ-C and ι-C solutions remained negative during the whole titration, which could be attributed to the low pK_a value of sulfate group, resulting in no protonation during the titration. EEPs for all LPI-carrageenan systems were determined at pH below the pI of LPI and shifted closer to pI as the mixing ratio increased. The EEPs for 8:1 LPI-κ-C, 12:1 LPI-κ-C, and 12:1 LPI-ι-C were found at pH 3.5, 4.0, and 3.7, respectively, all corresponding to their pH_{opt} points (Figure 5.2B & C). Surface charge of 4:1 LPI-κ-C and 4:1 LPI-

ι-C remained negative during the whole titration, suggesting both carrageenan polysaccharides were saturated in the systems, and thus, no pH_{opt} points were identified.

5.4.2 Effects of pH and mixing ratio on the emulsifying properties of LPI-κ-C and LPI-ι-C complexes

5.4.2.1 Emulsion characteristics

The stability of emulsions (1.0% (w/w)) at pH 6 and 3.5 stabilized by homogeneous LPI, and LPI-κ-C and LPI-ι-C complexes formed at 4:1, 8:1, 12:1 mixing ratios over 48 h was determined through creaming (Table 5.2). These two pH values were chosen to compare the emulsifying properties of soluble complexes and precipitated complexes, where soluble complexes were yielded at pH 6 and pH 3.5 was closed to the pH_{opt} points for most mixtures to maximize precipitated complexes. Emulsion stability (ES) of LPI emulsions at pH 6 and pH 3.5 remained 100% after 30 min but dropped dramatically to 20% and 18% after 24 h, respectively. Sediment of LPI were observed in both emulsions after 48 h (data not shown), which could be due to the low solubility of LPI resulting in low ES at 24 and 48 h. For comparison purpose, emulsions were also prepared at pH 6 and 3.5 using homogeneous κ-C and ι-C at concentrations equivalent to the carrageenan amount (w/w) at their corresponding emulsions at 4:1, 8:1, 4:1 mixing ratios. Emulsion stability was not determined for κ-C and ι-C at 1% due to gel formation. For all κ-C and ι-C emulsions, separation occurred rapidly after emulsions were formed, and a layer of oil was observed for each sample after 30 min, indicating both carrageenan polysaccharides are not good emulsifiers and extensive droplet coalescence occurred. The stability of κ-C emulsions at concentration equivalent of 4:1, 8:1, and 12:1 mixing ratio at pH 6 was 65%, 51%, and 50%, respectively, and their corresponding emulsions at pH 3.5 remained 22%, 20%, and 25% stability, respectively, at 30 min. Emulsion stability of ι-C emulsions at concentration equivalent of 4:1, 8:1, and 12:1 at pH 6 was 68%, 52%, and 47%, respectively, at 30 min, and the stability of their corresponding emulsions at pH 3.5 was 31%, 27%, 21%, respectively. All emulsions destabilized completely after 24 h for each sample with a layer of oil on the top and aqueous solution at the bottom. These results suggested that both κ-C and ι-C at pH 6 could slow down the droplet movement at increased concentration, indicating that viscosity might play an important role in the systems; however, this effect was temporary, suggesting a more effective emulsifier is needed to stabilize emulsions. Both κ-C and ι-C at pH 3.5 did not show good properties to enhance emulsion

stability. For emulsions prepared with soluble complexes at pH 6, the addition of κ-C and ι-C at all three different mixing ratios led to improvement in ES over 48 h. All emulsions had 100% stability after 30 min, where ES of 4:1 LPI-κ-C and LPI-ι-C emulsions remained 100% for 48 h. ES of 8:1 LPI-ι-C emulsion decreased to 86% at 24 h ($p<0.05$) and 83% at 48 h ($p<0.05$), while ES of 8:1 LPI-κ-C emulsion dropped to 42% at 24 h ($p<0.05$) and 35% at 48 h ($p<0.05$). Both ES for emulsions at 12:1 mixing ratio dropped to about 34% ($p<0.05$) at 24 h and below 30% after 48 h ($p<0.05$). ES of emulsions prepared with insoluble complexes (pH 3.5) were all lower than those prepared at pH 6 at 30 min ($p<0.05$). ES of 4:1 LPI-κ-C emulsion was found to be 89% at 30 min, then decreased to 74% at 24 h ($p<0.05$) and remained stable till 48 h ($p>0.05$). 4:1 LPI-ι-C emulsion displayed a higher ES of 98% at 30 min, but the decrease is more rapid at 24 h and 48 h for 57% and 55%, respectively. ES of 8:1 LPI-κ-C and 8:1 LPI-ι-C emulsions were only 42% and 36% at 30 min, respectively. The ES dropped to 36% ($p<0.05$) and 31% ($p<0.05$) at 24 h, respectively, and remained stable ($p>0.05$). ES for 12:1 LPI-κ-C and 12:1 LPI-ι-C emulsions was 53% and 40%, respectively, and the decline for both emulsions were minor after 30 min ($p>0.05$). Emulsion destabilization is due to gravitational separation, which could be controlled through reducing droplet size, lessening droplet flocculation or coalescence, and modifying continuous phase rheology (McClements, 2015).

Table 5.2 Critical parameters of for emulsions stabilized by homogeneous lentil protein isolate (LPI) solutions and mixtures of LPI with κ-, ι-carrageenan at various mixing ratio at pH 6 and pH 3.5. Data represents the mean ± one standard deviation (n = 3).

	Emulsion Stability (%)			droplet size D[3.2] (μm)	droplet size D[4.3] (μm)	droplet charge (mV)	Interfacial tension (mN/m)
	0.5 h	24 h	48 h				
pH 6							
homo LPI	100.0 ± 0.0^{Aa}	19.6 ± 0.4^{Ae}	19.2 ± 0.4^{Af}	11.23 ± 0.43^{Aa}	24.06 ± 3.18^{Aa}	-38.63 ± 1.18^{Be}	4.9 ± 0.2^{Aa}
4: 1 LPI: k-C	100.0 ± 0.0^{Aa}	100.0 ± 0.0^{Aa}	100.0 ± 0.0^{Aa}	8.83 ± 0.46^{Bd}	19.39 ± 1.14^{Bb}	-69.57 ± 1.46^{Aab}	5.3 ± 0.4^{Ba}
8: 1 LPI: k-C	100.0 ± 0.0^{Aa}	42.3 ± 1.3^{Ac}	34.8 ± 3.2^{Ac}	10.16 ± 0.15^{Bbc}	21.40 ± 0.39^{Bab}	-71.53 ± 2.48^{Ba}	4.8 ± 0.3^{Ba}
12: 1 LPI: k-C	100.0 ± 0.0^{Aa}	34.0 ± 1.8^{Bd}	29.6 ± 0.7^{Bd}	10.42 ± 0.58^{Bab}	22.77 ± 0.11^{Bab}	-66.67 ± 0.61^{Bbc}	4.8 ± 0.4^{Ba}
4: 1 LPI: ι-C	100.0 ± 0.0^{Aa}	100.0 ± 0.0^{Aa}	100.0 ± 0.0^{Aa}	9.40 ± 0.11^{Acd}	23.18 ± 1.66^{Bab}	-63.50 ± 1.05^{Acd}	5.0 ± 0.5^{Ba}
8: 1 LPI: ι-C	100.0 ± 0.0^{Aa}	85.8 ± 0.7^{Ab}	83.3 ± 1.4^{Ab}	10.26 ± 0.08^{Bbc}	24.48 ± 0.04^{Ba}	-63.57 ± 1.34^{Acd}	4.9 ± 0.5^{Ba}
12: 1 LPI: ι-C	100.0 ± 0.0^{Aa}	33.8 ± 2.9^{Ad}	25.2 ± 0.4^{Be}	10.71 ± 0.14^{Bab}	25.05 ± 0.71^{Ba}	-59.47 ± 2.18^{Bd}	4.9 ± 0.7^{Ba}
pH 3.5							
homo LPI	100.0 ± 0.0^{Aa}	18.1 ± 1.7^{Ae}	18.1 ± 1.7^{Ae}	12.04 ± 0.96^{Ae}	26.34 ± 1.49^{Af}	39.3 ± 0.20^{Aa}	12.0 ± 0.6^{Bc}
4: 1 LPI: k-C	88.6 ± 1.3^{Bb}	74.0 ± 0.4^{Ba}	73.1 ± 0.6^{Ba}	14.70 ± 1.26^{Ade}	39.28 ± 2.82^{Ae}	-51.13 ± 0.15^{Be}	14.2 ± 0.2^{Aa}
8: 1 LPI: k-C	42.3 ± 0.7^{Bd}	36.3 ± 1.7^{Bd}	36.3 ± 1.7^{Ad}	38.08 ± 1.10^{Ac}	59.89 ± 1.34^{Ac}	10.27 ± 1.27^{Ac}	13.7 ± 0.1^{Aab}
12: 1 LPI: k-C	53.3 ± 3.8^{Bc}	45.6 ± 4.5^{Ac}	45.4 ± 4.3^{Ac}	17.96 ± 1.91^{Ad}	47.49 ± 4.10^{Ad}	27.37 ± 1.18^{Ab}	12.9 ± 0.6^{Abc}
4: 1 LPI: ι-C	97.5 ± 1.3^{Ba}	57.1 ± 0.7^{Bb}	54.8 ± 0.4^{Bb}	12.12 ± 0.70^{Ae}	30.75 ± 2.66^{Af}	-56.07 ± 2.18^{Bf}	13.3 ± 0.5^{Aab}
8: 1 LPI: ι-C	35.6 ± 1.1^{Be}	31.0 ± 3.2^{Bd}	30.8 ± 3.1^{Bd}	61.14 ± 2.90^{Aa}	85.07 ± 3.52^{Ab}	-6.45 ± 0.26^{Bd}	12.0 ± 0.3^{Ac}
12: 1 LPI: ι-C	40.0 ± 2.1^{Bde}	36.9 ± 1.7^{Ad}	36.7 ± 1.9^{Ad}	51.64 ± 3.05^{Ab}	123.69 ± 2.42^{Aa}	9.42 ± 1.54^{Ac}	14.0 ± 0.1^{Aa}

- Upper letters indicate comparison between samples with the same mixing ratio and materials at different pH values
- Lower letters indicate comparison between samples at the same pH

Emulsion stability can be improved by forming very small droplets to against gravitational separation according to Stoke law. Droplet size distributions for all emulsions showed a multimodal distribution (Figure A5.1, Appendix), and the average droplet diameter ($D_{3,2}$ and $D_{4,3}$) is given in Table 5.2. Emulsions prepared at pH 6 all gave similar distribution curves with the dominant peak ranging from below 10 to 100 µm and the small peak at 1 µm. LPI emulsion at pH 6 was found to have $D_{3,2}$ of 11 µm and $D_{4,3}$ of 24 µm (Table 5.2). Emulsions stabilized with LPI-κ-C and LPI-ι-C soluble complexes for all mixing ratios resulted in $D_{3,2}$ below 11 µm and $D_{4,3}$ below or similar to 24 µm, where smaller $D_{3,2}$ and $D_{4,3}$ values were observed as mixing ratio decreased. LPI emulsion at pH 3.5 was found to have similar droplet size distribution and average droplet diameter with LPI emulsion at pH 6 ($p>0.05$). In contrast, the $D_{3,2}$ and $D_{4,3}$ values increased for all other emulsions at pH 3.5. 4:1 LPI-κ-C emulsion was found to have $D_{3,2}$ of 15 µm and $D_{4,3}$ of 40 µm, and the $D_{3,2}$ and $D_{4,3}$ values for 8:1 emulsion were 38 and 60 µm, respectively, and for 12:1 LPI-κ-C emulsion were 18 and 48 µm, respectively. 4:1 LPI-ι-C emulsion at pH 3.5 was found to have $D_{3,2}$ of 12 µm and $D_{4,3}$ of 31 µm. $D_{3,2}$ and $D_{4,3}$ for 8:1 LPI-ι-C and 12:1 LPI-ι-C emulsions were larger than 50 and 80 µm, respectively (Table 5.2). Emulsions at pH 6 and LPI emulsion at pH 3.5 formed very small droplets leading to a lower rate of creaming, so they all had ES of 100% at 30 min. 4:1 LPI-κ-C and 4:1 LPI-ι-C emulsions at pH 3.5 also formed small droplets and thus had ES of ~90%. Other emulsions formed larger droplets resulting in the low ES. As reported by Liu and co-authors (2010), soluble complexes were smaller in size, which could also be reflected as low OD values in Figure 5.1, allowing the complexes to rapidly migrate towards and adsorb into the oil-water interface. Also, κ-C and ι-C polysaccharides were interacting with small LPI-LPI aggregates at pH 6, and the interactions were weaker compared to complexes formed at pH 3.5 due to the overall negative surface charge of LPI, and sulfate groups on carrageenan were only interacting with the positive patches on LPI (Figure 5.2A). It is hypothesized that more flexible complexes were formed so that the LPI could re-align easily to unfold and expose the hydrophobic amino acids towards the oil phase and hydrophilic moieties towards the water phase. Therefore, smaller droplet formation was resulted. On the contrary, insoluble complexes formed at pH 3.5 were more prominent and larger in size (higher OD in Figure 5.1), and the interactions were more significant, which caused slower diffusion and less flexibility of the complexes to re-position onto the interface, as a result of less integration to cover the interface and larger droplet formation. The change of the complexes structure from loose at soluble

complexes to compact at insoluble complexes was also observed in an ovalbumin-carboxymethyl cellulose system (Xiong et al., 2020). The morphology of their complexes observed under the scanning electron microscopy suggested that the complexes prepaed at lower pH were denser due to stronger electrostatic interaction than complexes prepared at higher pH, agreed with our hypothesis.

Emulsion stability could also be enhanced by highly charged droplets to prevent droplet flocculation and further coalescences. Droplet charge for each system was provided in Table 5.2. The droplet charge of LPI emulsion at pH 6 was -38.6 mV, which slightly decreased compared to LPI solution at pH 6 of -31.3 mV (Figure 5.2A), indicating the increase of exposure of negatively charged groups on LPI upon emulsification process. Droplet charges were between -59 to -71 mV for all other emulsions at pH 6, where the charge of their corresponding solutions was between -35 to -47 mV (Figure 5.2B & C). It was hypothesized that LPI from the complexes unfolded and exposed the hydrophobic groups toward to oil phase and the hydrophilic moieties with carrageenan polysaccharides toward continuous phase during homogenization resulting in the more negatively charged droplets, which was also observed in the previous work (Wang et al., 2019b). The zeta potential for LPI emulsion at pH 3.5 was 39.3 mV, which increased comparing to the zeta potential of its solution at 29.4 mV, suggesting that more positively charged groups were exposed. The droplet charge for 4:1, 8:1, 12:1 LPI-κ-C emulsions at pH 3.5 was -51.1, 10.3, 27.4 mV, respectively. For 4:1, 8:1, 12:1 LPI-ι-C emulsions, droplet charge was found at -56.1, -6.5, and 9.4 mV, respectively. The droplet charge for both 4:1 LPI-κ-C and LPI-ι-C emulsions were more negative compared to their corresponding solutions' surface charge of -25.8 and -27 mV, respectively, contributing to the previous hypothesis. However, the droplet charge increased for 8:1, 12:1 LPI-κ-C, and -ι-C emulsions compared to the surface charge of their corresponding solutions. This observation suggested that the increase of LPI's zeta potential was more prominent in 8:1 and 12:1 mixing ratio; however, the influence of LPI became less affective since the carrageenan polysaccharides were saturated in 4:1 mixing ratio. Droplet charge greater than +/- 50 mV is considered to be efficient for supporting droplet electrostatic repulsion. The less charge of 8:1 and 12:1 LPI-κ-C, and -ι-C emulsions at pH 3.5 lead to significant droplet flocculation and increased gravitational separation at 30 min.

5.4.2.2 Interfacial tension

Interfacial tension (IT) for homogeneous LPI, LPI-κ-C and LPI-ι-C solutions at all mixing ratios at pH 6 and 3.5 were given in Table 5.2. All the solutions were surface active and led to interfacial tension lower than oil-water interface (22.0 mN/m). The interfacial tension for all solutions at pH 6 were ~5.0 mN/m ($p>0.05$). Solutions at pH 3.5 generally led to higher interfacial tension ($p<0.05$) with LPI solution at pH 3.5 of 12.0 mN/m. Interfacial tension for other LPI-carrageenan solutions at pH 3.5 were between 12 and 14 mN/m. The lower interfacial tension values for solutions at pH 6 could be attributed to the looser LPI-carrageenan structure at pH 6, causing more flexible LPI to unfold and re-position at the interface. It was observed that insoluble complexes formed at pH 3.5 settled down quickly during the measurement suggesting that only soluble complexes were able to align at the oil-water interface to lower the interfacial tension during the measurement. Therefore, solutions at pH 6 that contained more soluble complexes could lower the interfacial tension to a greater extent. Settling of insoluble complexes were also observed in the previous study for LPI-carboxymethyl cellulose, LPI-gum Arabic, LPI-alginate, and LPI-ι-C systems (Wang et al., 2019b). The greater ability for soluble complexes to lower the interfacial tension could help to disrupt the droplet and results in small droplet formation since all emulsions were treated with the same energy input during emulsion preparation. Thus, all emulsions prepared at pH 6 resulted in smaller droplet diameter. It is worth mentioning that the droplet size of LPI emulsions at pH 3.5 remained small although the interfacial tension of corresponding solution was high, indicating the biopolymer conformation plays a more important role than interfacial tension in terms of droplet size.

5.4.2.3 Emulsion and continuous phase rheology

Emulsion stability could also be affected by enhancing continuous phase rheology to slow down the droplet movement (McClements, 2015). Flow diagrams of continuous phase and emulsion viscosities for all system were shown in Figure A5.2 and A5.3, respectively (Appendix). The flow curves were fitted with the Power-law model to conduct the consistency coefficient (m) and the flow behavior index (n) (Table 5.3). For emulsions at pH 6, emulsion viscosity increased as LPI-carrageenan mixing ratio decreased (both LPI-κ-C and LPI-ι-C systems). The type of carrageenan added did not significantly affected the emulsion viscosity except the higher emulsion viscosity of 4:1 LPI-κ-C emulsion than 4:1 LPI-ι-C emulsions ($p<0.05$). The viscosity of

emulsions could be attributed to the corresponding continuous phase viscosity, droplet volume fraction, droplet size, and inter-droplet interaction (McClements, 2015). Also, since the emulsion was prepared at pH 6, where small size and number of soluble complexes were formed (Figure 5.1; Liu et al, 2010) and droplet charge was highly negative (Table 5.2), the interactions between droplets should remain low. The main factor thus would be continuous phase viscosity. A similar trend compared to emulsion viscosity was observed in continuous phase viscosity, where continuous phase viscosity increased as LPI-carrageenan mixing ratio decreased. κ-C and ι-C polysaccharides were well-known as thickening and gelling reagents (Li et al., 2014) to contribute the continuous phase viscosity. Different from emulsion viscosity, 4:1 LPI-ι-C solution displayed the highest viscosity ($p<0.05$), followed by 8:1 LPI-ι-C solution and 4:1 LPI-κ-C solution with similar continuous phase viscosity ($p>0.05$), which could be attributed to the formation of microgel of ι-C under the presence of salts (within the ash) (Table A1, Appendix). All other solutions at pH 6 displayed similar viscosities. As high continuous phase viscosity slowed down the droplet movement, ES of 4:1 LPI-κ-C and LPI-ι-C emulsions remained 100% at 48 h, and 8:1 LPI-ι-C emulsion remained the second highest ES of 83% at 48 h (Table 5.2). However, low continuous phase viscosity was observed in LPI emulsion leading to the low ES after 24 h. It is worth to mention that the continuous phase viscosities of 4:1 and 8:1 LPI-ι-C solutions were significantly higher than their corresponding emulsions' viscosities ($p<0.05$). It was assumed that the microgels of ι-C were broken down with applied mechanical shearing upon emulsification process, leading to the decrease of viscosity. The same mechanical shearing was therefore applied to the 4:1 and 8:1 LPI-ι-C solutions to prove the theory. The apparent viscosity at 1 s^{-1} for 4:1 and 8:1 LPI-ι-C solutions after emulsification process decreased to 0.08 and 0.02 Pa s, respectively, and both solutions' viscosity values became slightly lower than their corresponding emulsion viscosities, confirming the hypothesis of breaking of microgels of ι-C.

Table 5.3 Critical parameters of for emulsions stabilized by homogeneous lentil protein isolate (LPI) solutions and mixtures of LPI with κ-, ι-carrageenan at various mixing ratio at pH 6 and pH 3.5. Data represents the mean ± one standard deviation (n = 3).

	Continuous phase			Emulsion	
	Consistency coefficient (Pa s)	Flow behavior index	ηD/ηC	Consistency coefficient (Pa s)	Flow behavior index
pH 6					
homo LPI	0.03 ± 0.01^{Bc}	0.53 ± 0.04^{Ac}	1.90	0.06 ± 0.02^{Bc}	0.46 ± 0.06^{Ad}
4: 1 LPI: k-C	0.07 ± 0.01^{Bbc}	0.74 ± 0.03^{Aa}	0.81	0.16 ± 0.00^{Ba}	0.68 ± 0.01^{Ac}
8: 1 LPI: k-C	0.04 ± 0.00^{Bc}	0.68 ± 0.01^{Aa}	1.43	0.04 ± 0.01^{Bcd}	0.79 ± 0.04^{Ab}
12: 1 LPI: k-C	0.03 ± 0.00^{Ac}	0.67 ± 0.02^{Aa}	1.90	0.03 ± 0.01^{Bd}	0.79 ± 0.04^{Ab}
4: 1 LPI: ι-C	0.25 ± 0.04^{Aa}	0.56 ± 0.03^{Abc}	0.23	0.09 ± 0.01^{Ab}	0.82 ± 0.02^{Ab}
8: 1 LPI: ι-C	0.08 ± 0.00^{Ab}	0.65 ± 0.01^{Aab}	0.71	0.04 ± 0.00^{Bcd}	0.86 ± 0.01^{Aab}
12: 1 LPI: ι-C	0.03 ± 0.01^{Ac}	0.68 ± 0.06^{Aa}	1.90	0.02 ± 0.00^{Bd}	0.91 ± 0.03^{Aa}
pH 3.5					
homo LPI	0.11 ± 0.01^{Ab}	0.37 ± 0.02^{Bd}	0.52	0.14 ± 0.04^{Ab}	0.37 ± 0.02^{Ae}
4: 1 LPI: k-C	0.26 ± 0.08^{Aa}	0.39 ± 0.03^{Bcd}	0.22	0.48 ± 0.03^{Aa}	0.43 ± 0.01^{Bde}
8: 1 LPI: k-C	$2.06 \pm 0.39^{A*}$	0.06 ± 0.03^{Be}	0.03	0.06 ± 0.01^{Abc}	0.55 ± 0.05^{Bbc}
12: 1 LPI: k-C	0.03 ± 0.01^{Abc}	0.60 ± 0.07^{Aab}	1.90	0.10 ± 0.00^{Abc}	0.48 ± 0.02^{Bcd}
4: 1 LPI: ι-C	0.08 ± 0.02^{Bbc}	0.58 ± 0.04^{Aab}	0.71	0.05 ± 0.01^{Bc}	0.73 ± 0.04^{Ba}
8: 1 LPI: ι-C	0.04 ± 0.01^{Bbc}	0.51 ± 0.05^{Bbc}	1.43	0.12 ± 0.03^{Abc}	0.46 ± 0.02^{Bcde}
12: 1 LPI: ι-C	0.01 ± 0.00^{Bc}	0.67 ± 0.04^{Aa}	5.70	0.45 ± 0.05^{Aa}	0.58 ± 0.06^{Bb}

- *Denotes samples that were not included in the statistical analysis
- Upper letters indicate comparison between samples with the same mixing ratio and materials at different pH values
- Lower letters indicate comparison between samples at the same pH

For emulsions prepared at pH 3.5, the highest emulsion viscosity was observed at 4:1 LPI-κ-C and 12:1 LPI-ι-C emulsion ($p>0.05$), followed by LPI emulsion, and then 8:1 LPI-ι-C, 8:1 and 12:1 LPI-κ-C emulsions, with 4:1 LPI-ι-C emulsion displaying the lowest viscosity. For continuous phase viscosity, 8:1 LPI-κ-C solution was found to have the highest viscosity, followed by 4:1 LPI-κ-C ($p<0.05$), then homogeneous LPI, and 12:1 LPI-κ-C, 4:1 and 8:1 LPI-ι-C solutions, and then 12:1 LPI-ι-C solution. The high emulsion viscosity of 4:1 LPI-κ-C emulsion were resulted from the high corresponding continuous phase viscosity. The larger $D_{4,3}$ of 4:1 LPI-κ-C emulsion compared to 4:1 LPI-ι-C emulsion could be due to the high continuous phase viscosity which slowed down the complexes to migrate to the interface leading to larger droplet formation, and consequently lower ES at 30 min (Table 5.2). In contrast, the lowest viscosity of 4:1 LPI-ι-C emulsion could be attributed to not only the lower continuous phase viscosity, but also highly negative droplet charge to weaken droplet attractions (Table 5.2), and small size and number of complexes formation (low OD in Figure 5.1B). The highest continuous phase viscosity of 4:1 LPI-κ-C solution resulted the highest ES at 48 h for all emulsion at pH 3.5, while 4:1 LPI-ι-C emulsion had lower ES with the lower continuous phase viscosity. It was observed that the emulsion viscosity of 8:1 LPI-κ-C emulsion decreased significantly ($p<0.05$) compared its continuous phase viscosity, while the 12:1 LPI-ι-C emulsion with high emulsion viscosity had a very low corresponding continuous phase viscosity, suggesting the destabilization of both emulsions during the measurements. Continuous phase viscosity is an important factor in emulsion formation, as an optimum range of ratios of disperse-to-continuous phase viscosity ($\frac{\eta_D}{\eta_C}$), generally agreed with $0.05<\frac{\eta_D}{\eta_C}<5$, needs to be achieved to disrupt a larger droplet into a smaller one (McClements, 2015; Walstra, 1993; Walstra, 2003; Wooster et al., 2008). The very high viscosity of 8:1 LPI-κ-C solution and very low viscosity of 12:1 LPI-ι-C solution led to the $\frac{\eta_D}{\eta_C}$ out of the optimal range with the ratios of 0.03 and 5.70, respectively (Table 5.3). Therefore, elongation of droplets would occur in 8:1 LPI-κ-C system, and droplet deformation was interrupted in 12:1 LPI-ι-C system, both leading to less stable emulsions and large droplet formation. The $\frac{\eta_D}{\eta_C}$ values for other systems were in the range of 0.05 to 5 (Table 5.3).

As seen in the flow behavior, all the solutions and emulsions are shear thinning (Figure A5.2 & A5.3, Appendix). The pseudoplastic behavior (i.e. flow behavior index, n value) for

emulsions at pH 6 increased (n value decreased) as LPI-carrageenan mixing ratio decreased for both LPI-κ-C and LPI-ι-C systems; however, n value of LPI emulsion at pH 6 was significantly lower than all other emulsions ($p<0.05$). It was assumed that a less homogenous and less stable system was resulted due to the relatively larger droplet size and less charged system. Therefore, the droplet flocculation and coalescence were thought to be more significant during shearing leading to the larger changes of LPI emulsion viscosity. LPI-κ-C continuous phase solutions at all mixing ratios at pH 6 showed similar pseudoplastic behavior ($p>0.05$), and the pseudoplastic behavior for LPI-ι-C solutions increased as LPI-ι-C mixing ratio decreased. Similar to emulsion, LPI solution at pH 6 at displayed the strongest pseudoplastic behavior. For emulsions at pH 3.5, 4-1 LPI-ι-C emulsion was found to have the weakest pseudoplastic behavior ($p<0.05$), which could be attributed to low emulsion viscosity, the small droplet size formation to become a more homogeneous system, and highly charged system to against shearing. On the contrary, significantly increased pseudoplastic behavior of 4:1 LPI-κ-C emulsion was observed ($p<0.05$) since it had the highest emulsion viscosity. 8:1 and 12:1 LPI-carrageenan emulsions had similar pseudoplastic behavior regardless of the type of carrageenan. Again, the strongest pseudoplastic behavior was found in LPI emulsion and LPI continuous phase solution (except 8:1 LPI- κ-C solution).

5.4.2.4 CLSM images

CLSM images were taken for LPI, 4:1 LPI-κ-C and -ι-C emulsions at pH 6 and pH 3.5 at 24 h for comparison purposes since 4:1 LPI-carrageenan emulsions showed the greatest ES (Figure 5.3). For LPI emulsions, a lot of very large droplets were observed at both pH values (Figure 5.3A & B) suggesting droplet coalescences occurred. Droplets remained small for 4:1 LPI-κ-C and -ι-C emulsions at pH 6 corresponding to their ES of 100% at 24 h (Figure 5.3C & E). The larger droplets for these two emulsions were around 20 μm; some very small droplets were also observed, which corresponded to two peaks found at droplet size distribution (Figure A5.1, Appendix). Both images for 4:1 LPI-κ-C and -ι-C emulsions at pH 3.5 showed larger droplets corresponding to their lower ES, where larger droplets were seen at 4:1 LPI-κ-C emulsion compared to 4:1 LPI-ι-C emulsion, which could be attributed to the larger droplet size formation at fresh emulsion (Figure 5.3D & F).

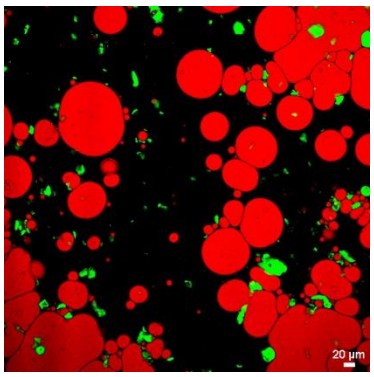

A) LPI pH 6

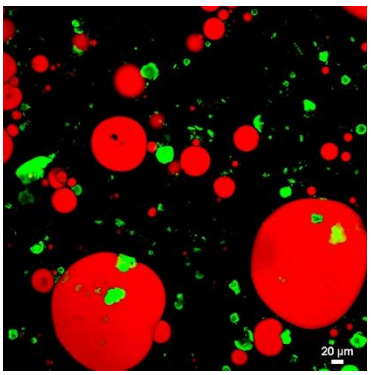

B) LPI pH 3.5

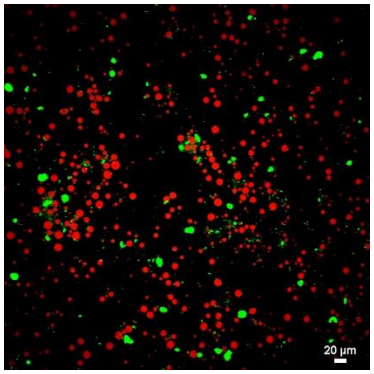

C) 4:1 LPI-κ-C pH 6

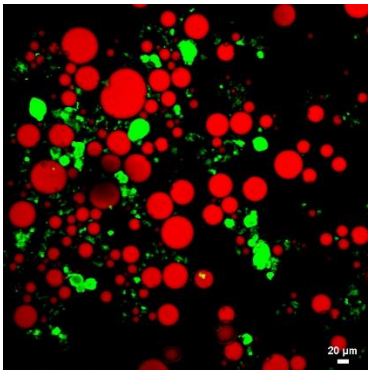

D) 4:1 LPI-κ-C pH 3.5

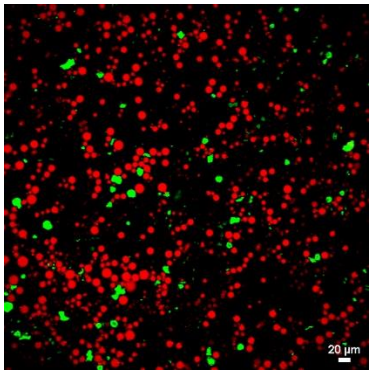

E) 4:1 LPI-ι-C pH 6

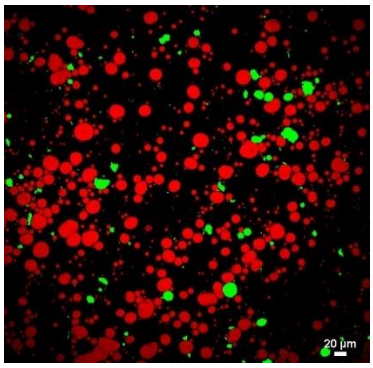

F) 4:1 LPI-ι-C pH3.5

Figure 5.3 Confocal laser scanning microscopy images of oil-in-water emulsions stabilized by lentil protein isolate (LPI) at pH 6 and pH 3.5 (A and B, respectively), 4:1 LPI-κ-Carrageenan at pH 6 and pH 3.5 (C and D, respectively), and 4:1 LPI-ι-Carrageenan at pH 6 and pH 3.5 (E and F, respectively) were taken after 24-hour of preparation. The scale bar represents 20 µ.

5.5 Conclusions

This worked explored the emulsifying behaviors between LPI and carrageenan polysaccharides by first investigating the effects of pH on the formation of LPI-κ-C and LPI-ι-C complexes at 4:1, 8:1, and 12:1 biopolymer mixing ratios. Suppression of the turbidity curves was observed with the addition of κ-C and ι-C into the LPI solution during all the turbidimetric pH acid-titration measurements. Critical pH values (pH_c, $pH_{\phi 1}$, pH_{opt}, $pH_{\phi 2}$) shifted to more acidic pH values, and max OD values decreased as biopolymer mixing ratio decreased in both LPI-κ-C and LPI-ι-C systems. The resulting soluble complexes (at pH 6) and insoluble complexes (at pH 3.5) were then used to examine the emulsifying properties. Improvement of emulsion stability was observed in all LPI-carrageenan emulsions at 24 h and 48 h compared to LPI emulsions at both pH values, where emulsions made with soluble complexes at pH 6 generally showed higher ES than those made at pH 3.5 for each sample. ES of all emulsions at pH 6 remained 100% at 30 min, and smaller and more uniform droplets with highly negative charge of -50 to -71 mV were formed. Interfacial tension was also lowered to a greater extent for solutions at pH 6 due to more soluble complexes formed. The high continuous phase viscosity of 4:1 LPI-κ-C, 4:1 LPI-ι-C, and 8:1 LPI-ι-C solutions at pH 6 contributed to their high ES. The greatest ES over time was found in 4:1 LPI-κ-C and -ι-C emulsions at pH 6. CLSM images confirmed that the droplet size of 4:1 LPI-κ-C and LPI-ι-C emulsions at pH 6 remained small at 24 h. All these findings suggested that LPI-carrageenan (both types) soluble complexes formed at pH 6 could effectively lower the interfacial tension and led to smaller droplet formation, and the excessive carrageenan in the system increased the viscosity, all contributing to the enhanced emulsion stability; our future work will thus focus in these two systems and try to explore more potential applications, such as microencapsulation of omega-3 oil through complexation of LPI-carrageenan.

5.6 Linkage to the next study

Within this chapter, the complexation behavior between LPI-ι-C and LPI-κ-C as a function of pH and biopolymer mixing ratio was studied. Emulsions were also made by using the resulting soluble and insoluble complexes. The most stable emulsions were found and could be prepared by 4:1 LPI-ι-C and 4:1 LPI-κ-C soluble complexes at pH 6. In the next study, these stable emulsions were finally prepared to encapsulate edible oil such as flaxseed oil, and drying were applied to result dried microcapsules. In chapter 6, LPI-carrageenan based emulsions were first prepared to

encapsulate flaxseed oil by using LPI-κ-C or LPI-ι-C, and maltodextrin as the coating wall materials. Subsequent drying such as spray-drying and freeze-drying were applied to produce dried microencapsulated powders.

6. MICROENCAPSULATION OF FLAXSEED OIL BY LENTIL PROTEIN ISOLATE-κ-CARRAGEENAN AND - ι-CARRAGEENAN BASED WALL MATERIALS THROUGH SPRAY AND FREEZE DRYING

6.1 Abstract

Lentil protein isolate (LPI)-κ-carrageenan (κ-C) and -ι-carrageenan (ι-C) based microcapsules were prepared through spray-drying and freeze-drying to encapsulate flaxseed oil to reach the final oil levels of 20% and 30%. The corresponding emulsion properties, the microcapsules' physical properties, surface oil, encapsulation efficiency, oil oxidation stability, and *in vitro* oil release were determined. For emulsion properties, all LPI-κ-C and LPI-ι-C emulsions remained 100% stable after 48 h, while the LPI emulsions destabilized quickly after homogenization mainly due to low emulsion viscosity. Emulsions were then spray dried or freeze dried. For spray-dried microcapsules, the highest yield was attributed to LPI-ι-C with 20% oil, followed by LPI-κ-C 20% and LPI-ι-C 30%, and all other systems resulted very low yields. The spray-drying capsules showed lower water activity (a_w) and more whiteness compared to the freeze-drying capsules. Flaxseed oil was oxidized more significantly among the spray-dried capsules compared to untreated oil due to heat applied during drying. Flaxseed oil was more stable in all the freeze-dried capsules and showed significant lower oil oxidation than the untreated oil after 8 weeks of storage. For *in vitro* oil release profile, higher amount of oil was released for LPI-κ-C powders due to digestive enzymes under simulated gastric fluid (SGF), while more oil was released for LPI-ι-C powders due to digestive enzymes under simulated gastric fluid and simulated intestinal fluid (SGF + SIF) regardless of drying method and oil content. This study enhanced the emulsion stability by applying carrageenan to LPI and showed the potential to make plant-based microcapsules to deliver omega-3 oils.

6.2 Introduction

Flaxseed oil contains a rich source of polyunsaturated fatty acids such as α-linolenic acid (ALA; ~50%), oleic acid (~20%) and linoleic acid (~15%) (Mohanan et al., 2018; Shim et al., 2015). ALA, an omega-3 fatty acid, provides health benefits such as developing the brain and nervous system in infants, preventing cardiovascular diseases and immune response disorders, and reducing cholesterol levels (Reifen et al., 2015). Also, ALA acts as the precursor of eicosapentaenoic acid (EPA) and docosahexaenoic acid (DHA) for humans (Menin et al., 2018). However, polyunsaturated fatty acids are highly susceptible to oxidation under the presence of light, heat, or reactive oxygen species leading to oil rancidity, loss of nutritional value and flavor, as well as texture and color changes (Mohanan et al., 2018). Microencapsulation can be an effective method to enhance the oxidative stability of flaxseed oil.

Encapsulation is a process to produce microcapsules with sizes ranging from less than 1 μm to more than 1000 μm, where the bioactive core is entrapped in the wall materials to ensure the functionality of the bioactive compounds and to provide their controlled delivery (Chang et al., 2016; Gharsallaoui et al., 2007; Eghbal & Ghoudhary, 2018). Microencapsulation by complex coacervation, followed by drying is one of the most widely used encapsulation technique for entrapping a lipid core (Bakry et al., 2016). In terms of production, a coacervate-based emulsion containing the core materials is first prepared, followed by drying, typically spray-drying and freeze-drying, to yield dried powders (Koupantsis et al., 2014; Chang et al., 2016). Coacervation encapsulation is a simple, solvent-free, and low-cost process, which is excellent for the industrial scale (Xiao et al., 2014). Complex coacervation occurs involving the electrostatic attraction between biopolymers such as proteins and polysaccharides during an acid pH titration, where soluble complexes are formed at the initially detectable change in turbidity and formation of insoluble complexes happens at further acidification with greater protein-polysaccharide interactions (Ye, 2008; Turgeon & Laneuville, 2009). Spray-drying involves the atomization of the emulsion into spherical dry powders with embedded oil at elevated temperature (Drusch, 2006). It is a common drying method widely used in the food industry due to its low cost compared and easy handled (Gharsallaoui et al., 2007). However, spray-drying requires wall materials to have good solubility and leads to a lot of energy waste due to heat loss in the drying chamber and final products with lower oxidative stability (Bakry et al., 2016; Gharsallaoui et al., 2007). Freeze-drying is an attractive drying method due to its simple process and easy handling. Freeze drying is

normally applied for heat sensitive products and results in volatile compounds with longer retention times (Krokida & Philippopoulos, 2006). During the process, the emulsion is frozen between – 90 °C to – 40 °C, and the pressure is reduced by the vacuum pump, which leads to the sublimation of the frozen water (Bakry et al., 2016). Nevertheless, freeze-drying requires long processing time, higher cost, and high energy consumption. Studies have been conducted on investigating microencapsulated powders prepared by coacervation and subsequent drying such as microcapsules of encapsulated palm oil by chitosan-xanthan coacervates with spray-drying (Rutz et al., 2017), β-pinene containing microcapsules by milk proteins-carboxymethylcellulose coacervates and freeze-drying (Koupantsis, et al., 2014), β-carotene containing microcapsules were prepared by chitosan-sodium tripolyphosphate coacervates or chitosan-carboxymethyl cellulose coacervates with freeze-drying (Rutz et al., 2016), and tuna oil encapsulated microcapsules with whey protein-gum Arabic and both spray- and freeze-drying (Eratte et al., 2014).

The selection of biopolymers is critical as their characteristics can greatly affect coacervation, spray-drying, and freeze-drying process. The use of plant protein ingredients within the food industry is increasing rapidly due to their lower cost, greater environmental sustainability, perceived safety concerns related to consuming animal products, and consumer dietary preferences. Lentil proteins are gaining tremendous interests because of their non-GMO status, low allergenicity, high solubility among plant proteins, and abundance in Canada (Liang & Tang, 2014). The dominant proteins in lentil proteins are globulin-type (50-65%) and albumin-type (10-25%) proteins (Jarpa-Parra, 2018). Carrageenan is widely applied in foods because of its texture improving property and its ability to produce products with high encapsulation efficiency in control-delivery systems (Li et al., 2014; Van de Velde et al., 2002). Carrageenan is a linear sulfated galactans with β (1-3) and α (1-4) linkages that extracted from red seaweeds in the class *Rhodophyceae* (Necas & Bartosikova, 2013). Carrageenan can be classified into κ-, ι-, and λ-carrageenan with 1, 2, and 3, respectively, sulfate groups per disaccharide unit (Necas & Bartosikova, 2013). Maltodextrin (MD) is an ingredient that is obtained from the enzymatic (e.g. α-amylase) or acid hydrolysis of starch, followed by drying (Rezende & Hashizume, 2018). Maltodextrin has dextrose equivalent (DE) value less than 20, and a larger DE value means a higher degree of hydrolysis of starch (Qi & Tester, 2018). Maltodextrin is a common secondary wall material for microencapsulation due to the excellent functional properties such as high

solubility, low viscosity at higher concentration, and low affinity to hydrophobic compounds (Suryabhan et al., 2019; Carneiro et al., 2013).

Studies have been conducted on using protein only to microencapsulate omega-3 oil, such as flaxseed oil containing microcapsules by whey protein concentrate and spray-drying (Carneiro et al., 2013), flaxseed oil containing microcapsules by LPI and freeze-drying (Avramenko et al., 2016), and fish oil containing microcapsules by soy protein isolate and spray-drying (Di Giorgio et al., 2019). However, the encapsulation efficiency of oil for these systems were all below 65% when the oil level was 20%. Investigations on using insoluble complexes for microencapsulation have also been conducted, such as tuna oil containing microcapsules by whey protein isolate-gum Arabic insoluble complexes and freeze-drying (Eratte et al., 2014) and β-pinene containing microcapsules by milk proteins-carboxymethylcellulose insoluble complexes and freeze-drying (Koupantsis et al., 2014). However, our previous work (Wang et al., 2021) suggested more stable emulsions were prepared by using soluble complexes rather than insoluble complexes within the systems of LPI-κ-C and LPI-ι-C at all investigated LPI: carrageenan mixing ratios (i.e. 4:1, 8:1, & 12:1) or homogeneous LPI. That was because soluble complexes were smaller in size compared to LPI aggregates and insoluble complexes, and soluble complexes lowered the interfacial tension to a greater extent. In that work, the most stable emulsion was prepared by soluble complexes at 4:1 LPI: carrageenan (both κ-C and ι-C) at pH 6. Therefore, the objective of this work was to look at the possible use of lentil protein isolate-carrageenan based materials to encapsulate edible oil by first incorporating κ-C and ι-C to LPI to form stable emulsions, along with MD to the system as a coating wall material. Subsequent spray-drying and freeze-drying were then applied to produce microencapsulated powders with better qualities such as higher encapsulation efficiency, oxidative stability, and release properties.

6.3 Materials and methods

6.3.1 Materials

Lentil protein isolate (LPI) used in this study was generously donated by KeyLeaf Corp. (Saskatoon, SK), and was produced by alkaline extraction (pH 9.5) followed by isoelectric precipitation (pH 4.5), followed by neutralization and spray drying. κ-Carrageenan (κ-C; Lot#: 0001432063) and ι-carrageenan (ι-C; Batch #: 075K1808) were purchased from Sigma-Aldrich Co (Oakville, ON, Canada). Maltodextrin (MALTRIN M100, dextrose equivalent of 9.0–12.0)

was donated by Grain Processing Corporation (Muscatine, IA, USA). Flaxseed oil, which was produced by cold pressing, was provided from Bioriginal Food and Science Crop. (Saskatoon, SK). All other chemicals used in this study were of reagent grade and purchased through Sigma-Aldrich Co (Oakville, ON, Canada). Water was filtered through a Milli-Q purification system (Millipore Corporation, MA, USA).

6.3.2 Proximate analysis

Proximate analysis of all materials including moisture, ash, lipid and crude protein (reported on a dry weight basis (d.b.)) was determined according to the Association of Official Analytical Chemists (AOAC) methods 925.10, 923.03, 920.85, and 920.87, respectively (AOAC, 2003). Carbohydrate content was calculated based on percent differential from 100%. Lentil protein isolate (LPI) was found to contain 80.6% (d.b.) protein, whereas κ- and ι-carrageenan had 77.6% (d.b.) and 71.2% (d.b.) carbohydrate, respectively. Maltodextrin contained 99.3% (d.b.) carbohydrate. Complete proximate composition results are given in Table A1 (Appendix).

6.3.3 Emulsion characteristics

6.3.3.1 Emulsion preparation

Homogeneous LPI, 4:1 LPI-κ-C, and 4:1 LPI-ι-C plus maltodextrin were used as wall materials to encapsulate flaxseed oil. Four hundred milli-litres of each initial emulsion were prepared, and the ratio of oil: (LPI/ LPI-κ-C/ LPI-ι-C): MD were 5:1:19 and 7.5:1:16.5 (w/w/w) to achieve the final oil level of 20% or 30% respectively in dried powders. The details of the compositions of formulations were given the Table A2 (Appendix). In brief, LPI, κ-C, and ι-C powders were dispersed on Milli-Q water under magnetic stirring at 500 rpm for 16 h stirring on room temperature (21-23 °C). The LPI, LPI-κ-C and LPI-ι-C solutions were then mixed at pH 6 for another hour. The resulting solutions were then mixed with 20 g or 30 g of flaxseed oil at 500 rpm for 15 min. Homogenization process was then applied to the resulting mixture at 15,000 rpm using a rotor stator system (Polytron PT2100 homogenizer) (Kinematica AG, Lucerne, Switzerland) equipped with a 12 mm PT-DA 2112/2EC generating probe for 5 min. In parallel, maltodextrin was dispersed in Milli-Q water for 1 h with magnetic stirring at 500 rpm, and the pH of solution was adjusted to 6. The emulsions were then mixed with maltodextrin solution for another 15 min stirring. The resulting emulsions were then re-homogenized with the same

homogenizer at the same speed for another 5 min. All emulsions were prepared in triplicate and reported as the mean ± one standard deviation (n = 3).

6.3.3.2 Emulsion stability (ES)

ES was determined according to Wang et al. (2019a) based on creaming overtime at room temperature (21–23 °C). Ten milli-liters of the fresh emulsion was transferred to a 10 mL graduated cylinder (inner diameter = 9.60 mm; height = 114.96 mm; measured by a digital caliper) and allowed to separate for 48 h. The percentage of ES was determined using Eq. (6.1), where V_B and V_A are the volume of the aqueous phase before emulsification (8.0 mL) and after drainage at each time point, respectively.

$$\%ES = \frac{V_B - V_A}{V_B} \times 100\% \quad (6.1)$$

All measurements were performed in triplicate and reported as the mean ± one standard deviation (n = 3).

6.3.3.3 Droplet size and distribution

Each freshly prepared emulsion and reconstituted emulsion (1 g powder in 4 mL Milli-Q water) were placed in a Mastersizer 2000 laser light scattering instrument (Malvern Instruments Ltd., Worcestershire, UK) equipped with a Hydro 2000S sample handling unit at room temperature (21–23 °C) as described by Can Karaca et al. (2013) to measure the average droplet size and distribution. The relative refractive index of emulsion was 1.112, which was calculated as the ratio of the refractive index of flaxseed oil (1.479) to the refractive index of water (1.33). The particle size was reported as surface-average diameter ($D_{3,2}$) and volume-average diameter ($D_{4,3}$) expressed using Eq. (6.2) and (6.3), respectively.

$$D_{3,2} = \frac{\sum_{i=1} N_i d_i^3}{\sum_{i=1} N_i d_i^2} \quad (6.2)$$

$$D_{4,3} = \frac{\sum_{i=1} N_i d_i^4}{\sum_{i=1} N_i d_i^3} \quad (6.3)$$

where N_i is the total number of particles of diameter (*di*) (McClements, 2015). All measurements were performed in triplicate, and two measurements were made for each replicate. The average

value of two measurements in each replicate was collected and reported as the mean ± one standard deviation (n = 3).

6.3.3.4 Droplet charge

For the droplet charge of emulsions, ten drops of each of the fresh emulsion were dispersed into 100 mL Milli-Q water at the corresponding pH values, and the dispersions were shaken gently to become homogeneous and used to measure droplet charge.

The electrophoretic mobility (i.e., velocity of a particle within an electric field, U_E) was used to calculate the zeta potential (ς) by using the Henry equation.

$$U_E = \frac{2\varepsilon \times \xi \times f(\kappa\alpha)}{3\eta} \quad (6.4)$$

where η is the dispersion viscosity (water in this study), ε is the permittivity, and $f(\kappa\alpha)$ is a function related to the Debye length (κ) and the ratio of particle radius (α) (Aryee & Nickerson, 2012). *f*(κα) equals to 1.5 according to the Smoluchowski approximation. All the measurements were performed at room temperature (22.5 °C) in triplicate, and two measurements were made for each replicate. The average value of two measurements in each replicate was collected and reported as the mean ± one standard deviation (n = 3).

6.3.3.5 Emulsion viscosity

Each solution or emulsion (~0.62 mL) were placed onto the AR-G2 Rheometer (TA Instruments, New Castle, DE) equipped with a 40 mm diameter 2° acrylic cone (Hopkins et al., 2015). Apparent viscosity was measured as a function of shear rate (2 to 200 s^{-1}), and 10 data points were collected per logarithmic decade. Data were then fitted with the power-law model:

$$\log \text{viscosity} = (n-1) \log \text{shear rate} + \log m \quad (6.5)$$

where m is the consistency coefficient (equivalent to the apparent viscosity at 1 s^{-1}) and n is the flow behavior index. All measurements were performed in triplicate, and the m, n values were reported as the mean ± one standard deviation (n = 3).

6.3.3.6 Confocal laser scanning microscopy (CLSM)

LPI-carrageenan stabilized emulsions prepared as previously described were imaged through CLSM using 543 and 633nm lasers (Wang et al., 2019a). Nile red (0.01% (w/w)) with a maximum excitation and emission wavelength of 543 nm and 573-613 nm, respectively was added into the flaxseed oil with stirring overnight at room temperature (21-23 °C) prior to emulsion preparation. 0.1% (w/w) of Fast green in water with the excitation and emission at 633 and 650 nm, respectively was mixed with emulsions to bind with protein in the continuous phase to reach the final fast green concentration at 0.01% (w/w). Emulsions were made in triplicate, and 4 images were taken per slide with the use of a 60x objective lens.

6.3.4 Characteristics of microencapsulated powders

6.3.4.1 Microencapsulation by spray drying and freeze drying

The freshly prepared emulsions were spray dried using a benchtop Buchi Advanced Mini Spray Drier B-290 (Buchi Labortechnik AG, Flawil, Switzerland) equipped with an atomizing nozzle (0.7 mm diameter). The air flow was set at 473 L/h and 0.41, and the aspiration rate was 38 m^3/h. The emulsion was stirring at 200 rpm before going into the chamber to avoid droplets aggregation, and the emulsion was pumped at 3 mL/ min. The inlet temperature was 135°C ± 1 °C, and the outlet temperature was 95°C ± 2 °C. Microcapsules produced from spray drying for each formula were performed in triplicate.

For freeze drying, each emulsion was poured into a small aluminum pan and frozen at –80 °C. All the samples were then freeze dried in a Labconco Free Zone 6 freeze dryer (Labconco Corp., Kansas City, MO, USA). The freeze dryer was initially at –20 °C for a few hours and was then raised to –4 °C for the rest of the drying time until the samples were completely dried.

6.3.4.2 Recovered solid yield

The yield of recovered solid was calculated as the ratio of the powders collected after drying process and weight of core material and wall materials, shown in equation:

$$Recovered\ solid\ yield\ (\%) = \frac{weight\ of\ powders\ collected\ (g)}{weight\ of\ core\ and\ wall\ materials\ (g)} \times 100\% \qquad (6.6)$$

6.3.4.3 Physical characteristics

Moisture content of microcapsules was determined according to the Association of Official Analytical Chemists (AOAC) methods 925.10 moisture (AOAC, 2003). The water activity (a_w) of microcapsules was measured with an AquaLab 4TE water activity meter (Decagon Devices, Inc., Pullman, WA, USA) with a 0.001 sensitivity at 22 °C.

The color of microcapsules was measured using a Hunter Colorimeter (ColorFlex EZ 45/0, Hunter Associates Laboratory, Inc., Reston, VA, USA), and the *L* (lightness), *a* (redness), and *b* (yellowness) were reported.

Wettability of microcapsules was measured according to Chew et al., (2018) with some modification. 0.5 gram of microcapsules was added into 50 mL Milli-Q water with magnetic stirring at 150 rpm at room temperature (21–23 °C). The time of microcapsules to be full dissolution was recorded.

All the measurements were performed in triplicate, and two measurements were made for each replicate. The average value of two measurements in each replicate was collected and reported as the mean ± one standard deviation (n = 3).

6.3.4.4 Surface oil and encapsulation efficiency

Surface oil and encapsulation efficiency were determined based on Haq & Chun (2018) with some modifications. A 50 mL centrifuge tube was used to weight 1 g of microcapsules and 30 mL of hexane. The tube was then vortexed for 30 s to extract the surface oil. The solvent was then filtered twice using #1 Whatman filter paper (Whatman International Ltd., Maidstone, UK), and the organic solvent was collected a 100 mL beaker and evaporated in a fume hood for overnight, followed by drying at 105 °C for 30 min. The surface oil of microcapsules was weighted. Surface oil (SO) and entrapment efficiency (EE) was calculated based on the definition:

$$SO = \frac{weight\ of\ surface\ oil\ on\ the\ microcapsules\ (g)}{weight\ of\ microcapsules\ (g)} \times 100\% \quad (6.7)$$

$$EE = \frac{total\ oil\ (\%) - surface\ oil\ (\%)}{total\ oil\ (\%)} \times 100\% \quad (6.8)$$

Where total oil is the oil content of 20% or 30%. Measurements were performed in triplicate and reported as the mean ± one standard deviation (n = 3).

6.3.4.5 Microcapsule morphology

Surface morphology of the spray- and freeze-dried powders was imaged using a scanning electron microscope (SEM) of Phenom G2Pure (Phenom-World, Eindhoven, Netherlands). The microcapsules were coated with gold and imaged at 1000X magnification.

6.3.4.6 Oxidative stability

Oxidative stability of the encapsulated flaxseed oil in microcapsules were determined by measuring peroxide value (PV) and 2-thiobarbituric acid reactive substances (TBARS) every week of storage over an 8-week period at room temperature (21–23 °C). Modified from Can Karaca and co-workers (2013), encapsulated oils were extracted by dissolving about 1.5 g microcapsules in 6 mL Milli-Q water, followed by 15 min-stirring at 500 rpm. Mixture of 40 mL hexane/isopropanol (3:1, v/v) was added to extract the oil with another 15 min stirring. Aluminum foil was applied to the beaker to prevent light-induced oil oxidation. The resulting mixtures were centrifuged at 4,193 × g for 15 min at room temperature. The organic solvent (top layer) was then transferred to a 250 mL Erlenmeyer flask and dried under a stream of nitrogen in the fume hood. The oxidative stability of the untreated flaxseed oil was used as the control sample, and same extraction process was applied. Only the powders using mixed wall materials were conducted since the LPI-20% and 30% formed poor capsules due to emulsion instability.

6.3.4.6.1 Peroxide value (PV)

Experiment was conducted according to Chang et al. (2016) and Koc et al. (2015). About 0.2 g of flaxseed oil was mixed with 10 mL of acetic acid/chloroform solution (3:2, v/v) and 200 µL of saturated potassium iodide (KI). The solution was allowed to react for 1 min with occasional shaking, and 10 mL of Milli-Q water was added to stop the reaction. The solution was then titrated with 0.001 N sodium thiosulfate ($Na_2S_2O_3$) with the presence of 1% (w/v) cooked corn starch indicator until the violet color disappeared. PV of oil was calculated using the following formula:

$$PV = \frac{(S-B)\times N\times 1000}{W} \quad (6.9)$$

where S is the volume (mL) of $Na_2S_2O_3$ solution used to titrate the encapsulated and untreated oils, B is the volume (mL) of $Na_2S_2O_3$ solution used to titrate the blank (without oils), N is the normality

of $Na_2S_2O_3$ solution, and W is the oil weight (g). Measurements were performed in triplicate and reported as the mean ± one standard deviation (n = 3).

6.3.4.6.2 2-Thiobarbituric acid reactive substances (TBARS)

TBARS test was performed according to Akhlaghi & Bandy (2010) with some modifications. Solutions including 50 μL of 8.1% (w/v) SDS, 375 μL of 20% acetic acid (~ pH 3.5), 375 μL of 0.8% (w/v) 2-thiobarbituric acid (TBA), 8.25 μL of 0.02% (w/v) butylated hydroxytoluene (BHT) (in dimethyl sulfoxide (DMSO)) and 200 μL of the emulsified oil mixture (about 15 mg of oil dissolved in 10 mL of 2% SDS-20 mM acetic acid-sodium acetate buffer at pH 3.5) were added in a 2.0 mL centrifuge tube. The blank was prepared under the same experimental conditions except that 200 μL of 2% SDS-20 mM acetic acid-sodium acetate buffer was added. A standard curve was prepared using malondialdehyde (MDA) (0.25 - 5 nM) under the same conditions. Samples and standards were then heated at 95 °C for 1 h, followed by 5 min cooling and 10 min centrifugation at 4000 ×g (Eppendorf Centrifuge 5424, Hamburg, Germany). Absorbance at 532 nm for all solutions was measured. TBA values were expressed as mg MDA/g oil. All the measurements were performed in triplicate, and two measurements were made for each replicate. The average value of two measurements in each replicate was collected and reported as the mean ± one standard deviation (n = 3).

6.3.4.7 Oil release characteristics

The release profile of the encapsulated flaxseed oil was examined by an in vitro assay simulating gastric and intestinal conditions with some modifications (Can Karaca et al., 2013). Simulated gastric fluid (SGF; 1 L at pH 1.2) contained 3.2 g pepsin, 2 g NaCl, and 7.0 mL 36% HCl, and simulated intestinal fluid (SIF; 1 L at pH 6.8) was prepared by adding 10 g pancreatin, 6.8 g K_2HPO_4. For exposure to SGF, approximately 1 g of microcapsules was mixed with 10 mL SGF and incubated in a shaking water bath at 100 rpm for 2 h at 37 °C. The solution was then vortexed with the 15 mL of hexane to extract the release oil, followed by centrifugation at 4,193 × *g* for 10 min at room temperature. The oil was determined gravimetrically similar to previous described. For exposure to SGF and SIF in sequence, 1 g of powder was mixed the 10 mL SGF and incubated under the same conditions. The pH of the resulting solution was then adjusted the pH 6.8 with the addition of 10 mL SIF, followed by 3 h incubation at 37 °C at 100 rpm. The

solution was then vortexed with the 30 mL of hexane to extract the release oil, and the oil was determined gravimetrically. In parallel, same conditions except that no digestive enzyme was added were applied to each sample to measure the amount of oil release without enzymes. Finally, each oil release value was reported as the percentage of oil released under the use of digestive enzymes minus the percentage of oil released without the use of digestive enzymes. Measurements were performed in triplicate and reported as the mean ± one standard deviation (n = 3). Only the mixed wall materials were used since the LPI-20% and 30% formed poor capsules due to emulsion instability.

6.3.5 Statistics

A one-way analysis of variance with a Scheffe test were performed to determine differences for all emulsions and reconstituted emulsions in emulsion stability, consistency coefficient and flow behavior index of emulsion viscosity, droplet size ($D_{3,2}$, $D_{4,3}$), droplet charge. Also, it was used to determine the difference for powders within each type of drying method for water activity, moisture, color (L, a, b), wettability, surface oil, encapsulation efficiency. Peroxide value and TBARS were determined through a Tukey HSD test. The independent T-test was performed to access the differences of droplet size ($D_{3,2}$, $D_{4,3}$) between the initial emulsion and its corresponding reconstituted spray- or freeze-drying emulsions. All statistics were performed using SPSS software.

6.4 Results and discussion

6.4.1 Emulsion characteristics

Initial emulsions were first homogenized by LPI, LPI-κ-C, or LPI-ι-C solutions at pH 6, followed by a second homogenization with MD solutions to alter the final viscosity of the emulsions. Each initial emulsion contained 5% or 7.5% flaxseed oil to deliver 20% or 30% of final oil respectively in the dried microencapsulated powders. Details of each formula were given in Table A2 (Appendix). In terms of naming, for instance, the initial LPI emulsion containing 5% oil was prepared to deliver 20% oil, so it was named as LPI 20% in all tables and figures. Emulsion characteristics such as emulsion stability (via creaming), droplet charge, emulsion viscosity, and droplet size were determined (Table 6.1 & 6.2). For emulsion stability, gravitational separation occurred rapidly after emulsification for LPI 20% and LPI 30% emulsions. Emulsions stabilized

by LPI-κ-C or LPI-ι-C complexes showed significant increase in stability against creaming, where all emulsions with 20% or 30% final oil remained 100% stability after 48 h (Table 6.1).

Table 6.1 Emulsions characteristics for emulsions stabilized by homogeneous lentil protein isolate (LPI) solutions and mixtures of LPI with κ-, ι-carrageenan at pH 6 to deliver 20% and 30% oil. Data represents the mean ± one standard deviation (n = 3).

Type of emulsions[1]	Emulsion stability at 48 h (%)	Droplet charge (mV)	Consistency coefficient (mPa s)	Flow behavior index
LPI 20%	n.d.	-40.40 ± 0.95^{d}	23.7 ± 4.4^{d}	0.69 ± 0.04^{bc}
LPI 30%	n.d.	-43.43 ± 1.58^{d}	19.9 ± 5.4^{d}	0.74 ± 0.04^{ab}
LPI-ι-C 20%	100.0 ± 0.0^{a}	-58.80 ± 0.82^{c}	270.2 ± 7.9^{a}	0.61 ± 0.01^{c}
LPI-ι-C 30%	100.0 ± 0.0^{a}	-61.27 ± 1.64^{bc}	277.3 ± 4.8^{a}	0.62 ± 0.00^{c}
LPI-κ-C 20%	100.0 ± 0.0^{a}	-65.55 ± 1.24^{a}	68.6 ± 13.2^{c}	0.83 ± 0.03^{a}
LPI-κ-C 30%	100.0 ± 0.0^{a}	-63.92 ± 0.98^{ab}	116.8 ± 26.3^{b}	0.75 ± 0.03^{ab}

- Emulsion stability was not determined for LPI 20% and 30% emulsions as they rapidly destabilized in a few minutes after emulsification. Abbreviation: n.d., not determined.
- Droplet charge and Power-law parameters were determined immediately after homogenization.
- [1]Type of emulsions: the percentage on the name of the samples represents the final oil content in dried powders

Table 6.2 Droplet size of fresh emulsions and reconstituted emulsions. Data represents the mean ± one standard deviation (n = 3).

	Emulsions		Reconstituted spray-drying emulsions		Reconstituted freeze-drying emulsions	
	droplet size $D_{3,2}$ (μm)	droplet size $D_{4,3}$ (μm)	droplet size $D_{3,2}$ (μm)	droplet size $D_{4,3}$ (μm)	droplet size $D_{3,2}$ (μm)	droplet size $D_{4,3}$ (μm)
LPI 20%	11.85 ± 0.58^{a}	20.74 ± 0.42^{bc}	n.d.	n.d.	11.25 ± 1.01^{a}	23.84 ± 1.24^{b}
LPI 30%	12.66 ± 1.71^{a}	21.12 ± 2.95^{bc}	n.d.	n.d.	11.84 ± 0.35^{a}	27.13 ± 1.24^{ab}
LPI-ι-C 20%	10.83 ± 0.18^{a}	28.78 ± 1.82^{a}	7.33 ± 0.09^{a}	20.48 ± 1.70^{a}	10.57 ± 0.79^{a}	29.80 ± 2.27^{a}
LPI-ι-C 30%	10.34 ± 0.45^{a}	25.06 ± 0.68^{ab}	7.30 ± 0.28^{a}	19.14 ± 1.63^{a}	10.47 ± 0.11^{a}	32.02 ± 2.50^{a}
LPI-κ-C 20%	7.68 ± 0.28^{b}	19.60 ± 1.27^{c}	4.05 ± 0.15^{b}	11.34 ± 0.66^{b}	8.22 ± 0.40^{b}	23.29 ± 1.30^{b}
LPI-κ-C 30%	6.77 ± 0.46^{b}	21.66 ± 0.79^{bc}	*	*	7.34 ± 0.58^{b}	23.80 ± 1.88^{b}

- *Indicates the very low yield of the powders of LPI-κ-C 30%; Abbreviation: n.d., not determined.
- The percentage on the name of the samples represents the final oil content in dried powders.

In terms of droplet size, LPI-κ-C 20% and 30% emulsions formed the smallest droplets ($p<0.05$) with $D_{3,2}$ of 6.8 μm and 7.7 μm, respectively, and $D_{4,3}$ of 19.6 μm and 21.7 μm, respectively (Table 6.2). The smaller values of $D_{3,2}$ ($p<0.05$) for both LPI-κ-C emulsions suggested the formation of larger numbers of smaller droplets. $D_{3,2}$ of LPI 20%, LPI 30%, LPI-ι-C 20%, and LPI-ι-C 30% emulsions were all found to range from 10 to 12 μm ($p>0.05$). $D_{4,3}$ values of LPI 20% and LPI 30% emulsions were ~20 μm, which were similar as in the LPI-κ-C 20% and 30% emulsions ($p>0.05$). LPI-ι-C 20% and 30% emulsions showed the largest $D_{4,3}$ among all systems of 28.8 and 25.1 μm, respectively ($p<0.05$) suggesting the presence of some large droplets. Since the average droplet sizes of all systems were comparable, other factors such as droplet charge and viscosity are hypothesized to cause the rapid gravitational separation for the LPI 20% and 30% emulsions. Droplet charge of each emulsion was given in Table 6.1. The strongest electrostatic repulsion was attributed to LPI-κ-C 20% and 30% emulsions with charges of -66 and -64 mV, respectively. Droplet charge for LPI-ι-C 20% and 30% emulsions was -59 and -61 mV, respectively, which was slightly smaller than both LPI-κ-C emulsions ($p<0.05$) but still providing significant electrostatic repulsive forces. LPI 20% and 30% emulsions generated the least electrostatic repulsion ($p<0.05$) against droplet aggregation with droplet charges of -40 and -43 mV. However, the electrostatic repulsion was still considered to be moderate (McClements, 2015).

Emulsion viscosity could also have an effect on emulsion stability. The consistency coefficient (m) and the flow behavior index (n) for each system was given in Table 6.1 (See flow curves, Figure A6.1). LPI 20% and 30% emulsions showed the lowest viscosity ($p<0.05$) with the m-values of 24 and 20 mPa s, respectively, and this low viscosity led to a remarkable high rate of creaming. Incorporating κ-C and ι-C into the systems both led to higher emulsion viscosity, where LPI-ι-C 20% and 30% emulsions showed the greatest emulsion viscosity ($p<0.05$) of 270 and 277 mPa s, respectively, followed by LPI-κ-C 30% with m-value of 117 mPa s ($p<0.05$), and then LPI-κ-C 20% of 69 mPa s ($p<0.05$). At pH 6, LPI was forming soluble complexes with κ-C and ι-C, and excessing carrageenan was contributing to the viscosity to reduce creaming effect, as both carrageenan polysaccharides are good thickening reagents and have good water binding properties (Li et al., 2014; McClements, 2015). Within these two carrageenan polysaccharides, ι-C contains two sulfate groups per disaccharide unit and was able to bind with more water molecules to contribute to a higher viscosity in LPI-ι-C 20% and 30% emulsions (Necas & Bartosikova, 2013). As the oil content of the initial emulsions did not vary (i.e. 5% and 7.5% oil), the viscosity of two

emulsions within each type of system showed no difference between each other ($p>0.05$). It was also worth to mention that the larger $D_{4,3}$ values of LPI-ι-C 20% and 30% emulsions were resulted from the higher emulsion viscosities. Studies have suggested that suppression of breaking up droplets during homogenization might occur as the viscosity of an emulsion continuous phase increased (McClements, 2015; Walstra, 1993; Wooster et al., 2008). All emulsions were shear thinning as shown in the flow curves (Figure A6.1). The highest n-value was attributed to the LPI-κ-C 20% emulsion, followed by LPI-κ-C 20%, LPI 30%, and LPI 20% emulsions. LPI-ι-C 20% and 30% emulsions showed the smallest n-values, corresponding to their larger average droplet size and in terms of less homogeneous systems. Viscosity can not only affect emulsion stability but is also extremely important in the subsequent spray-drying process to prepare dried powders. Studies suggested that liquid that fed in the spray dryer generally should not have its viscosity exceed 300 mPa s to prevent the formation of large or elongated droplets and air inclusion in the droplets during atomization, which in terms will cause negative effects on dried powder's characteristics (Di Battista et al., 2015). In this study, all emulsion viscosities were below 300 mPa s.

Confocal laser scanning microscopy images were taken for each fresh initial emulsion (Figure 6.1). For both LPI 20% and 30% emulsions, very large droplets were observed, confirming the rapid destabilization of the emulsions due to droplet coalescence (Figure 6.1A & B). In contrast, small droplets were seen in LPI-κ-C 20% & 30% and LPI-ι-C 20% & 30% emulsions with some larger size at about 20-25 μm and a lot of them below 10 μm, corresponding to their average droplet size (Figure 6.3C - F; Table 6.2). The protein aggregates in both LPI 20% and 30% emulsions were also larger in size (marked as green; Figure 6.1A & B) compared to all other LPI-κ-C and LPI-ι-C emulsions (Figure 6.3C – F), which suggested the incorporation of carrageenan could suppress the formation of large protein aggregates, corresponding to our previous findings (Wang et al., 2019a; Wang et al., 2019b). It was also confirmed that the oil droplets were surrounded by LPI, LPI-κ-C, or LPI-ι-C complexes. A representative image of LPI-ι-C 20% emulsion was provided in Figure A6.2 (Appendix).

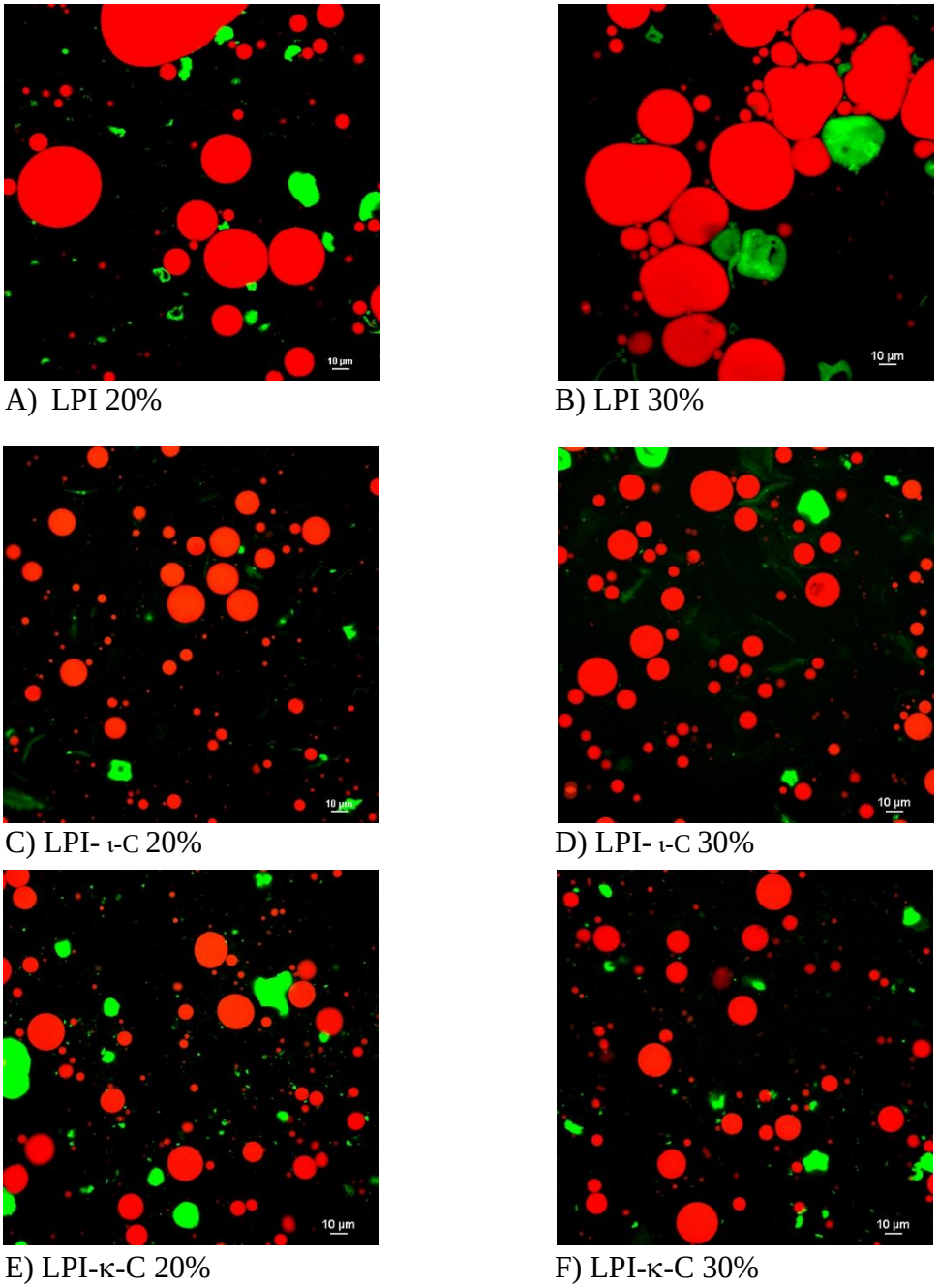

A) LPI 20% B) LPI 30%

C) LPI- ι-C 20% D) LPI- ι-C 30%

E) LPI-κ-C 20% F) LPI-κ-C 30%

Figure 6.1 Confocal laser scanning microscopy (CLSM) images of oil-in-water emulsions for systems of LPI 20% and 30% (A and B, respectively), LPI-ι-carrageenan (LPI-ι-C) 20% and 30% (C and D, respectively), and LPI-κ-carrageenan (LPI-κ-C) 20% and 30% (E and F, respectively). Red color represents oil droplets, and green color represents proteins. All the scale bars represent 10 µ. The percentage on the name of the samples represents the final oil content in dried powders.

6.4.2 Physical characteristics of spray-drying powders and freeze-drying powders

6.4.2.1 Yield of dried powders

The initial emulsions were either spray-dried and freeze-dried to give fine powders with 20% and 30% oil. As the LPI 20% and 30% emulsions were highly unstable, these two emulsions were not applied to spray-drying. However, they were applied to freeze-drying since emulsions were frozen at -80 °C prior. All the solids (i.e. powders) were collected from freeze-drying, but only part of the powders were able to be collected during the spray-drying process. The yields of LPI-ι-C 20%, LPI-ι-C 30%, LPI-κ-C 20%, and LPI-κ-C 30% powders from spray drying were 32.8%, 16.8%, 20.5%, and below 5%, respectively. Due to the very low yield of LPI-κ-C 30% powders, no further experiments were conducted on this system. Yield of powders may have also been affected by oil content in the powders. Both LPI-ι-C and LPI-κ-C powders with 20% final oil showed higher yield to their corresponding powders with 30% oil, which could be attributed to lack of sufficient coverage of wall materials to the oil (Polavarapu, Oliver, Ajlouni, & Augustin, 2011), leading to more samples sticking on the surface of the cylinder and cyclone during drying. Lower yield caused by higher encapsulated oil was also observed in the encapsulation of fish oil in soybean protein powders (Di Giorgio et al., 2019).

6.4.2.2 Physical characteristics of dried powders

The physical properties including moisture content, water activity, color, and wettability of spray drying (LPI-ι-C 20% & 30%, LPI-κ-C 20%) and freeze drying (LPI 20% & 30%, LPI-ι-C 20% & 30%, LPI-κ-C 20% & 30%) powders were given in Table 6.3. Moisture contents of all spray drying powders were similar ranging between 2.6% to 3.1% ($p>0.05$). The freeze-drying powders had moisture content ranging from 2.7% to 4.1%. It was suggested by the food industry that dry powders should contain 3-4% moisture to ensure good stability during storage (Klaypradit & Huang, 2008; Goyal et al., 2015). Similar moisture contents were also reported in the encapsulated flaxseed oil-modified starch spray-drying powders (Barroso et al., 2014), kenaf seed oil-sodium caseinate spray-drying powders (Chew et al., 2018), and flaxseed oil-LPI-MD freeze-drying powders (Avramenko et al., 2016). Water activity (a_w), which measured the availability of free water in foods, was found to be 0.09 for both LPI-ι-C 20% and 30% powders ($p>0.05$). The a_w of LPI-κ-C 20% powder was significantly lower with a_w value of 0.06 ($p<0.05$), which might be due to the smaller number of sulfate group on per disaccharide unit to bind less water molecules

and lower water solubility of κ-C (Barbeyron et al., 2000), thereby resulting in a more prominent dehydration during spray-drying process and consequently lower a_w value. The a_w values for all freeze-drying powders were ranging from 0.09 to 0.12, again with LPI-κ-C 30% powder showing the lowest a_w value of 0.09. Generally, a_w should be below 0.60 for food products to against microbial spoilage, and for dry powders a_w should not exceed 0.30 (Klaypradit & Huang, 2008; Quek et al., 2007). It is also agreed that non-enzymatic browning and enzymatic activities are inhibited in foods with a_w around 0.3 (Alvarez-Henao et al., 2018; Gamboa-Santos et al., 2013). Therefore, powders produced in this study should be able to against chemical and microbial spoilage well during storage. However, the a_w values of our powders seemed to be lower when compared with those powders with similar moisture contents that referenced above, whose a_w values were ranging from 0.15 to 0.40 (Barroso et al., 2014; Chew et al, 2018; Avramenko et al., 2016). The lower a_w values for powders in current study could be attributed to the large amount of MD (dextrose equivalent [DE]: 9 -12) in wall materials, and similar a_w values were also observed in spray-drying powders where MD with the same DE was the major wall material (Can Karaca et al., 2013; Kuang et al., 2015). The low a_w values might not be ideal to against lipid oxidation in food products. Some studies suggested that a_w of food products should be near the water monolayer (i.e. a_w: 0.2 – 0.3) to minimize lipid oxidation (Chew & Nyam, 2016; Velasco et al., 2003).

Table 6.3 Physical characteristics of spray-drying and freeze-drying powders. Data represents the mean ± one standard deviation (n = 3).

	Water activity	moisture	Color			Wettability (s)	Surface oil (%)	Encapsulation efficiency (%)
			L	a	b			
Spray drying								
LPI-ι-C 20%	0.090 ± 0.008^{a}	2.57 ± 0.21^{a}	93.58 ± 0.31^{a}	0.00 ± 0.06^{a}	10.35 ± 0.39^{b}	441 ± 27^{a}	3.19 ± 0.15^{b}	84.05 ± 0.75^{a}
LPI-ι-C 30%	0.093 ± 0.005^{a}	2.96 ± 0.45^{a}	92.39 ± 0.06^{b}	-0.01 ± 0.07^{a}	13.10 ± 0.35^{a}	459 ± 21^{a}	4.95 ± 0.65^{a}	83.51 ± 2.16^{a}
LPI-κ-C 20%	0.064 ± 0.009^{b}	3.07 ± 0.29^{a}	93.44 ± 0.22^{a}	-0.02 ± 0.03^{a}	10.58 ± 0.53^{b}	412 ± 8^{a}	2.95 ± 0.28^{b}	85.23 ± 1.38^{a}
LPI-κ-C 30%	-	-	-	-	-	-	-	-
Freeze drying								
LPI 20%	0.107 ± 0.005^{ab}	3.91 ± 0.30^{ab}	89.68 ± 0.06^{c}	0.36 ± 0.02^{b}	16.41 ± 0.19^{c}	82 ± 7^{b}	16.21 ± 0.26^{b}	18.94 ± 1.30^{c}
LPI 30%	0.115 ± 0.007^{a}	3.39 ± 0.15^{b}	89.21 ± 0.27^{c}	0.54 ± 0.10^{a}	19.08 ± 0.18^{a}	101 ± 11^{b}	25.17 ± 0.25^{a}	16.10 ± 0.84^{c}
LPI-ι-C 20%	0.103 ± 0.007^{ab}	4.08 ± 0.17^{a}	91.94 ± 0.19^{ab}	0.12 ± 0.05^{c}	14.11 ± 0.22^{d}	239 ± 19^{a}	5.04 ± 0.37^{d}	74.82 ± 1.84^{a}
LPI-ι-C 30%	0.115 ± 0.004^{a}	3.50 ± 0.05^{b}	91.06 ± 0.12^{b}	0.31 ± 0.02^{b}	17.77 ± 0.15^{b}	271 ± 12^{a}	13.51 ± 0.74^{c}	54.95 ± 2.48^{b}
LPI-κ-C 20%	0.102 ± 0.009^{ab}	3.88 ± 0.14^{ab}	92.13 ± 0.07^{a}	0.08 ± 0.04^{c}	13.52 ± 0.29^{d}	234 ± 15^{a}	4.84 ± 0.47^{d}	75.80 ± 2.37^{a}
LPI-κ-C 30%	0.086 ± 0.012^{b}	2.68 ± 0.05^{c}	91.56 ± 0.63^{ab}	0.23 ± 0.02^{bc}	16.25 ± 0.76^{c}	235 ± 6^{a}	14.51 ± 0.66^{c}	51.64 ± 2.21^{b}

- Notes: LPI (20 and 30%) emulsions were too unstable for the spray drying process. LPI-κ-C 30% showed to low of yield in the spray dryer for further measurements.
- Statistics were run within each type of drying method.
- The percentage on the name of the samples represents the final oil content in dried powders.
- Surface oil was calculated as weight of surface oil on the powders divided by weight of powders. Encapsulation efficiency was calculated as the difference of total oil and surface oil divided by total oil.

Color parameters for each powder including *L* (lightness), *a* (redness), and *b* (yellowness) were given in Table 6.3. Spray-drying powders showed stronger lightness ($p<0.05$) with *L* values ranging from 92.4 – 93.6 than freeze-drying powders, whose *L* values were from 89.2 – 92.1. Among freeze-drying powders, LPI 20% and 30% powders showed the strongest darkness ($p<0.05$), which could be attributed to the rapid destabilization of their corresponding emulsions and more oil got separated out. The *a* values of spray-drying powders were all closed to zero ($p>0.05$), while *a* values of freeze-drying powders increased suggesting the freeze-drying powders showed more redness. Stronger whiteness was observed in spray-drying powders, reflected by the lower *b* values, and freeze-drying powders showed more yellowness due to their higher *b* values. The yellowness increased as the final oil level increased among each wall-type of powders ($p<0.05$). Wettability of powders that showed the ability to absorb water was also reported in Table 6.3. A shorter time for a product to become reconstituted in water is more desirable (Chew et al., 2018; Edris et al., 2016). Wettability was significantly affected by wall materials, and LPI 20% and 30% freeze-drying powders showed significantly stronger wettability than other freeze-drying powders ($p<0.05$). Addition of polysaccharide to system led to lower wettability was also observed in LPI-MD based and LPI-MD-alginate based powders (Chang et al., 2016). Wettability was also influenced by drying methods, where all spray-drying powders were more difficult to be wetted than freeze-drying powders ($p<0.05$). The wettability among each spray-drying powder was similar ($p>0.05$) and was compatible with other spray-drying powders such as modified starch-based powders (Barroso et al., 2014) and gum Arabic-sodium caseinate-based powders (Chew et al., 2018).

The average droplet size for each reconstituted emulsion was provided in Table 6.2. For spray-drying powders, the $D_{3,2}$ values of LPI-ι-C 20%, 30%, and LPI-κ-C 20% reconstituted emulsions were 7.3, 7.3, and 4.1 μm, respectively, and the $D_{4,3}$ values were 20.5, 19.1, and 11.3 μm, respectively. All these values were significantly smaller than their corresponding average values in initial fresh emulsions ($p<0.05$), attributing to the samples lose or sample degradation during spray-drying process. The decrease of average dropet size in the reconstituted emulsions were also observed in the chickpea protein-based powders with 10% flaxseed oil (Can Karaca et al., 2013). In terms of freeze-drying reconstituted emulsions, all the $D_{3,2}$ values were similar to their corresponding average values in initial fresh emulsions ($p>0.05$). However, increased $D_{4,3}$ values ($p<0.05$) for LPI 20%, 30%, LPI-ι-C 30%, and LPI-κ-C 20% reconstituted emulsions were

determined, suggesting the presence of larger droplets, which could be due to coalescence that occurred within the non-encapsulated oils. A layer of flaxseed oil was also observed in both LPI 20% and 30% reconstituted freeze-drying emulsions (data not shown), confirming the destabilization of the emulsions prior to freezing.

6.4.3 Surface oil and encapsulation efficiency of dried powders

Surface oil and encapsulation efficiency for each powder were determined and given in Table 6.3. The more desirable powders should contain less amount of surface oil as it negatively affects powder quality such as oxidative stability (Can Karaca et al., 2013). For oil encapsulated powders, this should be less than 2% surface oil and 98% entrapment efficiency (Drusch & Berg, 2008). For spray-drying powders, LPI-ι-C 20% and LPI-κ-C 20% powders showed similar surface oil content at ~3% ($p>0.05$), and the surface oil increased to 5% for LPI-ι-C 30%, indicating there was lack of sufficient wall materials (i.e. LPI-ι-C complexes) to encapsulate the oil. That an increase in final oil content resulted an increase in surface oil content was also reported in chickpea protein-based powders (Can Karaca et al., 2013) and corn zein based powders (Quispe-Condori et al., 2011). The encapsulation efficiency of LPI-ι-C 20%, 30%, and LPI-κ-C 20% powders were 84.1%, 83.5%, and 85.2%, respectively (Table 6.3). For freeze-drying powders, the lowest surface oil content ($p<0.05$) was attributed to LPI-ι-C 20% and LPI-κ-C 20% powders with surface oil of 5% and 4.8%, respectively. As the final oil content increased to 30%, the surface oil increased to 13.5% and 14.5% for LPI-ι-C 30% and LPI-κ-C 30% powders, respectively, again indicating the insufficient coverage of oil. The surface oil was very high at 16.2% and 25.2% for LPI 20% and 30% powders, respectively, due to the low stability of their corresponding emulsions. The emulsions started to destabilize prior to freezing -80 °C, and thus, the encapsulation efficiency for LPI 20% and 30% powders was both below 20%. Encapsulation efficiency for LPI-ι-C 20% & 30% and LPI-κ-C 20% & 30% powders was 74.8%, 55.0%, 75.8%, and 51.6%, respectively. It was also observed that surface oil was lower for spray-dried powders than freeze-dried powders ($p<0.05$). Similar trends were found by Eratte and co-authors (2014), who compared the surface tuna oil contents with whey protein-gum Arabic based spray-drying and freeze-drying powders. Quispe-Condori and co-authors (2011) also reported a lower surface flax oil in corn zein spray-drying powders than the corresponding freeze-drying powders. One reason might be due to the loss of some surface oil in the cyclone separator during the spray drying process, resulting in the lower

surface oil values of spray-drying powders. Another hypothesis could be attributed to the structural difference between spray-drying and freeze-drying powders (see section 6.4.4).

6.4.4 Surface morphology of dried powders

Surface morphology of each spray- and freeze-dried powder was provided in Figure 6.2 and Figure A6.3 (Appendix). All the spray-drying powders exhibited wrinkled spherical structure (Figure 6.2A & B, Figure A6.3A, Appendix). The size of the all the spray-drying powders were ranging from below 10 to 30 μm, corresponding to their average droplet sizes. Collapse of some spray-dried LPI-ι-C 30% powders were observed (Figure 6.2B), again indicating the lack of sufficient wall materials (i.e. LPI-ι-C 30% complexes) to encapsulate the flaxseed oil as oil content increased. In contrast, irregular structure was imaged for all the freeze-drying powders (Figure 6.2C & D, Figure A6.3B-E, Appendix). Some pores were seen in freeze-dried LPI-ι-C 20% powders (Figure 6.2C), and more pores were found as the oil content of the powders increased to 30% (Figure 6.2D). The formation of the porous structure in the freeze-dried powders was due to the sublimation of the ice crystals during primary drying cycle in freeze drying (Morais et al., 2016). Similar findings was also reported by Eratte and co-authors (2014), where spray dried powders gave a more compact and wrinkled spherical structure and freeze-drying powders were more in irregular shape and highly porous. The authors also stated that the porous structure of freeze-dried powders might lead to more leakage of oil and consequently a higher surface oil content. Due to this oil leakage, the higher surface oil content of freeze-drying powders compared to their corresponding spray-drying powders was observed in this study (Table 6.3).

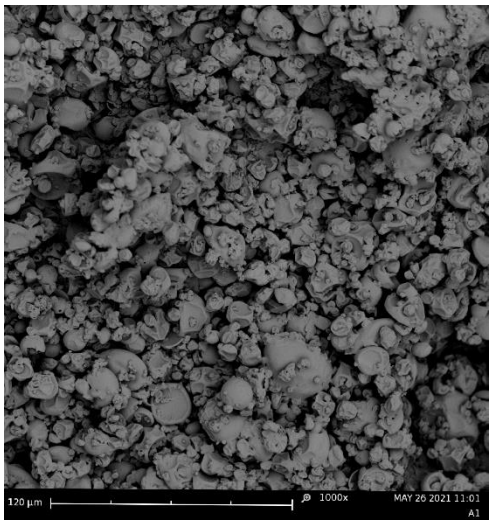

A) Spray-dried LPI- ι-C 20%

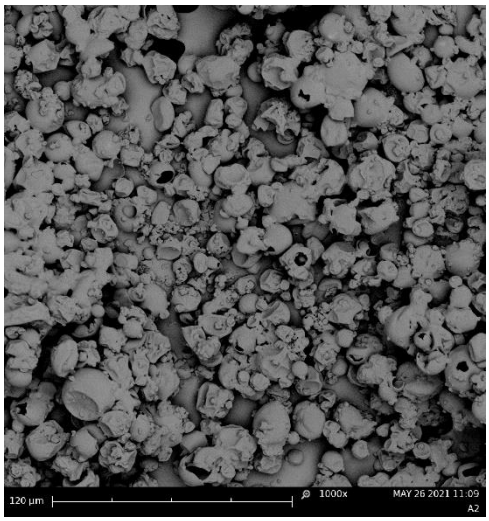

B) Spray-dried LPI- ι-C 30%

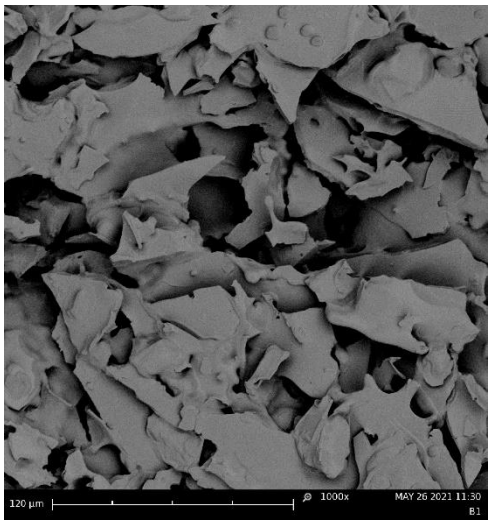

C) Freeze-dried LPI- ι-C 20%

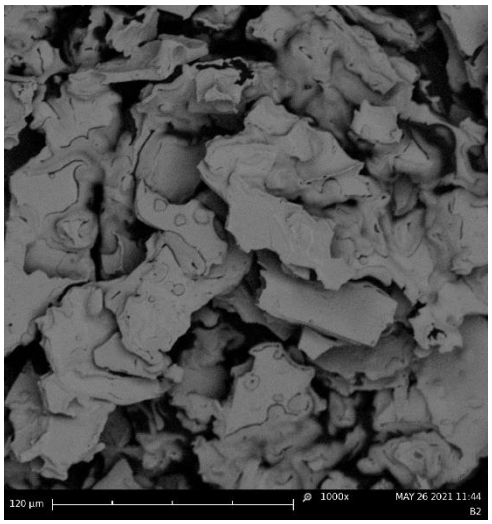

D) Freeze dried LPI- ι-C 30%

Figure 6.2 Scanning electron microscopy (SEM) images of the spray-dried LPI-ι-carrageenan (LPI-ι-C) 20% and 30% powders (A and B, respectively), and freeze-dried LPI-ι-C 20% and 30% powders (C and D, respectively) at 1000X magnification. All the scale bars represent 120 µm.

6.4.5 Lipid oxidation of dried powders

Flaxseed oil is highly susceptible to lipid oxidation due to its high unsaturation of over 95% (Chang & Nickerson, 2018). Lipid oxidation can occur chemically with the presence of oxygen through a free radical mechanism to produce primary oxidative products (i.e. peroxides and hydroperoxides), which are highly unstable and will further decompose to form secondary oxidative products (i.e. aldehydes, hydroxy acids, and ketones) (Di Giorgio et al., 2019; Lagarde, 2010). Primary lipid oxidation can be determined by measuring peroxide values (PV), and 2-Thiobarbituric acid reactive substances (TBARS) assay can be used to measure secondary lipid oxidation to access the formation of one of the main resulted compounds—malondialdehyde (MDA) (Chang et al., 2016). PV and TBARS values for each powder under 8-week of storage were given in Figure 6.3.

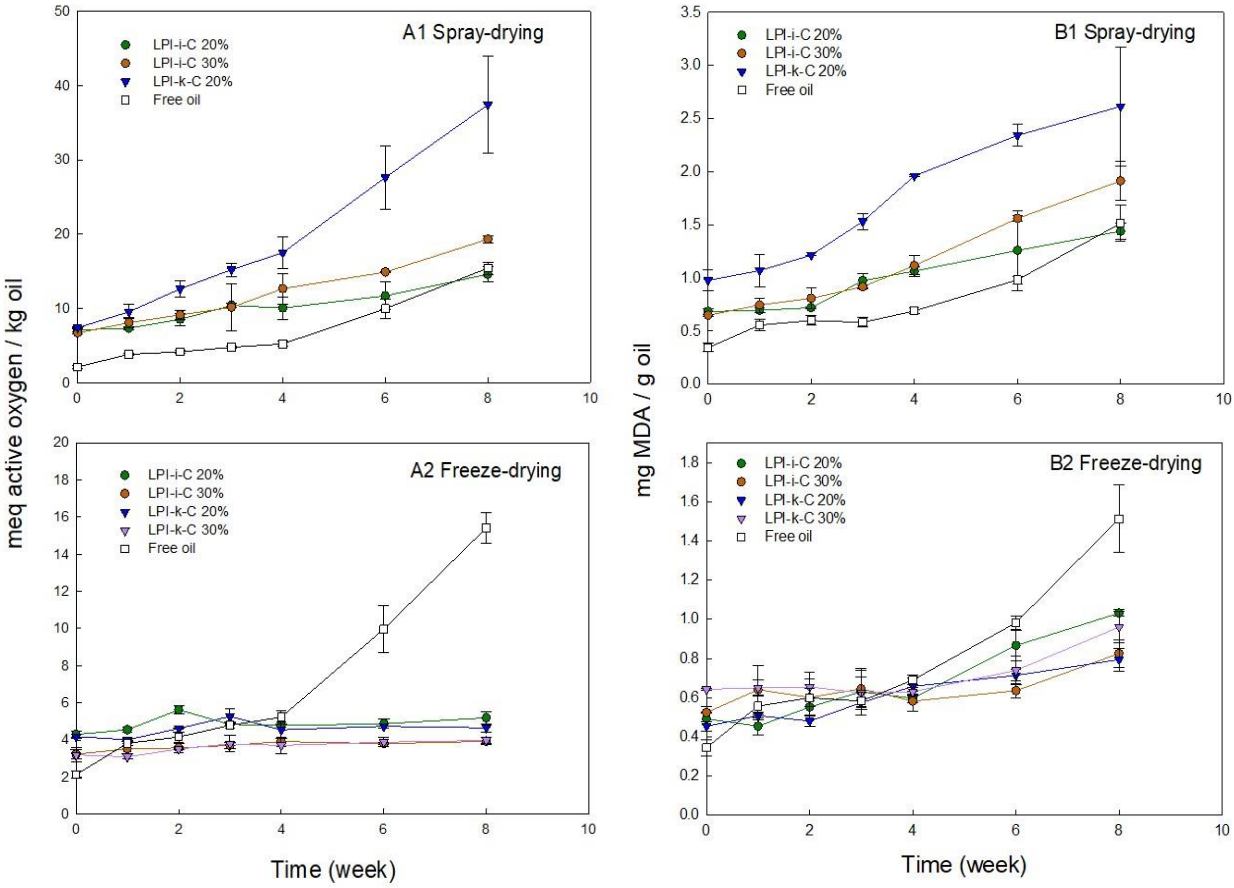

Figure 6.3 Changes in (A) peroxide value (PV) and (B) 2-thiobarbituric acid reactive substances (TBARS) for the untreated and encapsulated flaxseed oil through spray-drying (1) and freeze-drying (2) over 8 weeks of storage at room temperature (21-23 °C). Note that untreated oil was not spray dried nor freeze dried. Both LPI 20% & 30% powders were not included in the oxidation tests as their corresponding emulsions rapidly destabilized after emulsification. The percentage on the name of the samples represents the final oil content in dried powders. It is worth to mention that the Y-axis are different between spray- and freeze-drying to show the trends. Data represent the mean ± one standard deviation (n=3).

PV value of untreated flaxseed oil before encapsulation process was 2.1 meq active oxygen/ kg oil (Figure 6.3A). After emulsification and spray-drying processes, the PV values for LPI-ι-C 20%, 30%, and LPI-κ-C 20% powders increased to 7.1, 6.7, and 7.4 meq active oxygen/ kg oil, respectively (Figure 6.3A). The increase in PV values for freeze-drying powders was less prominent ($p<0.05$) with PV values of 4.3, 3.2, 4.2, and 3.2 meq active oxygen/ kg oil for LPI-ι-C 20% & 30% and LPI-κ-C 20% & 30% powders, respectively (Figure 6.3B). The higher PV values for all the fresh powders compared to untreated oil could be attributed to the emulsification process, where flaxseed oil was blending with solutions and oxygen (Can Karaca et al., 2013). In addition to emulsification, heat was also applied in spray-drying process (inlet and outlet temperature: 135°C & 95°C) and was hypothesized to initiate the oxidation more prominent, resulting a larger increase of PV values in all spray-drying powders. Dried powders with higher PV value compared to untreated oil were also reported in the fish oil-soybean protein-based spray-drying powders (Di Giorgio et al., 2019). During 8-week of storage, PV values for untreated oil increased 2-fold to 4.2 meq active oxygen/ kg oil ($p<0.05$) after 2 weeks, followed by slow increase to 5.2 meq active oxygen/ kg oil at week 4. The increment then became more significantly to 10.0 ($p<0.05$) and 15.4 ($p<0.05$) meq active oxygen/ kg oil at week 6 and 8, respectively. The smaller increment in the first month could be attributed to less free radicals being present. As there was no protection to the untreated oil during storage, the oil started to react with oxygen to produce peroxides, and the formation of peroxides became more prominent after week 4. Unlike untreated oil, the PV values for all freeze-drying powders were quite stable during 8-week of storage (Figure 6.3A2), where PV values of LPI-ι-C 20% and LPI-κ-C 20% powders showed no difference ($p>0.05$) in 8 weeks, suggesting the efficiency of encapsulation process to prevent lipid oxidation. The PV values for LPI-ι-C 30% and LPI-κ-C 30% powders increased slightly ($p<0.05$) by about 1 meq active oxygen/ kg oil from time 0 to week 8, because higher surface oil contents within these two powders were determined. That higher surface oil content led to stronger oil oxidation was also reported in flaxseed oil-chickpea-based powders (Can Karaca et al., 2013). For spray-drying powders (Figure 6.3A1), the increment of PV values for all powders were higher compared to the freeze-drying powders since heat was applied during spray-drying process. PV values increased slowly for LPI-ι-C 20% powders from 7.1 meq active oxygen/ kg oil at time 0 to 11.7 meq active oxygen/ kg oil at week 6 ($p>0.05$), then more significantly to 14.6 meq active oxygen/ kg oil at week 8 ($p<0.05$). Similarly, PV values of LPI-ι-C 30% powders increased gradually from time 0 to week 4 and then

more significantly till week 8. Although the PV values for all spray-drying powders were similar ($p>0.05$) at time 0, the increment of PV for LPI-κ-C 20% powders during storage was more rapid, with PV reaching 37.4 meq active oxygen/ kg oil at week 8. The surface oil contents were similar in all spray-drying powders, indicating other factors rather than surface oil contributing a more important role in oil oxidation during storage. One assumption might be the lower a_w value of 0.06 of LPI-κ-C 20% spray-drying powders compared to a_w values of 0.09 for both LPI-ι-C 20% and 30% powders (Table 6.3). As mentioned above, a_w near the water monolayer (between 0.2 - 0.3) would show lowest lipid oxidation. At this point, water molecules could provide a barrier by hydrogen-bonding to lipid hydroperoxides, preventing the direct exposure to air and increasing the relative stability (Chew & Nyam, 2016; Karel & Heidelbaugh, 1973). Since the a_w value was very low for LPI-κ-C 20% powder, there was lack of coverage of water against lipid oxidation.

For TBARS, the amount of MDA for untreated oil at time 0 was 0.34 mg/ g oil (Figure 6.3B). Higher level of MDA was determined in freeze-drying powders at time 0 since emulsification was implemented (Figure 6.3B2). The amount of MDA found in LPI-ι-C 20% & 30% and LPI-κ-C 20% and 30% powders was 0.49, 0.52, 0.45, and 0.64 mg/ g oil, respectively. Both powders with 30% oil showed higher MDA values compared to their corresponding powders with 20% oil, which could be attributed to the higher surface oil level. Increment of MDA was more significantly ($p<0.05$) for spray-drying powders at time 0 as both emulsification and heat treatment were applied (Figure 6.3B1). During 8 week of storage, MDA values of untreated oil increased slowly from time 0 to week 3 ($p>0.05$), then more rapidly starting from week 4 ($p<0.05$). All freeze-drying powders showed similar growth trends, where the increment of MDA was more steadily from time 0 to week 4 and became more significantly ($p<0.05$) at week 6 and week 8. The increase of MDA value for each freeze-drying powder was about two-fold from time 0 to week 8. The amount of MDA detected for all freeze-drying powders were smaller than MDA measured at week 8 for untreated oil, suggesting the encapsulation process could lower lipid oxidation. For spray-drying powders, the growth of MDA levels was more significantly than the freeze-drying powders during 8 week of storage, where the increase of MDA of LPI-κ-C 20% powders was the most prominent. The increase of MDA values for LPI-ι-C 20% & 30% spray-drying powders was more steadily ($p>0.05$) from time 0 to week 2 and became more prominent ($p<0.05$) starting from week 3. For LPI-κ-C 20% powders, MDA values remained stable till week 3 and then increased significantly since week 4. After 8-week of storage, MDA value increased 2-fold for LPI-ι-C 20%

powders, and the increment of MDA was 3-fold for LPI-ι-C 30% powders and LPI-κ-C 20% powders.

6.4.6 Oil release characteristics of dried powders

The flaxseed oil release profile for each powder under simulated gastric fluid (SGF) and sequential exposure to simulated gastric fluid and simulated intestinal fluid (SGF + SIF) was given in Figure 6.4. In this figure, each result was reported as oil release due to digestive enzyme, which is percentage (%) of oil released from the dried powders under the use of digestive enzymes minus % of oil released from the dried powders without the use of enzymes. Under SGF, the pepsin in the SGF could break down the proteins and led to partial oil being released from the powders. The amount of oil release due to enzyme under SGF for LPI-ι-C 30% and LPI-κ-C 20% spray-drying powders was about 31% ($p>0.05$), and slightly lower for LPI-ι-C 20% at 26% ($p<0.05$) (Figure 6.4A). For freeze-drying powders, the highest amount of oil release under SGF was 37% for LPI-κ-C 20% powders, followed by 34% and 33% for LPI-ι-C 30% and LPI-κ-C 30% powders, respectively. Again LPI-ι-C 20% powders had the least amount of oil released of 26% ($p<0.05$). This result might suggest that the LPI-ι-C 20% powders were more resistance to the acidic conditions in SGF despite on the drying method. Under SGF + SIF, pancreatin broke down the wall materials (i.e. MD and lentil protein) more excessively as pancreatin contains amylase, lipase, and protease. Generally, it was observed that less oil was released ($p<0.05$) from LPI-κ-C powders than LPI-ι-C powders under SGF + SIF despite on the drying method. The amount of oil release for both LPI-ι-C 20% and 30% spray-dried powders were about 56%, followed by LPI-κ-C 20% powders at about 40% (Figure 6.4A). For freeze-drying powders, over 50% of oil got released from for both LPI-ι-C 20% and 30% powders ($p>0.05$), followed by LPI-κ-C 20% and 30% powders at about 30% (Figure 6.4B). The reason for less oil released in all the LPI-κ-C powders (including both oil contents and both drying methods) was due to the higher amount of oil released without the use of enzymes (data not shown), indicating the less resistance of the LPI-κ-C powders against pH change, the presence of various salts in the SGF during measurement.

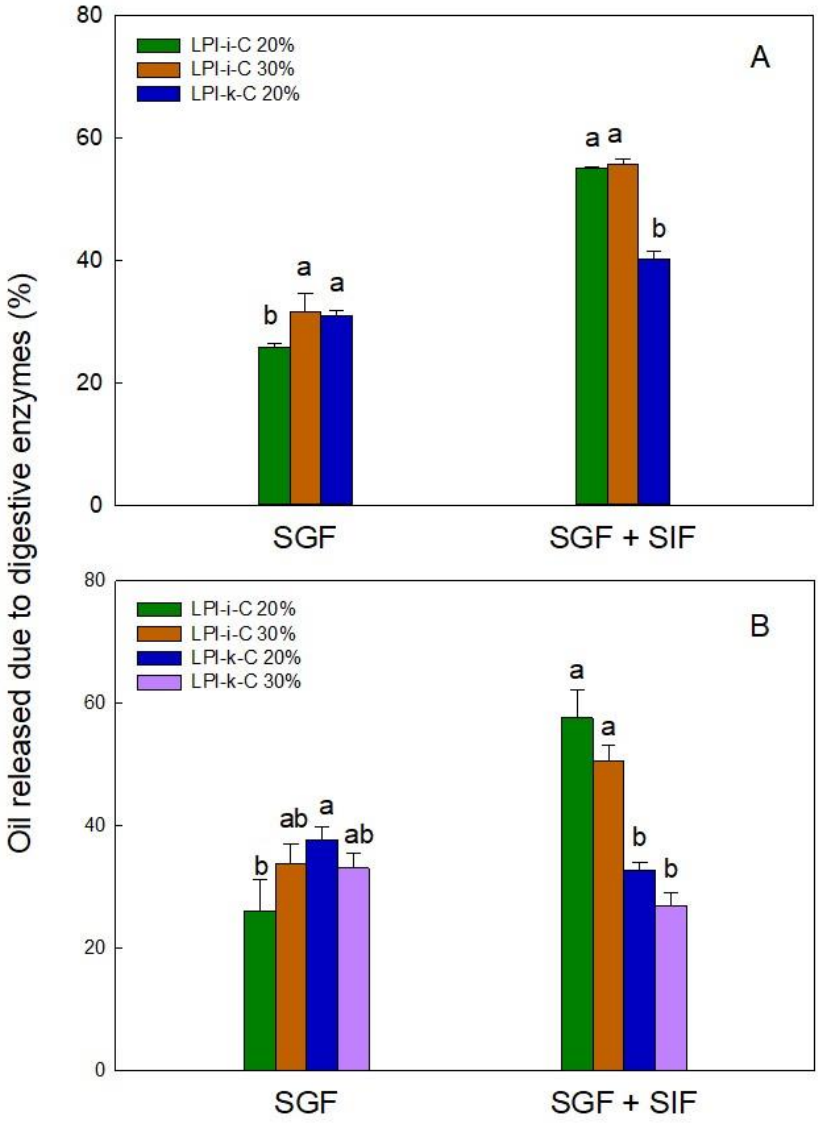

Figure 6.4 The release of flaxseed oil due to digestive enzymes from spray-drying (A) and freeze-drying (B) microcapsules under simulated gastric fluid (SGF) and sequential exposure to simulated gastric fluid and simulated intestinal fluid (SGF + SIF). Each value was reported as the percentage of oil released with the use of digestive enzymes minus the percentage of oil released without the use of digestive enzymes. Data represent the mean ± one standard deviation (n=3). The percentage on the name of the samples represents the final oil content in dried powders.

6.5 Conclusions

This study prepared microencapsulated powders through complex coacervation of LPI-κ-C and LPI-ι-C by spray-drying and freeze-drying. Initial emulsions' stability was enhanced remarkably with using LPI-κ-C and LPI-ι-C complexes compared to homogeneous LPI, which could be mainly attributed to the improvement of emulsion viscosity. Emulsions were then either spray-dried or freeze-dried. All the solids were able to be recovered for freeze-drying powders, however significant loss was found during the spray-drying process, with the highest yield of 33% of LPI-ι-C 20% powders. The physical characteristics of each powders including moisture content, a_w, color, wettability, and droplet size were determined. For a_w values, all the powders resulted in this study showed low a_w values ranging from 0.06 to 0.12. Spray-drying powders showed lower surface oil content and higher encapsulation efficiency compared to freeze-drying powders possibly due to the more compact structure of spray-drying powders to provide better protection. However, spray-drying powders showed very strong oil oxidation during 8 weeks of storage, mainly attributing to the heat effect during spray-drying process. Encapsulation of flaxseed oil through freeze-drying process showed significantly lower oxidation than the untreated oil, suggesting the encapsulation process was successful. The oil release profile suggested that more oil got released due to digestive enzymes for LPI-κ-C powders under SGF and more oil got released due to digestive enzymes for LPI-ι-C powders under SGF + SIF regardless of drying method and oil content.

Learning from the results obtained from current study, more work can be done in the future study to improve the quality of the microencapsulated powders. For instances, high energy emulsification process can be applied to form emulsion with higher stability and to find out if the yield of the spray-drying powders can be improved, as Di Giorgio et al. (2019) and Fernandes et al. (2016) have reported the increase of yield of powders after applying ultrasonic emulsification. In this study, no powders within both drying methods with surface oil below 2% was achieved. In order to achieve food industry's goal, some improvements could be implemented in the future study, such as increasing the concentration of LPI-ι-C and LPI-κ-C to achieve better coverage of oil droplets (e.g. from 1% LPI-ι-C to 2% LPI-ι-C). Moreover, it seems that the lipid oxidation was accelerated by the very low a_w value; therefore, the replacement of part of MD to other simple sugars such as sucrose can be taken into consideration. A study has reported the incorporation of

sucrose to the spray-drying powders could effectively increase a_w of the powders (Kuang et al., 2015).

7. GENERAL DISCUSSION

This research explored the potential of using LPI-polysaccharide complexes to encapsulate flaxseed oil as a means for bioactive delivery. Initially, the complexation behavior between LPI and various polysaccharides were examined, and the emulsifying properties of their resulting complexes were characterized. Select systems that formed the most stable emulsions were then investigated for their potential as a wall material in the microencapsulation process. The research aimed to find value-added uses for lentil protein as a food ingredient, and to develop functional food ingredient which can improve the heart health of consumers.

In order to gain knowledge of the complexation behavior between LPI and polysaccharides, LPI and CMC with different DS (0.7, 0.9 and 1.2%) and MM (90 and 250 kDa) was first selected and investigated in study 1 to test the effect of linear charge density and molecular mass on coavervation (Chapter 3). A bell-shaped OD curve as a function of pH was observed for homogeneous LPI solutions. The maximum OD value was 0.476 occurring at pH 4.4, corresponding to the protein's isoelectric point of pH 4.6. Also, OD remained relatively flat at the maximum over the pH range of 3.6-4.8 due to reduced solubility caused by the increased protein-protein interactions. With the addition of CMC (DS: 0.7%, MM: 250 kDa) into the LPI solution, as the amount of CMC increases within the mixing ratio, the scattering curves shifted to lower pH values, and the bell-shaped curve changed to have a longer rise in OD as pH decreased prior to the maximum, a narrower peak region and, a lower maximum OD. For all mixtures, pH_c and $pH_{\phi 2}$ remained unchanged as the mixing ratio increased; however, $pH_{\phi 1}$ and pH_{opt} shifted to higher pH values with increasing mixing ratio until reaching a plateau at a 4:1 mixing ratio. Max OD value in all mixing ratios was also found at 4:1 LPI-CMC ratio with OD value of 0.495. Based on these results, the optimal mixing ratio was conducted at 4:1 and for the following experiments. The effect of DS and MM of CMC on the formation of electrostatic complexes with LPI was then examined. Both DS and MM of CMC had minor effects on the critical pH values. However, CMC with higher DS could suppress of formation of LPI-LPI aggregates and consequently a lowder max OD (less complexes being formed) due to the higher charge density on the CMC chains that

generated more electrostatic repulsion within neighboring chains in solution (Warnakulasuriya et al., 2018). One more reason could be the structural differences between these CMCs. Increased DS means bigger constituent groups ($-CH_2OH \rightarrow -CH_2OCH_2COOH$) are generated, and steric effect might occur, which negatively affects the complexation between LPI and CMC, resulting lower maximum OD values (Zhivkov, 2013). A larger OD_{max} reading was also observed at a lower molecular mass of CMC with LPI. It was hypothesized that CMC (90 kDa) with smaller sizes could interact with LPI easier compared to CMC (250 kDa) due to less steric effects resulting more LPI-CMC interaction. To understand the thermodynamic behavior during complexation of LPI-polysaccharide, isothermal titration calorimetry (ITC) was performed for all LPI-CMC systems at 4:1 mixing ratio. The results suggested that the complexation reaction was energetically favorable as the thermograms obtained for all systems were exothermic. Larger enthalpy values were observed in LPI-CMC as DS of CMC increased or MM of CMC decreased. Binding stoichiometry was greatly influence by CMC molecular mass, where one protein was interacting with two CMC chains at 90 kDa and only interacted with one CMC chain at 250 kDa. From study 1, the optimal biopolymer mixing ratio was conducted on 4:1, and as no significantly different complexation was observed between CMC with different DS and MM, CMC with 0.7% DS and 250kDa was selected for the next study.

In Chapter 4, GA, AL, ι-C were introduced to contrast with CMC (0.7% DS, 250 kDa) to interact with LPI in order to obtain stronger protein-polysaccharide interactions. Turbidimetric measurements were conducted on the LPI-polysaccharide mixing ratio of 4:1. LPI-GA and LPI-CMC systems formed coacervate-type structures since greater max OD than the LPI control was observed. In contrast, LPI-AL and LPI-ι-C mixtures formed precipitate-type of structures, reflected by their lower max OD values. Significant chain repulsion of the polysaccharides (AL and ι-C) was thought to occur in both LPI-AL and LPI-ι-C systems due to their higher linear charge density, which resulted in suppression of LPI-LPI aggregation. Critical pH values (pH_c, $pH_{\phi1}$, pH_{opt}, $pH_{\phi2}$) varied significantly for each system. CLSM was conducted on each system at their corresponding pH_{opt}, and different number and sizes of each type of complexes were observed, where LPI-ι-C complexes were the smallest in size due to the large electrostatic repulsive forces exerted between ι-C chains in solution. The resulting complexes at pH_{opt} was then used to prepare emulsions. For their corresponding emulsions, the greatest emulsion stability was attributed to LPI-ι-C emulsion, with its stability of 100% at 0.5 h and 87.5% at 48 h. The stability of the

emulsion can be impacted by coverage of the viscoelastic film, charge, size/conformation of the aggregates, and the continuous phase viscosity, all of which acts to inhibit coalescence (McClements, 2007; Walstra & van Vliet, 2008). In all the LPI-polysaccharide and LPI control emulsions, LPI-ι-C emulsion formed the smallest and highly negative-charged droplets, and displaced the higher continuous phase and emulsion viscosities, all contributing to a greater emulsion stability. All other LPI-polysaccharide systems showed lower stability than LPI (control) stabilized emulsions mainly due to the larger complex's sizes, larger droplet size, and higher interfacial tension which was hypothesized to inhibit their ability to migrate and align at the oil-water interface to form a stable viscoelastic film. From this work, LPI-ι-C system was selected for the following study. Additionally, LPI-ι-C complexes was formed at pH_{opt} in this study so that a great extent of the complexes was insoluble and couldn't align on the interface. Therefore, it will be interesting to look at the emulsifying properties of the soluble complexes.

Chapter 5 continued to explore the complexation behavior and emulsifying behavior between LPI and carrageenan polysaccharides. κ-Carrageenan was introduced in this study to contrast with ι-carrageenan since the linear charge density was different (i.e., κ-C and ι-C have 1 and 2 sulfate groups, respectively). For the carrageenan polysaccharides, κ-carrageenan and ι-carrageenan are gelling polysaccharides whereas λ-carrageenan is more contributed to thickening (Li et al., 2014). Thus, this study focused on κ- and ι-carrageenan only since κ- and ι-types are more closely related in terms of their functional attributes. Additionally, these two carrageenan could develop a weak gel network, which could possibly improve emulsion stability. The complexation behavior of LPI-κ-C and LPI-ι-C complexes at 4:1, 8:1, and 12:1 biopolymer mixing ratios as a function of pH was first examined. Through a turbidimetric pH acid-titration, suppression of the turbidity curves was observed within the LPI-κ-C and LPI-ι-C systems compared to LPI control system. For both LPI-κ-C and LPI-ι-C systems, all the critical pH values (pH_c, $pH_{\phi 1}$, pH_{opt}, $pH_{\phi 2}$) shifted to more acidic pH values, and max OD values decreased with the decrease of biopolymer mixing ratio. Both 12:1 LPI-carrageenan mixtures and the 8:1 LPI-κ-C mixture showed the bell-shaped curves. For 4:1 LPI-κ-C, 4:1 LPI-ι-C, and 8:1 LPI-ι-C, electrostatic repulsion was very strong. The OD values of these systems increased gradually without going through a transition state of forming insoluble complexes, but the formed complexes started to precipitate out, and the OD values became stable, suggesting the saturation of the κ-C or ι-C. The resulting complexes (both soluble and insoluble) were then used to prepare emulsions.

LPI emulsions at pH 6 and pH 3.5 remained 100% stability after 30 min but dropped dramatically to around 20% after 24 h. Enhanced emulsion stability was observed in all LPI-carrageenan emulsions at 24 h and 48 h compared to LPI emulsions at both pH values (pH 6 and pH 3.5). Within all the LPI-carrageenan emulsions, emulsions made with soluble complexes (pH 6) displaced higher emulsion stability than those made with insoluble complexes (pH 3.5) at each sample. All emulsions at pH 6 remained 100% stability at 30 min, and smaller and more uniform droplets with highly negative charge were formed at each system to against gravitational separation and to prevent droplet flocculation and further coalescences. Interfacial tension was also lowered to a greater extent for LPI-carrageenan solutions at pH 6 compared to solutions at pH 3.5. After 48 h, both 4:1 emulsions at pH 6 remained 100% stability, followed by 8:1 LPI-ι-C and 4:1 LPI-κ-C emulsions with 83% and 74% stability, respectively. The greatest stability over time was found in 4:1 LPI-κ-C and -ι-C emulsions at pH 6 mainly attributed to high continuous phase viscosity. All the findings suggested that LPI-carrageenan (both κ-C and ι-C) soluble complexes could effectively lower the interfacial tension and led to smaller droplet formation, and the excessive carrageenan in the system increased the viscosity, which all led to the greater emulsion stability. This study found a more stable emulsions compared to those in Chapter 4, and these stable emulsions (4:1 LPI-κ-C and -ι-C emulsions at pH 6) could be used for encapsulation.

Microencapsulated powders containing 20% and 30% flaxseed oil with LPI-κ-C-MD based and LPI-ι-C-MD based materials were prepared through spray-drying and freeze-drying in Chapter 6. LPI and LPI-carrageenan emulsions were prepared, and MD was also added into the systems as the coating materials. Initial emulsion stability was improved remarkably by using LPI-κ-C and LPI-ι-C complexes compared to homogeneous LPI mainly due to the improvement of emulsion viscosity. All LPI-κ-C or LPI-ι-C emulsions with 20% or 30% final oil remained 100% stability after 48 h, while gravitational separation occurred rapidly after emulsification for LPI 20% and LPI 30% emulsions. Emulsions were then either spray-dried or freeze-dried. All the solids were recovered for freeze-drying powders, while significant loss was found in the spray-drying powders, with the highest yield of 33% of LPI-ι-C 20% spray-dried powders. As oil content increased to 30%, the yield decreased, which could be attributed to lack of sufficient coverage of wall materials to the oil; thus, more samples were stuck on the surface of the cylinder and cyclone during drying (Polavarapu et al., 2011). The average droplet size of the reconstituted spray-drying emulsions decreased compared to their droplet size of initial emulsions again suggested the sample lose after

the spray drying process. Moisture contents of all dried powders were similar ranging 2.6% to 4.1%, meeting the requirement to ensure good stability during storage (Klaypradit & Huang, 2008; Goyal et al., 2015). All the dried powders had very low a_w values ranging from 0.06 to 0.12, and it was able to inhibit the non-enzymatic browning and enzymatic activities in foods (Alvarez-Henao et al., 2018). Spray-drying powders showed more whiteness compared to the freeze-drying powders, which could be due to the lower surface oil content on spray-drying powders. The lower surface oil content of spray-drying powders was attributed to the compact structure. In contrast, porous structure was seen in freeze-drying powders under SEM, which resulted in the higher surface oil content. For oil oxidation, flaxseed oil within the spray-dried powders was oxidized more rapidly during 8 weeks of storage compared to untreated oil due to the heat effect during spray-drying process. The increase in PV and TBARS values were more significantly in LPI-κ-C 20% powders compared to LPI-ι-C 20% and 30% powders possibly due to the lower a_w value of 0.06 of LPI-κ-C 20% spray-drying powders. Water activity near the water monolayer (between 0.2 - 0.3) could lower oil oxidation by providing a barrier through hydrogen-bonding to lipid hydroperoxides, which prevented the direct exposure to air and increasing the relative stability (Chew & Nyam, 2016). Thus, there was lack of coverage of water against lipid oxidation for LPI-κ-C 20% powder. Flaxseed oil in all the freeze-dried powders showed significant lower oil oxidation than the untreated oil, and PV values of all the freeze-dried powders remained similar upon 8-week of storage, all suggesting the success of the encapsulation process. oil release due to digestive enzyme for each powder under simulated gastric fluid (SGF) and sequential exposure to simulated gastric fluid and simulated intestinal fluid (SGF + SIF) was finally examined. Pepsin in the SGF could partially break down the proteins and led to partial oil being released from the powders, and pancreatin broke down the wall materials (i.e. MD and lentil protein) more excessively. Our findings suggested that more oil got released due to digestive enzymes for LPI-κ-C powders under SGF, indicating its less resistance to the acidic conditions in SGF despite on the drying method. More oil was released due to digestive enzymes for LPI-ι-C powders under SGF + SIF regardless of drying method and oil content.

8. GENERAL CONCLSUONS

The overall goal of this thesis was to explore the potential of using lentil protein-polysaccharide based microcapsules to encapsulate omega-3 fatty acid rich oil. In this research, the complexation behavior between LPI and selected polysaccharides as a function of biopolymer mixing ratio and pH was first investigated. The resulting LPI-polysaccharide electrostatic complexes (both soluble and insoluble) was used to prepare emulsions to examine their emulsifying properties and to select the stable emulsions. After that, subsequent spray drying or freeze drying was applied to the select emulsions to produce dried powders. Therefore, four studies were included in this research.

In Chapter 3, the complexation behavior of LPI and CMC with different molecular mass (90 and 250 kDa) and degree of substitution (0.7. 0.9, and 1.2%) was investigated through a turbidimetric pH acid-titration over a pH (8.0-1.5) and mixing ratio (LPI: CMC; 1:1-10:1) rang and ITC. For LPI-CMC (0.7% DS, 250 kDa), the level of maximum complex formation was found to increase from OD of 0.317 at the 1:1 LPI: CMC mixing ratio to 0.495 at the 4:1 ratio, followed by a plateau region till 10:1. Therefore, optimal complexation was conducted at 4:1. For critical pH values, pH_c and $pH_{\phi 2}$ remained unchanged at all mixing ratios. In contrast, $pH_{\phi 1}$ and pH_{opt} were also found to increase as the mixing ratio increased, which indicated more LPI-LPI aggregates were interacting with CMC. Electrical equivalence points shifted to higher pH values within increasing mixing, but all of which was below the isoelectric point of LPI. It was hypothesized that CMC with different DS and MM would have different complexation behaviour with LPI. However, the effects of DS and MM of CMC on the turbidimetric curves and critical pH values were minor. DS and MM of CMC only influenced the size and number of complexes formed as reflected by their max OD values. A higher DS of CMC generated more electrostatic repulsion within neighboring chains in solution, which could suppress of formation of protein aggregates and led to a lower max OD reading complexes being formed. In contrast to the hypothesis, a lower MM of CMC with LPI resulted in increase of max OD readings since CMC with smaller MM would have less effect on suppression of protein aggregation. CLSM conducted at pH_{opt} also

suggested that increase number of aggregates were observed as the DS or MM of CMC decreased. Through the ITC, larger enthalpy values were found in LPI-CMC as DS of CMC increased or MM of CMC decreased. Binding stoichiometry was affected by MM of CMC, where one protein was interacting with one CMC (250 kDa) chain but could interact with two CMC (90 kDa) chains.

Chapter 4 investigated the complexation behaviour between LPI and four anionic polysaccharides (CMC, GA, AL, and ι-C) at 4:1 LPI-polysaccharide mixing ratio. The resulting emulsifying properties of the complexes being formed at pH_{opt} was then evaluated. LPI-GA and LPI-CMC systems formed coacervate-type structures, while LPI-AL and LPI-ι-C mixtures formed precipitate-type of structures, which was consistent with our hypothesis. It was assumed that more water could be entrapped in the LPI-GA and LPI-CMC mixtures due to relatively weaker attraction between LPI and CMC as well as LPI and GA; therefore, coacervate-type structures were formed. In contrast, AL and ι-C generated stronge electrostatic attraction with LPI, and less water was entrapped within the LPI-AL and LPI-ι-C mixture, leading to the formation of precipitate-type of structures. The max OD values for LPI-GA, LPI-CMC, LPI-AL, and LPI-ι-C were found to be 0.716, 0.486, 0.310, and 0.190, respectively, and the critical pH values (pH_c, $pH_{\phi 1}$, pH_{opt}, $pH_{\phi 2}$) of four mixtures varied significantly. It was hoping that emulsion stability could be increased under LPI-polysaccharide complex stabilized emulsions; however, for their corresponding emulsions, only LPI-CAR emulsion showed higher stability than LPI control emulsion. The great stability of LPI-ι-C was due to its higher continuous phase and emulsion viscosities, lower mean droplet sizes, and negatively charged droplets. Very small LPI-ι-C complexes were formed within solution due to the large electrostatic repulsive forces exerted between ι-C chains in solution. All other LPI-polysaccharide systems showed lower stability than LPI (control) stabilized emulsions mainly due to the larger complex's sizes, larger droplet size, and higher interfacial tension. In contrast to the hypothesis of a stronge film formation at the oil-water interface due to complexation, the ability of the resulting complexes at pH_{opt} to migrate and align at the oil-water interface was inhibited.

Chapter 5 explored the complexation behavior of LPI-κ-C and LPI-ι-C complexes at 4:1, 8:1, and 12:1 biopolymer mixing ratios as a function of pH and the emulsifying properties of their resulting soluble complexes at pH 6 and insoluble complexes at pH 3.5. Based on the findings from chapter 4, emulsions were not stable when they were prepared with complexes formed at pH_{opt} (i.e. insoluble complexes). Thus, soluble complexes were introduced in this chapter to examine the emulsion properties. In the first part of the chapter, through a turbidimetric pH acid-

titration, suppression of the turbidity curves was observed within the LP-κ-C and LPI-ι-C systems compared to LPI control system. For both LPI-κ-C and LPI-ι-C systems, all the critical pH values (pH_c, $pH_{\phi1}$, pH_{opt}, $pH_{\phi2}$) shifted to more acidic pH values, and max OD values decreased with the decrease of biopolymer mixing ratio. The resulting complexes (both soluble and insoluble) were then used to prepare emulsions in the second part of chapter. Enhanced emulsion stability was observed in all LPI-carrageenan emulsions at 24 h and 48 h compared to LPI emulsions at both pH values. Agreed with the hypothesis, within all the LPI-carrageenan emulsions, emulsions made with soluble complexes displaced higher emulsion stability than those made with insoluble complexes at each sample. All emulsions at pH 6 remained 100% stability at 30 min, and smaller and more uniform droplets with highly negative charge were formed. Interfacial tension was also lowered to a greater extent for LPI-carrageenan solutions at pH 6. The greatest stability over time was found in 4:1 LPI-κ-C and -ι-C emulsions at pH 6 mainly attributed to high continuous phase viscosity. CLSM images confirmed that droplets formed in 4:1 LPI-κ-C and LPI-ι-C emulsions at pH 6 remained small at 24 h. All these findings suggested that LPI-carrageenan (both types) soluble complexes could effectively lower the interfacial tension and led to smaller droplet formation, and the excessive carrageenan in the system increased the viscosity, all contributing to the greater emulsion stability.

Chapter 6 prepared microencapsulated powders with 20% and 30% flaxseed oil through LPI-κ-C-MD based and LPI-ι-C-MD based materials by spray-drying and freeze-drying. This chapter evaluated their corresponding emulsion properties, the microcapsules' physical properties, surface oil, encapsulation efficiency, oil oxidation stability, and *in vitro* oil release. LPI and LPI-carrageenan emulsions were first made, and initial emulsions' stability was improved remarkably by using LPI-κ-C and LPI-ι-C complexes compared to homogeneous LPI mainly due to the improvement of emulsion viscosity. Emulsions were then either spray-dried or freeze-dried. All the solids were recovered for freeze-drying powders, while significant loss was found in the spray-drying powders, with the highest yield of 33% of LPI-ι-C 20% spray-dried powders. For the physical characteristics, all the powders resulted in this chapter showed very low a_w values ranging from 0.06 to 0.12, and spray-drying powders showed more whiteness compared to the freeze-drying powders. Spray-drying powders gave a more compact structure, while porous structure was seen in freeze-drying powders under SEM, which resulted in a lower surface oil content and higher encapsulation efficiency for spray-dried powders compared to freeze-dried powders. However,

flaxseed oil was oxidized more significantly among the spray-dried powders during 8 weeks of storage compared to untreated oil due to the heat effect during spray-drying process as well as the low water activity of the powders. Flaxseed oil in all the freeze-dried powders showed significant lower oil oxidation than the untreated oil suggesting the success of the encapsulation process. The oil release profile suggested that more oil got released due to digestive enzymes for LPI-κ-C powders under SGF and more oil got released due to digestive enzymes for LPI-ι-C powders under SGF + SIF regardless of drying method and oil content.

9. FUTURE STUDIES

The potential of using LPI-polysaccharide based wall materials to encapsulate omega-3 oils was conducted in this research. Within all four studies, the complexation behavior between LPI and various polysaccharides (CMC with different DS and MM, GA, AL, κ-C, ι-C) as a function of biopolymer mixing ratio and pH was investigated through turbidimetric titration measurements and ITC. The resulting LPI-polysaccharide electrostatic complexes (both soluble and insoluble) was used to prepare emulsions to examine their emulsifying properties. Finally, soluble complexes formed at 4:1 LPI-κ-C and LPI-ι-C solutions were selected to prepare emulsions. In the following chapter, subsequent spray drying and freeze drying was applied to the select emulsions to produce dried powders with 20% and 30% flaxseed oil.

Although current work has already investigated quite a few works on complexation behavior, there is still more work that can be done in the future. For instance, Chapter 3 only looked into the thermodynamic parameters of LPI-CMC complexes at pH 3, where the greatest number of insoluble complexes were formed. The thermodynamic properties of soluble complexes can be examined in the future since our findings in this thesis suggested soluble complexes showed better emulsifying property than insoluble complexes. It will be interesting to examine the complexation behavior for LPI-GA, LPI-AL, and LPI-ι-C systems as a function of biopolymer mixing ratio as only 4:1 LPI: polysaccharide mixing ratio was investigated in Chapter 4. Their thermodynamic properties can be examined as well. Similarly, it will be worth to look into the thermodynamic properties of LPI-κ-C and LPI-ι-C systems at pH 3.5 and pH 6, where insoluble and soluble complexes were formed, respectively.

Based on the results from the current work, more research can also be done in the future study to improve the quality of the microencapsulated powders. In the current work, emulsions were all prepared using the rotor-stator homogenizers, and the size of the droplets were relatively large (e.g. $D_{4,3}$ of formed droplets around 20 μm in Chapter 4). Therefore, high energy emulsification process can be applied to produce emulsions with higher stability and smaller droplets. For instance, high-pressure homogenizers can be introduced to produce more uniform

droplets with very small size (i.e. less than 1 μm) since it can generate stronger disruptive forces (Maindarkar et al., 2015; Lee et al., 2009). Emulsions with higher stability might also lead to the higher yield of powders after spray-drying. In the current work, the highest yield of the spray dried powders was 33% for LPI-ι-C 20% powders, followed by 20.5% for LPI-κ-C 20% powders, and 16.8% for LPI-ι-C 30% powders. All other systems resulted below 5% of yield. Di Giorgio et al. (2019) and Fernandes et al. (2016) have reported the significant increase of yield of powders after applying high energy emulsification process—ultrasonic emulsification.

Powders containing less amount of surface oil are more desirable because surface oil negatively affects powder quality such as oxidative stability (Can Karaca et al., 2013). Food industry aims to produce oil encapsulated powders with less than 2% surface oil (Drusch & Berg, 2008). However, no powders produced in the current work under both drying methods with surface oil below 2% was achieved. The surface oil content for all the powders in the current work was ranging from 3% to 25%. In order to achieve food industry's goal, some improvements could be implemented in the future study, for example, the concentration of LPI-ι-C and LPI-κ-C can be increased to form a stronger viscoelastic film on the oil and water interface and achieve better coverage of oil droplets (e.g. from 1% LPI-ι-C to 2% LPI-ι-C).

Moreover, it seems that the lipid oxidation was accelerated by the very low a_w value of the powders made in the current work with the a_w values ranging from 0.09 to 0.11. These low a_w values might not be ideal to against lipid oxidation in food products, as some studies have suggested that a_w of food products should be near the water monolayer (i.e. a_w: 0.2 – 0.3) to minimize lipid oxidation (Chew & Nyam, 2016; Velasco, Dobarganes, & Marquez-Ruiz, 2003). At water monolayer, water molecules are able to provide a barrier by hydrogen-bonding to lipid hydroperoxides, preventing the direct exposure to air, and subsequently increase the relative stability (Chew & Nyam, 2016; Karel & Heidelbaugh, 1973). The very low a_w values for powders in current study was due to the large amount of MD (dextrose equivalent [DE]: 9 -12) used as the coating materials. Similar a_w values were also observed in the oil encapsulated spray-drying powders, where MD with the same DE was the major wall material (Can Karaca et al., 2013; Kuang et al., 2015). One solution could be replacing part of MD to other simple sugars such as sucrose. That the incorporation of sucrose to the spray-drying powders could effectively increase a_w of the powders has been reported by Kuang and co-authors (2015).

10. REFERENCES

Agyare, K. K., Addo, K., & Xiong, Y. L. (2009). Emulsifying and foaming properties of transglutaminase-treated wheat gluten hydrolysate as influenced by pH, temperature and salt. *Food Hydrocolloids, 23*(1), 72-81. doi:10.1016/j.foodhyd.2007.11.012.

Akhlaghi, M., & Bandy, B. (2010). Dietary broccoli sprouts protect against myocardial oxidative damage and cell death during ischemia-reperfusion. *Plant Foods for Human Nutrition*, *65*(3), 193–199. doi:10.1007/s11130-010-0182-4

Ali, B. H., Ziada, A., & Blunden, G. (2009). Biological effects of gum arabic: A review of some recent research. *Food and Chemical Toxicology*, *47*(1), 1–8. doi: 10.1016/j.fct.2008.07.001

Aloys, H., Korma, S. A., Alice,T. M., Chantal, N., Ali, A. H., Abed, S. M., & Ildephonse, H., (2016). Microencapsulation by complex coacervation: methods, techniques, benefits, and applications - a review. *American Journal of Food Science and Nutrition Research. 3*(6),188-192. http://www.openscienceonline.com/journal/archive2?journalId=744&paperId=3564

Alvarez-Henao, M. V., Saavedra, N., Medina, S., Jiménez Cartagena, C., Alzate, L. M., & Londoño-Londoño, J. (2018). Microencapsulation of lutein by spray-drying: Characterization and stability analyses to promote its use as a functional ingredient. *Food Chemistry, 256*, 181-187. doi:10.1016/j.foodchem.2018.02.059

Antonov, Y., Dmitrochenko, A., & Leontiev, A. (2006). Interactions and compatibility of 11 S globulin from Vicia Faba seeds and sodium salt of carboxymethylcellulose in an aqueous medium. *International Journal of Biological Macromolecules*. 38(1): 18-24. doi.org/10.1016/j.ijbiomac.2005.12.011

AOAC (2003). Official method of analysis (17th ed.) Virginia: Association of Official Analytical Chemists, Inc.

Aryee, F. N., & Nickerson, M. T. (2012). Formation of electrostatic complexes involving mixtures of lentil protein isolates and gum Arabic polysaccharides. *Food Research International, 48*(2), 520-527. doi:10.1016/j.foodres.2012.05.012.

Aryee, F. N., & Nickerson, M. T. (2014). Effect of pH, biopolymer mixing ratio and salts on the formation and stability of electrostatic complexes formed within mixtures of lentil protein isolate and anionic polysaccharides (κ-carrageenan and gellan gum). *International Journal of Food Science & Technology, 49*(1), 65-71. doi:10.1111/ijfs.12275.

Avramenko, N. A., Chang, C., Low, N. H., & Nickerson, M. T. (2016). Encapsulation of flaxseed oil within native and modified lentil protein-based microcapsules. *Food Research International, 81*, 17–24. doi: 10.1016/j.foodres.2015.12.028

Aydemir, L. Y., & Yemenicioğlu, A. (2013). Potential of Turkish Kabuli type chickpea and green and red lentil cultivars as source of soy and animal origin functional protein alternatives. *LWT - Food Science and Technology, 50*(2), 686-694. doi:10.1016/j.lwt.2012.07.023.

Bakry, A. M., Abbas, S., Ali, B., Majeed, H., Abouelwafa, M. Y., Mousa, A., & Liang, L. (2016). Microencapsulation of oils: a comprehensive review of benefits, techniques, and applications. *Comprehensive Reviews in Food Science and Food Safety, 15*, 143-182. doi: 10.1111/1541-4337.12179

Barbeyron, T., Michel, G., Potin, P., Henrissat, B., & Kloareg, B. (2000). ι-Carrageenases constitute a novel family of glycoside hydrolases, unrelated to that of κ-carrageenases. *Journal of Biological Chemistry, 275*(45), 35499–35505. doi: 10.1074/jbc.m003404200

Barroso, A. K., Pierucci, A. P., Freitas, S. P., Torres, A. G., & Rocha-Leão, M. H. (2014). Oxidative stability and sensory evaluation of microencapsulated flaxseed oil. *Journal of Microencapsulation, 31*(2), 193-201. doi:10.3109/02652048.2013.824514

Bhatty, R. (1988). Composition and quality of lentil (*Lens culinaris Medik*): a review. *Canadian Institute of Food Science and Technology Journal*. 21(2): 144-160. doi: 10.1016/S0315-5463(88)70770-1

Biswal, D., & Singh, R. (2004). Characterisation of carboxymethyl cellulose and polyacrylamide graft copolymer. *Carbohydrate Polymers, 57*(4), 379-387. doi:10.1016/j.carbpol.2004.04.020.

Bonilla, J., Atarés, L., Vargas, M., & Chiralt, A. (2012). Edible films and coatings to prevent the detrimental effect of oxygen on food quality: possibilities and limitations. *Journal of Food Engineering*, *110*(2), 208–213. doi: 10.1016/j.jfoodeng.2011.05.034

Borrega, R., Tribet, C., & Audebert, R. (1999). Reversible gelation in hydrophobic polyelectrolyte/protein mixtures: an example of cross-links between soft and hard colloids. *Macromolecules*. 32(23): 7798-7806. doi:10.1021/ma981872c

Boye, J., Zare, F., & Pletch, A. (2010). Pulse proteins: processing, characterization, functional properties and applications in food and feed. *Food Research International, 43*(2), 414-431. doi:10.1016/j.foodres.2009.09.003.

Bu, H., Kjøniksen, A.-L., Knudsen, K. D., & Nyström, B. (2004). Rheological and structural properties of aqueous alginate during gelation via the ugi multicomponent condensation reaction. *Biomacromolecules*, *5*(4), 1470–1479. doi: 10.1021/bm049947

Bungenberg De Jong, H. G., & Kruyt, H. R. (1929). Coacervation (partial miscibility in colloid system). *Proceeding Royal Academy Amsterdam*. 32: 849-856. https://www.dwc.knaw.nl/DL/publications/PU00015781.pdf

Burgess, D. (1990). Practical analysis of complex coacervate systems. *Journal of Colloid and Interface Science*. 140(1): 227-238. doi.org/10.1016/0021-9797(90)90338-O

Campos-Vega, R., Loarca-Piña, G., & Oomah, B. D. (2010). Minor components of pulses and their potential impact on human health. *Food Research International, 43*(2), 461-482. doi:10.1016/j.foodres.2009.09.004.

Can Karaca, A., Low, N., & Nickerson, M. (2011). Emulsifying properties of canola and flaxseed protein isolates produced by isoelectric precipitation and salt extraction. *Food Research International, 44*(9), 2991-2998. doi:10.1016/j.foodres.2011.07.009.

Can Karaca, A., Low, N., & Nickerson, M. (2013). Encapsulation of flaxseed oil using a benchtop spray dryer for legume protein–maltodextrin microcapsule preparation. *Journal of Agricultural and Food Chemistry*, *61*(21), 5148–5155. doi:10.1021/jf400787j

Can Karaca, A., Nickerson, M., & Low, N. H. (2013). Microcapsule production employing chickpea or lentil protein isolates and maltodextrin: Physicochemical properties and oxidative protection of encapsulated flaxseed oil. *Food Chemistry*, *139*(1-4), 448–457. doi: 10.1016/j.foodchem.2013.01.040

Capek, I. (2004). Degradation of kinetically-stable o/w emulsions. *Advances in Colloid and Interface Science, 107*, 125–155. doi:10.1016/s0001-8686(03)00115-5.

Carneiro, H. C., Tonon, R. V., Grosso, C. R., & Hubinger, M. D. (2013). Encapsulation efficiency and oxidative stability of flaxseed oil microencapsulated by spray drying using different combinations of wall materials. *Journal of Food Engineering, 115*(4), 443–451. doi: 10.1016/j.jfoodeng.2012.03.033

Chakraborty, P., Sosulski, F., & Bose, A. (1979). Ultracentrifugation of salt-soluble proteins in ten legume species. *Journal of the Science of Food and Agriculture, 30*(8), 766-771. doi:10.1002/jsfa.2740300804.

Chang, C. & Nickerson, M. (2018). Stability and *in vitro* release behaviour of encapsulated omega fatty acid-rich oils in lentil protein isolate-based microcapsules. *International Journal of Food Sciences and Nutrition, 69*(1), 12-23. doi: 10.1080/09637486.2017.1336513

Chang, C., Tu, S., Ghosh, S., & Nickerson, M. T. (2015). Effect of pH on the inter-relationships between the physicochemical, interfacial and emulsifying properties for pea, soy, lentil and canola protein isolates. *Food Research International, 77,* 360-367. doi: 10.1016/j.foodres.2015.08.012

Chang, C., Varankovich, N., & Nickerson, M. (2016). Microencapsulation of canola oil by lentil protein isolate-based wall materials. *Food Chemistry, 212*, 264–273. doi: 10.1016/j.foodchem.2016.05.136

Chew, S. C., Tan, C. P., & Nyam, K. L. (2018). Microencapsulation of refined kenaf (hibiscus cannabinus l.) seed oil by spray drying using β-cyclodextrin/gum arabic/sodium caseinate. *Journal of Food Engineering, 237*, 78-85. doi:10.1016/j.jfoodeng.2018.05.016

Chew, S., & Nyam, K. (2016). Microencapsulation of kenaf seed oil by co-extrusion technology. *Journal of Food Engineering, 175*, 43-50. doi:10.1016/j.jfoodeng.2015.12.002

Chiu, Y. T., Chiu, C. P., Chien, J. T., Ho, G. H., Yang, J., & Chen, B. H. (2007). Encapsulation of lycopene extract from tomato pulp waste with gelatin and poly(γ-glutamic acid) as carrier. *Journal of Agricultural and Food Chemistry, 55*(13), 5123–5130. doi: 10.1021/jf0700069

Chuah, A. M., Kuroiwa, T., Kobayashi, I., & Nakajima, M. (2014). The influence of polysaccharide on the stability of protein stabilized oil-in-water emulsion prepared by

microchannel emulsification technique. *Colloids and Surfaces A: Physicochemical and Engineering Aspects*, *440*, 136–144. doi: 10.1016/j.colsurfa.2012.09.051

Conto, L. C., Grosso, C. R., & Gonçalves, L. A. (2013). Chemometry as applied to the production of omega-3 microcapsules by complex coacervation with soy protein isolate and gum Arabic. *LWT - Food Science and Technology*. 53(1): 218-224. doi:10.1016/j.lwt.2013.02.017

Croy, R. R., Gatehouse, J. A., Tyler, M., & Boulter, D. (1980). The purification and characterization of a third storage protein (convicilin) from the seeds of pea (Pisum sativumL.). *Biochemical Journal, 191*(2), 509-516. doi:10.1042/bj1910509.

da Silva, P. T., Fries, L. L. M., de Menezes, C. R., Holkem, A. T., Schwan, C. L., Wigmann, E. F., Bastos, J. D., & da Silva, C. D. (2014). Microencapsulation: concepts, mechanisms, methods and some applications in food technology. *Ciencia Rural, 44,* 1304-1311. doi:10.1590/0103-8478cr20130971

de Jong, S., & van de Velde, F. (2007). Charge density of polysaccharide controls microstructure and large deformation properties of mixed gels. *Food Hydrocolloids, 21*(7), 1172-1187. doi:10.1016/j.foodhyd.2006.09.004.

de Kruif, C. G., Weinbreck, F., & de Vries, R. (2004). Complex coacervation of proteins and anionic polysaccharides. *Current Opinion in Colloid & Interface Science, 9*(5), 340-349. doi:10.1016/j.cocis.2004.09.006.

Devi, N. & Maji, T. K. (2011). Study of complex coacervation of gelatin A with sodium carboxymethyl cellulose: microencapsulation of neem (*Azadirachta indica A. Juss*.) seed oil (NSO). *International Journal of Polymeric Materials*. 60(13): 1091-1105. doi:10.1080/00914037.2011.553851

Devi, N., & Maji, T. K. (2009). A novel microencapsulation of neem (*Azadirachta Indica A. Juss*.) seed oil (NSO) in polyelectrolyte complex of κ-carrageenan and chitosan. *Journal of Applied Polymer Science, 113*(3), 1576–1583. doi: 10.1002/app.30038

Di Battista, C.A., Constenla, D., Ramírez-Rigo, M.V., & Pi˜na, J. (2015). The use of Arabic gum, maltodextrin and surfactants in the microencapsulation of phytosterols by spray drying. *Powder Technol. 286*, 193–201. doi:10.1016/j.powtec.2015.08.016

Di Giorgio, L., Salgado, P. R., & Mauri, A. N. (2019). Encapsulation of fish oil in soybean protein particles by emulsification and spray drying. *Food Hydrocolloids, 87*, 891-901. doi:10.1016/j.foodhyd.2018.09.024

Dickinson, E. (1992). Introduction to food colloids. Oxford, UK: Oxford University Press.

Djordjevic, D., Kim, H. J., McClements, D.J., & Decker, E. A. (2006). Physical stability of whey protein-stabilized oil-in-water emulsions at pH 3: Potential ω-3 fatty acid delivery systems (Part A). *Journal of Food Science, 69*(5). doi:10.1111/j.1365-2621.2004.tb10696.x.

Dong, Z., Ma, Y., Hayat, K., Jia, C., Xia, S., & Zhang, X. (2011). Morphology and release profile of microcapsules encapsulating peppermint oil by complex coacervation. *Journal of Food Engineering, 104,* 455–460. doi:10.1016/j.jfoodeng.2011.01.011

Doublier, J., Garnier, C., Renard, D., & Sanchez, C. (2000). Protein–polysaccharide interactions. *Current Opinion in Colloid & Interface Science, 5*(3-4), 202-214. doi:10.1016/s1359-0294(00)00054-6.

Doublier, Jean-Louis., Garnier, C., & Cuvelier, G. (2017). Gum and hydrocolloids (Chapter 7). In Carbohydrates in food, Third edition. Edited by Eliasson. Ann-Charlotte. A CRC title, New York, 285-332.

Dror, Y., Cohen, Y., & Yerushalmi-Rozen, R. (2006). Structure of gum arabic in aqueous solution. *Journal of Polymer Science Part B: Polymer Physics, 44*(22), 3265-3271. doi:10.1002/polb.20970.

Drusch, S. (2006). Sugar beet pectin: a novel emulsifying wall component for microencapsulation of lipophilic food ingredients by spray-drying. *Food Hydrocolloids, 21,* 1223-1228. doi:10.1016/j.foodhyd.2006.08.007

Drusch, S., & Berg, S. (2008). Extractable oil in microcapsules prepared by spray-drying: Localisation, determination and impact on oxidative stability. *Food Chemistry, 109*(1), 17-24. doi:10.1016/j.foodchem.2007.12.016

Ducel, V., Richard, J., Saulnier, P., Popineau, Y., & Boury, F. (2004). Evidence and characterization of complex coacervates containing plant proteins: application to the microencapsulation of oil droplets. *Colloids and Surfaces A: Physicochemical and Engineering Aspects, 232*(2-3), 239-247. doi:10.1016/j.colsurfa.2003.11.001.

Duhoranimana, E., Yu, J., Mukeshimana, O., Habinshuti, I., Karangwa, E., Xu, X., Muhoza, B., Xia, S., & Zhang, X. (2018). Thermodynamic characterization of gelatin–sodium

carboxymethyl cellulose complex coacervation encapsulating conjugated linoleic acid (CLA). *Food Hydrocolloids*. 80: 149-159. doi:10.1016/j.foodhyd.2018.02.011

Dukhin, S. S., J. Sjoblom, D. T. Wasan, and O. Saether (2001). Coalescence coupled with either coagulation or floocculation in dilute emulsions. *Colloids and Surfaces A: Physicochemical and Engineering Aspects. 180*(3): 223–234. doi:10.1016/S0927-7757(00)00696-8

Dukhin, S. S., N. A. Mishchuk, G. Loglio, L. Liggieri, and R. Miller (2003). Coalescence coupling with floocculation in dilute emulsions within the primary and/or secondary minimum. *Advances in Colloid and Interface Science. 100*: 47–81. doi:10.1016/S0001-8686(02)00073-8

Dziuba, J., Szerszunowicz, I., Nałęcz, D., & Dziuba, M. (2014). Proteomic analysis of albumin and globulin fractions of pea (Pisum sativum L.) seeds. *Acta Scientiarum Polonorum Technologia Alimentaria, 13*(2), 181-190. doi:10.17306/j.afs.2014.2.7.

Edris, A. E., Kalemba, D., Adamiec, J., & Piątkowski, M. (2016). Microencapsulation of nigella sativa oleoresin by spray drying for food and nutraceutical applications. *Food Chemistry, 204*, 326-333. doi:10.1016/j.foodchem.2016.02.143

Eghbal, N., & Choudhary, R. (2018). Complex coacervation: Encapsulation and controlled release of active agents in food systems. *Lwt, 90*, 254–264. doi: 10.1016/j.lwt.2017.12.036

Eghbal, N., Yarmand, M. S., Mousavi, M., Degraeve, P., Oulahal, N., & Gharsallaoui, A. (2016). Complex coacervation for the development of composite edible filmsbased on LM pectin and sodium caseinate. *Carbohydrate Polymers*. 151: 947-956. doi:10.1016/j.carbpol.2016.06.052

El-Adawy, T., Rahma, E., El-Bedawey, A., & El-Beltagy, A. (2003). Nutritional potential and functional properties of germinated mung bean, pea and lentil seeds. *Plant Foods for Human Nutrition*. 58(3): 1-13. doi:10.1023/B:QUAL.0000040339.48521.75

Eratte, D., Wang, B., Dowling, K., Barrow, C. J., & Adhikari, B. P. (2014). Complex coacervation with whey protein isolate and gum arabic for the microencapsulation of omega-3 rich tuna oil. *Food Funct., 5*(11), 2743-2750. doi:10.1039/c4fo00296b

Ercelebi, E. A., & Ibanog˘lu, E. (2007). Influence of hydrocolloids on phase separation and emulsion properties of whey protein isolate. *Journal of Food Engineering, 80*, 454–459. doi:10.1016/j.jfoodeng.2006.05.027

Espinosa-Andrews, H., Baez-Gonzalez, J. G., Cruz-Sosa, F., &Vernon-Carter, E. J. (2007). Gum Arabic-chitosan complex coacervation. *Biomacromolecules*. 8: 1313-1318. doi-org.cyber.usask.ca/10.1021/bm0611634

Evans, M., Ratcliffe, I., & Williams, P. (2013). Emulsion stabilisation using polysaccharide–protein complexes. *Current Opinion in Colloid & Interface Science*, *18*(4), 272–282. doi: 10.1016/j.cocis.2013.04.004

Fernandes, R. V., Borges, S. V., Silva, E. K., Da Silva, Y. F., De Souza, H. J., Do Carmo, E. L., de Oliveira, C. R., Yoshida, M. I., & Botrel, D. A. (2016). Study of ultrasound-assisted emulsions on microencapsulation of ginger essential oil by spray drying. *Industrial Crops and Products, 94*, 413-423. doi:10.1016/j.indcrop.2016.09.010

Flores, Z., Martín, D. S., Villalobos-Carvajal, R., Tabilo-Munizaga, G., Osorio, F., & Leiva-Vega, J. (2016). Physicochemical characterization of chitosan-based coating-forming emulsions: Effect of homogenization method and carvacrol content. *Food Hydrocolloids*, *61*, 851–857. doi: 10.1016/j.foodhyd.2016.07.007

Freire, E., Mayorga, O. L., & Straume, M. (1990). Isothermal titration calorimetry. *Analytical Chemistry, 62*(18), 950A-959A. doi:10.1021/ac00217a002.

Friberg, S. E., & Larsson, K. (1997). Food emulsions (3rd ed.). New York: Marcel Dekker.

Gamboa-Santos, J., Soria, A. C., Villamiel, M., & Montilla, A. (2013). Quality parameters in convective dehydrated carrots blanched by ultrasound and conventional treatment. *Food Chemistry, 141*(1), 616-624. doi:10.1016/j.foodchem.2013.03.028

Gharsallaoui, A., Roudaut, G., Chambin, O., Voilley, A., & Saurel, R. (2007). Applications of spray-drying in microencapsulation of food ingredients: an overview. *Food Research International, 40,* 1107-1121. doi:10.1016/j.foodres.2007.07.004

Girard, M., Sanchez, C., Laneuville, S. I., Turgeon, S. L., & Gauthier, S. F. (2004). Associative phase separation of β-lactoglobulin/pectin solutions: a kinetic study by small angle static light scattering. *Colloids and Surfaces B: Biointerfaces, 35*(1), 15-22. doi:10.1016/j.colsurfb.2004.02.002.

Girard, M., Turgeon, S. L., & Gauthier, S. F. (2003). Thermodynamic parameters of β-lactoglobulin−pectin complexes assessed by isothermal titration calorimetry. *Journal of Agricultural and Food Chemistry, 51*(15), 4450-4455. doi:10.1021/jf0259359.

Girard, M., Turgeon, S., & Paquin, P. (2002). Emulsifying properties of whey protein-carboxymethylcellulose complexes. *Journal of Food Science*. 67(1): 113-119. doi:10.1111/j.1365-2621.2002.tb11369.x

Gouin, S. (2004). Microencapsulation: industrial appraisal of existing technologies and trends. *Trends in Food Science & Technology, 15,* 330-347. doi:10.1016/j.tifs.2003.10.005

Goyal, A., Sharma, V., Sihag, M. K., Tomar, S., Arora, S., Sabikhi, L., & Singh, A. (2015). Development and physico-chemical characterization of microencapsulated flaxseed oil powder: a functional ingredient for omega-3 fortification. *Powder Technology, 286*, 527-537. doi:10.1016/j.powtec.2015.08.050

Graca, C., Raymundo, A., & Sousa, I. D. (2016). Rheology changes in oil-in-water emulsions stabilized by a complex system of animal and vegetable proteins induced by thermal processing. *Lwt*, *74*, 263–270. doi: 10.1016/j.lwt.2016.07.055

Grindrod, J. & Nickerson, T.A. (1968). Effect of various gums on skim milk and purified milk proteins. *Journal of Dairy Science*. 51: 834–841. doi:10.3168/jds.S0022-0302(68)87089-4

Gueguen, J., & Barbot, J. (1988). Quantitative and qualitative variability of pea (*Pisum sativum L.*) protein composition. *Journal of the Science of Food and Agriculture, 42*(3), 209-224. doi:10.1002/jsfa.2740420304.

Guzey, D. & McClements, D. J. (2006). Formation, stability and properties of multilayer emulsions for application in the food industry. *Advances in Colloid and Interface Science, 128*, 227-248. doi:10.1016/j.cis.2006.11.021

Hader, R. N., Waldeck, W. F., & Smith, F. W. (1952). Carboxymethylcellulose. *Industrial and Engineering Chemistry*. 44(12): 2803-2812. doi-org.cyber.usask.ca/10.1021/ie50516a016

Haq, M., & Chun, B.-S. (2018). Microencapsulation of omega-3 polyunsaturated fatty acids and astaxanthin-rich salmon oil using particles from gas saturated solutions (PGSS) process. LWT, 92, 523–530. doi:10.1016/j.lwt.2018.03.009

Harnsilawat, T., Pongsawatmanit, R., & Mcclements, D. (2006). Characterization of β-lactoglobulin–sodium alginate interactions in aqueous solutions: a calorimetry, light scattering, electrophoretic mobility and solubility study. *Food Hydrocolloids, 20*(5), 577-585. doi:10.1016/j.foodhyd.2005.05.005.

Heinzelmann, K., Franke, K., Jensen, B., & Haahr, A.-M. (2000). Protection of fish oil from oxidation by microencapsulation using freeze-drying techniques. *European Journal of*

Lipid Science and Technology, *102*(2), 114–121. doi: 10.1002/(sici)1438-9312(200002)102:2<114::aid-ejlt114>3.3.co;2-s

Heinzen, C. (2002). Microencapsulation solve time dependent problems for foodmakers. *European Food and Drink Review, 3*, 27–30.

Hopkins, E. J., Chang, C., Lam, R. S., & Nickerson, M. T. (2015). Effects of flaxseed oil concentration on the performance of a soy protein isolate-based emulsion-type film. *Food Research International, 67*, 418-425. doi:10.1016/j.foodres.2014.11.040.

Hosseini, S. M., Emam-Djomeh, Z., Razavi, S. H., Moosavi-Movahedi, A. A., Saboury, A. A., Mohammadifar, M. A., Farahnaky, A., Atri, M. S., & van der Meeren, P. V. (2013). Complex coacervation of β-lactoglobulin – κ-carrageenan aqueous mixtures as affected by polysaccharide sonication. *Food Chemistry, 141*(1), 215-222. doi:10.1016/j.foodchem.2013.02.090.

Hsiao, Y., Hsia, S., Chan, Y., & Hsieh, J. (2017). Complex coacervation of soy proteins, isoflavones and chitosan. *Molecules*. 22(12): 1022. doi:10.3390/molecules22061022

Idris, O., Williams, P., & Phillips, G. (1998). Characterisation of gum from Acacia senegal trees of different age and location using multidetection gel permeation chromatography. *Food Hydrocolloids*, *12*(4), 379–388. doi: 10.1016/s0268-005x(98)00058-7

Janjarasskul, T., & Krochta, J. M. (2010). Edible packaging materials. *Annual Review of Food Science and Technology*, *1*(1), 415-448. doi:10.1146/annurev.food.080708.100836.

Jarpa-Parra, M. (2018). Lentil protein: A review of functional properties and food application. An overview of lentil protein functionality. *International Journal of Food Science & Technology,53*(4), 892-903. doi:10.1111/ijfs.13685.

Jelesarov, I., & Bosshard, H. R. (1999). Isothermal titration calorimetry and differential scanning calorimetry as complementary tools to investigate the energetics of biomolecular recognition. *Journal of Molecular Recognition, 12*(1), 3-18. doi:10.1002/(sici)1099-1352(199901/02)12:13.0.co;2-6.

Johnson, G. H., Keast, D. R., & Kris-Etherton, P. M. (2007). Dietary modeling shows that the substitution of canola oil for fats commonly used in the United States would increase compliance with dietary recommendations for fatty acids. *Journal of the American Dietetic Association, 107*(10), 1726–1734. doi: 10.1016/j.jada.2007.07.015

Kamide, K., Okajima, K., Kowsaka, K., Matsui, T., Nomura, S., & Hikichi, K. (1985). Effect of the distribution of substitution of the sodium salt of carboxymethylcellulose on its absorbency toward aqueous liquid. *Polymer Journal, 17*(8), 909-918. doi:10.1295/polymj.17.909.

Karel, M., & Heidelbaugh, N. D. (1973). Recent research and development in the field of low-moisture and intermediate-moisture foods. *C R C Critical Reviews in Food Technology, 3*(3), 329-373. doi:10.1080/10408397309527144

Kaushik, P., Dowling, K., Barrow, C. J., & Adhikari, B. (2015). Microencapsulation of omega-3 fatty acids: a review of microencapsulation and characterization methods. *Journal of Functional Foods, 19,* 868-881. doi:10.1016/j.jff.2014.06.029

Kayitmazer, A. B. (2017). Thermodynamics of complex coacervation. *Advances in Colloid and Interface Science, 239,* 169-177. doi:10.1016/j.cis.2016.07.006.

Kayitmazer, A. B., Koksal, A. F., & Iyilik, E. K. (2015). Complex coacervation of hyaluronic acid and chitosan: effects of pH, ionic strength, charge density, chain length and the charge ratio. *Soft Matter, 11*(44), 8605-8612. doi:10.1039/c5sm01829c.

Kishimoto, A., Ushida, K., Phillips, G. O., Ogasawara, T., & Sasaki, Y. (2006). Identification of intestinal bacteria responsible for fermentation of gum Arabic in pig model. *Current Microbiology, 53*(3), 173–177. doi: 10.1007/s00284-005-0219-3

Kizilay, E., Kayitmazer, A. B., & Dubin, P. L. (2011). Complexation and coacervation of polyelectrolytes with oppositely charged colloids. *Advances in Colloid and Interface Science,167*(1-2), 24-37. doi:10.1016/j.cis.2011.06.006.

Klassen, D. R., Elmer, C. M., & Nickerson, M. T. (2011). Associative phase separation involving canola protein isolate with both sulphated and carboxylated polysaccharides. *Food Chemistry,126*(3), 1094-1101. doi:10.1016/j.foodchem.2010.11.138.

Klaypradit, W., & Huang, Y. (2008). Fish oil encapsulation with chitosan using ultrasonic atomizer. *LWT - Food Science and Technology, 41*(6), 1133-1139. doi:10.1016/j.lwt.2007.06.014

Klemmer, K., Waldner, L., Stone, A., Low, N., & Nickerson, M. (2012). Complex coacervation of pea protein isolate and alginate polysaccharides. *Food Chemistry, 130*(3), 710-715. doi:10.1016/j.foodchem.2011.07.114.

Koc, M., Gungor, O., Zungur, A., Yalcin, B., Selek, I., Ertekin, F. K., & Otles, S. (2015). Microencapsulation of extra virgin olive oil by spray drying: effect of wall materials

composition, process conditions, and emulsification method. *Food Bioprocess Technology, 8,* 301-318. doi:10.1007/s11947-014-1404-9

Koupantsis, T., Pavlidou, E., & Paraskevopoulou, A. (2014). Flavour encapsulation in milk proteins – CMC coacervate-type complexes. *Food Hydrocolloids, 37,* 134-142. doi:10.1016/j.foodhyd.2013.10.031.

Krokida, M., & Philippopoulos, C. (2006). Volatility of apples during air and freeze drying. *Journal of Food Engineering*, *73*(2), 135–141. doi: 10.1016/j.jfoodeng.2005.01.012

Kuang, P., Zhang, H., Bajaj, P. R., Yuan, Q., Tang, J., Chen, S., & Sablani, S. S. (2015). Physicochemical properties and storage stability of lutein microcapsules prepared with maltodextrins and sucrose by spray drying. *Journal of Food Science*, *80*(2). doi:10.1111/1750-3841.12776

Kyriakoudi, A., & Tsimidou, M. Z. (2018). Properties of encapsulated saffron extracts in maltodextrin using the Büchi B-90 nano spray-dryer. *Food Chemistry, 266*, 458–465. doi: 10.1016/j.foodchem.2018.06.038

Lagarde, M. (2010). Oxygenated metabolites of polyunsaturated fatty acids: formation and function in blood and vascular cells. *European Journal of Lipid Science and Technology, 112*(9), 941-947. doi:10.1002/ejlt.201000045

Lam, R. S., & Nickerson, M. T. (2013). Food proteins: a review on their emulsifying properties using a structure–function approach. *Food Chemistry*, *141*(2), 975–984. doi: 10.1016/j.foodchem.2013.04.038

Lam, R. S., & Nickerson, M. T. (2014). The properties of whey protein–carrageenan mixtures during the formation of electrostatic coupled biopolymer and emulsion gels. *Food Research International,66,* 140-149. doi:10.1016/j.foodres.2014.08.006.

Lee, S.-H., Lefèvre, T., Subirade, M., & Paquin, P. (2009). Effects of ultra-high pressure homogenization on the properties and structure of interfacial protein layer in whey protein-stabilized emulsion. *Food Chemistry*, *113*(1), 191–195. doi: 10.1016/j.foodchem.2008.07.067

Lemetter, C. Y. G., Meeuse, F. M., & Zuidam, N. J. (2009). Control of the morphology and the size of complex coacervate microcapsules during scale-up. *AIChE Journal*, *55*(6), 1487–1496. doi: 10.1002/aic.11816

Li, L., Ni, R., Shao, Y., & Mao, S. (2014). Carrageenan and its applications in drug delivery. *Carbohydrate Polymers*, *103*, 1–11. doi: 10.1016/j.carbpol.2013.12.008

Li, Y., & McClements, D. J. (2011). Controlling lipid digestion by encapsulation of protein-stabilized lipid droplets within alginate–chitosan complex coacervates. *Food Hydrocolloids, 25*(5), 1025-1033. doi:10.1016/j.foodhyd.2010.09.024.

Li, Y., Xia, J., & Dubin, P. L. (1994). Complex formation between polyelectrolyte and oppositely charged mixed micelles: static and dynamic light scattering study of the effect of polyelectrolyte molecular weight and concentration. *Macromolecules, 27*(24), 7049-7055. doi:10.1021/ma00102a007.

Liang, H., & Tang, C. (2014). Pea protein exhibits a novel Pickering stabilization for oil-in-water emulsions at pH 3.0. *LWT - Food Science and Technology, 58*(2), 463-469. doi:10.1016/j.lwt.2014.03.023.

Lin, C.-Y., & Chen, L.-W. (2008). Comparison of fuel properties and emission characteristics of two- and three-phase emulsions prepared by ultrasonically vibrating and mechanically homogenizing emulsification methods. *Fuel*, *87*(10-11), 2154–2161. doi: 10.1016/j.fuel.2007.12.017

Lin, L., Allemekinders, H., Dansby, A., Campbell, L., Durance-Tod, S., Berger, A., & Jones, P. J. (2013). Evidence of health benefits of canola oil. *Nutrition Reviews*, *71*(6), 370–385. doi: 10.1111/nure.12033

Liu, C., Li, M., Liang, C., & Wang, W. (2013a). Measurement and analysis of bimodal drop size distribution in a rotor-stator homogenizer. *Chemical Engineering Science. 102*, 622-631. doi:10.1016/j.ces.2013.08.030

Liu, H., Cui, Y., Li, P., Zhou, Y., Chen, Y., Tang, Y., & Lu, T. (2013b). Polyphosphonate induced coacervation of chitosan: encapsulation of proteins/enzymes and their biosensing. *Analytica Chimica Acta*, *776*, 24–30. doi: 10.1016/j.aca.2013.03.040

Liu, S., Cao, Y., Ghosh, S., Rousseau, D., Low, N. H., & Nickerson, M. T. (2010). Intermolecular interactions during complex coacervation of pea protein isolate and gum Arabic. *Journal of Agricultural and Food Chemistry, 58*(1), 552-556. doi:10.1021/jf902768v.

Liu, S., Low, N. H., & Nickerson, M. T. (2009). Effect of pH, salt, and biopolymer ratio on the formation of pea protein isolate−gum Arabic complexes. *Journal of Agricultural and Food Chemistry, 57*(4), 1521-1526. doi:10.1021/jf802643n.

Liu, Z., Zhou, J., Zeng, Y., & Ouyang, X. (2004). The enhancement and encapsulation of Agaricus bisporus flavor. *Journal of Food Engineering*, *65*, 391–396. doi:10.1016/j.jfoodeng.2004.01.038

Madene, A., Jacquot, M., Scher, J., & Desobry, S. (2006). Flavor encapsulation and controlled release – a review. *International Journal of Food Science and Technology*, *4,* 1-21. doi-org.cyber.usask.ca/10.1111/j.1365-2621.2005.00980.x

Maindarkar, S. N., Hoogland, H., & Henson, M. A. (2015). Predicting the combined effects of oil and surfactant concentrations on the drop size distributions of homogenized emulsions. *Colloids and Surfaces A: Physicochemical and Engineering Aspects*, *467*, 18–30. doi: 10.1016/j.colsurfa.2014.11.032

Mao, L., Roos, Y. H., O'Callaghan, D. J., & Miao, S. (2013). Volatile release from whey protein isolate–pectin multilayer stabilized emulsions: effect of ph, salt, and artificial salivas. *Journal of Agricultural and Food Chemistry*, *61*(26), 6231–6239. doi: 10.1021/jf4011615

McClements, D. J. (2005). Food emulsions: principles, practice and techniques (2nd ed). Boca Raton, FL, USA: CRC Press Taylor & Francis Group.

McClements, D. J. (2007). Critical review of techniques and methodologies for characterization of emulsion stability. *Critical Reviews in Food Science and Nutrition, 47*(7), 611-649. doi:10.1080/10408390701289292.

McClements, D. J. (2012). Advances in fabrication of emulsions with enhanced functionality using structural design principles. *Current Opinion in Colloid and Interface Science, 17*, 235–245. doi:10.1016/j.cocis.2012.06.002

McClements, D. J. (2015). Food emulsions: principles, practice and techniques (3rd ed). Boca Raton, FL, USA: CRC Press Taylor & Francis Group.

McClements, D. J., & Rao, J. (2011). Food-grade nanoemulsions: formulation, fabrication, properties, performance, biological fate, and potential toxicity. *Critical Reviews in Food Science and Nutrition*, *51*(4), 285–330. doi: 10.1080/10408398.2011.559558

Mehmood, T., Ahmad, A., Ahmed, A., & Ahmed, Z. (2017). Optimization of olive oil based O/W nanoemulsions prepared through ultrasonic homogenization: A response surface methodology approach. *Food Chemistry*, *229*, 790–796. doi: 10.1016/j.foodchem.2017.03.023

Menin, A., Zanoni, F., Vakarelova, M., Chignola, R., Donà, G., Rizzi, C., Mainente, F., Zoccatelli, G. (2018). Effects of microencapsulation by ionic gelation on the oxidative stability of flaxseed oil. *Food Chemistry*, *269*, 293–299. doi: 10.1016/j.foodchem.2018.06.144

Mi, F.-L., Sung, H.-W., & Shyu, S.-S. (2002). Drug release from chitosan–alginate complex beads reinforced by a naturally occurring cross-linking agent. *Carbohydrate Polymers*, *48*(1), 61–72. doi: 10.1016/s0144-8617(01)00212-0

Mishchuk, N. A. (2005). Theoretical analysis of coagulation kinetics in Brownian disperse systems. *Colloid Journal, 67*(3): 341–350. doi.org/10.1007/s10595-005-0102-8

Mohanan, A., Nickerson, M. T., & Ghosh, S. (2018). Oxidative stability of flaxseed oil: effect of hydrophilic, hydrophobic and intermediate polarity antioxidants. *Food Chemistry*, *266*, 524–533. doi: 10.1016/j.foodchem.2018.05.117

Morais, A. R., Alencar, É. do, Xavier Júnior, F. H., Oliveira, C. M., Marcelino, H. R., Barratt, G., Fessi, H., Egito, E. S., & Elaissari, A. (2016). Freeze-drying of emulsified systems: a Review. International Journal of Pharmaceutics, 503(1-2), 102–114. doi:10.1016/j.ijpharm.2016.02.047

Narsaiah, K., Jha, S. N., Wilson, R. A., Mandge, H. M., & Manikantan, M. R. (2014). Optimizing microencapsulation of nisin with sodium alginate and guar gum. *Journal of Food Science and Technology*, *51*(12), 4054–4059. doi: 10.1007/s13197-012-0886-6

Necas, J., & Bartosikova, L. (2013). Carrageenan: a review. *Veterinární Medicína*, *58*(No. 4), 187–205. doi: 10.17221/6758-vetmed

Nesterenko, A., Alric, I., Silvestre, F., & Durrieu, V. (2013). Vegetable proteins in microencapsulation: a review of recent interventions and their effectiveness. *Industrial Crops and Products, 42,* 469-479. doi:10.1016/j.indcrop.2012.06.035

Nunes, M., Raymundo, A., & Sousa, I. (2006). Rheological behaviour and microstructure of pea protein/κ-carrageenan/starch gels with different setting conditions. *Food Hydrocolloids*. 20(1): 106-113. doi:10.1016/j.foodhyd.2005.03.011

O'Sullivan, A. C. (1997) Cellulose: the structure slowly unravels. *Cellulose. 4*, 173-207. doi:10.1023/A:1018431705579.

Ou, Z., & Muthukumar, M. (2006). Entropy and enthalpy of polyelectrolyte complexation: Langevin dynamics simulations. *The Journal of Chemical Physics*, *124*(15), 154902. doi:10.1063/1.2178803.

Paramera, E. I., Konteles, S. J., & Karathanos, V. T. (2011). Microencapsulation of curcumin in cells of Saccharomyces cerevisiae. *Food Chemistry*, *125*(3), 892–902. doi: 10.1016/j.foodchem.2010.09.063

Park, S. J., Kim, T. W., & Baik, B. (2010). Relationship between proportion and composition of albumins, and in vitro protein digestibility of raw and cooked pea seeds (Pisum sativum L.). *Journal of the Science of Food and Agriculture*, *90*(10), 1719-1725. doi:10.1002/jsfa.4007.

Pawar, S. N., & Edgar, K. J. (2012). Alginate derivatization: a review of chemistry, properties and applications. *Biomaterials*, *33*(11), 3279–3305. doi: 10.1016/j.biomaterials.2012.01.007

Perry, S., Li, Y., Priftis, D., Leon, L., & Tirrell, M. (2014). The effect of salt on the complex coacervation of vinyl polyelectrolytes. *Polymers*, *6*(12): 1756-1772. doi:10.3390/polym6061756

Pillai, P. K., Stone, A. K., Guo, Q., Guo, Q., Wang, Q., & Nickerson, M. T. (2019). Effect of alkaline de-esterified pectin on the complex coacervation with pea protein isolate under different mixing conditions. *Food Chemistry, 284*, 227-235. doi:10.1016/j.foodchem.2019.01.122.

Piorkowski, D. T. & McClements, D. J. (2014). Beverage emulsions: recent developments in formulation, production, and applications. *Food Hydrocolloids, 42,* 5–41. doi:10.1016/j.foodhyd.2013.07.009

Polavarapu, S., Oliver, C. M., Ajlouni, S., & Augustin, M. A. (2011). Physicochemical characterisation and oxidative stability of fish oil and fish oil–extra virgin olive oil microencapsulated by sugar beet pectin. *Food Chemistry*, *127*(4), 1694-1705. doi:10.1016/j.foodchem.2011.02.044

Pothakamury, U. R. & Barbosa-Canovas, G. V. (1995). Fundamental aspects of controlled release in foods. *Trends in Food Science & Technology, 6,* 397-406. doi:10.1016/s0924-2244(00)89218-3

Primozic, M., Duchek, A., Nickerson, M., & Ghosh, S. (2018). Formation, stability and in vitro digestibility of nanoemulsions stabilized by high-pressure homogenized lentil proteins isolate. *Food Hydrocolloids, 77,* 126-141. doi:10.1016/j.foodhyd.2017.09.028.

Qi, X., & Tester, R. F. (2018). Is starch or maltodextrin "glucose?" *Starch - Stärke*, *70*(9-10), 1700304. doi: 10.1002/star.201700304

Qian, C., & McClements, D. J. (2011). Formation of nanoemulsions stabilized by model food-grade emulsifiers using high-pressure homogenization: factors affecting particle size. *Food Hydrocolloids, 25*(5), 1000-1008. doi:10.1016/j.foodhyd.2010.09.017.

Quek, S. Y., Chok, N. K., & Swedlund, P. (2007). The physicochemical properties of spray-dried watermelon powders. *Chemical Engineering and Processing: Process Intensification, 46*(5), 386-392. doi:10.1016/j.cep.2006.06.020

Quispe-Condori, S., Saldaña, M. D., & Temelli, F. (2011). Microencapsulation of flax oil with zein using spray and freeze drying. *LWT - Food Science and Technology, 44*(9), 1880-1887. doi:10.1016/j.lwt.2011.01.005

Rajaram, S. (2014). Health benefits of plant-derived α-linolenic acid. *The American Journal of Clinical Nutrition*, *100*(supplement). doi: 10.3945/ajcn.113.071514

Reifen, R., Karlinsky, A., Stark, A. H., Berkovich, Z., & Nyska, A. (2015). α-Linolenic acid (ala) is an anti-inflammatory agent in inflammatory bowel disease. *The Journal of Nutritional Biochemistry, 26*(12), 1632-1640. doi:10.1016/j.jnutbio.2015.08.006

Reineccius, G. A. (2004). The spray drying of food flavors. *Drying Technology, 22,* 1289- 1324. doi:10.1081/drt-120038731

Rezende, G., & Hashizume, L. N. (2018). Maltodextrin and dental caries: a literature review. *RGO - Revista Gaúcha De Odontologia, 66*(3), 257-262. doi:10.1590/1981-86372018000300003288

Rubilar, M., Morales, E., Contreras, K., Ceballos, C., Acevedo, F., Villarroel, M., & Shene, C. (2012). Development of a soup powder enriched with microencapsulated linseed oil as a source of omega-3 fatty acids. *European Journal of Lipid Science and Technology*, *114*(4), 423–433. doi: 10.1002/ejlt.201100378

Rutz, J. K., Borges, C. D., Zambiazi, R. C., Crizel-Cardozo, M. M., Kuck, L. S., & Noreña, C. P. (2017). Microencapsulation of palm oil by complex coacervation for application in food systems. *Food Chemistry, 220,* 59–66. doi: 10.1016/j.foodchem.2016.09.194

Rutz, J. K., Borges, C. D., Zambiazi, R. C., Rosa, C. G. D., & Silva, M. M. D. (2016). Elaboration of microparticles of carotenoids from natural and synthetic sources for applications in food. *Food Chemistry, 202,* 324–333. doi: 10.1016/j.foodchem.2016.01.140

Schmitt, C., Sanchez, C., Desobry-Banon, S., & Hardy, J. (1998). Structure and technofunctional properties of protein-polysaccharide complexes: a review. *Critical Reviews in Food Science and Nutrition, 38*(8), 689-753. doi:10.1080/10408699891274354.

Seyrek, E., Dubin, P. L., Tribet, C., & Gamble, E. A. (2003). Ionic strength dependence of protein-polyelectrolyte interactions. *Biomacromolecules, 4*(2), 273-282. doi:10.1021/bm025664a.

Shi, J. (2002). Steric stabilization. Croup inorganic materials science – literature review. The Ohio State University. Columbus, USA.

Shieh J., & Glatz C.E. (1994). Precipitation of proteins with polyelectrolytes: role of polymer molecular weight. In: Dubin P., Bock J., Davis R., Schulz D.N., Thies C. (eds) macromolecular complexes in chemistry and biology. Springer, Berlin, Heidelberg.

Shim, Y. Y., Gui, B., Wang, Y., & Reaney, M. J. (2015). Flaxseed (*Linum usitatissimum L*.) oil processing and selected products. *Trends in Food Science & Technology*, *43*(2), 162–177. doi: 10.1016/j.tifs.2015.03.001

Singh, S. S., Siddhanta, A., Meena, R., Prasad, K., Bandyopadhyay, S., & Bohidar, H. (2007). Intermolecular complexation and phase separation in aqueous solutions of oppositely charged biopolymers. *International Journal of Biological Macromolecules, 41*(2), 185-192. doi:10.1016/j.ijbiomac.2007.02.004.

Souza, C. J. & Garcia-Rojas, E. E. (2015). Effects of salt and protein concentrations on the association and dissociation of ovalbumin-pectin complexes. *Food Hydrocolloids*. 47: 124-129. doi:10.1016/j.foodhyd.2015.01.010

Sovilj, V. J., & Petrović, L. B. (2006). Influence of hydroxypropylmethyl cellulose–sodium dodecylsulfate interaction on the solution conductivity and viscosity and emulsion stability. *Carbohydrate Polymers*, *64*(1), 41–49. doi: 10.1016/j.carbpol.2005.10.030

Stone, A. K., Avarmenko, N. A., Warkentin, T. D., & Nickerson, M. T. (2015a). Functional properties of protein isolates from different pea cultivars. *Food Science and Biotechnology, 24*(3), 827-833. doi:10.1007/s10068-015-0107-y.

Stone, A. K., Cheung, L., Chang, C., & Nickerson, M. T. (2013). Formation and functionality of soluble and insoluble electrostatic complexes within mixtures of canola protein isolate and (κ-, ι- and λ-type) carrageenan. *Food Research International, 54*(1), 195-202. doi:10.1016/j.foodres.2013.06.009.

Stone, A. K., Karalash, A., Tyler, R. T., Warkentin, T. D., & Nickerson, M. T. (2015b). Functional attributes of pea protein isolates prepared using different extraction methods and cultivars. *Food Research International, 76,* 31-38. doi:10.1016/j.foodres.2014.11.017.

Stone, A. K., Teymurova, A., & Nickerson, M. T. (2014). Formation and functional attributes of canola protein isolate—gum Arabic electrostatic complexes. *Food Biophysics, 9*(3), 203-212. doi:10.1007/s11483-014-9334-7.

Stone, A.K., Teymurova, A., Chang, C., Cheung, L., and Nickerson, M.T. (2015). Formation and functionality of canola protein isolate with both high- and low-methoxy pectin under associative conditions. *Food Science and Biotechnology*, 24, 1209-2018. doi:10.1007/s10068-015-0155-3

Sulatha, M. S. & Natarajan, U. (2015). Molecular dynamics simulations of adsorption of poly(acrylic acid) and poly(methacrylic acid) on dodecyltrimethylammonium chloride micelle in water: effect of charge density. *The Journal of Physical Chemistry B*. 119(38): 12526-12539. doi:10.1021/acs.jpcb.5b04680

Suryabhan, P., Lohith, K., & Anu-Appaiah, K. (2019). Sucrose and sorbitol supplementation on maltodextrin encapsulation enhance the potential probiotic yeast survival by spray drying. *Lwt*, *107*, 243–248. doi: 10.1016/j.lwt.2019.03.002

Timilsena, Y. P., Wang, B., Adhikari, R., & Adhikari, B. (2016). Preparation and characterization of chia seed protein isolate–chia seed gum complex coacervates. *Food Hydrocolloids*, *52*, 554–563. doi: 10.1016/j.foodhyd.2015.07.033

Tolstoguzov, V. B. (1991). Functional properties of food proteins and role of protein-polysaccharide interaction. *Food Hydrocolloids*. 4(6): 429-468. doi:10.1016/s0268-005x(09)80196-3

Tolstoguzov, V.B. (1997). Protein-polysaccharide interactions. In Damodaran. S. & Paraf. A. (Eds.), food proteins and their applications (171–199). New York, NY: Marcel Dekker.

Tsianou, M., Kjøniksen, A., Thuresson, K., & Nyström, B. (1999). Light scattering and viscoelasticity in aqueous mixtures of oppositely charged and hydrophobically modified polyelectrolytes. *Macromolecules*. 32(9): 2974-2982. doi:10.1021/ma981619c

Turgeon, S. L., & Laneuville, S. I. (2009). Protein polysaccharide coacervates and complexes. *Modern Biopolymer Science,* 327-363. doi:10.1016/b978-0-12-374195-0.00011-2.

Tyagi, V. V., Kaushik, S. C., Tyagi, S. K., & Akiyama, T. (2011). Development of phase change materials based microencapsulated technology for building: a review. *Renewable and Sustainable Energy Reviews, 15*, 1373-1391. doi:10.1016/j.rser.2010.10.006

Uruakpa, F. O., & Arntfield, S. (2005). Emulsifying characteristics of commercial canola protein–hydrocolloid systems. *Food Research International, 38*(6), 659-672. doi:10.1016/j.foodres.2005.01.004.

Van De Velde, F., Lourenço, N. D., Pinheiro, H. M., & Bakker, M. (2002). Carrageenan: a food-grade and biocompatible support for immobilisation techniques. *Advanced Synthesis & Catalysis*, *344*(8), 815–835. doi: 10.1002/1615-4169(200209)344:8<815::aid-adsc815>3.0.co;2-h

Vargas, M., Perdones, Á., Chiralt, A., Cháfer, M., & González-Martínez, C. (2011). Effect of homogenization conditions on physicochemical properties of chitosan-based film-forming dispersions and films. *Food Hydrocolloids*, *25*(5), 1158–1164. doi: 10.1016/j.foodhyd.2010.11.002

Velasco, J., Dobarganes, C., & Márquez-Ruiz, G. (2003). Variables affecting lipid oxidation in dried microencapsulated oils. *Grasas Y Aceites, 54*(3). doi:10.3989/gya.2003.v54.i3.246

Velasco, P., Soengas, P., Vilar, M., Cartea, M. E., & Rio, M. D. (2008). Comparison of glucosinolate profiles in leaf and seed tissues of different brassica napus crops. *Journal of the American Society for Horticultural Science*, *133*(4), 551–558. doi: 10.21273/jashs.133.4.551

Verbeken, D., Dierckx, S., & Dewettinck, K. (2003). Exudate gums: occurrence, production, and applications. *Applied Microbiology and Biotechnology*, *63*(1), 10–21. doi: 10.1007/s00253-003-1354-z

Vikelouda, M., & Kiosseoglou, V. (2004). The use of carboxymethylcellulose to recover potato proteins and control their functional properties. *Food Hydrocolloids*. 18(1): 21-27. doi:10.1016/s0268-005x(03)00038-9

Walstra, P. (1993). Principles of emulsion formation. *Chemical Engineering Science*, *48*(2), 333–349. doi: 10.1016/0009-2509(93)80021-h

Walstra, P. (2003). Physical chemistry of foods. New York: Marcel Dekker.

Walstra, P., & van Vliet, T. (2008). Dispersed systems: Basic considerations. In S. Damordaran, K. L. Parkin, & O. R. Fennema (Eds.), Fennema's food chemistry (pp. 783–847) (4th ed.). Boca Raton: CRC Press.

Wang, B., Adhikari, B., & Barrow, C. J. (2014). Optimisation of the microencapsulation of tuna oil in gelatin–sodium hexametaphosphate using complex coacervation. *Food Chemistry*, *158*, 358–365. doi: 10.1016/j.foodchem.2014.02.135

Wang, J., Dumas, E., & Gharsallaoui, A. (2019c). Low methoxyl pectin / sodium caseinate complexing behavior studied by isothermal titration calorimetry. *Food Hydrocolloids*, *88*, 163-169. doi:10.1016/j.foodhyd.2018.10.006.

Wang, X., Yuan, Y., & Yue, T. (2015). The application of starch-based ingredients in flavor encapsulation. *Starch - Stärke*, *67*(3-4), 225–236. doi: 10.1002/star.201400163

Wang, Y., Ghosh, S., & Nickerson, M. T. (2019a). Effect of pH on the formation of electrostatic complexes between lentil protein isolate and a range of anionic polysaccharides, and their resulting emulsifying properties. *Food Chemistry*, *298*, 125023. doi: 10.1016/j.foodchem.2019.125023

Wang, Y., Ghosh, S., & Nickerson, M. T. (2021). Effect of biopolymer mixing ratios and aqueous phase conditions on the interfacial and emulsifying properties of lentil protein isolate–κ-carrageenan and lentil protein isolate–ι-carrageenan complexes. *Cereal Chemistry*. doi: 10.1002/cche.10465

Wang, Y., Pillai, P. K., & Nickerson, M. T. (2019b). Effect of molecular mass and degree of substitution of carboxymethyl cellulose on the formation electrostatic complexes with lentil protein isolate. *Food Research International*, *126*, 108652. doi: 10.1016/j.foodres.2019.108652

Warnakulasuriya, S., Pillai, P. K., Stone, A. K., & Nickerson, M. T. (2018). Effect of the degree of esterification and blockiness on the complex coacervation of pea protein isolate and commercial pectic polysaccharides. *Food Chemistry*, *264*, 180-188. doi:10.1016/j.foodchem.2018.05.036.

Weinbreck, F., de Vries, R., Schrooyen, P., & de Kruif, C. G. (2003b). Complex coacervation of whey proteins and gum Arabic. *Biomacromolecules*, *4*(2), 293-303. doi:10.1021/bm025667n.

Weinbreck, F., Nieuwenhuijse, H., Robijn, G. W., & de Kruif, C. G. (2003a). Complex formation of whey proteins: exocellular polysaccharide EPS B40. *Langmuir, 19*(22), 9404-9410. doi:10.1021/la0348214.

Weinbreck, F., Nieuwenhuijse, H., Robijn, G. W., & de Kruif, C. G. (2004). Complexation of whey proteins with carrageenan. *Journal of Agricultural and Food Chemistry, 52*(11), 3550-3555. doi:10.1021/jf034969t.

Wooster, T. J., Golding, M., & Sanguansri, P. (2008). Impact of oil type on nanoemulsion formation and Ostwald ripening stability. *Langmuir, 24*(22), 12758-12765. doi:10.1021/la801685v.

Xiao, J. X., Yu, H. Y., & Yang, J. A. (2011). Microencapsulation of sweet orange oil by complex coacervation with soybean protein isolate/gum Arabic. *Food Chemistry, 125*, 1267-1272. doi:10.1016/j.foodchem.2010.10.063

Xiao, Z., Liu, W., Zhu, G., Zhou, R., & Niu, Y. (2013). A review of the preparation and application of flavour and essential oils microcapsules based on complex coacervation technology. *Journal of the Science of Food and Agriculture*, *94*(8), 1482–1494. doi: 10.1002/jsfa.6491

Xiong, W., Deng, Q., Li, J., Li, B., & Zhong, Q. (2020). Ovalbumin-carboxymethylcellulose complex coacervates stabilized high internal phase emulsions: comparison of the effects of pH and polysaccharide charge density. *Food Hydrocolloids*, *98*, 105282. doi:10.1016/j.foodhyd.2019.105282

Xiong, W., Ren, C., Tian, M., Yang, X., Li, J., & Li, B. (2017). Complex coacervation of ovalbumin-carboxymethylcellulose assessed by isothermal titration calorimeter and rheology: effect of ionic strength and charge density of polysaccharide. *Food Hydrocolloids, 73*, 41-50. doi:10.1016/j.foodhyd.2017.06.031.

Xu, A. Y., Melton, L. D., Jameson, G. B., Williams, M. A., & Mcgillivray, D. J. (2015). Structural mechanism of complex assemblies: characterisation of beta-lactoglobulin and pectin interactions. *Soft Matter, 11*(34), 6790-6799. doi:10.1039/c5sm01378j.

Yang, J.-S., Xie, Y.-J., & He, W. (2011). Research progress on chemical modification of alginate: a review. *Carbohydrate Polymers*, *84*(1), 33–39. doi: 10.1016/j.carbpol.2010.11.048

Ye, A. (2008). Complexation between milk proteins and polysaccharides via electrostatic interaction: Principles and applications – a review. *International Journal of Food Science & Technology, 43*(3), 406-415. doi:10.1111/j.1365-2621.2006.01454.x .

Yin, B., Deng, W., Xu, K., Huang, L., & Yao, P. (2012). Stable nano-sized emulsions produced from soy protein and soy polysaccharide complexes. *Journal of Colloid and Interface Science, 380*(1), 51–59. doi: 10.1016/j.jcis.2012.04.075

Zhivkov, A. M. (2013). Electric properties of carboxymethyl cellulose. *Cellulose - Fundamental Aspects*. doi:10.5772/56935.

11. APPENDICES

11.1 Tables

Table A1 Proximate composition of lentil protein isolate, carboxymethyl cellulose polymers, gum Arabic, alginate, ι-carrageenan, κ-carrageenan, and maltodextrin. Data represents the mean ± one standard deviation (n = 3). All data is reported as the percentage on a dry weight basis.

Materials	**Protein[1]**	**Lipid**	**CHO[2]**	**Ash**	**Select minerals**			
					Na^+	**K^+**	**Ca^{2+}**	**Mg^{2+}**
Lentil protein isolate	80.6 ± 0.3	0.8 ± 0.1	13.0	5.6 ± 0.4	1.80	0.67	0.03	0.07
Carboxymethyl cellulose								
DS 0.7, 250 kDa	Nil	Nil	81.3	18.7 ± 0.2	8.20	0.00	0.00	0.00
DS 0.9, 250 kDa	Nil	Nil	81.4	18.6 ± 0.3	8.40	0.10	0.00	0.00
DS 1.2, 250 kDa	Nil	Nil	75.0	25.0 ± 0.5	10.0	0.10	0.00	0.00
DS 0.7, 90 kDa	Nil	Nil	80.4	19.6 ± 0.5	8.10	0.10	0.00	0.00
Gum Arabic	1.8 ± 0.2	Nil	94.8	3.4 ± 0.1	0.00	0.90	0.70	0.20
Alginate	Nil	Nil	73.9	26.1 ± 0.1	10.30	0.20	0.20	0.10
ι-Carrageenan	Nil	Nil	71.2	28.8 ± 0.2	1.40	5.50	4.00	0.20
κ-Carrageenan	Nil	Nil	77.6	22.4 ± 0.2				
Maltodextrin	Nil	Nil	99.3	0.7 ± 0.0				

Notes: [1]Nitrogen conversion factor (6.25)

[2]Carbohydrate (CHO) was determined based on the dry weight difference 100% and (protein + ash + lipid) levels.

Table A2 Formulations used for the initial emulsions to deliver 20% and 30% oil within microcapsules with both types of lentil protein isolate-carrageenan (LPI-ι-C) formulations.

Sample	%Final oil	Initial emulsions (%, w/w)				Spray dried microcapsules (%, w/w)				
		% Oil	LPI/ LPI-ι-C/ LPI-κ-C	MD	Total solid	Core: wall	Oil	LPI/ LPI-ι-C/ LPI-κ-C	MD	Total solid
LPI 20%	20	5	1	19	25	1:4	20	4	76	100
LPI 30%	30	7.5	1	16.5	25	1:2.3	30	4	66	100
LPI-ι-C 20%	20	5	1	19	25	1:4	20	4	76	100
LPI-ι-C 30%	30	7.5	1	16.5	25	1:2.3	30	4	66	100
LPI-κ-C 20%	20	5	1	19	25	1:4	20	4	76	100
LPI-κ-C 30%	30	7.5	1	16.5	25	1:2.3	30	4	66	100

- The percentage on the name of the samples represents the final oil content in dried powders.

11.2 Figures

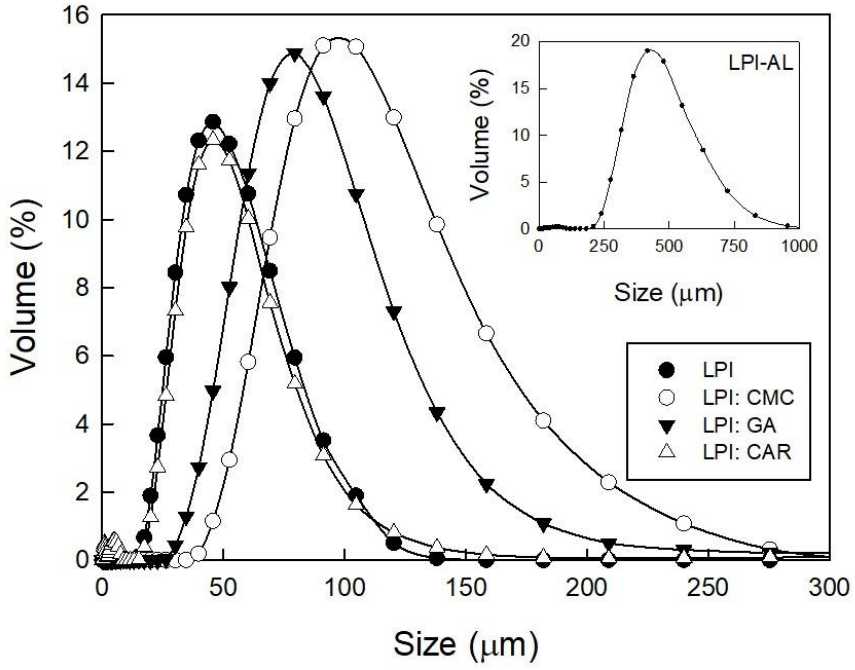

Figure A4.1 Droplet size distribution for emulsions stabilized by homogenous LPI solutions and mixtures of lentil protein isolate (LPI) with carboxymethyl cellulose (CMC), gum Arabic (GA), alginate (AL) and ι-carrageenan (ι-C). Data represents the mean ± one standard deviation (n = 3).

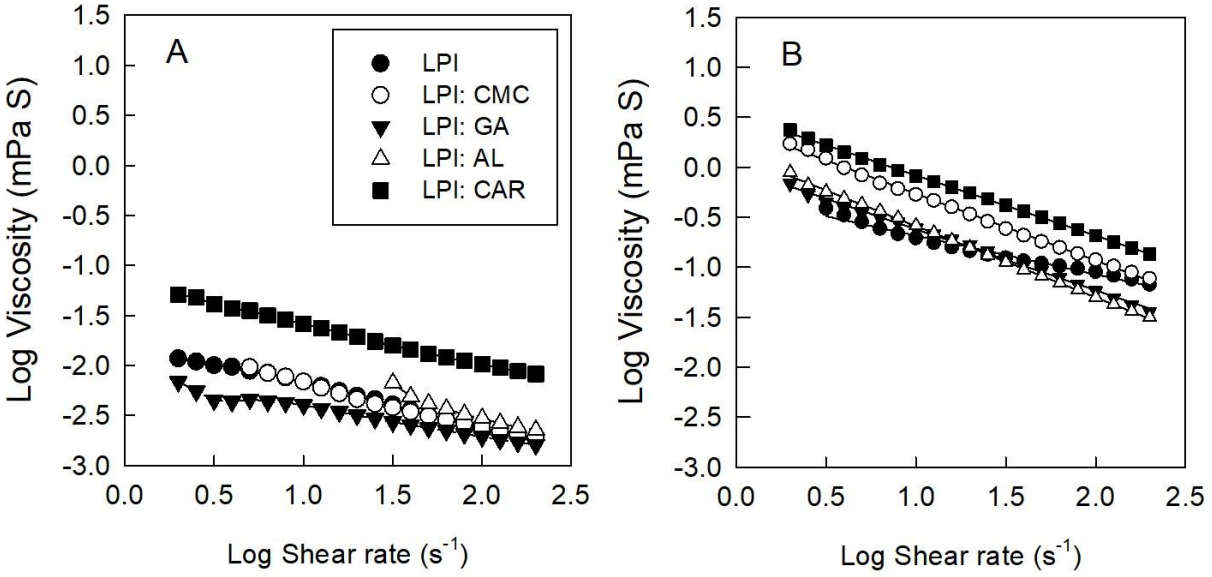

Figure A4.2 Flow diagrams as fitted using the Power-law model parameters for (A) homogenous LPI solutions and mixtures of LPI with carboxymethyl cellulose (CMC), gum Arabic (GA), alginate (AL) and ι-carrageenan (ι-C) and (B) emulsions stabilized by corresponding solutions. Data represents the mean ± one standard deviation (n = 3).

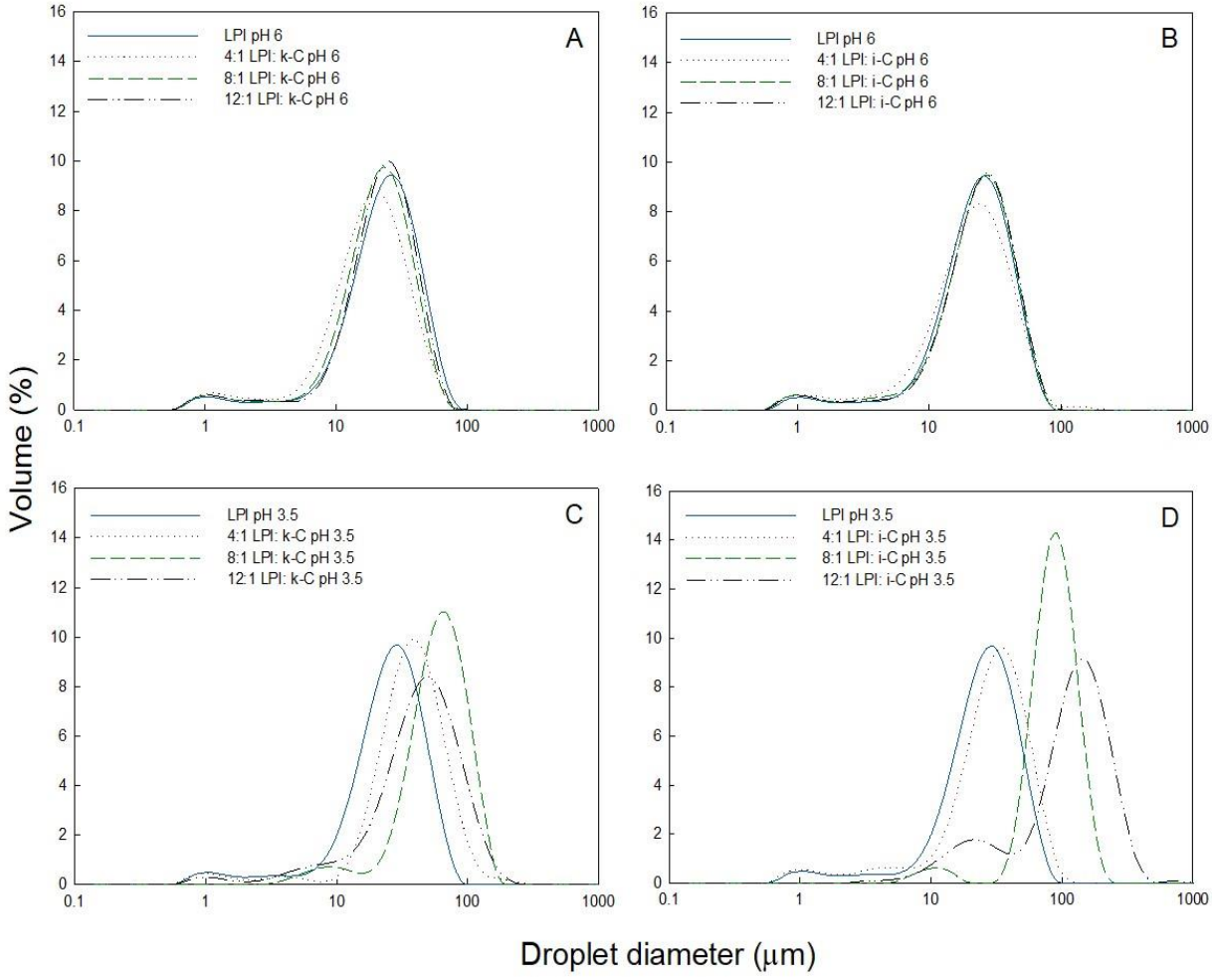

Figure A5.1 Droplet size distribution for emulsions stabilized by homogeneous lentil protein isolate (LPI) solutions and mixtures of LPI with κ-, ι-carrageenan at various mixing ratio at pH 6 and pH 3.5. Data represents the mean ± one standard deviation (n = 3).

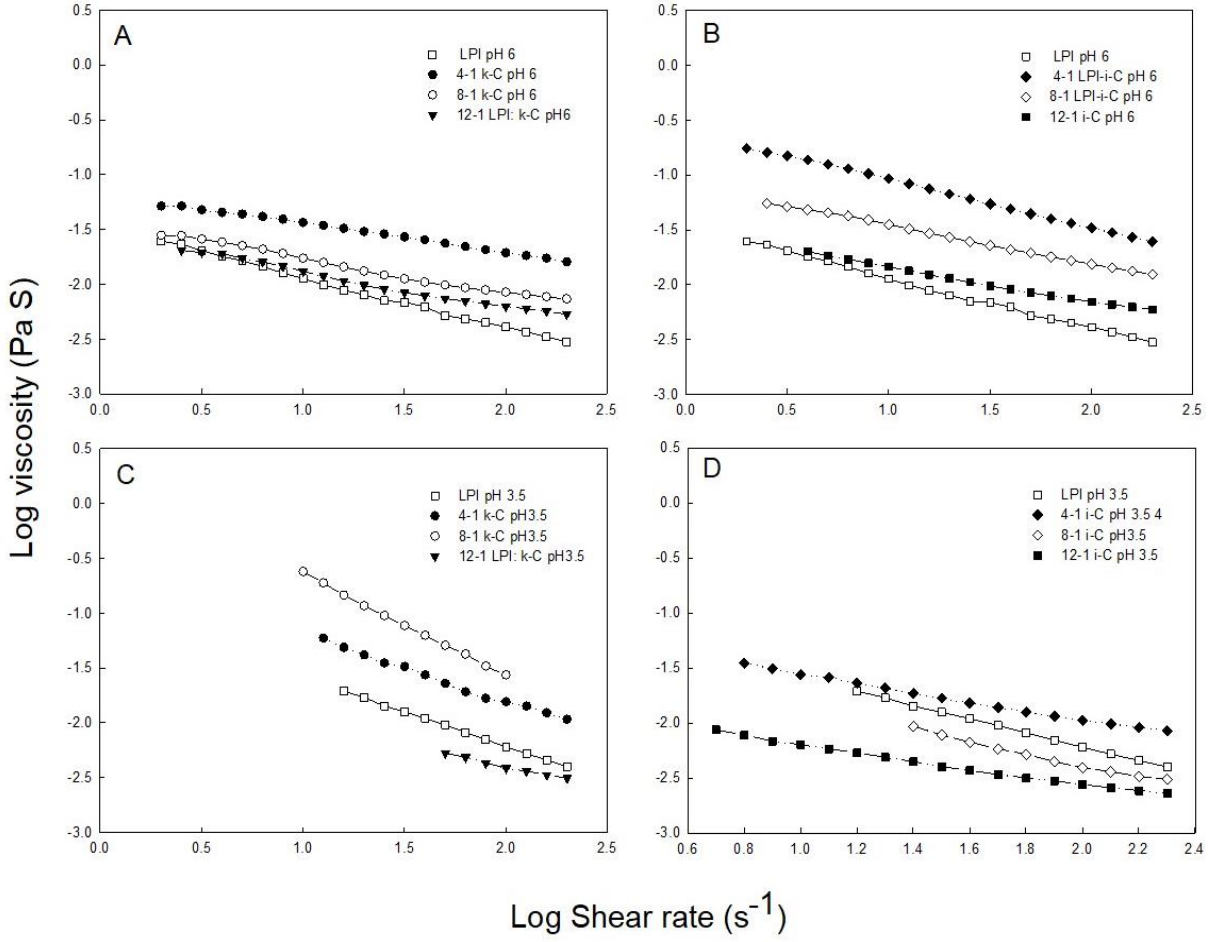

Figure A5.2 Flow diagrams as fitted using the Power-law model parameters for 1% (w/w) homogeneous lentil protein isolate (LPI) solutions and mixtures of LPI with κ-, ι-carrageenan at various mixing ratio at pH 6 and pH 3.5. Data represents the mean ± one standard deviation (n = 3).

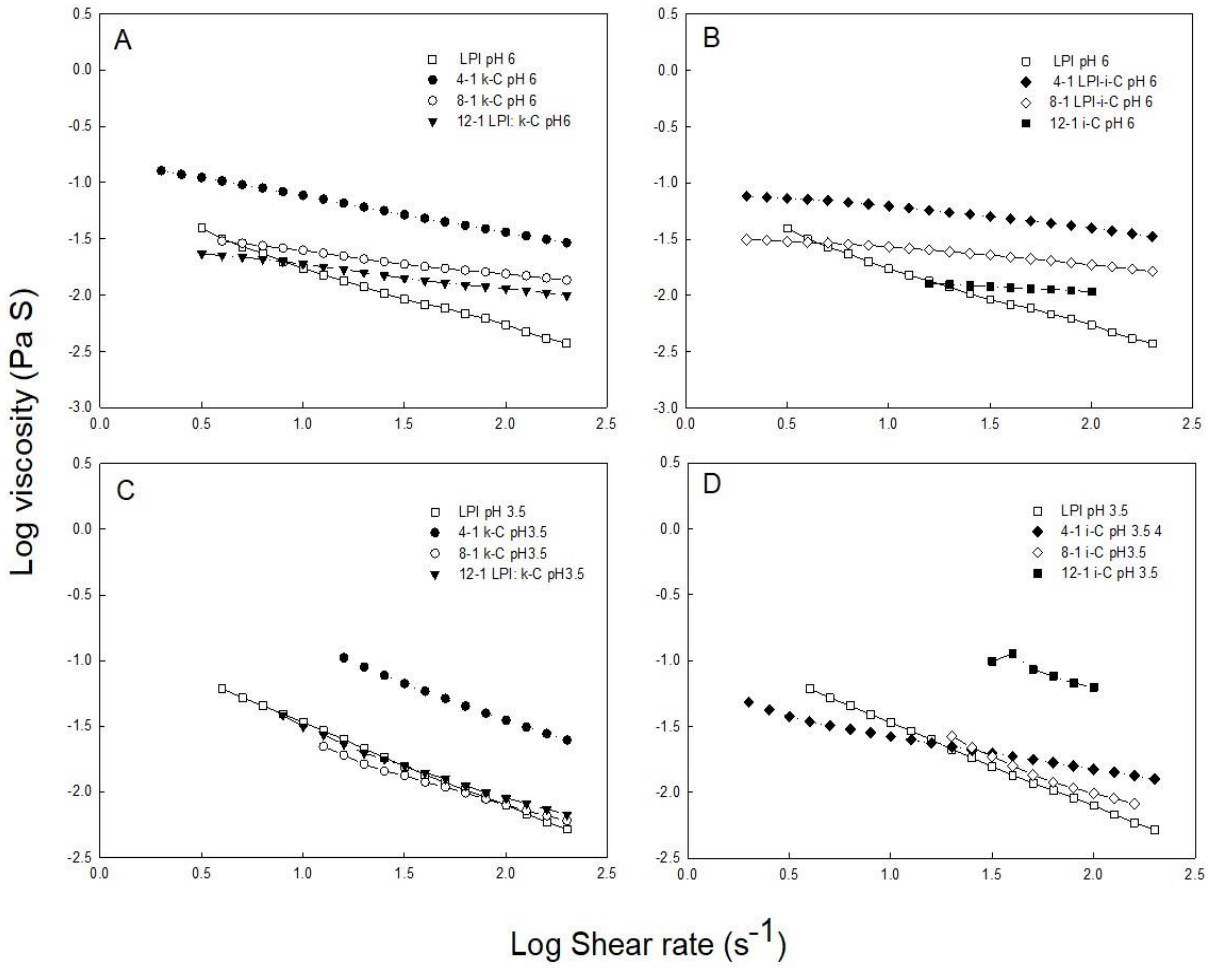

Figure A5.3 Flow diagrams as fitted using the Power-law model parameters for emulsions stabilized by homogeneous lentil protein isolate (LPI) solutions and mixtures of LPI with κ-, ι-carrageenan at various mixing ratio at pH 6 and pH 3.5. Data represents the mean ± one standard deviation (n = 3).

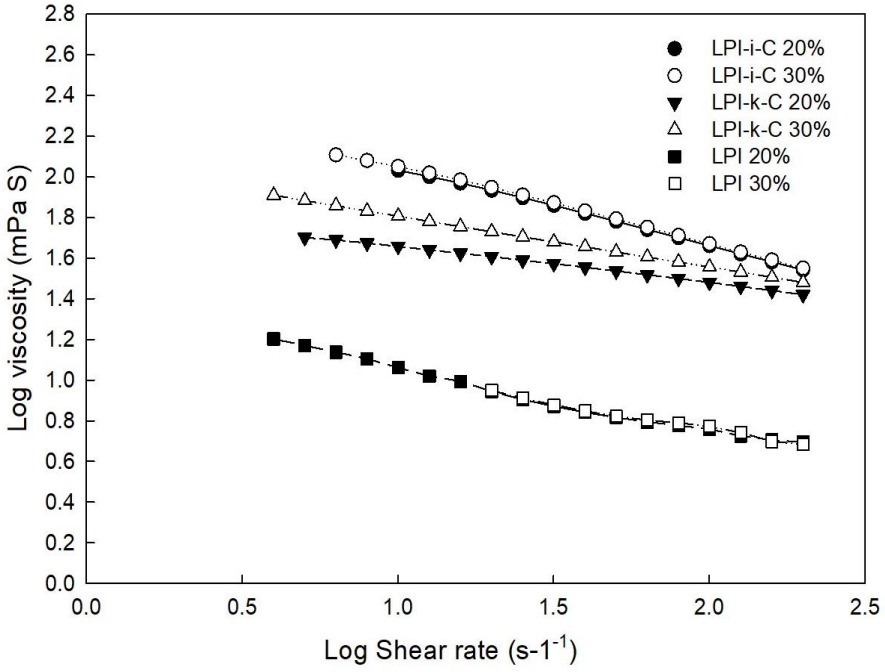

Figure A6.1 Flow diagram as fitted using the Power-law model parameters for emulsions stabilized by homogeneous lentil protein isolate (LPI) solutions and mixtures of LPI with κ-, λ-carrageenan at pH 6 to deliver 20% and 30% oil. Data represents the mean ± one standard deviation (n = 3). The percentage on the name of the samples represents the final oil content in dried powders.

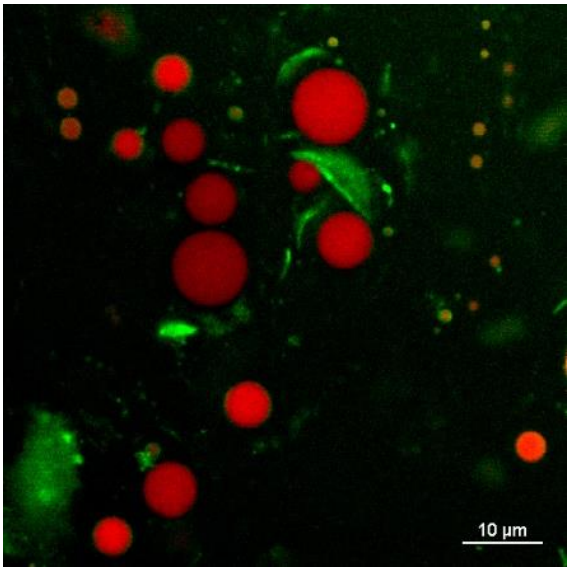

LPI- ι-C 20%

Figure A6.2 Confocal laser scanning microscopy (CLSM) images of a representative image for system of LPI-ι-carrageenan 20% to show the protein (green) surrounding the oil droplets (red). The scale bar represents 10 µ. The percentage on the name of the sample represents the final oil content in dried powder.

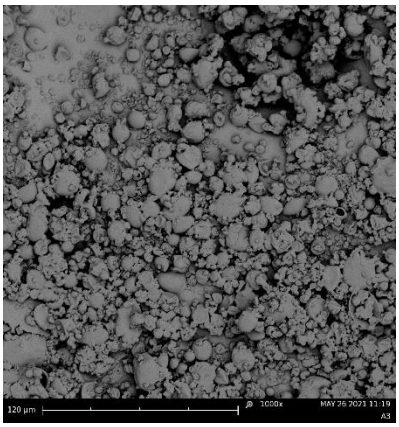

A) Spray-dried LPI- κ-C 20%

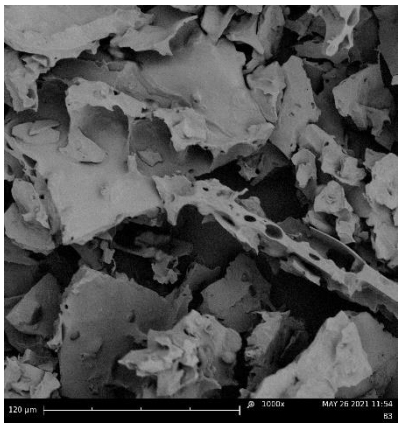

B) Freeze-dried LPI- κ-C 20%

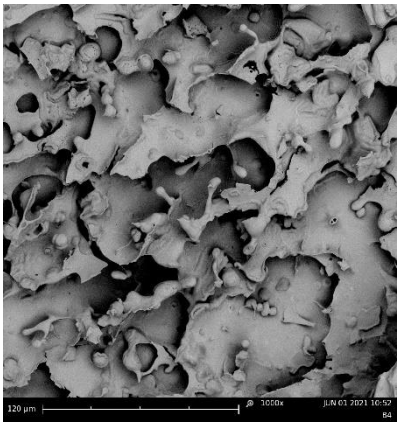

C) Freeze-dried LPI- κ-C 30%

D) Freeze-dried LPI 20%

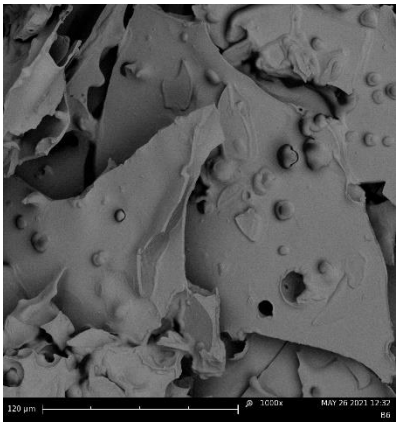

E) Freeze-dried LPI 30%

Figure A6.3 Scanning electron microscopy (SEM) images of the spray-dried LPI-κ-carrageenan **(**LPI-κ-C) 20% powder (A), freeze-dried LPI-κ-C 20% and 30% powders (B and C, respectively), freeze-dried LPI 20% and 30% powders (D and E, respectively) at 1000X magnification. All the scale bars represent 120 µ.